A Novel Homeostatic Mechanism Tunes PI(4,5)P_2-dependent Signaling at the Plasma Membrane

by

Rachel Christine Wills

B.A., Thiel College, 2012

Submitted to the Graduate Faculty of the

School of Medicine in partial fulfillment

of the requirements for the degree of

Doctor of Philosophy

University of Pittsburgh

2022

UNIVERSITY OF PITTSBURGH

SCHOOL OF MEDICINE

This dissertation was presented

by

Rachel Christine Wills

It was defended on

July 8, 2022

and approved by

Marijn G.J. Ford, Associate Professor, Department of Cell Biology

Adam V. Kwiatkowski, Associate Professor, Department of Cell Biology

Ora A. Weisz, Professor, Department of Cell Biology; Department of Medicine, Renal-Electrolyte Division

Guillermo G. Romero, Associate Professor, Department of Pharmacology and Chemical Biology

Dissertation Director: Gerry R.V. Hammond, Associate Professor, Department of Cell Biology

A Novel Homeostatic Mechanism Tunes PI(4,5)P_2-dependent Signaling at the Plasma Membrane

Rachel Christine Wills, PhD

University of Pittsburgh, 2022

The lipid molecule phosphatidylinositol (4,5)-bisphosphate (PI(4,5)P_2) controls virtually all aspects of plasma membrane (PM) function in animal cells. These functions range from cellular signaling to selective membrane permeability to the attachment of the cytoskeleton. Upon the reduction of PI(4,5)P_2 these cellular functions are dysregulated. The majority of PI(4,5)P_2 is synthesized by type 1 phosphatidylinositol 4-phosphate 5-kinase (PIP5K). However, the mechanism by which PIP5K localizes to the PM to access its substrate phosphoinositide 4-phosphate (PI4P) is not well known. Therefore, understanding the regulation of this kinase is critical for determining how the cell maintains PI(4,5)P_2 homeostasis. We observed PM localization of over-expressed PIP5K isoforms and endogenously tagged PIP5K1A to determine the potential mechanisms for PM association. After experimentally altering the phosphoinositide composition of the PM, we were able to observe the acute corresponding changes in PIP5K localization. PIP5K remained localized with the PM in the presence of PI4P and PI(4,5)P_2. Furthermore, we determined that two basic residues in the C-terminal tail are necessary for this PM interaction. The crystal structure of PIP5K displays these two residues opposite the activation loop and near an unstructured insert loop. Ultimately, we believe that the insert loop functions as a PI(4,5)P_2 binding pocket or confers allosteric regulation to reveal a cryptic PI(4,5)P_2 binding site on PIP5K to facilitate its PM localization.

On the other hand, increased levels of $PI(4,5)P_2$ are also associated with a wide range of diseases. Yet, it remains unclear how cells sense and maintain $PI(4,5)P_2$ levels without exceeding the basal level. Here, we show that the type 2 phosphatidylinositol 5-phosphate 4-kinase (PIP4K) family of enzymes, that synthesize $PI(4,5)P_2$ via a minor pathway, also function as sensors of tonic $PI(4,5)P_2$ levels. We show that PIP4K inhibits the synthesis of $PI(4,5)P_2$ and that this is done through a direct interaction with PIP5K. Furthermore, PIP4K is recruited to the membrane to interact with PIP5K in a $PI(4,5)P_2$ dependent manner. Perturbation of this simple homeostatic mechanism reveals differential sensitivity of $PI(4,5)P_2$-dependent signaling to elevated $PI(4,5)P_2$ levels. We find that a subset of $PI(4,5)P_2$ mediated functions may drive diseases associated with disrupted $PI(4,5)P_2$ homeostasis.

Table of Contents

List of Tables

List of Figures

Preface

The path to obtaining my PhD has certainly been long and can be quite eloquently summarized by Dr. Seuss.

"You'll start in a race down long wiggled roads at a break-necking pace and grind on for miles across weirdish wild space, headed, I fear, toward a most useless place. The Waiting Place… But on you will go though the weather be foul. On you will go though your enemies prowl… You'll get mixed up, of course, as you already know. You'll get mixed up with many strange birds as you go. So be sure when you step. Step with care and great tact and remember that Life's a Great Balancing Act… And will you succeed? Yes! You will, indeed! (98 and ¾ percent guaranteed.)"

The success that I have had is not mine alone and I would like to take the time to thank everyone who helped get me here.

First and foremost, I want to thank Gerry Hammond, my advisor and mentor. Gerry, thank you for taking a risk and making the time to train a novice graduate student. Thank you for your advice, support, and patience during my time in your lab. You have mentored me into an excellent scientist, capable of planning, performing, and analyzing experiments with the best of them.

I would also like to thank the Hammond lab, past and present. In particular, I must extend the greatest thanks to James Zewe and Colleen Doyle. James, thank you for teaching me and imparting a fragment of your scientific wisdom. Colleen, thank you for teaching me how to teach and allowing me to guide you through the wonders of research. Thank you both for being wonderful lab mates and life-long friends.

The work presented here would have never been completed without the help of Scott Hansen. Thank you for your collaboration and for performing experiments that we could never have imagined running ourselves. I am deeply grateful for your trust in the story and for your insightful comments and suggestions.

I must also thank my thesis committee. Marijn Ford, Adam Kwiatkowski, Ora Weisz, Guillermo Romero, and Linton Traub. Thank you for all your scientific inputs and recommendations for my projects. Additionally, thank you all for taking the time to assist me as a person, both scheduled meetings and impromptu hallway chats. Your mentorship and guidance have been truly invaluable in navigating the difficulties that are graduate school.

This work was supported through various funding agencies. Thank you to the University of Pittsburgh School of Medicine Cell Biology Teaching Fellowship and the Ruth L. Kirschstein Pre-doctoral Fellowship from the National Cancer Institute.

My scientific career humbly began at Thiel College. Thank you to the various professors that I had during my four years. I am deeply grateful to both Joyce Cuff and Kathryn Frantz. Without your mentorship, I would have never pursued a career in research.

Thank you to the many friends that I have made during my time at the University of Pittsburgh. I am appreciative for the many, many conversations about science, graduate school, and life in general. I can never return the kindness and love you have all shown me. Thank you for always making space for me, even when you didn't have space to spare. I could not have done this without each and every one of you.

I cannot fully articulate the immense gratitude that I have for my family. To my wife, Chelsea, I am so deeply appreciative for you during this entire process, particularly the last three

months. Thank you for listening to me rant and rave during every low and every high. I know it is my job to make the coffee but thank you for doing it when I could not.

To my parents, I am eternally grateful for you teaching me the definition of hard work. I would have never been able to achieve any of what I have today without that lesson. Thank you endlessly for always buying me the K'NEX sets that I asked for and letting me take up the entire dining room table for months at a time. That truly allowed me to think both logically and creatively from such an early age.

1.0 Introduction

1.1 Phospholipids and Phosphoinositides

Phospholipids, sphingolipids, and sterols are essential for the formation of cellular membranes and play a crucial role in regulating membrane fluidity, curvature, and the local recruitment of proteins (*1*–*3*). A large repertoire of lipid building blocks are used to generate unique membranes with exquisite spatio-temporal regulation of cellular processes (*3*, *4*). Therefore, understanding the cellular distribution, function, and metabolism of these lipid species has become an increasingly important endeavor to uncover both homeostatic function and pathological mis-regulation (*5*–*8*).

1.2 Phosphoinositides

Phosphatidylinositol (PI) is a unique phospholipid possessing a *myo*-inositol headgroup which can be reversibly phosphorylated in up to three different positions, generating seven different polyphosphoinositides (PPIns) (*9*). The *myo*-inositol headgroup is linked to the diacylglycerol backbone at the D1 position, and phosphorylation can occur at positions 3, 4, or 5 (*9*, *10*). Also unique to this class of phospholipid, there is an increased prevalence of arachidonic acid at the sn-2 position of the glycerol backbone (*9*, *11*). It has been hypothesized that these arachidonic acid containing lipids can be specifically targeted by enzymes involved in PPIns metabolism (*9*, *12*). The most common tail at the sn-1 position is steric acid (*9*). PPIns function in

several essential and dynamic roles in cell biology. As such, a great deal of effort has gone into understanding their function, cellular distribution, and metabolism (*8*).

Arguably, one of the important PPIns is the dually phosphorylated phosphatidylinositol 4,5-bisphosphate ($PI(4,5)P_2$). $PI(4,5)P_2$ is found in the inner leaflet of the plasma membrane (PM) and orchestrates most of the cellular activities that occur here (*9*, *10*). These functions will be discussed in detail below. The cellular levels of $PI(4,5)P_2$ are held at a very tight baseline, though the exact mechanism behind this spatiotemporal regulation is poorly understood.

1.3 $PI(4,5)P_2$ Metabolism

1.3.1 Synthesis

The foundation to the generation of all PPIns is through the initial synthesis of PI in the endoplasmic reticulum (ER) (*13–16*). This process first starts with the metabolism of precursor phosphatidic acid (PA) to cytidine-diphosphate diacylglycerol (CDP-DAG) (*13*). This occurs through the enzymatic reaction between cytidine-triphosphate (CTP) and PA by CDP-DAG synthase (CDS) (*15*, *17*). From here, CDP-DAG is conjugated with *myo*-inositol by the PI synthase (PIS) enzyme to form PI in the ER (*13*, *18*). From here, PI is shuttled from the ER to the PM by the lipid transfer protein, Nir2 (*19–22*). Very little PI remains in the PM at any point in time (*23*, *24*), and it is quickly metabolized into phosphatidylinositol 4-phosphate (PI4P) (*9*, *25*). This reaction is performed at the PM by phosphatidylinositol 4-kinase type III α (PI4Kα) (*26*, *27*). Alternatively, PI in endomembranes (*23*, *24*) can be metabolized to phosphatidylinositol 3-phosphate (PI3P) by the class III phosphatidylinositol 3-kinase (PI3K) Vps34 (*28*). From here,

PI3P is further phosphorylated to phosphatidylinositol 3,5-bisphosphate ($PI(3,5)P_2$ by PIKfyve, a PI3P 5-kinase (*29*). At this point, $PI(3,5)P_2$ is degraded by myotubularin-related protein (MTMR), a 3-phosphatase, to produce phosphatidylinositol 5-phosphate (PI5P) (*30*, *31*).

$PI(4,5)P_2$ can be synthesized via three independent routes. Two of these paths involve the secondary phosphorylation of either PI4P or PI5P (*9*). The third pathway involves the dephosphorylation of phosphatidylinositol 3,4,5-trisphosphate ($PI(3,4,5)P_3$) to $PI(4,5)P_2$ (*9*). An illustration of each of these pathways can be seen in **Figure 1.1**. Upon completed synthesis of $PI(4,5)P_2$, this lipid molecule can be cleaved by phospholipase C (PLC) into diacylglycerol (DAG) and inositol 1,4,5-trisphosphate (IP_3) (*9*, *32–36*). From here, DAG is phosphorylated into PA which is transported to the ER by Nir2 (*19–22*). As previously mentioned, Nir2 is responsible for the transport of both PA from the PM to the ER and that of PI from the ER to the PM (*19–22*). In the ER, PA is then converted back into CDP-DAG (*15*, *17*), and the PI cycle is free to continue again.

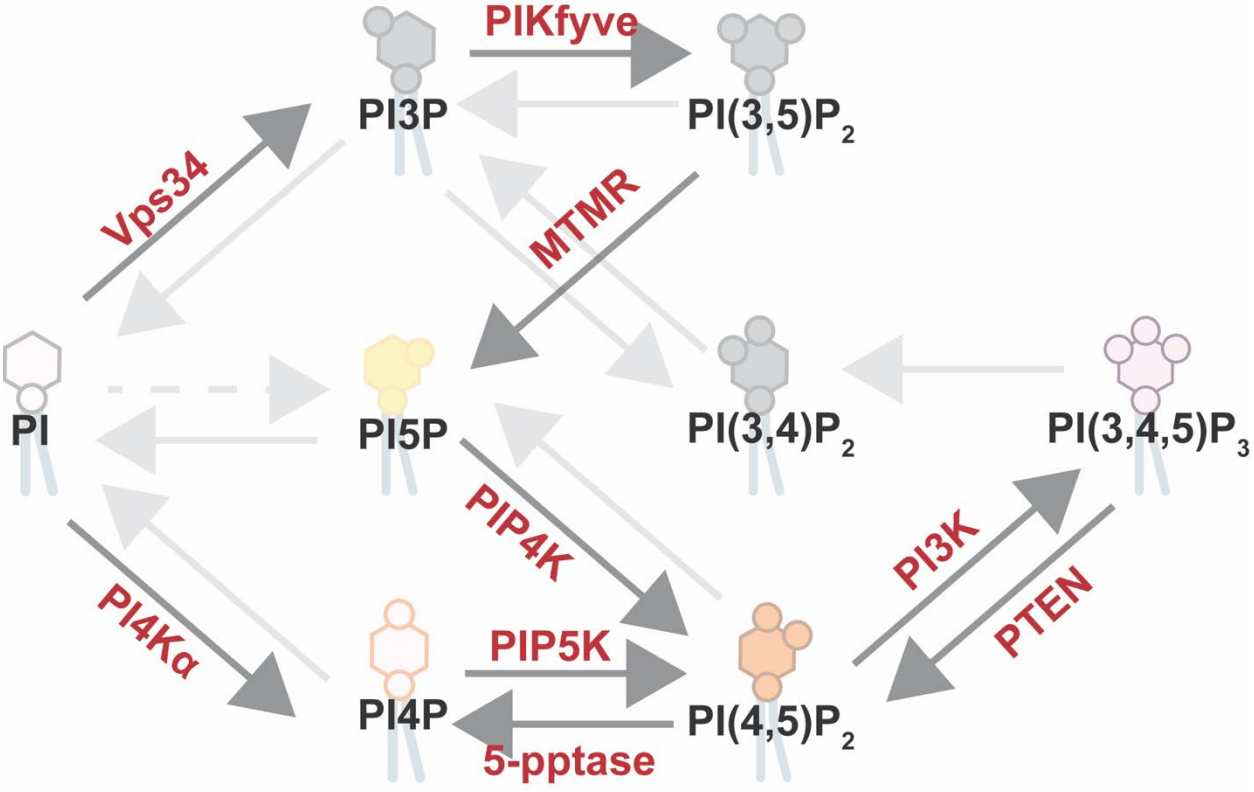

Figure 1.1 PI and the Seven Phosphoinositides.

A schematic outlining the synthesis and degradation pathways involved in phosphoinositide metabolism. PPIns discussed in this work are shown with associated colors while those not discussed in detail are shown in grey. The enzymes discussed in this work are shown in red.

1.3.1.1 PIP4K

One kinase family is composed of phosphoinositide 5-phosphate 4-kinase (PIP4K). This kinase phosphorylates PI5P at the 4-OH position of the inositol ring (*37–40*). The crystal structure of PIP4K2B suggests that localization with membranes is likely based off non-specific electrostatic interactions (*41*). Furthermore, the unique flattened kinase domain allows for PIP4K to associate with membranes (*41*). For example, the activation loop, the G-loop, the insert loop, and the N-terminus all appear as unstructured regions in PIP4K structures. However, this differs from the activation loop in the related phosphoinositide 4-phosphate 5-kinase (PIP5K), which

organizes as an alpha helix when interacting with membranes (*42*). Furthermore, the G-loop is predicted to stabilize an ATP bound confirmation of the protein; the same function as in other structurally related protein kinases (*41*). Yet, the insert loop and the N-terminal region have no known structure or function. These unique structural components likely lead to further regulation of PIP4K.

The PIP4K family is made up of three isoforms, A, B, and C with varying cellular concentrations and catalytic activities. All isoforms of PIP4K are reported to show a primarily cytosolic localization (*43–45*). Additionally, PIP4K2A can localize with the PM (*43*), PIP4K2B is found in the nucleus (*44*), and PIP4K2C shows intracellular membrane localization (*45*). Of the three isoforms, PIP4K2A is the most active (*45–48*), followed by PIP4K2B (*46–48*), and PIP4K2C is the least active (*45*, *48*). There is extensive variability in catalytic activity between the three isoforms of PIP4K; PIP4K2C displays little to no catalytic activity when compared to PIP4K2A and PIP4K2A is 10,000-fold more active than PIP4K2B (*45–48*). Furthermore, both PIP4K2A and PIP4K2C use ATP to phosphorylate PI5P but PIP4K2B preferentially utilizes GTP (*49*, *50*). Interestingly, the activity levels of the PIP4K isoforms are inversely related to their cellular concentrations. PIP4K2A universally has the lowest copy number, while PIP4K2B has the highest concentration in multiple tissues (*45*) and PIP4K2C is found most abundantly in HeLa and HEK293A cells (*51*, *52*). The presence of various isoforms with differing activity and cellular abundance further indicates that PIP4K is highly regulated.

To further complicate the cellular functionality of PIP4K, these proteins exist as obligate dimers in cells (*41*). Furthermore, PIP4K isoforms may either homo- (*41*) or heterodimerize (*45–47*). As such, it has been proposed that the more abundant, but less active, isoforms of PIP4K may be responsible for targeting the cellular localization of other PIP4K isoforms (*45–47*). Thus, less

abundant isoforms of PIP4K can undergo acute spatiotemporal regulation, adding further regulation to PIP4K function.

The proposed functions of this kinase range from $PI(4,5)P_2$ synthesis (*39*, *40*) to depletion of PI5P (*53–55*) to inhibiting the activity of PIP5K (*56*) to impacting insulin signaling (*53*, *56*). Overall, it is not thought that PIP4K is the main route of $PI(4,5)P_2$ synthesis, as PI5P comprises a minor portion of the PPIns pool (*9*, *40*, *57*). However, the ultimate physiological role of PIP4K has not yet been elucidated, and is still heavily debated (*53*, *58–61*).

1.3.1.2 PIP5K

The PIP5K is a second type of PPIns kinase which phosphorylates PI4P on the 5-OH position of the inositol headgroup (*62–65*). PIP5K is expected to produce the bulk of $PI(4,5)P_2$, specifically in the inner leaflet of the PM. However, the mechanism of regulation of the mammalian PIP5K remains elusive. In comparison, the yeast homolog of PIP5K, Mss4, has a well characterized regulatory mechanism (*66*, *67*). Mss4 localizes to the PM in a cluster or oligomeric patch, which allows for the rapid and continued production of $PI(4,5)P_2$ (*67*). Moreover, this PM association of Mss4 is dependent on PI4P (*67*); this substrate mediated localization is a potential mechanism of regulation of the kinase. As $PI(4,5)P_2$ is produced, a low affinity $PI(4,5)P_2$ binding protein, Opy1, is recruited to the PM (*67*). Upon recruitment to the PM, Opy1 interacts with and inhibits further activity of Mss4 (*67*). Thus, Opy1 acts as a coincidence detector to interact with both $PI(4,5)P_2$ and Mss4 to negatively regulate $PI(4,5)P_2$ synthesis at the PM in yeast (*67*).

Structurally, PIP5K is composed of a catalytic kinase core, an unstructured N-terminus, and a longer unstructured C-terminal tail (*64*, *65*, *68*, *69*) (**Figure 1.2**). The kinase domain of PIP5K shares similarity with that of both PIP4K2B and protein kinase A (PKA) (*70*). PIP5K1A, like PIP4K2B, has a net positive charge around the active site of the protein, away from the

dimerization interface (*70*). This could likely indicate that PIP5K membrane association is due to electrostatic interactions (*70*, *71*). The kinase domain of PIP5K also contains an activation loop, an insert loop, and a G-loop (*70*). It is speculated that the G-loop interacts with ATP and stabilizes the ATP-bound conformation, as in other protein kinases (*41*). However, this loop remained unstructured when ATP was soaked into the crystals, so this functionality is still up for debate (*72*). The activation loop of PIP5K serves two purposes. First, the activation loop regulates substrate specificity and the ability of PIP5K to interact with PI4P at the PM (*73*). Second, this unstructured segment organizes as an alpha helix when interacting with membranes, allowing for membrane sensing and interaction (*42*). As with PIP4K, neither the insert loop or the N-terminal region have any known structure or function. Again, it is likely that these unstructured features of PIP5K allow for further regulation of catalytic activity or subcellular localization.

There are three isoforms of PIP5K, A, B, and C (*64*, *65*, *68*, *74*). The A and B isoforms were discovered around the same time by two different groups in either mouse (*64*) or human (*68*). These two isoforms were named reciprocally between these two organisms, ie mouse A is human B and vice versa. As with most manuscripts, we will use human nomenclature here. The PIP5K1C is unique among the isoforms as six splice variants have been identified, giving rise to more variety in the PIP5K family (*65*, *74–76*). Each of these isoforms and splice variants has a unique C-terminal tail which may be responsible for specialized protein-protein interactions and spatiotemporal regulation at the PM.

Each of the PIP5K isoforms are found localized generally at the PM of cells (*9*, *77*). PIP5K can interact with several proteins, reviewed here: (*9*, *77–79*). In brief, PIP5K seems to interact with and be stimulated by the small GTPases Rho, Rac, and ADP-ribosylation factors 1 and 6 (ARF1 and ARF6). Additionally, the interaction of PIP5K with Dishevelled, via its DIX domain, also

stimulates the activity (*70*, *79*). In terms of protein interactions to simply direct subcellular localization, PIP5K can bind with Bruton's tyrosine kinase (BTK) to assist in recruiting PIP5K to the PM where it can subsequently produce $PI(4,5)P_2$ for further production of $PI(3,4,5)P_3$ and downstream calcium signaling (*79*). Furthermore, the scaffolding protein IQ motif containing GTPase activating protein 1 (IQGAP1) has been shown to recruit both PIP5K and PI3K to the PM to establish signaling platforms (*80–82*). Other than the PM, PIP5K has also been found in the nucleus (*75*). Here, PIP5K can interact with both pRB (*79*) and p53 (*83*). In terms of isoform specific interactions, PIP5K1A is localized specifically at membrane ruffles (*84*) and PIP5K1B to the apical surface of polarized cells (*85*). PIP5K1C-v1 and v-6 seem to be the only two splice variants localized primarily to the inner leaflet of the PM (*65*, *76*). PIP5K1C-v2 has been found to specifically localize with either AP-2 (*86*, *87*) or with talin (*88*, *89*). And PIP5K1C-v3 and -v5 have been shown to localize with unique and yet unidentified cytoplasmic domains (*75*, *90*). Finally, PIP5K1C-v4 has been found localized to the nucleus of both HeLa and MCF10A cells (*75*). These isoform specific differences further showcase the unique ways which PIP5K is regulated cellularly.

As with the PIP4Ks, the PIP5K isoforms have differing concentrations and catalytic activities (*77*). PIP5K1A is the most abundant in HEK293A and HeLa cells (*51*, *52*). This isoform also was very abundant in most tissues, particularly skeletal muscle (*68*). PIP5K1B is the least abundant isoform in tissues, except for the heart where it is highly expressed (*68*). It is also least abundant isoform in HEK293A cells (*52*) and not even detected in HeLa cells (*51*). PIP5K1C is the most abundant isoform in brain tissue (*65*, *74*) but is less abundant than PIP5K1A in both HEK293A and HeLa cells (*52*). In terms of catalytic activity, PIP5K1A is the highest of the three and PIP5K1B has the lowest catalytic activity (*65*, *91*). There is much less difference in catalytic

activity between the three PIP5K isoforms; the difference between the most active PIP5K1A and the least active PIP5K1B differs by only ~3-fold (*65*). Again, this is uniquely opposite to the expression levels of the PIP5K isoforms. These variations in isoform specific PIP5K expression and catalytic activity likely allow for specific and regulated tuning of $PI(4,5)P_2$ synthesis.

Another similarity between the PIP4K and PIP5K family is the ability of these molecules to dimerize. However, unlike PIP4K, PIP5K seems to exist in solution as both a monomer and as a dimer (*70*, *92*). Though, the activity of PIP5K is regulated by dimerization (*70*). The dimer interface of PIP5K is also slightly different than the head-to-head arrangement of PIP4K (*41*). PIP5K forms a side-to-side dimer which is held together due to both hydrophobic contact points and electrostatic interactions (*70*). The electrostatic interactions are made up of a double aspartate (D) and an arginine (R) salt bridge formed between two molecules (*70*). Dimerization does not seem to be necessary for the ability of PIP5K to interact with membranes, but it increases kinase activity (*70*). Furthermore, dimerization appears to allosterically regulate the catalytic activity in a yet unknown way (*92*). Little work has been done, to date, to assess whether the PIP5K isoforms can heterodimerize and whether this would further impact the activity or localization of various isoforms.

The catalytic activity of PIP5K seems to be regulated by phospholipids. For example, all three isoforms of PIP5K are stimulated by PA (*93*, *94*). Furthermore, PIP5K can interact directly with phospholipase D (PLD), an enzyme responsible for PA production (*95*). PIP5K1C displays the most robust increase in activity when stimulated by PA, though PIP5K1A and PIP5K1B are both stimulated to a lesser degree (*65*). This PA stimulation is unique to the PIP5K family of $PI(4,5)P_2$ producing enzymes, and was historically used to determine the difference between the PIP4K and PIP5K enzymes (*65*). PIP5K can also be inhibited by its product, $PI(4,5)P_2$ (*64*, *69*), an

interaction which may be competition within the active site (*73*). Finally, more than just the lipid headgroup may influence the activity of PIP5K. The PM of mammals is predominately made up of lipids with one saturated and one unsaturated acyl chain, primarily in the inner leaflet (*96*). Furthermore, the unsaturated fatty acid is polyunsaturated in 67% of the PM lipids (*96*). Previous research has shown that PIP5K has a preference in the acyl chain of lipids it interacts with (*91*), a feature also demonstrated by DAG kinase (DGK) (*97*). All three isoforms were activated most by 1-stearoyl-2-oleoyl PI4P but 1-stearoyl-2arachidonoyl PI4P also stimulated activity, when compared with 1,2-dipalmitoyl PI4P (*91*). Moreover, PIP5K stimulation was not dependent on the fatty acid tails that make up PA (*91*), suggesting that this stimulation may be the result of the head group interaction only. Overall, this selectivity of PIP5K for certain substrates may allow for specific pools of PI4P to be metabolized preferentially, which may further aid in PIP5K feedback.

PIP5K is regulated in multiple means from protein-protein interactions to PTMs to PPIns interactions. This myriad of mechanisms available for positive and negative regulation of PIP5K underscores the overall importance of maintaining $PI(4,5)P_2$ homeostasis.

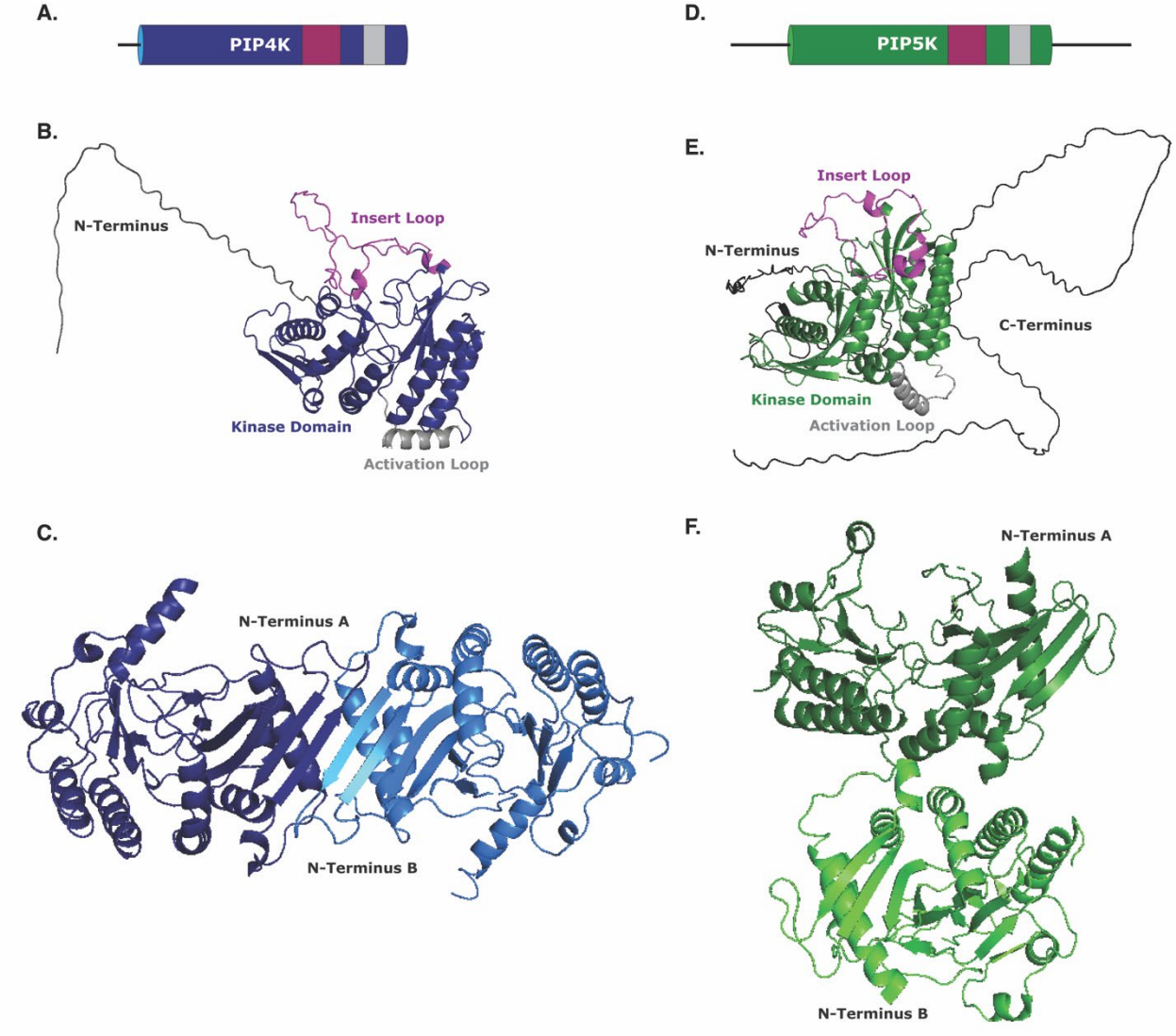

Figure 1.2 A comparison of the PIP4K and PIP5K structures.

(**A**) The linear structure of the PIP4K enzyme. Regions of interest and discussion are delineated with different colors. (**B**) The tertiary structure of PIP4K2C. This structure was adapted from AlphaFold predictions. The highlighted regions in the structure correspond to the regions of interest in the linear structure. These regions of interest include the N-terminus (black), kinase domain (blue), activation loop (grey), and insert loop (magenta). (**C**) Two tertiary PIP4K2B molecules as a dimer. Molecule A (blue) and molecule B (cyan) dimerize in a head-to-head fashion. This structure was taken from the Protein Data Bank: 1BO1. (**D**) The linear structure of the PIP5K enzyme. Regions of interest and discussion are delineated with different colors, similar to PIP4K. (**E**) The tertiary structure of PIP5K1A. This structure was adapted from AlphaFold predictions. The highlighted regions in the structure correspond to the regions of interest in the linear structure. These regions of interest include the N-terminus (black), kinase domain

(green), activation loop (grey), insert loop (magenta), and C-terminus (black). (**F**) Two PIP5K1A molecules as a dimer. The zebra fish structure of molecule A (dark green / top) and molecule B (light green / bottom) dimerize in a side-to-side manner, different than that of the PIP4K molecules. This structure was taken from the Protein Data Bank: 4TZ7.

1.3.1.3 PTEN

$PI(4,5)P_2$ can also be synthesized by the degradation of PPIns. In particular, phosphatase and tensin homolog on chromosome 10 (PTEN) acts as a 3-phosphatase to generate $PI(4,5)P_2$ from $PI(3,4,5)P_3$. To function, PTEN must target the PM, and this can be done in two main ways. First, PTEN contains a C2 domain which allows for the interaction with the PM either through non-specific electrostatic interactions or via a direct interaction with phosphatidylserine (PS) (*98*). Second, PTEN has a $PI(4,5)P_2$ binding motif (PBM) (*98*) which targets the phosphatase to the PM. Specifically, PTEN seems to negatively regulate the cellular levels of $PI(3,4,5)P_3$ and directly competes with class I PI3Ks (see below) (*9*). As such, this pathway is not likely to contribute to the bulk of $PI(4,5)P_2$ production in cells but is rather a mechanism to control the flux between $PI(4,5)P_2$ and $PI(3,4,5)P_3$ (*99*, *100*).

1.3.2 Degradation

Broadly, $PI(4,5)P_2$ can be removed from the PM in two main ways. First, $PI(4,5)P_2$ can be degraded into different lipid based products, such as IP_3 and DAG. Or secondly, $PI(4,5)P_2$ can be transformation into another PPIns, via dephosphorylation or phosphorylation.

1.3.2.1 Phospholipases

The PLC family of phospholipases use $PI(4,5)P_2$ as a substrate to produce DAG and IP_3, and have been reviewed extensively (*9*, *33*). Presently, there are 13 isoforms of PLC which have been divided into six different families (*9*). Some common features of these families, that pertain to this work include a PH domain, the catalytic regions, and a C2 domain (*9*, *33*). The PH-domain from PLCδ1 has been used as a $PI(4,5)P_2$ biosensor, and this domain is recruited to the PM in a $PI(4,5)P_2$ dependent manner (*9*). Additionally, the C2 domain is responsible for its PM localization and association, via in interaction with phosphatidylserine (PS) (*9*, *33*, *101*). PLCβ3 is an abundantly expressed isoform and is present in multiple tissues (*9*, *33*). Furthermore, PLCβ3 is readily activated by G protein-coupled receptors (GPCRs), specifically, via an interaction with the $G\alpha_q$ subunit (*9*, *33*). Here, PLCβ3 interacts with PM targeted $G\alpha_q$ via the C2 domain, and can therefore hydrolyze its substrate, $PI(4,5)P_2$ at the PM. However, the interaction of PLC with GPCRs and the associated G protein subunits is extensive and highly detailed (*33*). Moreover, the general regulation of PLC enzymes is very complex and is certainly beyond the scope of this work.

1.3.2.2 Class I PI3K

Class I phosphoinositide-3-kinases (PI3Ks) are responsible for the production of $PI(3,4,5)P_3$ by phosphorylating $PI(4,5)P_2$ at the 3-OH position of the inositol ring (*102*). Class I PI3Ks exist as dimers made up of a single p110 catalytic subunit (one of p110α, p110β, p110δ) and a single regulatory subunit (one of p85α, p85β, p55α, p55γ, p50α) (*103*). Upon activation of receptor tyrosine kinases (RTKs) or GPCRs, PI3K is recruited to the PM. This occurs through a direct interaction with Ras and with phosphorylated Tyr (pY) on adaptors or RTKs (*104*). The regulatory subunit possesses an SH2 domain that interacts with RTKs via their phosphorylated tyrosine kinase; this interaction breaks the autoinhibitory complex formed between the catalytic

and regulatory subunits to activate PI3K (*104*). There are multiple oncogenic activating mutations which are present in PI3Kα (*103*, *104*); E542K, E545K, and H1047R are all present in the p110α subunit (*104*). E542 and E545 mediate the autoinhibitory interaction with SH2, thus activating PI3Ka (*104*). H1047R increases the binding affinity for $PI(4,5)P_2$ at the PM and takes over the Ras binding activation, again increasing activity of PI3Kα (*104*). Overall, this pathway seems to provide the physiologically required amount of the potent signaling lipid $PI(3,4,5)P_3$, but this pathway is tightly controlled by the antagonizing activity of PTEN. However, the impact of basally elevated $PI(4,5)P_2$ levels on PI3K mediated $PI(3,4,5)P_3$ production is unknown.

1.3.2.3 Inositol 5-phosphatases

Inositol 5-phosphatase family of enzymes functions to dephosphorylate the 5 position of the inositol headgroup of PPIns (*9*). There are three types (II-IV) of enzymes which act to catalyze this reaction; historically, there are four types of 5-phosphatases, however, the type I enzyme does not act on PPIns (*9*). The type II and type IV inositol-5-phosphatases can all act on $PI(4,5)P_2$ (*9*, *105–107*). The type II family is made up of synaptojanin-1 (SYNJ1), SYNJ2, oculocerebrorenal syndrome of Lowe (OCRL), inositol polyphosphate-5-phosphatase B (INPP5B), INPP5J, and INPP5K (*9*, *105–107*). Finally, there is a single type IV 5-phosphatase, INPP5E (*9*, *106*). The type III inositol-5-phosphatases are SH2-domain containing inositol 5-phosphatase (SHIP1 or INPP5D) and SHIP2 (also known as INPPL1) (*9*, *108*). These enzymes are thought to primarily use $PI(3,4,5)P_3$ as a substrate to generate $PI(3,4)P_2$. Though, SHIP2 has been shown to also utilize $PI(4,5)P_2$ as a substrate to produce PI4P (*108*). Each of these proteins contains a 5-phosphatase domain which hydrolyzes $PI(4,5)P_2$ and/or $PI(3,4,5)P_3$, primarily on the inner leaflet of the PM (*109–111*). The inositol 5-phosphatases are found at several subcellular localizations, but to dephosphorylate their substrates the inositol 5-phosphatases must localize to the PM. Similar to

PTEN, it has been proposed that the role of these inositol 5-phosphatases negatively regulate $PI(4,5)P_2$ at other organelles (*112*). Each inositol 5-phosphatase has any number of domains which may further influence basal sub-cellular localization and allow for PM targeting (*9*, *105*).

Uniquely, SYNJ1 and SYNJ2 both contain a 5-phosphatase domain and a Sac1 domain (a 4-phosphatase) which can act synergistically to degrade $PI(4,5)P_2$ to PI (*9*, *105*, *113*). Both SYNJ1 and SYNJ2 are found primarily at the PM (*9*). This association is dependent on protein-protein interactions between SYNJ and endocytic machinery such as amphiphysin (*9*). SYNJ1 and SYNJ2B contain a proline-rich (PR) domain(s) (*9*, *105*) which localize to membranes via a hydrophobic interaction (*114*). The PR domain can also associate with src homology 3 (SH3) domains, which are found in several PM-associated proteins, and this can further direct these phosphatases (*114*).

OCRL is primarily a Golgi localized protein with some additional localization at the trans Golgi network (*9*). INPP5B is found at both the ER and the Golgi (*9*). OCRL and INPP5B share a similar linear structure, with similar domains to mediate membrane binding (*9*, *105*). These proteins each possess a PH domain and a RhoGAP domain. The PH domain mediates interactions with PPIns (*9*, *101*, *105*). The RhoGAP domain interacts with both Rac and Cdc42 to facilitate PM localization (*105*).

Both INPP5J and INPP5K have alternative names. INPP5J is alternatively known as proline-rich inositol-polyphosphate 5-phosphatase (PIPP) and INPP5K is known as skeletal muscle and kidney enriched inositol phosphatase (SKIP). INPP5J is often found at the PM, however its main functionality here is to metabolize $PI(3,4,5)P_3$ and not $PI(4,5)P_2$ (*9*). INPP5K is found at either the ER, the Golgi, or the PM (*9*, *115*). Furthermore, both INPP5J and INPP5K contain a SKIP carboxyl homology (SKICH) domain (*9*, *105*). This SKICH domain is essential to

direct localization of these 5-phosphatases specifically to membrane ruffles (*116*). INPP5J contains two PR domains, which again mediate membrane specific protein-protein interactions. Finally, INPP5E is found primarily at the Golgi, but can also be seen at the PM (*9*). INPP5E localizes to the PM due to a PR domain (*9*, *105*, *106*), which mediates protein-protein interactions, as discussed previously (*114*).

SHIP1 and SHIP2 are primarily localized in the cytosol of cells, but they can localize to the PM via protein-protein interactions (*9*, *117*). These two proteins contain SH2, C2, and PR domains (*9*, *105*). SH2 domains interact with phospho-tyrosine (pTyr) residues, prevalent in activated RTKs at the PM (*118*). SH2 domains can also display specificity in PPIns binding, specifically the SHIP1-SH2 domain displays a high selectivity for $PI(3,4,5)P_3$ and $PI(4,5)P_2$ (*119*, *120*). Upon the phosphorylation and activation of RTKs and the production of $PI(3,4,5)P_3$, SHIP1 and SHIP2 are efficiently recruited to the PM. Furthermore, as discussed above, the C2 and PR domains also help to direct the SHIP proteins to the PM (*9*, *117*). Evidence shows that SHIP2 interacts with intersectin1, a PM scaffolding protein, which further mediates the localization of these enzymes (*117*). In total, these enzymes are all able to further assist in the complex regulation of $PI(4,5)P_2$ levels in cells.

The multitude of enzymes that are involved in both the synthesis and the degradation of $PI(4,5)P_2$ highlights the importance of this essential lipid in cellular function. A variety of methods have emerged with which to quantify lipid levels and to observe the enzymes responsible for their metabolism (*9*, *121–125*).

1.4 Phosphatidylinositol 4,5-bisphosphate ($PI(4,5)P_2$) and PM identity

When compared to the overall lipid levels in cells, PPIns exist at relatively low molar percentages. However, each PPIn seems to have a specific distribution among distinct organelles (*126*). Furthermore, the local enrichment of lipid species within a specific organelle can result in a much higher local concentration of that lipid. For example, $PI(4,5)P_2$ makes up approximately ~1.4 molar percentage (mol%) of total cellular phospholipids, compared to that of the phosphatidylcholine (PC) which comprises ~25.4 mol% (*127–130*). However, virtually all of the $PI(4,5)P_2$ is found at the inner leaflet of the PM, while PC is found throughout organellar membranes, and in both the cytosolic and the exoplasmic leaflets (*9*, *123*, *127*, *128*, *131*, *132*).

How much $PI(4,5)P_2$ is in the inner leaflet of the PM? Assuming that the average leaflet of the bilayer can hold ~$1.5x10^6$ phospholipids/μm^2 (*11*, *128*) and that 60% of that space is not occupied by membrane proteins (*11*) there is space for a total of ~900,000 phospholipids/μm^2 in the inner leaflet of the PM. Various $PI(4,5)P_2$ densities have been experimentally determined and range from 4,000 molecules/μm^2 in a neuroblastoma cell line (*133*) to 34,000 molecules/μm^2 in adult rat pinealocytes (*11*), resulting in an average of ~20,000 $PI(4,5)P_2$ molecules/μm^2 (*134*). As a total percentage of the inner leaflet of the PM, $PI(4,5)P_2$ makes up anywhere from ~0.4 – 4% of the lipid density, resulting in an average of ~2.2% of the inner leaflet PM is $PI(4,5)P_2$ (*96*, *128*, *135*). Furthermore, accounting for the surface area of the PM at ~2000μm^2 (*129*, *130*), it can be determined that there are anywhere between $8x10^6$ and $6.8x10^7$ $PI(4,5)P_2$ molecules in the inner leaflet of the PM at any given time.

The enriched concentration of $PI(4,5)P_2$ allows for the targeting of proteins to the PM to specifically carry out membrane traffic, cytoskeletal arrangement, and cell signaling (*132*). Unlike $PI(4,5)P_2$, PI4P is found at multiple organelles, such as the Golgi, the PM, and endosomes (*127*,

128). PI4P binding proteins can then distinguish the PM from the Golgi by the presence or absence of various lipid species (*4*, *9*, *128*, *129*). The specific lipid makeup of membranes provides unique identities to various organelles, and this results in exquisite spatial and temporal regulation of cellular processes (*4*, *8*, *9*).

1.4.1 Signaling and PI(4,5)P_2

In addition to their function as markers of organelle identity, specific lipid species and their metabolites can function as second messengers within cells. PI(4,5)P_2 is a substrate for the PLC family of enzymes (*9*, *32*, *33*). PLC can be stimulated through G-protein coupled receptors (GPCRs) (*33*). Specifically, it was found that the stimulation of cells with acetylcholine or carbachol – known agonists of GPCRs - resulted in an activation of GPCRs, PLC, and subsequent degradation of PI4P and PI(4,5)P_2 (*32*, *33*). The breakdown of PI(4,5)P_2 generates two products, DAG and inositol 1,4,5-trisphosphate IP_3 (*9*, *32–36*). IP_3 interacts with receptors (IP_3R) in the endoplasmic reticulum (ER) to allow for the intracellular release of Ca^{2+} stores (*9*, *136*, *137*). The depletion of the intracellular Ca^{2+} triggers the refilling of the ER via a process called store operated Ca^{2+} entry (SOCE) (*9*, *136*, *138*, *139*). In brief, this process involves the recruitment of the ER Ca^{2+} sensitive protein, STIM1, and the PM Ca^{2+} channel, Orai1, to ER-PM contact sites (*9*, *136*, *138*, *139*). The C-terminus of STIM1 directly binds to PI(4,5)P_2 and allows for the stabilization of these ER-PM contacts (*136*, *138*, *140*, *141*). Once Ca^{2+} is moved into the cytosol via STIM1 and Orai1, sarco/endoplasmic reticulum Ca^{2+}-ATPase (SERCA) pumps Ca^{2+} back into the ER to refill intracellular stores (*136*, *142–144*).

After the initial release of intracellular Ca^{2+} into the cytosol, channels in the PM open to allow for continued extracellular Ca^{2+} influx (*9*, *145*, *146*). In response to membrane

depolarization, voltage gated Ca^{2+} (Cav) channels are able to open to allow for further influx of Ca^{2+} through the PM (*146–149*). However, $PI(4,5)P_2$ is also required for the channels to open fully (*150–152*). It has been proposed that Cav channels have two different $PI(4,5)P_2$ binding sites with different affinities for $PI(4,5)P_2$ (*150*, *152*). Transient receptor potential (TRP) channels are also found in the PM and allow for influx of Ca^{2+} (*148*, *149*, *153*). TRP channels can be regulated by factors such as voltage, mechanical stimuli, pH, and temperature (*148*, *149*, *153*). These TRP channels are additionally regulated by $PI(4,5)P_2$ (*148*, *149*, *153*, *154*). Both Cav and TRP channels require $PI(4,5)P_2$ to open and allow for the influx of extracellular Ca^{2+} into the cytosol.

Upon completion of Ca^{2+} induced cellular signaling, this ion must be removed from the cytosol. This occurs through two separate processes. First, the Ca^{2+} ions can be transported to the extracellular space by pumps in the PM. Two of these include the PM Ca^{2+} ATPase (PMCA) (*155*) and the Na^+/Ca^{2+} exchanger (NCX) (*156*). PMCA is known as a low-capacity Ca^{2+} transporter and has a high affinity for this ion (*157*, *158*). PMCA only requires ATP and $PI(4,5)P_2$ to efficiently pump Ca^{2+} across the PM, against its concentration gradient (*155*). NCX exchanges three Na+ ions for one Ca^{2+} ion and it has a low affinity for Ca^{2+} but is a high-capacity transporter (*157*, *158*). Additionally, NCX function relies on the electrochemical gradient of Na^+ to pump Ca^{2+} against its concentration gradient (*157*, *158*). NCX also relies on $PI(4,5)P_2$ to pump Ca^{2+} into the extracellular space quickly and efficiently (*157*, *158*). The second route by which cells clear the cytosolic Ca^{2+} is by pumping it into the ER using the SERCA pump, as discussed above (*136*, *142–144*, *155*). Uniquely, each of these stages of intracellular Ca^{2+} regulation, from release to refilling, require $PI(4,5)P_2$.

After PLC cleavage of $PI(4,5)P_2$, the synthesis of DAG results in the activation of either classical or novel protein kinase C (PKC), which can subsequently phosphorylate a plethora of

proteins, continuing the signaling cascade (*9*, *35*, *136*, *159*). DAG itself binds to C1 domains to facilitate the recruitment of proteins (*160–163*), such as Munc13, PKC, and DAG kinase (DGK) (*160*, *164*). Munc13 is an effector protein for vesicular exocytosis and will be discussed further below. PKCs are a family of protein serine/threonine kinases (*9*, *160*, *163*). PKCs phosphorylate and activate many cellular processes ranging from Golgi function (*165*) to muscle contraction (*166*, *167*) to T cell activation (*168*). DGK is a lipid kinase which uses DAG as a substrate to produce PA (*9*, *160*). PA itself stimulates the phosphorylation of NADPH oxidase components (*169*), recruits Raf-1 to the PM for MAPK signaling (*170*), and recruits KSR1 to the PM for ERK signaling (*171*). For these reasons, $PI(4,5)P_2$ is an essential component of PLC signaling.

In addition to being cleaved by PLC, $PI(4,5)P_2$ can be further phosphorylated by the class I phosphatidylinositol 3-kinase (PI3K) (*9*). PI3K phosphorylates the 3-OH position to produce phosphatidylinositol 3,4,5-trisphosphate ($PI(3,4,5)P_3$), which acts a potent growth and survival-promoting second messenger (*172–174*). The production of $PI(3,4,5)P_3$ can result in the recruitment and subsequent activation of enzymes such as protein kinase B (PKB/AKT) and Brunton's tyrosine kinase (BTK) (*9*, *111*). PI3K signaling can trigger cellular processes which include insulin signaling (*175*) and cell migration (*176–178*). Aberrant regulation of PI3K and $PI(3,4,5)P_3$ production can lead to prolonged inflammation (*111*) or cancer (*177*, *179–181*).

GPCRs regulate most physiological processes in humans (*182–184*). GPCRs all share similar structural components: an extracellular N-terminus, seven transmembrane helices which are connected by six cytosolic loops, and an intracellular C-terminus (*182–185*). The heterotrimeric G proteins, which interact with GPCRs, function as the downstream activators (*182–184*, *186*). The Gα subunit is inactive when bound to GDP and in this inactivated state it interacts with the Gβγ subunit (*182–184*). When a GPCR binds a ligand, the trimeric Gαβγ

interacts with the cytosolically facing C-terminal tail and loops of the GPCR (*182–184*). Upon binding, the Gα subunit undergoes a confirmational change and exchanges GDP for GTP, thereby activating the Gα subunit and separating it from the Gβγ subunit, again (*182–184*). From here, both the Gα and Gβγ subunits interact with downstream partners to initiate a myriad of signaling cascades (*182–184*). Finally, Gα hydrolyzes GTP back to GDP and the cycle continues (*182–184*).

Three class A GPCRs have been shown to bind to $PI(4,5)P_2$ with high specificity, including adenosine A2A, β1 adrenergic receptor, and neurotensin receptor 1 (*187*). Furthermore, the $PI(4,5)P_2$ interacting residues of GPCRs were mapped to the cytosolic loops which link specific transmembrane helices together (*187*). Moreover, this interaction with $PI(4,5)P_2$ is responsible for coupling the GPCR to the heterotrimeric $G\alpha_s\beta\gamma$ (*187*). The binding to $PI(4,5)P_2$ stabilizes the G-coupled GPCR and stimulates GTP hydrolysis (*187*). Further work has shown that $PI(4,5)P_2$ can stabilize the oligomeric state of adenosine A2A, which may lead to a multi-output signaling complexes (*188*).

GPCR signaling can be attenuated in two different ways: 1) receptor molecules can be internalized thereby slowing or stopping further ligand binding and the resulting cell signaling (*189*) or 2) the binding to G-proteins can be inhibited (*189*). Both of these steps can be accomplished by arrestins (*189*) Arrestins bind to GPCRs and inhibit their interaction with G-proteins as well as mediate their internalization (*189*). Recent work has shown that β-arrestin interacts with neurotensin receptor 1 (*190*). Furthermore, this interaction is facilitated by a $PI(4,5)P_2$ specific interaction with the C-lobe of β-arrestin and the transmembrane cytosolic loops (*190*). Other work has expanded on this and shown that the β-arrestin GPCR complex requires $PI(4,5)P_2$ to be fully stabilized (*191*). Additionally, the β-arrestin interaction with the PM may actually increase $PI(4,5)P_2$ levels to further facilitate GPCR internalization (*192*). $PI(4,5)P_2$ is

involved in both the stabilization of the GPCR-G-protein signaling complex as well as the GPCR-β-arrestin signaling termination complex. In these ways $PI(4,5)P_2$ is absolutely essential to the entire process of GPCR signaling.

1.4.2 Transport, Trafficking, and $PI(4,5)P_2$

Ion channels allow for the rapid flux of ions across the PM and allows for electrical excitability in nervous and muscular tissue (*147*, *193*, *194*). As previously discussed, several Ca^{2+} channels are regulated by $PI(4,5)P_2$. The Cav channel is voltage gated and opens in response to changes in voltage but is further opened and stabilized by binding to $PI(4,5)P_2$ (*146–149*). TRP channels were also previously discussed as Ca^{2+} channels, however they function overall as non-selective cation channels (*148*, *149*, *153*). Again, TRP channels are regulated by many external factors, including mechanical stimulation and temperature (*148*, *149*, *153*). Furthermore, many of the TRP channel family members are regulated by $PI(4,5)P_2$ via an interaction with positively charged residues in the cytosolic regions of the channel (*148*, *149*, *153*, *154*). The TRP channels have been shown to be either positively (*149*, *195–199*) or negatively regulated by their interaction with $PI(4,5)P_2$ (*200*, *201*). The P2X class of purinergic receptors are non-selective ATP-gated cation channels (*202*, *203*). These channels are a trimeric assembly of homologous subunits and allow for the movement of Ca^{2+}, Na^+, and K^+ (*202*, *203*). There are seven individual subunits, and it has been shown that $PI(4,5)P_2$ is necessary for the regulation of all seven (*202*, *203*). Specifically, it seems that $PI(4,5)P_2$ binds to a polybasic stretch of Arg and Lys residues in the C-terminal tail of P2X (*202*, *203*).

The epithelial Na^+ channel (ENaC) is a trimeric protein composed of three different subunits, α, β, and γ, which come together to form the channel structure (*204*). Each of these

subunits has a hairpin-like structure that contains a Gating Relief of Inhibition by Proteolysis (GRIP) domain and the α and γ GRIP domains are known to gate the channel and prevent ion flow (*204*). Upon proteolysis, these GRIP domains are cleaved, and the channel opens and can allow for the movement of Na^+ (*204*). Further opening of ENaC is regulated by $PI(4,5)P_2$ (*205–207*). Specifically, increased $PI(4,5)P_2$ increases ENaC activity via increased Na+ transport and a decrease in $PI(4,5)P_2$ decreases ENaC activity (*205–207*). Furthermore, both the β and γ subunits possess several basic residues, clustered to one side of the amphipathic helices in their cytosolic tails, which mediate the specific interaction between ENaC and $PI(4,5)P_2$ (*206*, *207*).

Voltage gated K^+ (Kv) channels are tetramers made up of a transmembrane pore that is flanked by four voltage sensor domains (*146*, *194*, *208*, *209*). Following membrane depolarization, the movement of the voltage sensor domain initiates conformation changes which allow for the opening of the Kv channels (*146*, *194*, *208*, *209*). Crystallization of Kv revealed that the channel interacts with lipids in the PM (*210*, *211*) and further work went to show that the lipid is $PI(4,5)P_2$ (*212*). $PI(4,5)P_2$ specifically interacts with the voltage sensor domain and regulates its movement in response to depolarization (*212*). Inward rectifying K^+ channels (Kir) allow K^+ ions to move across the PM into the cytosolic space to establish the resting membrane potential (*213*). These channels are tetrameric and are comprised of a transmembrane domain, which is K^+ selective, and a large cytosolic domain (*210*, *211*, *214–222*). It has been shown that all Kir channels are activated by $PI(4,5)P_2$ and this specific interaction has been mapped to Arg and Lys residues in the transmembrane helices and in the cytosolic domain (*210*, *211*, *214–222*). The binding to $PI(4,5)P_2$ both initiates and stabilizes an interaction between the cytosolic domain and the transmembrane domain which allows for the channel to open (*210*, *211*, *214–222*).

Cells also utilize active transport for the movement of ions. As previously discussed, PMCA and NCX are involved in transporting Ca^{2+} ions to the extracellular space (*155*, *156*). Both PMCA and NCX pump Ca^{2+} across the PM, against its concentration gradient, and both require ATP and $PI(4,5)P_2$ to do so (*156–158*). While PMCA functions to move only Ca^{2+}, NCX exchanges three Na^+ ions for one Ca^{2+} ion (*157*, *158*). There are two similar pumps that are responsible for further movement of Na^+ from the extracellular space to the intracellular space in exchange for other cations (*158*). First is the Na^+/H^+ exchanger (NHE) and second is a Na^+/Mg^{2+} exchanger of unknown identity (*158*). Both the NHE (*223*, *224*) and the Na^+/Mg^{2+} exchanger of unknown identity (*225*) require $PI(4,5)P_2$ to function for active cation transport. In the case of many ion transporters, passive or active and voltage-gated or not, $PI(4,5)P_2$ is an important regulator.

Intracellular trafficking of more than ions also requires $PI(4,5)P_2$ to recruit proteins to the PM for the initiation and regulation of both exo- and endocytosis (*9*, *226–228*). Exocytosis is a highly regulated process that leads to the release of intracellular components through the PM to the extracellular space (*226–229*). The three basic steps for exocytosis are vesicular docking, priming, and fusion (*229*). Docking involves the recruitment of vesicles and their tethering to the inner leaflet of the PM (*229*). The exocyst complex of proteins is essential for this tethering process of vesicles to the soluble N-ethylmaleimide-sensitive factor attachment protein receptors (SNAREs) (*230*, *231*). The exocyst complex is comprised of two independent subcomplexes; subcomplex-1 is made up of Exoc1-4 and subcomplex-2 is made up of Exoc5-8. A majority of the exocyst complex is present on the vesicular surface, and when in proximity to the PM this complex interacts with Exoc1 (Sec3 in yeast) to form the full exocyst complex (*230*). Exoc1 interacts with the PM initially due to an interaction with $PI(4,5)P_2$ and a PM anchored SNARE protein (*230–*

232). After this initial interaction, another exocyst protein, Exoc7 (Exo70 in yeast), is now able to interact with PI(4,5)P_2 at the PM as well, stabilizing the interaction of the vesicle with the PM and inducing membrane curvature (*229–231*). The next step, priming, is responsible for the maturation of PM tethered vesicles (*229*). Munc13 and Ca^{2+}-dependent activator protein for secretion (CAPS) are both required for the transition between docking and priming of vesicles (*229*, *231*). Specifically, Munc13 and CAPS are involved in the formation and stabilization of the SNARE complex once they are localized with the PM (*229*, *231*). Munc13 is recruited to the PM in a Ca^{2+} dependent manner, but once at the PM it interacts with and is stabilized by PI(4,5)P_2 (*229*, *231*, *233*, *234*). CAPS contains a PI(4,5)P_2 binding PH domain which allows for its recruitment to the PM (*229*, *231*, *233*, *235*). Finally, fusion allows for the vesicle to merge with the PM to release contents (*229*, *231*). Components of the SNARE complex include syntaxin-1 and synaptosomal-association protein of 25 kDa (SNAP-25). Syntaxin-1 is a transmembrane (TM) protein localized to the PM due to a hydrophobic C-terminal domain (*229*, *231*, *236*, *237*). SNAP-25, on the other hand, initially localizes with the PM due to a palmitoylation motif (*229*, *231*, *236*). Moreover, SNAP-25 has a polybasic stretch which is involved in stabilizing the interaction with PI(4,5)P_2 and other negatively charged phospholipids at the PM (*4*, *237*, *238*). Moreover, the loss of PI(4,5)P_2 at the PM results in dysregulation of exocytosis, hindering this process at all steps (*154*, *228*, *239–241*).

Opposite of exocytosis, endocytosis is the process of moving cargo from the extracellular surface into the interior of the cell (*226*, *227*). Clathrin-mediated endocytosis (CME) is the best characterized mechanism of endocytosis (*226*, *227*, *229*, *242*). The recruitment of clathrin to the PM is an essential step of CME; clathrin assembles into structures at the PM upon interaction with adaptor proteins (*242*, *243*). These adaptors include the AP-2 complex, Epsin, AP180, and

dynamin (*226*, *242*, *243*). Initially, AP-2 binds with PI(4,5)P_2 at the PM, after which clathrin is then recruited to initiate the formation of clathrin-labeled structures (*226*, *242–245*). After the initial formation of these AP-2 and clathrin labeled structures, AP180 and epsin are recruited to the PM to interact with AP-2, clathrin, and PI(4,5)P_2 to facilitate the further concentration of clathrin on the PM (*246*, *247*). The next stage of CME is invagination, and this is initiated by the Bin / amphiphysin / Rvs (BAR) domain containing proteins which induce curvature in the PM (*226*, *242*, *243*). Specifically, FCHo1/2 are BAR domain containing proteins that are recruited exclusively to the PM and initiate curvature in an AP-2, clathrin, and PI(4,5)P_2 dependent manner (*248*, *249*). Finally, the clathrin-coated pit can be separated from the PM via the constriction of the neck due to the action of dynamin (*226*, *242*, *243*). In this final stage of endocytosis, dynamin is recruited to the PM due its interaction with PI(4,5)P_2 (*250*). Loss of PI(4,5)P_2 hinders the ability for endocytosis to occur, again demonstrating the importance of this lipid in essential cellular processes (*154*, *228*, *239–241*).

1.4.3 Cytoskeletal organization and PI(4,5)P_2

The actin cytoskeleton regulates cellular processes ranging from endocytosis to cell motility to cytokinesis (*251*, *252*). Furthermore, the actin cytoskeleton undergoes many changes during these various activities (*251*, *252*). These cytoskeletal changes include actin filament assembly / disassembly, membrane association, and cell adhesion (*251*, *252*).

Actin filaments can be capped, at barbed ends, by the capping protein CapZ (*253–255*) to prevent both actin assembly and disassembly (*251*, *252*). CapZ can be removed from actin filaments due to an interaction with PI(4,5)P_2, thus allowing for either actin assembly or disassembly to occur, specifically at the PM (*253–255*). During endocytosis, the neuronal Wiskot-

Aldrich Syndrome protein (N-WASP) is recruited to the PM via an electrostatic interaction between the negatively charged inner leaflet, due in part to $PI(4,5)P_2$ (*4*), and a polybasic domain in N-WASP (*256*). Once localized at the PM, N-WASP activates the Actin related protein 2/3 (Arp2/3) complex (*257*, *258*). Upon activation, Arp2/3 is then able to nucleate new daughter filaments off of existing mother filaments to facilitate branching of actin, a necessary step for the endocytic process (*251*, *259*, *260*). Another protein involved in actin filament dynamics is profilin (*251*, *252*). In situations of low cellular $PI(4,5)P_2$, profilin is found bound to ATP-bound actin monomers, promoting actin nucleation (*261*, *262*). Profilin also binds to and regulates other actin-binding proteins, including Arp2/3, formins, and the Ena/VASP proteins. In this way profilin acts to assist in actin nucleation and F-actin assembly (*251*, *252*, *263*). In cases of high $PI(4,5)P_2$, profilin is recruited to the PM due to an interaction with $PI(4,5)P_2$, sequestering it away from monomeric actin (*261*, *262*). This interaction then negatively regulates the actin assembly. Finally, two proteins, gelsolin and cofilin act as actin severing or depolymerizing proteins (*251*, *252*). Again, the localization and therefore activity of both gelsolin (*264–266*) and cofilin (*267–269*) are regulated by $PI(4,5)P_2$. It is through these interactions that $PI(4,5)P_2$ can regulate both actin filament assembly and disassembly.

The actin cytoskeleton is linked to the PM due to interactions with several proteins (*251*, *252*). One such protein family involved in linking actin and microtubules to the PM are septins (*252*, *270*). Septins have been shown to interact with $PI(4,5)P_2$ via a polybasic domain that is separate from the actin / microtubule binding N-terminal domains (*270*, *271*). Spectrins are another family of proteins which similarly interact with actin and the PM (*251*, *252*). Specifically, β-spectrins contain a PH domain which has been shown in interact with $PI(4,5)P_2$, allowing for PM association (*272–274*). Furthermore, recent evidence suggests that both septins and spectrins may

be able to form $PI(4,5)P_2$ diffusion barriers; this essentially forms lipid corrals to limit lipid diffusion, potentially promoting further $PI(4,5)P_2$ linkage by both proteins (*275*). Finally, the ezrin, radixin, moesin family of (ERM) proteins function to link the actin cytoskeleton directly to the PM. The ERM proteins all contain a FERM domain, which has been shown to bind to $PI(4,5)P_2$ (*276–279*). The binding of the FERM domain to $PI(4,5)P_2$ allows for the unmasking of other binding sites in the ERM proteins which allow them to interact with other proteins of interest, such as F-actin or intracellular adhesion molecules (ICAMs) (*276–279*). These specific interactions only begin to highlight some of the mechanisms by which $PI(4,5)P_2$ regulates the linkage between actin and the PM.

Cellular adhesion to the extracellular matrix (ECM) is a pivotal functionality. Focal adhesions (FAs) are made up of a complex network of proteins that link the actin cytoskeleton to the ECM. The physical interaction with the ECM is facilitated by the extracellular portion of integrins (*280*). The intracellular portion of integrins then generates the integrin signaling layer (*280*). This layer contains integrins, paxillin, focal adhesion kinase (FAK), and talin (*280*). The force transduction layer is composed of talin, VASP, and vinculin (*280*). And finally, the actin regulatory layer is made up of VASP and α-actinin. Each of these layers contains at least one $PI(4,5)P_2$ interacting protein: FAK (*280–282*), talin (*276*, *277*, *283–285*), vinculin (*283*, *286–289*), and α-actinin (*286*). $PI(4,5)P_2$ is known to function, directly or indirectly, as either an activator or a stabilizer for each of these proteins in each layer of the FA. Aberrant $PI(4,5)P_2$ levels can lead to many changes in the organization or regulation of the actin cytoskeleton (*65*, *73*, *290–293*), again this exemplifies the importance of proper maintenance of $PI(4,5)P_2$ in cells. Furthermore, mutations in enzymes regulating these lipid-signaling pathways can lead to aberrant regulation of

the previously mentioned cellular processes and can lead to diseases, ranging from neurodegeneration to cancer (*8*).

1.5 Summary

In summary, we reviewed the following: $PI(4,5)P_2$ is generated in the inner leaflet of the plasma membrane by PIP4K and PIP5K, $PI(4,5)P_2$ serves as substrate for new PPIns or metabolites function as second messengers, and the vital function in regulating key cellular processes, from signaling to intracellular transport to cytoskeletal dynamics. At the core of every essential cellular mechanism lies the correct mass of $PI(4,5)P_2$ molecules to control the fate of cells, tissues, and organs. Tightly controlling such a key coordinator requires the ability to sense, upregulate, and downregulate its production to meet cellular demands. While this crucial fact is known and widely respected, the mechanism by which the cells regulate $PI(4,5)P_2$ has remained elusive. Throughout the course of these studies, we aim to demonstrate that the enzymes necessary for $PI(4,5)P_2$ production – PIP4K and PIP5K – cooperate in a beautifully orchestrated fashion to sense and regulate levels of $PI(4,5)P_2$ in order to maintain homeostasis and change $PI(4,5)P_2$ levels in response to physiological cues. In doing so, we propose a mechanism that can be interrogated and perturbed to adjust $PI(4,5)P_2$ levels, alter cellular processes, and effect disease progression.

2.0 Lipid detection and metabolism

This text has been pulled from a combination of reviews accepted by Molecular Biology of the Cell and book chapters published in Phosphoinositides, Methods and Protocols by Springer Protocols:

R.C. Wills, B.D. Goulden & G.R.V. Hammond. Genetically encoded lipid biosensors. *Mol Biol Cell* **29**, 1526–1532 (2018).

G.R.V. Hammond, M.M.C. Ricci, C.C. Weckerly, & R.C. Wills. An update on genetically encoded lipid biosensors. *Mol Biol Cell* **33**, tp2 (2022).

R.C. Wills, J. Pacheco, G.R.V. Hammond. Quantification of Genetically Encoded Lipid Biosensors. New York (NY): Springer Nature. Ch 4. (2021).

J. Pacheco, R.C. Wills, G.R.V. Hammond. Induced Dimerization Tools to Deplete Specific Phosphatidylinositol Phosphates New York (NY): Springer Nature. Ch 7. (2021).

Additionally, work on the $PI(3,4)P_2$ biosensor was published in the Journal of Cell Biology by previous Hammond Lab Member, Brady Goulden.

B.D. Goulden, J. Pacheco, A. Dull, J.P. Zewe, A. Deiters, G.R.V. Hammond. A high-avidity biosensor reveals plasma membrane $PI(3,4)P_2$ is predominantly a class I PI3K signaling product. *J Cell Biology* **218**, 1066–1079 (2019).

2.1 Overview

Lipids convey both structural and functional properties to eukaryotic membranes. Understanding the basic lipid composition and the dynamics of these important molecules, in the context of cellular membranes, can shed light on signaling, metabolism, trafficking, and even membrane identity. The development of genetically encoded lipid biosensors has allowed for the visualization of specific lipids inside individual, living cells. However, several caveats and considerations have emerged with the overexpression of these biosensors. Here, we provide a current list of available genetically encoded lipid biosensors. These tools are given along with criteria that are used to determine their reliability. We also provide some suggestions for the optimal utilization of these biosensors when both designing experiments and interpreting results.

2.2 Introduction

2.2.1 Phospholipids

Lipids are a central molecule in cellular biology and serve critical roles in energy storage, cellular membrane formation, and messengers for cellular activities (*131*). There are a variety of lipid species which provide discrete and functional properties to membranes (*126*, *131*). Phosphatidylinositol (PI) is a unique phospholipid possessing a *myo*-inositol headgroup which can be reversibly phosphorylated in up to three different positions, generating seven distinct phosphoinositides (PPIns) (*9*). The specific lipid makeup of membranes provides unique identities to various organelles, and this results in exquisite spatial and temporal regulation of cellular

processes (*4*, *9*). Understanding the cellular distribution and metabolism of various lipids has become a major focus of cellular biology (*8*). Mutations or expression differences in enzymes regulating these lipid-signaling pathways can lead to several diseases, such as neurodegeneration, cancer, diabetes, and others (*8*). As a result, there is an increased prevalence in methods aiming to quantify lipid levels and impact their metabolism (*9*, *121–125*).

2.2.2 Detection of lipids in cells

Historically, lipid species have been detected and quantified in cells using several labor-intensive methodologies, such as: mass spectroscopy (MS) (*57*, *294*, *295*), high-performance liquid chromatography (HPLC) (*296*), and thin-layer chromatography (TLC) (*297–299*). However, these measurements were obtained from a population of cells at a single time point, and therefore do not provide dynamic, temporal information. Microscopy techniques, on the other hand, allow for the real-time visualization of lipid dynamics. These approaches include total internal fluorescence microscopy (TIRFM), confocal microscopy, and super resolution imaging techniques. Additionally, microscopy allows for the observation of single cell dynamics over time, thus providing both spatial and temporal resolution (*122*).

2.2.3 Genetically encoded lipid biosensors

Using microscopy to visualize lipids presents a set of unique challenges. Proteins can be detected in cells using specific antibodies in immunocytochemistry or immunofluorescent assays. However, using antibodies for the labeling and detection of lipid species is challenging as typical protocols necessitate the fixation and permeabilization, or overall breakdown, of the lipid

containing membranes of interest (*109*). Proteins can also be detected by generating fusions with fluorescent proteins, such as GFP or mCherry (*123*, *125*, *300–303*). Fusing a lipid with a fluorophore has not provided an ultimate solution as there are still some issues with this method. But a unique approach has proven effective in the visualization of lipids. Some proteins possess specialized lipid-binding domains, known to associate with their cognate lipids (*302–304*). Additionally, bacterial effector proteins and toxins, namely those that target host membranes, have also proven to be efficient at binding unique lipid species (*304*). These proteins can be expressed as fluorescently conjugated fusions in living ces to allow for the visualization of specific lipids (**Figure 2.1A**). These fusion proteins have been termed biosensors, and this chapter will focus on qualitatively and quantitatively observing lipids via genetically encoded lipid biosensors.

2.3 Results

2.3.1 Genetically encoded biosensor visualization

The use of biosensors allows for the visualization of lipids in living cells and in real time. However, biosensors are not to be used as a binary means of determining lipid localization or definitive lipid amounts. Our group has developed three crucial criteria which should be considered when determining the validity of a biosensor (*123*). First, is the biosensor specific for the target lipid? Second, is the localization of the biosensor dependent on that lipid? Third, if dependent, is the lipid alone sufficient to localize the biosensor? **Table 2.1** provides a list of lipid-binding domains and illustrates whether each sensor meets the previously mentioned criteria.

Table 2.1 has been used as a guide for selecting appropriate biosensors for specific lipids, and we utilized this table to select the appropriate biosensors throughout this work.

The method of performing these biosensor experiments involves the transfection of plasmid DNA, containing the biosensor of interest, into cells. Living cells can then be visualized in real-time to determine the quiescent localization of lipids or, lipid levels can be perturbed using enzymes, growth factors, or other chemical treatments to mimic an array of cellular processes. To illustrate this point, we can express either GFP, PH-PLCδ1, or P4M, in HeLa cells to visualize the difference in localization of the fluorescent tag or biosensors (**Figure 2.1B**). GFP appears localized throughout the cytosol of the cell, as expected (**Figure 2.1B**). This is in stark contrast to the expression of the $PI(4,5)P_2$ biosensor PH-PLCδ1, which appears tightly localized with the PM (**Figure 2.1B**). Finally, the PI4P biosensor, P4M, can be seen at the PM, the Golgi, and endosomes (**Figure 2.1B**). This demonstrates how the localization of different lipid species can differentially localize the appropriate biosensor.

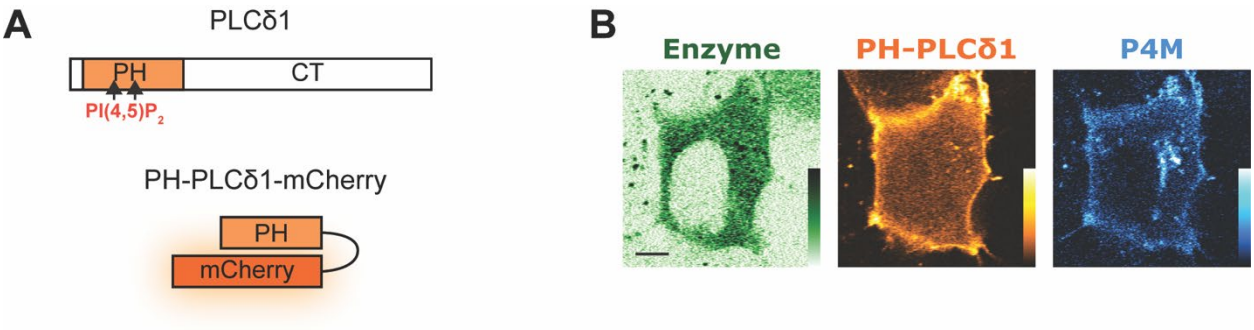

Figure 2.1 Genetically encoded lipid biosensors localize with specific organelle membranes.

(**A**) Domain structure of full-length PLCδ1 protein, along with the mCherry-PH domain from PLCδ1. (**B**) Confocal sections of cells expressing enzyme (green), PH-PLCδ1 (orange), and P4M (cyan), scale bar is 10 μm.

2.3.2 Quantification of biosensors in cells

The use and visualization of lipid biosensors via microscopy provides a real-time single-cell approach to monitor changes in fluorescence intensity. Images themselves are not able to be used as statistical data, but that does not mean the images cannot be used to obtain this type of quantitative data. The relative fluorescence intensity of a biosensor at a specific membrane directly corresponds to the amount of sensor bound and can indicate the relative amount of lipid in an organelle. For example, using a $PI(4,5)P_2$ probe would result in a high level of fluorescence at the plasma membrane (PM), visualized by either TIRFM or confocal microcopy (**Figure 2.2A**). Using tools (see below) to deplete $PI(4,5)P_2$ levels would result in a much lower membrane-associated fluorescence. The quantification of fluorescent images has been done in several ways. Our lab performs analysis on data collected from TIRFM and from confocal microscopy. TIRFM is a particularly efficient method of measuring changes in lipid level at the PM due to selective illumination of the bottom most ~100 nm of the cell. Confocal microscopy has been utilized for assaying lipid levels at various membrane compartments, including the PM. For TIRFM analysis, the fluorescence intensity is measured within the cell over time, and then the average pixel intensity of each frame is normalized to the average pixel intensity before treatment (F_t/F_{pre}) (**Figure 2.2A**). For confocal microscopy, the organelle of interest is used to generate a mask in which the biosensor intensity can be measured (**Figure 2.2B**). Once the mask is generated, the biosensor pixel intensity is measured in the mask relative to the intensity in the rest of a region of interest (ROI) that encompasses the whole cell, giving an organelle/cell ratio. Similarly, this can be done by measuring the intensity within the mask relative to a secondary ROI drawn in the cytoplasm yielding an organelle/cytosol ratio (**Figure 2.2C**).

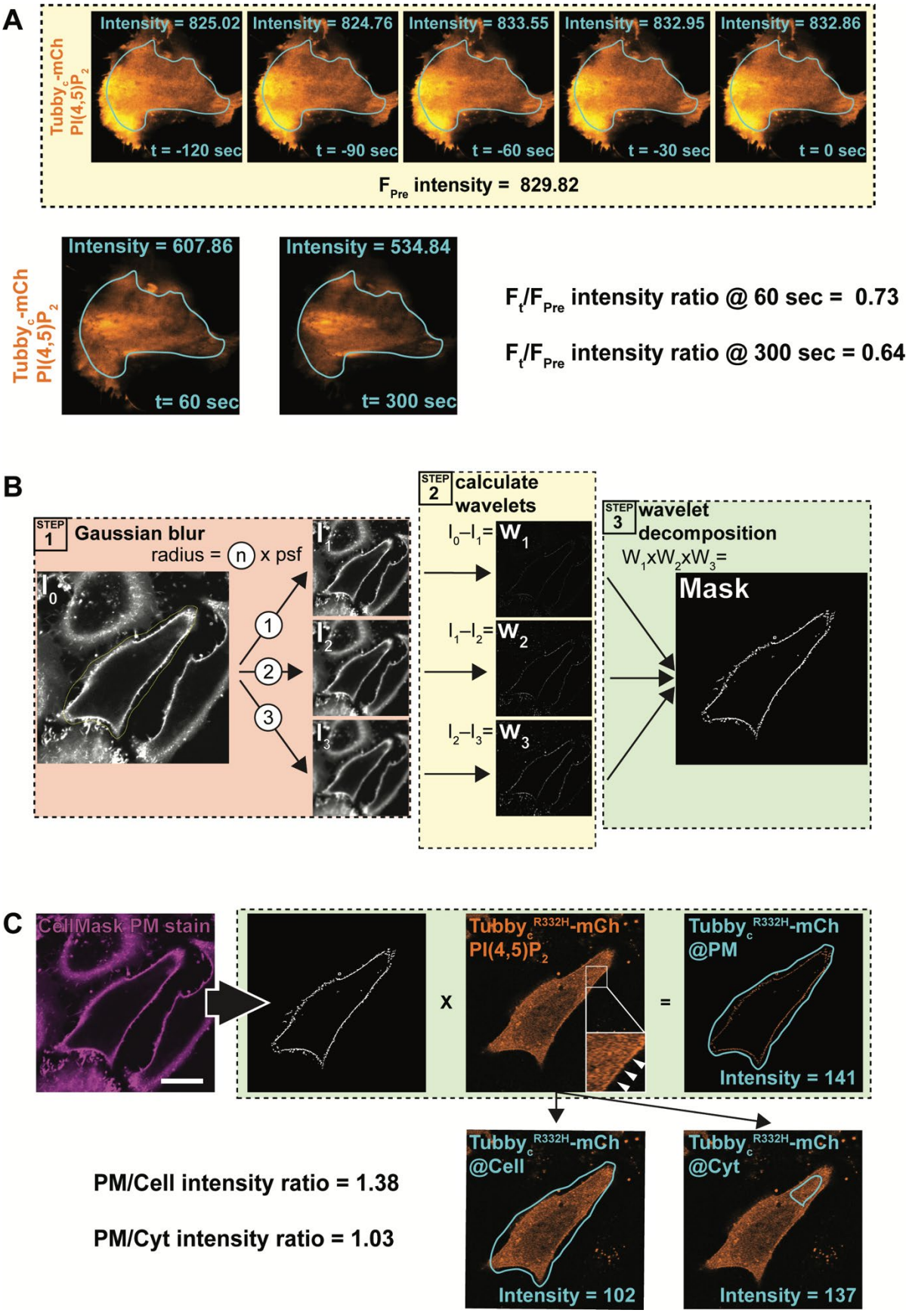
A
Tubby$_c$-mCh PI(4,5)P$_2$
Intensity = 825.02
t = -120 sec
Intensity = 824.76
t = -90 sec
Intensity = 833.55
t = -60 sec
Intensity = 832.95
t = -30 sec
Intensity = 832.86
t = 0 sec
F$_{Pre}$ intensity = 829.82
Intensity = 607.86
t= 60 sec
Intensity = 534.84
t= 300 sec
F$_t$/F$_{Pre}$ intensity ratio @ 60 sec = 0.73
F$_t$/F$_{Pre}$ intensity ratio @ 300 sec = 0.64
B
STEP 1 Gaussian blur
radius = n x psf
I$_0$
I$_1$
I$_2$
I$_3$
STEP 2 calculate wavelets
I$_0$–I$_1$= W$_1$
I$_1$–I$_2$= W$_2$
I$_2$–I$_3$= W$_3$
STEP 3 wavelet decomposition
W$_1$xW$_2$xW$_3$=
Mask
C
CellMask PM stain
X
Tubby$_c^{R332H}$-mCh PI(4,5)P$_2$
=
Tubby$_c^{R332H}$-mCh @PM
Intensity = 141
Tubby$_c^{R332H}$-mCh @Cell
Intensity = 102
Tubby$_c^{R332H}$-mCh @Cyt
Intensity = 137
PM/Cell intensity ratio = 1.38
PM/Cyt intensity ratio = 1.03

Figure 2.2 TIRF and confocal microscopy image analysis.

(**A**) Analysis of PI(4,5)P_2 biosensor in TIRF microscopy. The fluorescence intensity is measured in the first five frames before the addition of rapamycin to recruit a PI(4,5)P_2 degrading enzyme. The resulting intensity is averaged and generates F_{Pre}. The subsequent images (here t=60 and 300 sec) have their fluorescence intensity measured. These time points can be compared (as a ratio) to the baseline fluorescence as F_t/F_{Pre}. (**B**) Generation of a binary PM mask. Step 1 illustrates a ROI applied to the original image (I0). Images I1–I3 have had the Gaussian blur filter applied at increasing radii (In x pfs). Step 2 shows the generation of thresholded wavelets (W1–W3) from each pair of smoothed (I0–I3) images. Step three shows the final wavelet decomposition to generate the binary mask with the background cleared to reduce noise. (**C**) Analysis of PI(4,5)P_2 biosensor distribution with the aid of a binary mask. A PM stain, CellMask deep red, is used to generate a mask of the PM signal, as shown in Fig. 1. The cell is also expressing a low-affinity PI(4,5)P_2 biosensor, $Tubby_C^{R332H}$. This low-affinity biosensor is barely enriched at the PM (see inset in $Tubby_C^{R332H}$ image). Applying the binary mask allows the intensity of the biosensor to be easily measured at the PM and compared (as an intensity ratio) with the average intensity across the whole cell's optical section, or else a region of cytosol (Cyt).

2.3.3 Manipulation of lipids and biosensor readouts

2.3.3.1 Chemical dimerization

Dissecting PPIn function requires either traditional molecular genetic tools to manipulate protein expression of lipid metabolizing enzymes or modulating the lipids themselves in a chemically driven capacity (**Appendix Table 1.2**). Both approaches have proven challenging. PPIns can be sequestered by overexpressing PPIn-binding proteins, though this is often harder than typically realized (*305*). Alternatively, enzymes that synthesize or degrade the lipids can be overexpressed or knocked-down, though this causes chronic effects over several hours. Chemically induced dimerization (CID) approaches (and the more recent photoinduced dimerization) provide a powerful approach to induce rapid removal of lipids from precise intracellular locations, allowing

acute effects on downstream biology to be interrogated (*306*, *307*). In this chapter, we describe such an approach using the FKBP/FRB rapamycin inducible dimerization system.

2.3.3.2 FKBP-FRB

The origins of chemical dimerization systems come from pioneering work from Dr. Crabtree and colleagues, who rationalized that several receptors at the PM are activated when forming dimers. Crabtree's group successfully activated T-cell signaling by forcing dimer formation of cytosolic portions of T-cell receptors fused to FKBP12, an immunophilin that binds immunosuppressant drugs such as cyclosporine A (CsA), rapamycin, or FK506 (which gave the name to these receptors: FK506-Binding Protein) (*308*). The extended use of immunophilins as a heterodimerization system was adopted thanks to Schreiber's work, which showed that FKBP12 interacts with a minimal portion of the mechanistic Target of Rapamycin (mTOR), called FKBP12 Rapamycin-Binding (FRB) domain (*309*). The use of the FRB domain as an FKBP partner presented a major improvement in comparison with previous systems. FRB-tagged membrane anchors such as Giantin^{C129} (Golgi), LAMP1 (endolysosomes), AKAP^{N31} (mitochondria) (**Figure 2.3A**), or the myristoylated and palmitoylated peptide from Lyn kinase, Lyn$_{11}$ (PM) (**Figure 2.3B**) allow for the labeling of the associated organelles. The main advantages are the size since FRB comprises only 90 amino acid residues and 11 kDa instead of 2549 amino acid residues and 289 kDa of the whole human mTOR (*309*). FRB also binds FKBP12 with nanomolar binding affinity when rapamycin is used as a dimerizing agent. FRB and FKBP12 do not interact in the absence of rapamycin, and FRB shows a modest interaction with rapamycin by itself (K_d ~26 μM) (*310*). Therefore, labeling an organelle with FRB and an enzyme with FKBP allows for the recruitment of that enzyme to that specific cellular location (**Figure 2.3B**).

2.3.3.3 Rapamycin induced dimerization

While many ligands can be used to induce dimerization, several key positive attributes should be considered: high permeability, low molecular weight, high affinity, high specificity, and minimal secondary effects. Selection of the best ligand must be based on the experimental design to contrast the advantages and disadvantages of available drugs. For example, rapamycin is the most used compound for experiments on live cells with measurable effects in short periods of time (*311*). It should be noted that rapamycin is a potent inhibitor of mTOR (*312*). The inhibition of mTOR can result in the loss of the ability to sense cellular stress or to carry out cell growth and associated signaling (*312*). Many of these pathways are downstream of $PI(4,5)P_2$ and the use of rapamycin should be performed in the shortest time frame possible. **Figure 2.3B** shows the rapamycin induced recruitment of FKBP to the previously mentioned FRB-tethered organelles of interest.

2.3.3.4 Acute lipid manipulation

Generally speaking, acute lipid metabolism uses a dimerization system to target localization of a phosphatase to deplete a specific pool of PPIns. A PM-bound recruiter carrying an FRB domain (Lyn_{11}) is used to target the enzyme fused with the FKBP domain, here FKBP-INPP5E. Simultaneously, a lipid-binding domain fused to a fluorescent protein can be used to observe how lipid levels change at the specific cellular location. A prototypical protocol of depletion of $PI(4,5)P_2$ from the PM is described here. We observe rapid recruitment of FKBP-INPP5E from the cytosol to the PM, upon rapamycin addition (**Figure 2.3B**). Subsequently, we can observe the localization of the $PI(4,5)P_2$ biosensor PH-PLCδ1 from the PM to the cytosol (**Figure 2.3B**). Ultimately, lipid biosensors, enzymes, and membrane recruiters are interchangeable according to the experimenter's scope (**Table 2.1 and Appendix Table 1.2**).

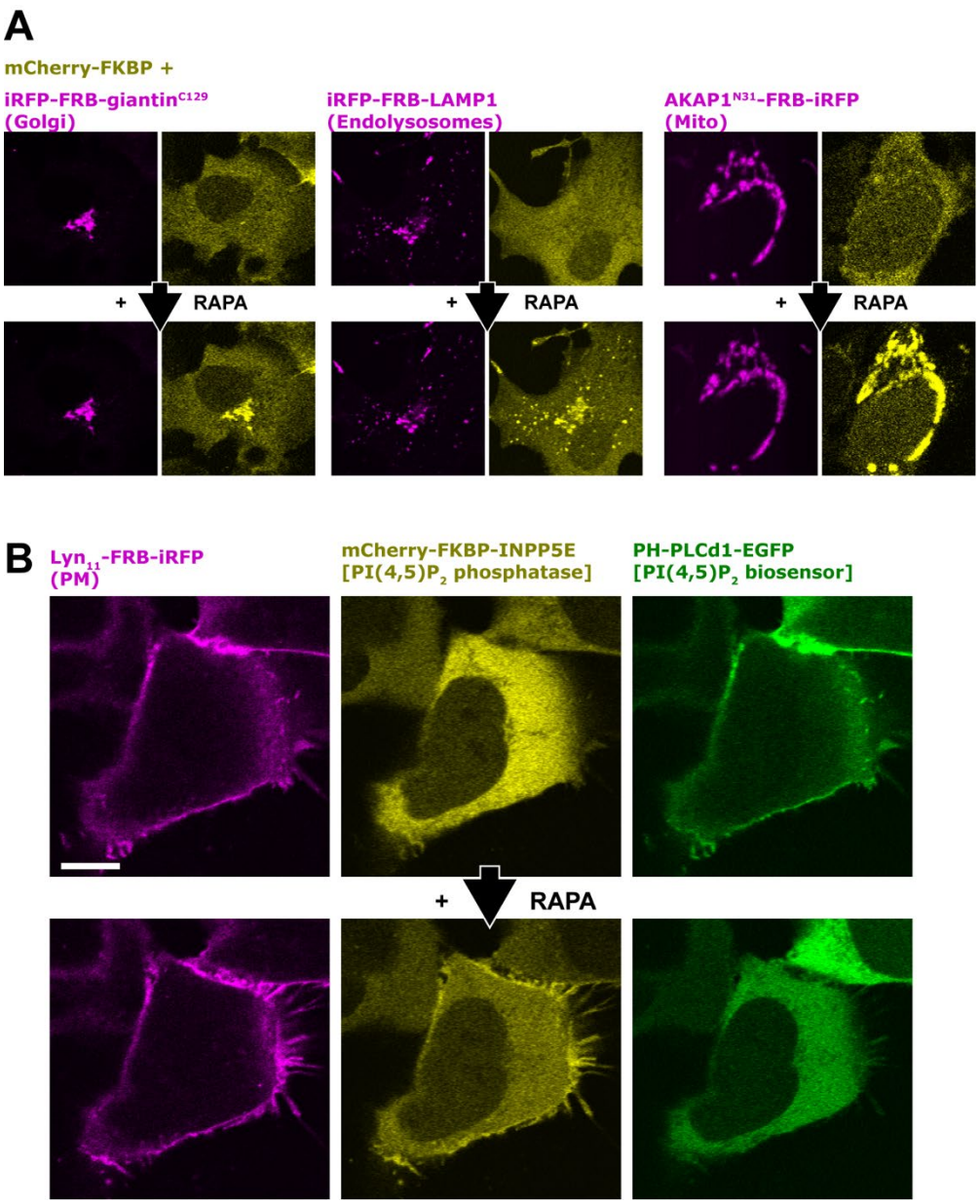

Figure 2.3 Target localization at different cellular compartments.

(**A**) Targeted recruitment of chimeric phosphatase PJ-Sac to specific subcellular localization. Giantin, Lamp1, and AKAP1 are membrane anchor proteins that target localization to the Golgi apparatus, lysosomes, and mitochondria, respectively. (**B**) Localized depletion of PI(4,5)P_2 from the PM after addition of rapamycin. Lyn$_{11}$-FRB-iRFP is used to drag the phosphatase INPP5E to the PM. Acute depletion of PI(4,5)P_2 is registered simultaneously with the biosensor PH-PLCδ1-GFP, scale bar is 10 μm.

2.3.4 Low or High affinity/avidity

Lipid binding proteins can have specific affinities for either individual or multiple lipid species (*304*, *313–315*). In the case of P4M, a specific PI4P biosensor, the localization of this sensor specifically indicates the presence of PI4P (*304*). Tubby$_C$ is readily used as a PI(4,5)P_2 biosensor but, Tubby$_C$ also binds to PI(3,4)P_2 and PI(3,4,5)P_3 (*315–317*). However, the cellular concentration of PI(4,5)P_2 is by far the highest of the three, so any changes seen in Tubby$_C$ localization are the result of changes in PI(4,5)P_2 levels, compared with the other two lipids (*99*, *100*).

Furthermore, biosensors can have modifications made to their lipid binding domains, generating sensors with higher or lower lipid binding affinity. The mutation of a single residue in Tubby$_C$, to generate Tubby$_C^{R332H}$, lowers the affinity of this probe for PI(4,5)P_2 (*316*). When deciding when to use a high or a low affinity probe, a few considerations can be taken. High-affinity probes can be used to detect low concentrations of lipid. However, if a majority of the biosensor is already bound to a potentially abundant lipid, then further increases in the lipid will be much more difficult to observe. Low-affinity probes are very useful to use when assaying small increases in lipid levels, as they exist in complex with their lipid of interest for much shorter periods of time. At the same time, this renders these probes less useful when observing and quantifying decreases in lipid species at organelles of interest.

To illustrate these examples the high- and low-affinity probes for PI(4,5)P_2, Tubby$_C$ and Tubby$_C^{R332H}$ (*316*) were used to detect acute perturbations in lipid levels (**Figure 2.4A**). To increase PI(4,5)P_2 levels at the PM we utilized a recruitable mutant of PIP5K1C. To this effect, we generated a truncation of PIP5K1C which contained only the kinase domain as a homodimeric mutant PIP5K1C_Kina$^{D101R/R304D}$ (PIP5K1C-HD) (*70*). Using the CID system, we recruited

PIP5K1C-HD to the PM and, with confocal, observed a slight increase in PM association of $Tubby_C$ and an even more robust increase in $Tubby_C^{R332H}$, over time (**Figure 2.4A**). In an alternative approach we used the CID system to recruit INPP5E to the PM. Again, using confocal microscopy, we observed a rapid loss of the $PI(4,5)P_2$ biosensors upon recruitment of INPP5E (**Figure 2.4B**). However, the loss of $Tubby_C$, fluorescence was more robust than that of its low-affinity counterpart (**Figure 2.4B**).

Like affinity, avidity of biosensors can also be altered by generating monomers (TAPP1 cPHx1) or multimers (TAPP1 cPHx3) to alter the binding potential of a sensor (*318*). The monomeric TAPP1 cPHx1 shows negligible localization with the PM (**Figure 2.4C,** adapted from (*318*)). However, a tandem dimer and trimer each show increasing PM association, due to their increased avidity (**Figure 2.4C,** adapted from (*318*)). Overall, these binding affinities and avidities result in transient, yet quantifiable, binding profiles. Furthermore, our lab often employs both high- and low-affinity or avidity biosensors dependent on the lipid species being studied and the assay being performed.

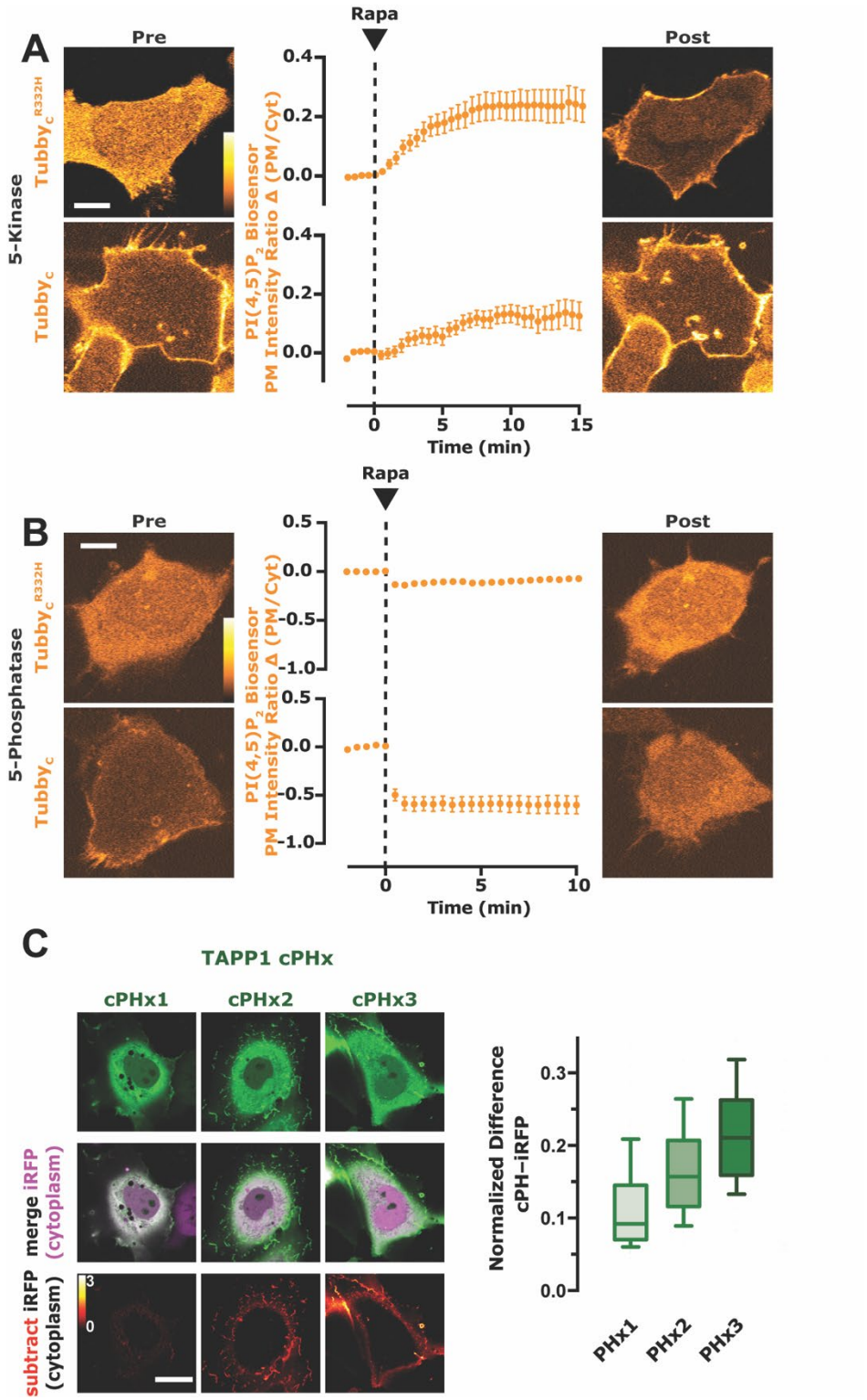

Figure 2.4 Go high or go low (affinity and avidity).

(**A** and **B**) These HEK293A cells are expressing either a low affinity (Tubby$_C^{R332H}$, top) or a high affinity (Tubby$_C$, bottom) version of a PI(4,5)P_2 biosensor. The images show the cells before and after activation of a (**A**) 5-kinase that

increases PI(4,5)P_2 in the plasma membrane or a (**B**) 5-phosphatase that decreases PI(4,5)P_2 in the plasma membrane. (**A**) The lower affinity biosensor is able to detect small changes in PI(4,5)P_2 synthesis and relocalize to the PM, whereas the higher affinity probe is already saturated at the plasma membrane. (**B**) The higher affinity biosensor is able to detect greater changes in PI(4,5)P_2 depletion and relocalize to the cytosol, whereas the lower affinity probe is already primarily localized in the cytosol. Scale bar for **A** and **B** is 10 μm. (**C**) cPHx2 and cPHx3 bind the PM in a PI(3,4)P_2-dependent manner in COS-7 grown in 10% serum. Confocal sections are shown of cells expressing EGFP-cPH plasmids and iRFP to mark the cytoplasm. Subtracting normalized iRFP signal from normalized EGFP reveals PM localization of cPHx2 and cPHx3. Scale bar is 20 μm. The box and whisker plots show median, interquartile range, and 10th–90th percentiles of 90–93 cells from three independent experiments, scale bar is 10 μm.

2.3.5 Treachery of images

User beware: increases in biosensor fluorescence do not always indicate that there is an increase in lipid. Cells expressing P4C show biosensor localization primarily at the Golgi and the PM (**Figure 2.5A**). Depletion of PM PI4P results in the loss of PM biosensor localization and the appearance of endosomal localization of the probe (*305*). This could be interpreted as the production of PI4P on the endosomal compartment (**Figure 2.5B**), however this observation is due only to the redistribution of the P4C sensor, which is now free to detect a smaller pool of PI4P, present on endosomes (*305*). The use of biosensors for the detection and observation of lipids presents various caveats (*123*). Utilizing this knowledge and **Table 2.1**, the best biosensor can be used for the experiment of interest.

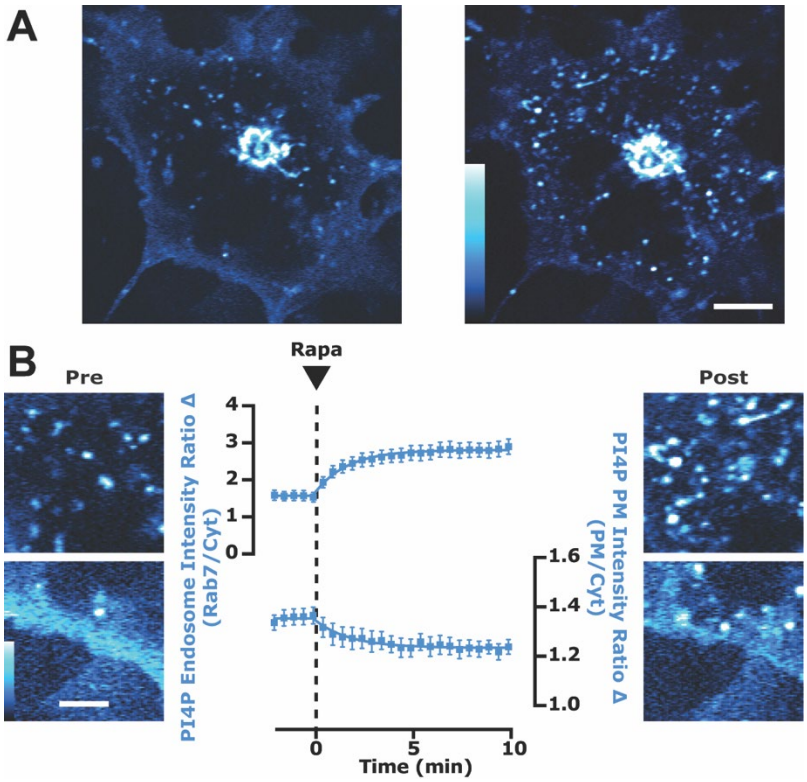

Figure 2.5 Ceci n'est pas une PIP ("This is not a PIP").

(**A**) This COS-7 cell is expressing P4C, a PI4P biosensor, scale bar is 10 µm. The images show the cell before and after a treatment that induces relocalization of the probe. What do you suppose this treatment was? See B for a careful explanation of answers. (**B**) The fluorescence intensity can be measured on different organelles. Observing and quantifying P4C localization on endosomes (top) reveals an increase in fluorescence intensity at this organelle. Conversely, quantifying the P4C localization at the PM (bottom) reveals a decrease in fluorescence intensity, scale bar is 2.5 µm.

2.4 Discussion

Genetically encoded lipid biosensors continue to be a powerful and convenient tool to study lipid dynamics and function in cell biology. In these works, we have discussed methods by which to visualize phosphoinositides with biosensors, acutely manipulate their cellular metabolism, and

quantify the resulting images. Brief considerations involving the proper selection of biosensors with differing affinities and avidities have also been discussed. Finally, we showed and discussed some potential caveats in terms of the interpretation of results obtained from using biosensors. As a whole, these considerations remind us of Rick Sanchez, the fictitious mad scientist from the sci-fi cartoon “Rick and Morty,” who once quipped: “Ok... well, sometimes science is more art than science... A lot of people don't get that.” Although biosensors may exhibit some limitations, when the experiments are properly controlled, quantified, and interpreted the probes provide invaluable information regarding lipid dynamics.

2.5 Experimental Procedures

2.5.1 Cell culture and lipofection

HeLa (ATCC CCL-2), Cos7 (ATCC CRL-1651), and HEK293A (ThermoFisher R705-07) cells were cultured in DMEM (low glucose; Life Technologies 10567022) supplemented with 10% heat-inactivated fetal bovine serum (Life Technologies 10438-034), 100 units/ml penicillin, 100μg/ml streptomycin (Life Technologies 15140122), and 1:1,000 chemically defined lipid supplement (Life Technologies 11905031) at 37˚C with a humidified atmosphere with 5% CO_2. Cells were passaged twice per week by diluting cells 1 in 5 after dissociation in TrpLE (Life Technologies 12604039).

2.5.2 Chemicals and reagents

Rapamycin (ThermoFisher BP2963-1) was dissolved in DMSO at 1 mM and stored as a stock at -20˚C, it was used in cells at 1 μM.

2.5.3 Plasmids and cloning

The EGFP (Aequorea victoria GFP containing F64L and S65T mutations) (*319*), mCherry (Discoma DsRed monomeric variant) (*320*), mTagBFP2 (Entacmaea quadricolor protein eqFP578) (*321*) and iRFP713 (Rhodopseudomonas palustris [Rp] bacteriophytochrome BphP2) (*322*) fluorophores were used in the Clontech pEGFP-C1 and -N1 backbones as described previously (*323*). Plasmids were obtained from the sources listed in **Table 2.2**.

2.5.4 Microscopy

For all live-cell imaging experiments, cells were imaged in 1.6 mL of experiment specific imaging media. Base imaging media contained FluoroBrite DMEM (Life Technologies A1896702) supplemented with 25 mM HEPES (pH 7.4), 10% fetal bovine serum, and 1:1000 chemically defined lipid supplement (CHIM). For treatments, 0.4 mL of experiment specific imaging media containing fivefold final concentration of compound was applied to the dish (or 0.5 ml for a second addition).

Confocal imaging was performed on a Nikon TiE A1R platform with acquisition in resonant mode with a 100x 1.45 NA plan-apochromatic objective. The signal-to-noise ratio was improved by taking 8 or 16 frame averages. Excitation of fluorophores was accomplished using a dual fiber-coupled LUN-V laser launch with 405-nm (BFP), 488-nm (EGFP and NG2), 561-nm (mCherry), and 640-nm (iRFP) lines. Emission was collected on four separate photomultiplier tubes with blue (425-475 nm), green (500-550 nm), yellow/orange (570-620 nm), and far-red (663-737 nm) filters. Blue and yellow/orange channels were recorded concurrently, as were green and far-red. The confocal pinhole was defined as 1.2x the Airy disc size of the longest wave-length channel used in the experiment. Nikon Elements denoising software was used to further enhance the signal-to-noise ratio.

For TIRF microscopy, a separate Nikon TiE platform coupled with a Nikon TIRF illuminator arm and 100x 1.45 NA plan-apochromatic objective was used. Excitation of fluorophores was accomplished using an Oxxius L4C laser launch with 405-nm (BFP), 488-nm (EGFP and NG2), 561-nm (mCherry), and 638-nm (iRFP) lines. Emission was collected through dual-pass filters (Chroma) with blue (420-480 nm) and yellow/orange (570-620 nm) together, and green (505-550 nm) and far-red (650-850 nm) together. An ORCA-Fusion BT sCMOS camera

(Hamamatsu) was used to capture images. Images were captured with 2x2 pixel binning and were registered in rolling shutter mode with 2x2 pixel binning with a 1.5x magnifier lens. Nikon Elements software was used to acquire all images for all experiments and all data was saved with the ND2 file extension.

2.5.5 Image analysis

Analysis of all images was accomplished using Fiji software (*324*) using the LOCI BioFormats importer (*325*). Custom macros were written to generate channel-specific montages displaying all x,y positions captured in an experiment in concatenated series. In these montages, individual regions of interest (ROIs) were generated around displayed cells.

For confocal images, the ratio or fluorescence intensity between specific compartments was analyzed as described previously (*323*). In brief, a custom macro was used to generate a compartment of interest specific binary mask through à trous wavelet decomposition (*326*). This mask was applied to measure the fluorescence intensity within the given compartment while normalizing to the mean pixel intensity in the ROI.

For TIRF microscopy images, a minimum intensity projection was used to generate ROIs within the smallest footprint of the cells. Background fluorescence was measured and subtracted from all images at all timepoints. The average pixel intensity in each frame (F_t) was normalized to the mean pixel intensity in the ROI of the time points before treatment (F_{pre}) to yield F_t/F_{pre}.

Quantitative data was imported into Prism 8 (GraphPad) for statistical analysis and the generation of graphs and plots. D'Agostino and Pearson normality tests showed data that significantly varied from normal distribution, data were then subjected to a nonparametric Kruskal-

Wallis test. If significant difference was found between sample medians, a post hoc Dunn's multiple comparison test was run.

Representative images were selected based on fluorescence measurements near the median of the sampled population, displayed typical morphology, and robust signal-to-noise ratio. If adjusting brightness or contrast, any changes were made across the entire image.

Table 2.1 Current genetically encoded lipid biosensors for a variety of selective lipid species

Lipid	Biosensor	Affinity	Lipid Specific?	Cellular localization of lipid		References
				Lipid dependent?	Lipid sufficient?	
Chol	D4-PFO + mutants	2-30 mol %	✓	✓	?	(*327–329*)
SM	Lysenin	K_D ~5 nM	✓	✓	?	(*330–332*)
PA	NES-PABD-spo20p$^{51-91}$ (PASS)	?	✗ -binds PI(4,5)P_2 and PIP_3 weakly	✓	?	(*333*)
	NES-2xPABD-spo20p$^{51-91}$	?	✗ - suspected to bind PI(4,5)P_2 and PIP_3 weakly	✓	?	(*334*)
	α-Syn-N	K_d ~6.6 μM (18:1/18:1 PA)	✓	✓	?	(*335*)
PS	C2-lactadherin	K_D ~0.5 μM	✓	✓	✓	(*336–338*)
DAG	C1ab-PDK1	K_i (PDBu) ~ 0.2 μM	✓	✓	✓	(*339*, *340*)
	C1ab-PKCε	K_D ~10 nM	✓	✓	?	(*341*, *342*)
PI	BcPI-PLC^{H82A}	?	✗ - binds to PC	✓	✓	(*343*)
	BcPI-PLC^{ANH}	?	✗ - binds DAG	✓	✓	(*343*)
PI3P	FYVE-Hrsx2	K_D ~2.5 μM	✓	✓	?	(*344–347*)
	FYVE-EEA1	K_D ~45 nM	✓	✓	?	(*344*, *345*, *348*)
	PX-p40phox	K_D ~5 μM	✓	✓	?	(*349–351*)
PI4P	P4M-SidM	K_D ~1 μM or ~18.2 nM FL	✓	✓	✓	(*352–354*)
	P4M-SidMx2	K_D < P4M-SidM	✓	✓	✓	(*354*, *355*)
	P4C-SidC	K_D ~250 nM	✓	✓	✓	(*356–358*)
	N-PH-ORP5, N-PH-ORP8	K_D ~5 μM for PI(4,5)P_2	✗ - binds PI4P and PI(4,5)P_2	✓	✗ - requires PI(4,5)P_2	(*359–361*)
	PH-OSBP, PH-FAPP1	K_D ~250 nM	✗ - binds PI(4,5)P_2	✓	✗ - requires Arf1	(*362–364*)
PI5P	3xPHD (ING2)	?	✗ - binds to PI3P	✓	✓	(*365*, *366*)
PI(3,4)P_2	PH-TAPP1-CT	K_D ~80 nM	✓	✓	✓	(*367–371*)
	eTapp1-PH†	K_D ~80 nM	✓	✓	✓	(*372*)
	TAPP1-cPHx3	K_D >80 nM	✓	✓	✓	(*373*)
PI(3,5)P_2	ML1-Nx2	K_D ~5.6 μM	✓	✓/✗*	✓/✗*	(*374*, *375*)
PI(4,5)P_2	PH-PLCδ1	K_D ~2 μM	✗ - binds to IP_3 ~20 fold more tightly than PI(4,5)P_2	✓	✓	(*376–381*)
	PH-PLCδ4	K_D > PH-PLCδ1	✗ - binds to IP_3	✓	✓	(*382*, *383*)
	Tubby$_c$	K_D > PH-PLCδ1	✗ - binds PI(3,4)P_2 and PI(3,4,5)P_3	✓	✓	(*383–386*)
	Tubby$_c^{R332H}$	K_D >Tubby	✗ - binds PI(3,4)P_2 and PI(3,4,5)P_3	✓	?	(*384*)
	ENTH/ANTH	K_D ~2 μM	✗ - binds to PI(3,4,5)P_3	✓	?	(*387–389*)
PI(3,4,5)P_3	PH-ARNO$^{2G-I303E}$x2	K_D ~170 nM	✗ - binds IP_4	✓	✓	(*373*)
	eMyoX-PHx2	K_D ~33 nM**	✗ - binds IP_4	✓	✓	(*372*, *390–392*)
	PH-Akt	K_D ~590nM	✗ - binds PI(3,4)P_2 and IP_4	✓	?	(*371*, *393*, *394*)
	PH-Btk	K_D ~80 nM	✗ - binds IP_4	✓	?	(*371*, *395–398*)
	PH-GRP1 (2G), PH-ARNO (2G)	K_D ~170 nM	✗ - binds IP_4	✓	✗-binds Arf/Arl	(*371*, *399–404*)

*The accuracy of this probe is disputed.

**The K_D value is derived from myosin-c tail and IP_4 headgroup binding.

† requires chemical ligation with a solvatochromic dye for optimal performance

Table 2.2 Plasmids used in this study

Plasmid	Vector	Insert	Reference
EGFP	pEGFP-C1	EGFP	This study
TagBFP2	pTagBFP2-C1	mTagBFP2	This study
$Tubby_C$-EGFP	pEGFP-N1	*Mus musculus* Tub(243-505):EGFP	(*405*)
$Tubby_C^{R332H}$-EGFP	pEGFP-N1	*Mus musculus* Tub(243-505)(R332H):mCherry	(*405*)
$Tubby_C$-mCherry	pmCherry-N1	*Mus musculus* Tub(243-505):mCherry	(*405*)
$Tubby_C^{R332H}$-mCherry	pmCherry-N1	*Mus musculus* Tub(243-505)(R332H):EGFP	(*405*)
PH-PLCδ1-mCherry	pmCherry-N1	PLCD1v2(1-170):mCherry	(*406*)
PH-PLCδ1-EGFP	pEGFP-N1	PLCD1v2(1-170):EGFP	(*406*)
NES-EGFP-P4Mx1	pEGFP-C1	X.leavis map2k1.L(32-44):EGFP:L. pneumophila SidM (546-647)	(*407*)
EGFP-P4C	pEGFP-C1	EGFP:L. pneumophila SidC (614-743)	(*407*)
NES-EGFP-cPHx1	pNES-EGFP-C1	X. laevis map2k1.L (32-44) : EGFP : PLEKHA1 (169-329)	(*318*)
NES-EGFP-cPHx2	pNES-EGFP-C1	X. laevis map2k1.L (32-44) : EGFP : PLEKHA1 (169-329) : GGSGGSGG:PLEKHA1 (169-329)	(*318*)
NES-EGFP-cPHx3	pNES-EGFP-C1	X. laevis map2k1.L (32-44) : EGFP : PLEKHA1 (169-329) : GGSGGSGG : PLEKHA1 (169-329) : GGSGGSGG : PLEKHA1 (169-329)	(*318*)
Lyn_{11}-FRB-iRFP	piRFP-N1	LYN(1-11):MTOR(2021-2113):iRFP	(*408*)
piRFP-FRB-$Giantin^{C129}$	piRFP-C1	iRFP:MTOR(2021-2113) : [GGSA]2 : GOLGB1 (3097-3226)	(*23*)
LAMP1-FRB-iRFP	piRFP-N1	LAMP1: MTOR (2021-2113) : iRFP	(*318*)
$AKAP1^{N31}$-FRB-iRFP	piRFP-N1	Mus musculus Akap1(1-31) M16L : MTOR (2021-2113) : iRFP	(*23*)
mCherry-FKBP	pmCherry-C1	mCherry : FKBP1A(3-108)	(*408*)
mCherry-FKBP-INPP5E	pmCherry-C1	mCherry : FKBP1A (3-108) : $[GGSA]_4GG$: INPP5E (214-644)	(*408*)
mCherry-$FKBPSAC1^{\Delta TMD}$	pmCherry-C1	mCherry:FKBP1A(3-108):[GGSA]4GG:SACM1L(1-521)	(*407*)

3.0 Determinants of PIP5K PM targeting

3.1 Overview

The plasma membrane (PM) is host to several intracellular processes, including membrane trafficking, cytoskeletal arrangement, and signal transduction. Phosphatidylinositol 4,5-bisphosphate ($PI(4,5)P_2$) is found in the inner leaflet of the PM and serves as a major regulatory lipid for these events. As expected, reduced levels of $PI(4,5)P_2$ lead to dysregulation of cellular functions. Type 1 phosphatidylinositol 4-phosphate 5-kinase (PIP5K) is a key player in the synthesis of $PI(4,5)P_2$ and therefore, understanding the regulation of this kinase is critical for determining how the cell maintains $PI(4,5)P_2$ homeostasis. To assess potential control mechanisms of this kinase, we observed PM localization of over-expressed PIP5K isoforms and endogenously tagged PIP5K1A. We were able to perturb the PM composition to observe the corresponding changes in PIP5K localization. PIP5K was continuously localized with the PM, but this was dependent on the presence of phosphatidylinositol 4-phosphate (PI4P) and $PI(4,5)P_2$. Furthermore, in assessing the domains of PIP5K required for this PM association, we determined that two basic residues in the C-terminal tail are necessary to mediate this PM interaction. The crystal structure of PIP5K displays these two residues opposite the activation loop and near an unstructured "insert" loop. We hypothesize that binding of its enzymatic product may serve as a positive feedback mechanism for both PIP5K activity and intracellular $PI(4,5)P_2$ levels.

3.2 Introduction

The inner leaflet of the plasma membrane (PM) is a hub for several intracellular processes and phosphatidylinositol 4,5-bisphosphate ($PI(4,5)P_2$) acts as a critical regulator of these processes (*8*, *9*, *409*). The $PI(4,5)P_2$ regulated cell processes include trafficking (*226*, *410*), cytoskeletal organization (*411*, *412*), ion transport (*8*, *409*), and the generation of the second messengers inositol trisphosphate (IP_3), diacylglycerol (DAG) (*36*), and $PI(3,4,5)P_3$ (*100*, *413*). Aberrant levels of this phosphoinositide can lead to dysregulation of these intracellular processes (*8*, *409*). In particular, reductions in $PI(4,5)P_2$ levels have been linked to improper organization of the actin cytoskeleton (*65*, *73*, *292*) and decreases in endocytosis (*239*, *240*). Conversely, mutations in $PI(4,5)P_2$ phosphatases, resulting in increased or mis-localized $PI(4,5)P_2$ have been linked to a failure of clathrin coat disassembly and improper actin assembly (*414*, *415*). As such, the levels of $PI(4,5)P_2$ are tightly regulated at the PM and a constant mass is maintained.

$PI(4,5)P_2$ can be synthesized by one of two biochemical routes, either the phosphorylation of phosphatidylinositol 5-phosphate (PI5P) or phosphatidylinositol 4-phosphate (PI4P) (*9*, *69*). Each of these precursor lipids are metabolized into $PI(4,5)P_2$ by a separate phosphoinositide kinases: phosphatidylinositol 5-phosphate-4 kinase (PIP4K) and phosphatidylinositol 4-phosphate-5 kinase (PIP5K) (*62*, *63*, *69*, *416*). PIP4K phosphorylates PI5P at the 4-OH position of the inositol ring (*37–40*). In cells, however, PIP4K is not the main route of synthesis as PI5P comprises a relatively minor portion of the phosphatidylinositol phosphate pool (*9*, *39*, *57*). The most well-known and studied route of $PI(4,5)P_2$ synthesis is that of PI4P to $PI(4,5)P_2$ (*25*, *417*). PIP5K is the enzymes responsible for the phosphorylation of PI4P on the 5-OH position of the inositol headgroup (*62–65*, *68*, *69*). PIP5K produces virtually all of the cellular $PI(4,5)P_2$ and it does so specifically at the PM, as this is where both enzyme (*73*) and substrate (*304*) are localized.

Moreover, PIP5K PM association has been shown to be the result of substrate binding (*72*, *73*, *292*), general electrostatic interactions (*71*), and product interaction (*92*, *418*). Further evidence has suggested that the PIP5K – $PI(4,5)P_2$ interaction may function as a positive feedback mechanism for $PI(4,5)P_2$ synthesis in purified systems (*92*, *418*).

During times of cellular signaling, $PI(4,5)P_2$ can be readily used as a substrate or a binding partner for many proteins involved in signal transduction (*9*). In the case of PLC activation, $PI(4,5)P_2$ levels can be depleted by up to ~80% in some cell types (*419*). After inactivation of PLC, the levels of $PI(4,5)P_2$ recover within 2-5 min (*124*, *419*), suggesting that PIP5K is capable of rapid resynthesis. Here, we provide our own evidence that PIP5K interacts with both PI4P and $PI(4,5)P_2$; this interaction may be facilitated by the uncharacterized "insert" loop. Ultimately, this interaction may serve as a positive feedback mechanism for $PI(4,5)P_2$ synthesis during periods of cellular signaling.

3.3 Results

3.3.1 PIP5K localization at the PM is regulated by C-terminal tail residues.

Mammalian PIP5K exists as three isoforms, A, B, and C (*64*, *65*, *68*, *69*) and each of these isoforms localizes to the PM (*71*, *73*, *292*, *420*). To confirm the PM localization in our own system, we developed plasmids for the transient over-expression of each of the isoforms for each of these enzymes. When over-expressed in HeLa cells, we observed exclusively PM-associated localization, as expected (**Figure 3.1A**). We further quantified these results using the PM/cell ratio and saw a significant increase in PM association compared to the EGFP control (**Figure 3.1A**).

The localization of PIP5K was strikingly different from that of PIP4K2A, as expected (*73*, *292*, *420*) (**Figure 3.1A, left**). We next sought to test whether PIP5K catalytic activity was a factor in PM localization (*421*). Catalytically dead mutants of each isoform were generated and similarly over-expressed (*74*, *292*, *420*, *422*). Again, each isoform was localized tightly with the PM, indicating that the catalytic activity was not necessary for this localization (**Figure 3.1A**).

Comparison of the amino acid sequences of PIP5K isoforms and PIP4K2A, we noted that the first main difference was the absence of a C-terminal tail in PIP4K2A. To further investigate the function of the C-terminal tail of PIP5K we generated plasmids for the expression of PIP5K1A truncations (**Figure 3.1B**). The PIP5K1A truncations all lacked the N-terminus and had different lengths of the C-terminal tail. Previous work had shown that two basic residues (either Lys-Lys in PIP5K1-A and -B or Arg-Lys in -C) in the C-terminal tail were essential for proper PM association (*423*). Removal of the entire C-terminal tail yielded the Kina fragment (**Figure 3.1B**) which was cytosolically localized when expressed in cells (**Figure 3.1C**). PIP5K1A with the full-length of the C-terminal tail ($Kina^{CTail}$) (**Figure 3.1B and C**) remained PM localized, similar to the full-length PIP5K1A. Finally, the PIP5K1A with the kinase domain and two basic C-terminal tail residues only ($Kina^{++}$) (**Figure 3.1B**) also showed significant PM localization, compared with EGFP control (**Figure 3.1C**).

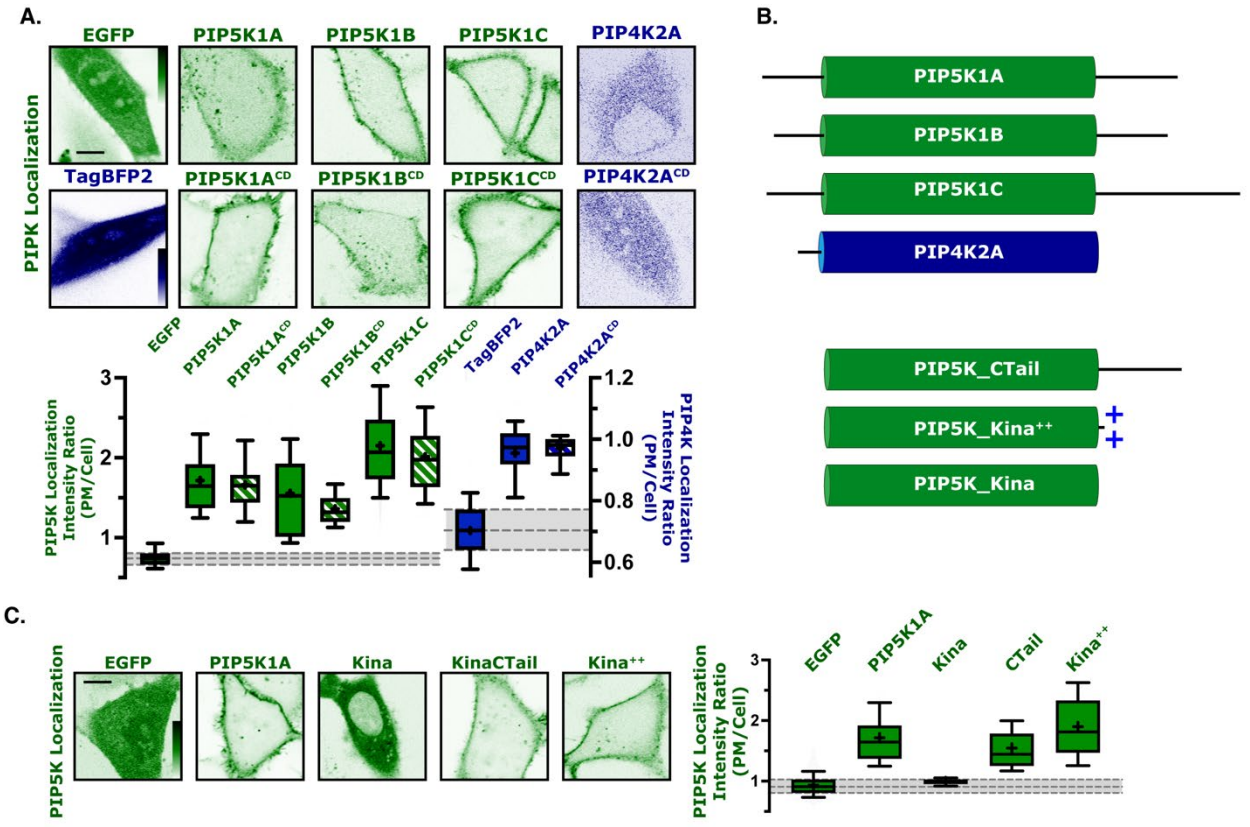

Figure 3.1 C-terminal tail residues are necessary for PIP5K1A localization at the PM.

(**A**) PIP5Ks localize with the PM independently of catalytic activity. Images show equatorial confocal sections of HeLa cells expressing EGFP-tagged catalytically active or dead PIP5K constructs (A, B, or C isoforms) (green), TagBFP2-tagged catalytically active or dead PIP4K2A (blue), or EGFP/TagBFP2 alone as control. PIP5K isoform localization is evident by increased EGFP fluorescence in the PM. PIP4K localization is cytosolically localized. Box and whisker plots show the mean fluorescence intensity ratio (PM/cell) of the fluorescently-tagged proteins from >90 cells imaged across at least three independent experiments (boxes displaying median and interquartile range, whiskers representing 10-90% of data and "+" represents mean), scale bar is 10 µm. (**B**) PIPkins have differential C-termini which mediate PM localization. Cartoon denotes the linear structure of PIP5K isoforms compared with PIP4K2A. Cartoons also show the linear structure of C-terminal truncations of PIP5K1A. (**C**) The C-terminal tail is necessary for PM association of PIP5K1A. Images show PIP5K1A truncations expressed in HeLa cells as in A. Box and whiskers from >90 cells imaged across at least three independent experiments as in A, scale bar is 10 µm.

3.3.2 Overexpressed PIP5K1A maintains PM localization even after lipid recomposition.

The necessity of the two basic residues in the Kina^{++} construct led us to hypothesize that PM localization of PIP5K1A was regulated by electrostatic interactions. To determine if this was the case, we used a chemically-induced dimerization (CID) system (**Figure 3.2A and B**) to recruit and deplete PI(4,5)P_2 and PI4P from the PM (*4*). We recruited the Sac phosphatase to deplete PI4P to PI and observed no change in either the full-length PIP5K1A localization or in the PI(4,5)P_2 biosensor, Tubby$_C$ (*316*), localization with the PM (**Figure 3.2C**). Upon recruitment of INPP5E, which depletes PI(4,5)P_2 to PI4P, we observed a decrease in Tubby$_C$ PM association (**Figure 3.2C**). Additionally, there was a slight decrease in PIP5K1A localization with the PM (**Figure 3.2C**). The dual phosphatase construct pseudojanin (PJ) (*4*) was also recruited to deplete both PI(4,5)P_2 and PI4P to PI. Upon recruitment, we observed no change in either PIP5K1A or Tubby$_C$ localization at the PM. Finally, we tested the recruitment of PLCβ3 to deplete PI(4,5)P_2 to DAG and IP_3 (**Figure 3.2B**). DAG lacks charge and must undergo a lengthier re-synthesis reaction, rather than reversible phosphorylation initiated by any of the phosphatases used previously. Upon recruitment, we observed the expected depletion of Tubby$_C$ from the PM, however we did not observe any loss of PIP5K1A from the PM (**Figure 3.2C**). We hypothesized that the catalytic activity of the over-expressed PIP5K1A was able to outcompete the phospholipase/phosphatases. To this end we over-expressed PIP5K1A^{CatDead} and again used PJ to deplete PI(4,5)P_2 and PI4P to PI (**Figure 3.2B**). Upon PJ recruitment there was a rapid loss of Tubby$_C$ from the PM (**Figure 3.2C**). Even before PJ recruitment, we noticed that there was a lower baseline value of PIP5K1A^{CatDead} at the PM, compared to PIP5K1A (**Figure 3.2C**). Furthermore, the recruitment of PJ resulted in further loss of PIP5K1A^{CatDead} from the PM. Taken together, these data support that PIP5K1A is recruited to and held at the PM in a PI4P (*42*, *73*, *292*) and PI(4,5)P_2 (*418*) dependent

manner. However, the over-expression and potential competition between the various enzymes yielded this system inadequate to accurately study the mechanism of PIP5K PM association.

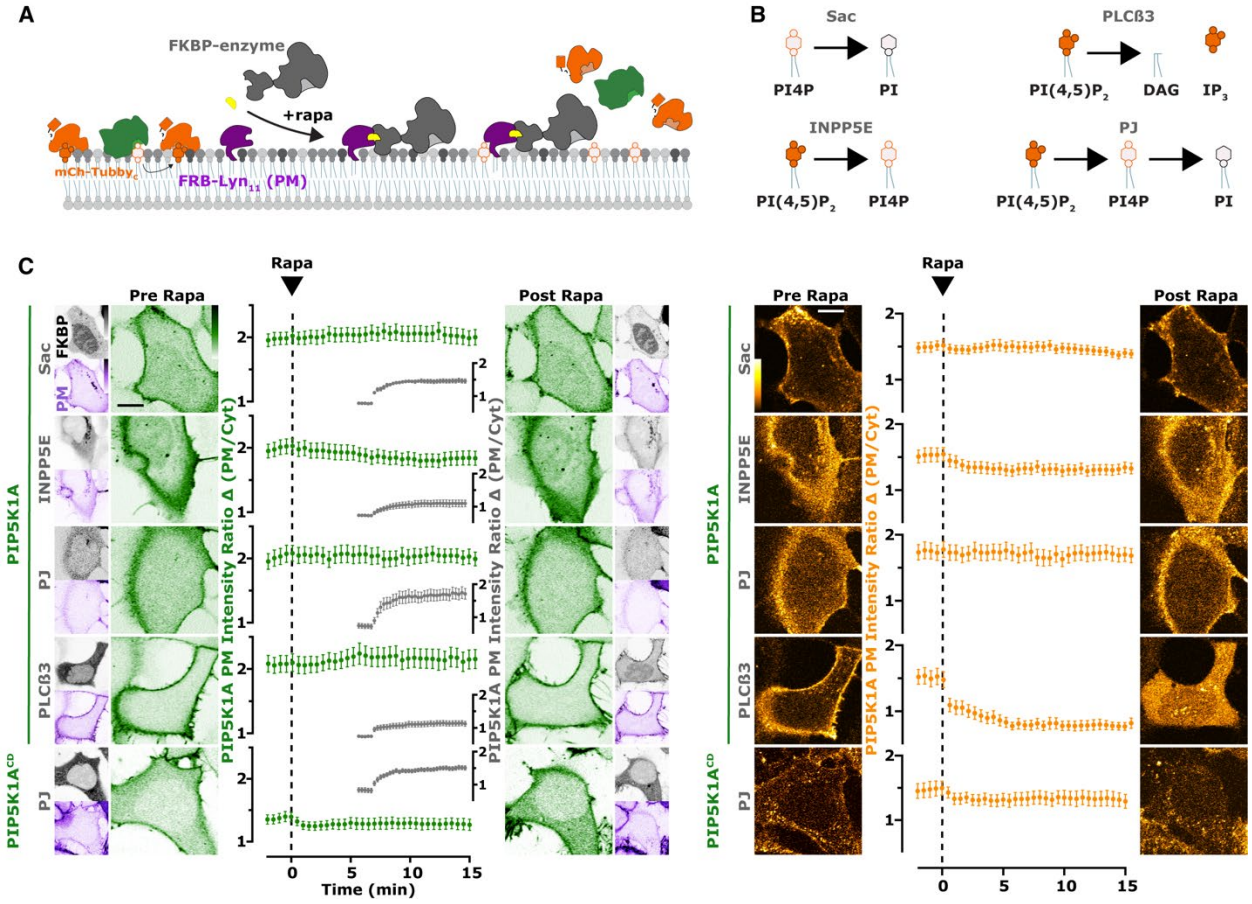

Figure 3.2 Over-expressed PIP5K1A is not sensitive to changes in PM lipid composition.

(**A**) Acute phosphatase / phospholipase recruitment to the PM. Cartoon schematics show the chemically induced dimerization (CID) system for FKBP-tagged enzymes, which dimerize with the PM-anchored FRB-Lyn$_{11}$ upon the addition of rapamycin (rapa). (**B**) Phosphatase / phospholipase recruitment alters PM lipid levels. Cartoon schematics show the expected changes in PM phosphoinositides upon the recruitment of the indicated phosphatase or phospholipase. (**C**) Phosphatase / phospholipase recruitment alters PM PI(4,5)P$_2$ levels, but not over-expressed PIP5K1A. HEK293A cells were transfected with PIP5K1A, FKBP-tagged proteins, the high affinity PI(4,5)P$_2$ indicator Tubby$_C$, and FRB-Lyn$_{11}$. During time-lapse confocal microscopy, cells were stimulated with 1 µM rapa as indicated. Graphs represent mean change in PIP5K1A localization or PI(4,5)P$_2$ sensor intensity ratio (PM/cell) ± s.e. for 37-55 cells imaged across three independent experiments, scale bar is 10 µm.

3.3.3 Endogenous PIP5K1A is localized at the PM.

As a way of circumventing any of the artifacts of our over-expression system, we turned to CRISPR-Cas9 to endogenously tag PIP5K1A with mNeonGreen2 (NG) (**Figure 3.3A**). We used HEK293A cells and added the NG tag to the N-terminus of PIP5K1A, the most abundant isoform in both HEK293A (*52*) and HeLa cells (*424*). The subsequent ePIP5K1A cells were genotyped using a NG specific forward primer and a PIP5K1A specific reverse primer to produce an expected amplicon of ~200 bp in the edited, but not the parental HEK293A cell line (**Figure 3.3B**). With TIRFM we could easily observe the PM localized population of ePIP5K1A molecules, which appeared to be diffraction-limited and had uniform intensity (**Figure 3.3B**). Using confocal, we observed a primarily PM localized ePIP5K1A (**Figure 3.3B**). Altogether, this data indicates endogenously tagging PIP5K1A does not alter its localization (**Figure 3.3B**).

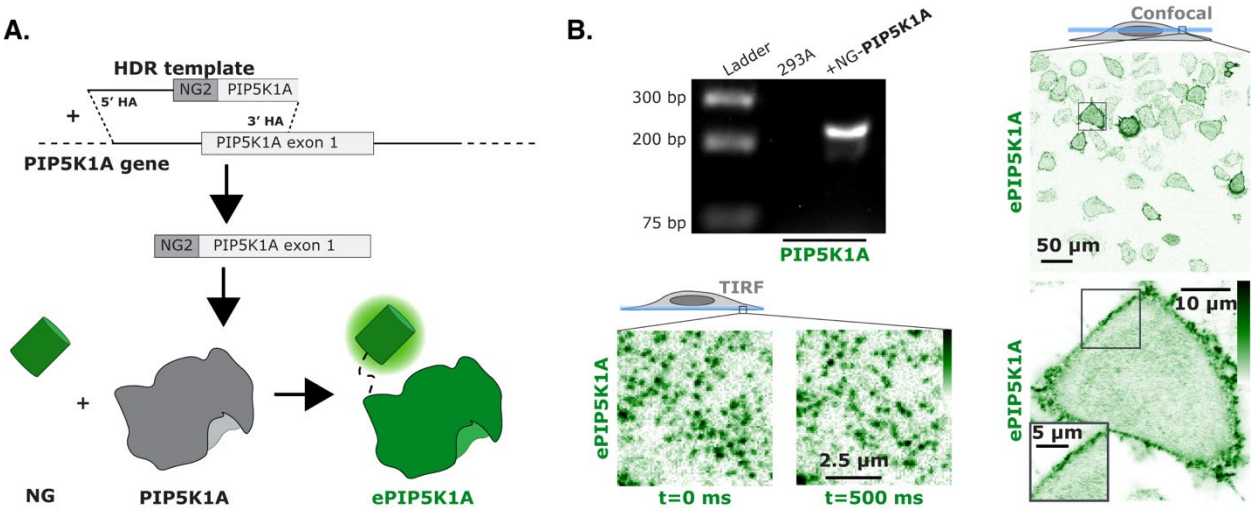

Figure 3.3 Endogenously tagged PIP5K1A is associated with the PM.

(**A**) Endogenous tagging of PIP5K1A. Brief cartoon schematic showing the mechanism of endogenous tagging employed for PIP5K1A with full-length mNeonGreen2 (NG2). The resulting cell line was termed ePIP5K1A. Cells were genotyped with a mNG specific forward primer and a PIP5K1A specific reverse primer yielding an edited product of ~200bp. (**B**) Image based characterization of ePIP5K1A. When imaged live by TIRF, dynamic, diffraction limited spots are observed on the membrane (compare differential localization at 0 and +0.5 s). Confocal images display the ePIP5K1A (green) in cells localized mainly at the PM, with the zoomed in image futher showing primary association of the enzyme to the PM.

3.3.4 Endogenous PIP5K1A PM localization is mediated by PI4P and PI(4,5)P_2.

With the new system of endogenously tagged PIP5K1A, we returned to test the potential of either an electrostatic or a lipid specific interaction of ePIP5K1A with the PM. We first used chemical treatment of cells to alter the electrostatic potential of the PM (**Figure 3.4A**). Dibucaine was added to decrease the net PM charge in two ways: 1) it is a cationic amphiphile which inserts directly into the PM and 2) it induces phosphatidylserine (PS) scrambling (*71*, *425*). Upon addition, there was a very rapid, and almost complete, loss of ePIP5K1A from the PM (**Figure 3.4A).** Ionomycin was added to trigger a cytosolic influx of calcium which can decrease the PM charge

in three ways: 1) the cation blocks the existing negative charges of the PM, 2) it promotes the PS scrambling, and 3) it actives PLC, which will further deplete phosphoinositides (*71*). With the addition of ionomycin we also observed a complete loss of ePIP5K1A from the PM (**Figure 3.4A**). These data all indicate that the negative charge of the PM is necessary for ePIP5K1A localization.

We next moved to replicate the experiments in **Figure 3.3**, with the depletion of specific phosphoinositides such as PI4P and PI(4,5)P_2. In confocal, we observed the localization of ePIP5K1A after the recruitment of either Sac, INPP5E, PJ, or PLCβ3 (**Figure 3.4B**). The only case that we observed any loss of ePIP5K1A PM localization was with the recruitment of PJ, depleting both PI4P and PI(4,5)P_2 (**Figure 3.4B**). These experiments were also performed with TIRF microscopy (**Figure 3.4C**). Again, we observed loss of ePIP5K1A puncta from the PM only upon the recruitment of PJ (**Figure 3.4C**). While Figure 3.4 deduced that the overall charge of the PM is important for ePIP5K1 recruitment, these experiments demonstrate that ePIP5K1A specifically associates with both PI4P and PI(4,5)P_2 at the PM for proper localization.

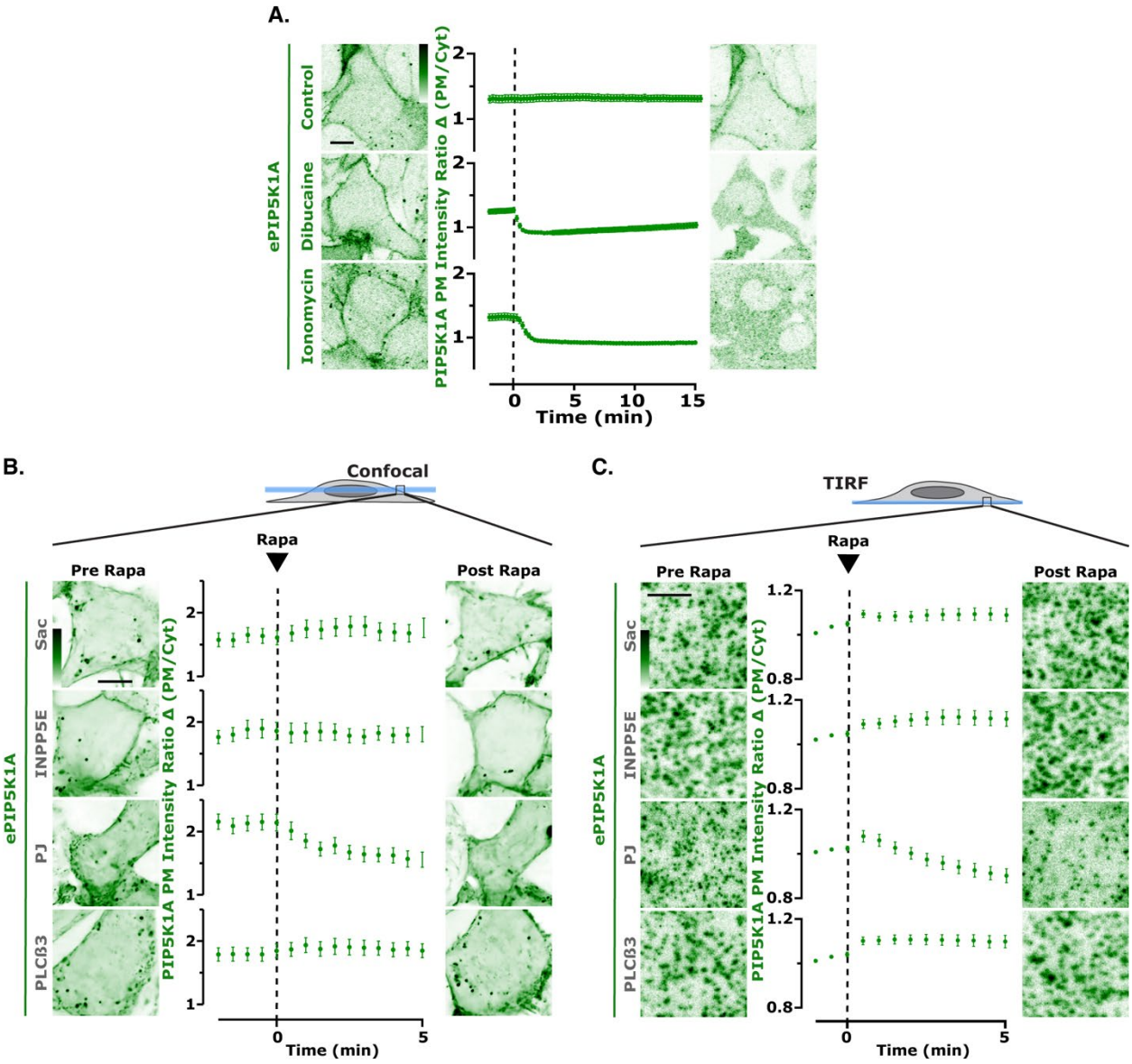

Figure 3.4 Endogenous PIP5K1A binds to PI4P and PI(4,5)P_2 to maintain PM localization.

(**A**) Chemical perturbation of PM lipids decreases ePIP5K1A PM localization. ePIP5K1A cells were transfected with the high affinity PI(4,5)P_2 indicator $Tubby_C$ and FRB-Lyn_{11}. During time-lapse confocal microscopy, cells were stimulated with 10 µM dibucaine or 1 mM ionomycin as indicated. Graphs represent mean change in ePIP5K1A intensity ratio (PM/cell) ± s.e. for 58-62 cells imaged across three independent experiments, scale bar is 10 µm. (**B**) Phosphatase / phospholipase recruitment alters ePIP5K1A localization. ePIP5K1A cells were transfected with FKBP-tagged proteins and FRB-Lyn_{11}. During time-lapse confocal microscopy, cells were stimulated with 1 µM rapa as indicated. Graphs represent mean change in ePIP5K1A localization intensity ratio (PM/cell) ± s.e. for 30-35 cells

imaged across three independent experiments, scale bar is 10 μm. (**C**) Phosphatase / phospholipase recruitment alters ePIP5K1A localization. ePIP5K1A cells were transfected with FKBP-tagged proteins and FRB-Lyn_{11}. During time-lapse TIRF microscopy, cells were stimulated with 1 μM rapa as indicated. Graphs represent mean change in ePIP5K1A localization intensity ratio (PM/cell) ± s.e. for 31-33 cells imaged across three independent experiments, scale bar is 2.5 μm.

3.3.5 PM association of over-expressed PIP5K isoforms differ.

The endogenous presence of three different isoforms of PIP5K led us to hypothesize that the different forms undergo different types of regulation. We returned to the over-expression system used in **Figure 3.2** to determine how PIP5K1B and PIP5K1C might be regulated in comparison to PIP5K1A. We utilized our CID system yet again to recruit Sac, INPP5E, PJ, or PLCβ3 to deplete PI4P and $PI(4,5)P_2$ to various other lipid species illustrated in **Figure 3.5A and B** (**repeated from Figure 3.2 A and B**). In the case of over-expressed PIP5K1B, the recruitment of either Sac, which depletes PI4P, we observed no change in TubbyC localization at the PM, as expected (**Figure 3.5C**). With the recruitment of INPP5E, which depletes $PI(4,5)P_2$, there was a slight decrease in $Tubby_C$ PM association (**Figure 3.5C**). In terms of PIP5K1B localization, we saw no change in PM association with recruitment of either Sac or INPP5E (**Figure 3.5C**). With the recruitment of PJ, we saw a slight decrease in $Tubby_C$ localization (**Figure 3.5C**) and a decrease in PIP5K1B localization (**Figure 3.5C**). Finally, the recruitment of PLCβ3 resulted in the greatest loss in both $Tubby_C$ and PIP5K1B PM association (**Figure 3.5C**). As was a concern with the over-expression of PIP5K1A, we hypothesized that the catalytic activity of PIP5K1B was able to outcompete the depletion of the PM lipids upon enzyme recruitment. We expressed $PIP5K1B^{CatDead}$ and again observed a lower baseline localization of the kinase (**Figure 3.5C**). This was followed by a greater decrease in both $Tubby_C$ and $PIP5K1B^{CatDead}$ localization from the PM

upon PJ recruitment and lipid breakdown (**Figure 3.5C**). Overall, PIP5K1B seems to localize to the PM in a PI4P (*42*, *73*, *292*) and PI(4,5)P_2 (*418*) dependent manner, but seems to be more sensitive to lipid changes than PIP5K1A.

The final isoform, PIP5K1C, was tested the same way. The recruitment of Sac resulted in no change in PM association of either Tubby$_C$ or PIP5K1C (**Figure 3.5D**). However, the recruitment of INPP5E resulted in a reduction in both Tubby$_C$ and PIP5K1C localization at the PM (**Figure 3.5D**). Recruiting PJ resulted in very little change in Tubby$_C$ localization at the PM but resulted in a rapid loss of PIP5K1C (**Figure 3.5D**). Utilizing PLCβ3 resulted in a lower baseline PM association of PIP5K1C (**Figure 3.5D**). Upon enzyme recruitment, there was loss of both Tubby$_C$ and PIP5K1C localization (**Figure 3.5D**). Again, to determine whether the catalytic activity had any impact on PIP5Ks ability to remain at the PM by producing PI(4,5)P_2 we utilized PIP5K1C^{CatDead}. This construct had a slightly lower PM association at baseline, and upon PJ recruitment there was a rapid and robust decrease in PM intensity (**Figure 3.5D**). Unlike with the over-expression of the active PIP5K1C, there was some loss of Tubby$_C$ localization when PIP5K1C^{CatDead} was expressed (**Figure 3.5D**). This data, collectively, show that PIP5K1C is sensitive to changes in either PI4P (*42*, *73*, *292*) and PI(4,5)P_2 (*418*) or just PI(4,5)P_2 (*418*). Moreover, PIP5K1C seems to be the isoform most sensitive to changes in phosphoinositide composition at the PM. The dependence of the PM association of three PIP5K isoforms with PI(4,5)P_2 could play an important role in a positive feedback mechanism of PIP5K, as it is able to both sense and bind to its catalytic product.

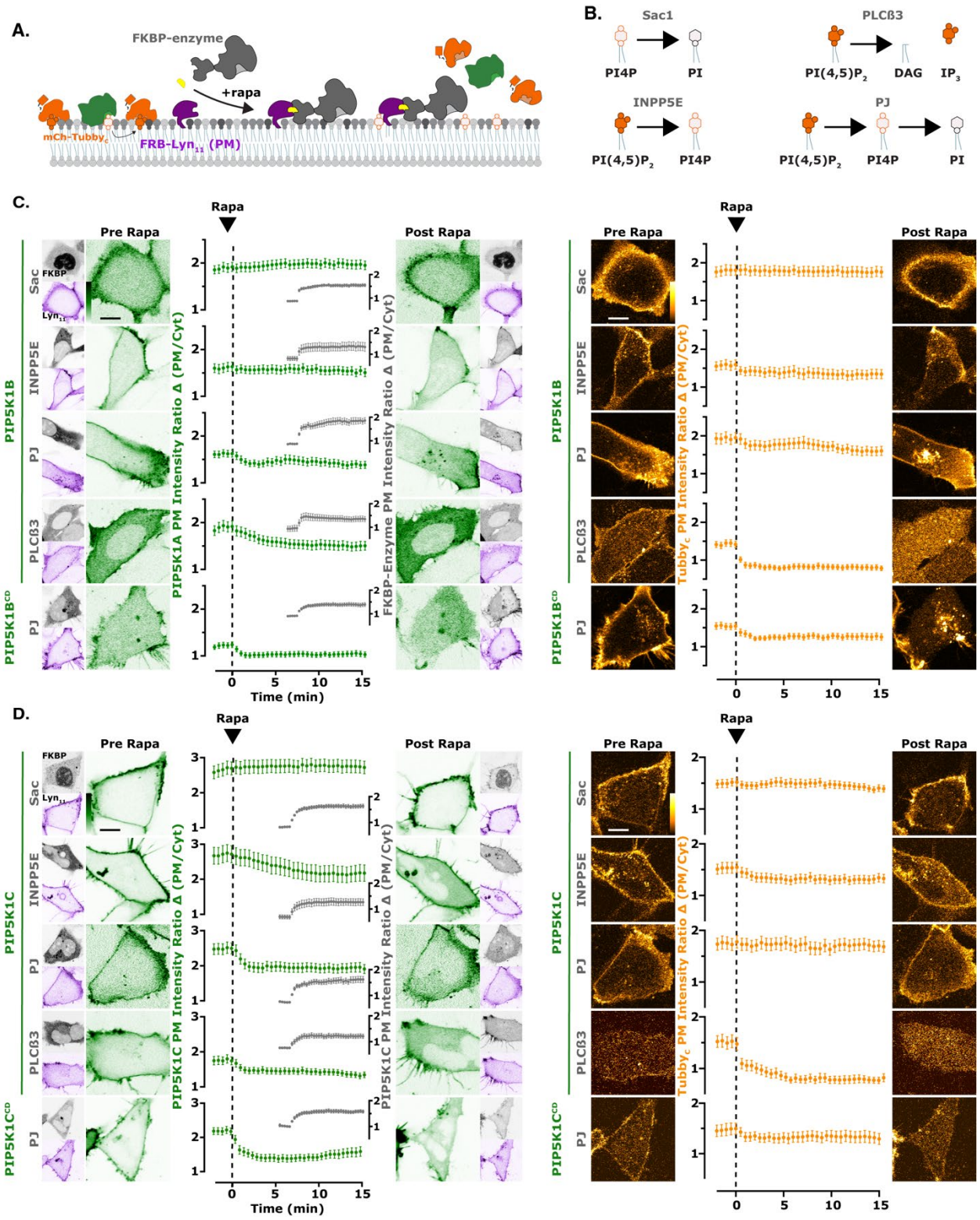
A.
FKBP-enzyme
+rapa
mCh-Tubby$_C$
FRB-Lyn$_{11}$ (PM)
B.
Sac1
PI4P
PI
PLCß3
PI(4,5)P$_2$
DAG
IP$_3$
INPP5E
PI(4,5)P$_2$
PI4P
PJ
PI(4,5)P$_2$
PI4P
PI
C.
Pre Rapa
Rapa
Post Rapa
PIP5K1B
PIP5K1B^{CD}
Sac
INPP5E
PJ
PLCß3
PJ
FKBP
Lyn$_{11}$
PIP5K1A PM Intensity Ratio Δ (PM/Cyt)
FKBP-Enzyme PM Intensity Ratio Δ (PM/Cyt)
Tubby$_C$ PM Intensity Ratio Δ (PM/Cyt)
Time (min)
D.
Pre Rapa
Rapa
Post Rapa
PIP5K1C
PIP5K1C^{CD}
PIP5K1C PM Intensity Ratio Δ (PM/Cyt)
Tubby$_C$ PM Intensity Ratio Δ (PM/Cyt)
Time (min)

Figure 3.5 Over-expressed isoforms of PIP5K are sensitive to changes in PM lipid composition.

(**A**) Acute phosphatase / phospholipase recruitment to the PM. Cartoon schematics show the chemically induced dimerization (CID) system for FKBP-tagged enzymes, which dimerize with the PM-anchored FRB-Lyn_{11} upon the addition of rapamycin (rapa), same from Figure 2. (**B**) Phosphatase / phospholipase recruitment alters PM lipid levels. Cartoon schematics show the expected changes in PM phosphoinositides upon the recruitment of the indicated phosphatase or phospholipase, same from Figure 2. (**C**) Phosphatase / phospholipase recruitment alters PIP5K1B localization. HEK293A cells were transfected with PIP5K1B, FKBP-tagged proteins, the high affinity $PI(4,5)P_2$ indicator $Tubby_C$, and FRB-Lyn_{11}. During time-lapse confocal microscopy, cells were stimulated with 1 μM rapa as indicated. Graphs represent mean change in PIP5K1B localization or $PI(4,5)P_2$ sensor intensity ratio (PM/cell) ± s.e. for 36-51 cells imaged across three independent experiments, scale bar is 10 μm. (**D**) Phosphatase / phospholipase recruitment differentially alters PIP5K1C localization. HEK293A cells were transfected with PIP5K1C, FKBP-tagged proteins, the high affinity $PI(4,5)P_2$ indicator $Tubby_C$, and FRB-Lyn_{11}. During time-lapse confocal microscopy, cells were stimulated with 1 μM rapa as indicated. Graphs represent either mean change in PIP5K1C localization or $PI(4,5)P_2$ sensor intensity ratio (PM/cell) ± s.e. for 37-53 cells imaged across three independent experiments, scale bar is 10 μm.

3.3.6 The specificity / activation loop and insert loop play a role in PM localization.

With the necessity of the two basic C-terminal tail residues for PM localization (*423*) (**Figure 3.1**), we sought to identify what other regions of may play a role in PIP5K membrane association. We used the published crystal structure (*70*) and AlphaFold predictive structure(s) (*426*, *427*) to identify the localization of the RK residues in PIP5K1C (**Figure 3.6A**). The activation loop of the PIP5K isoforms is important for both targeting to (*73*, *292*) and maintaining (*42*) enzyme localization at the PM. We hypothesized that these two structural features would be located near one another. To our surprise, the RK residues appeared to be localized on the opposite side of the PIP5K1C kinase domain from the activation loop (**Figure 3.6A**). However, we noticed

another large and unstructured region close to the RK residues, termed the insert loop (*48*, *70*) (**Figure 3.6A**). This region is ~50aa long and has high sequence variability between the PIP5K isoforms. To assess the functionality of both the activation loop and the insert loop we generated mutated PIP5K1C_Kina^{++} constructs and replaced these unstructured loops with flexible linkers (**Figure 3.6B**). We then assessed the PM association of these constructs as before, using confocal microscopy and quantifying the PM/cell ratio. The expression of full-length PIP5K1C, KinaCTail, and Kina^{++} all showed PM localization, compared to the expression of EGFP (**Figure 3.6C**). This was contrasted to the cytosolic only localization of the Kina fragment only (**Figure 3.6C**). Each of these results was consistent with the PIP5K1A truncations seen in **Figure 3.1**, as expected. The Kina^{++} fragment which contained the insert loop but lacked the activation loop (Kina^{++}ΔAct) was not localized to the PM, in fact it appeared excluded from the PM (**Figure 3.6B**). In contrast, the fragment with the activation loop but not the insert loop (Kina^{++}ΔIns) had slight enrichment with the PM, but was also still present in the cytosol, in contrast to the Kina^{++} fragment (**Figure 3.6C**). Taken together, we can conclude that the activation loop is necessary for PM association and the uncharacterized insert loop seems to enhance or stabilize PM localization, via an unknown mechanism.

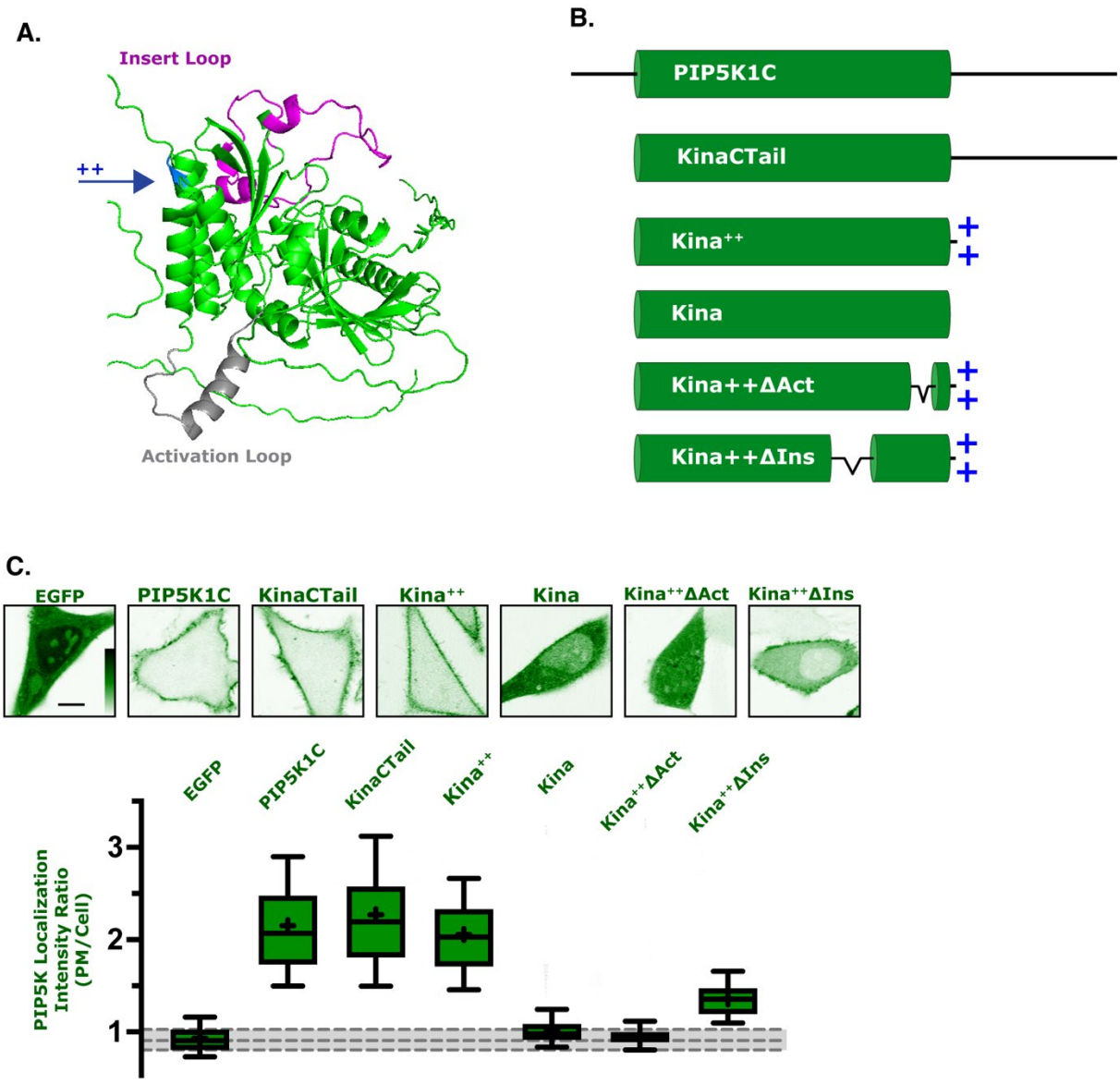

Figure 3.6 PIP5K1C structural elements play a role in PM localization.

(**A**) PIP5K1C contains multiple unstructured elements. Cartoon adapted from AlphaFold shows the annotated location of the "$^{++}$" residues, the activation loop, and the insert loop in relation to one another. (**B**) PIP5K1C unstructured loops can be mutated to assess function. Cartoon denotes the linear structure of PIP5K1C either with modifications to the C-terminal tail or the unstructured activation (Act) and insert (Ins) loops. (**C**) Unstructured loops play a role in PIP5K1C localization with the PM. Images show PIP5K1A truncations expressed in HeLa cells as in A. Box and whiskers from >90 cells imaged across at least three independent experiments as in A, scale bar is 10 μm.

3.4 Discussion

In conclusion, our results shed light on the mechanism by which PIP5K can localize with the PM and remain localized during periods of cellular signaling. With the kinase mediated production of $PI(4,5)P_2$, PIP5K can be further recruited to the PM in a manner consistent with positive feedback. Our data also indicate that the two basic residues in the C-terminal tail are necessary for this PM association. It was previously shown that the minimal construct of PIP5K1C_Kina^{++} was able to localize with the PM (*423*). Here we also show that that is the case for PIP5K1A_Kina^{++}. Taken together this indicates that the two basic residues adjacent to the kinase domain, in PIP5K, are necessary for PM localization.

The use of these minimal PIP5K fragments removed any isoform specific differences the C-terminal tail sequences (*9*). While all three isoforms seem to readily localize to the PM of cells, the differences in the C-terminal tails helps to differentially direct PIP5K isoforms to unique regions in cells. For example, PIP5K1A is reported to be found at membrane ruffles (*84*) and is required for receptor tyrosine kinase signaling (*84*, *428*). PIP5K1B is specifically localized to the apical surface of polarized cells and is required for apical endocytosis (*85*). And finally, PIP5K1C exists as multiple splice variants (*65*, *74*, *75*). PIP5K1C-v2 has been found to specifically localize with both AP-2 at endocytic structures (*86*, *87*) and with talin at focal adhesions (*88*, *89*).

Despite these differences in specific localization, we have shown that the three isoforms of PIP5K require both PI4P and $PI(4,5)P_2$ for PM association. It was previously shown that the interaction between PIP5K and the PM was due to electrostatic interactions (*71*). Due to the negative charge supplied by both PI4P and $PI(4,5)P_2$ (*4*), we further showed that this PM interaction is specific to PIP5K binding to both its substrate (*73*, *292*) and product (*418*). Furthermore, this effect was more striking when observed with either the catalytically inactive or

endogenous PIP5K, as the catalytic activity was unable to outcompete specific phosphatases. Upon stimulation of PLC signaling (**Figures 3.2, 3.4, and 3.5**) we also see the maintenance of PIP5K localization at the PM. It has been previously reported that PIP5K interacts with and is stimulated by phosphatidic acid (PA) (*94*, *429*), a lipid which is enriched at the PM during PLC signaling. Taken together, this provides a unique and specific mechanism by which PIP5K localization can be maintained at the PM.

Our results indicate that the activation loop and the insert loop each play a role in PM association. It has been previously demonstrated that the activation loop is essential for the interaction of PIP5K with PI4P (*73*). We observed partial PM localization of the Kina^{++}ΔIns construct, likely due to the transient interaction between both PI4P and PI(4,5)P_2 in the active site. We believe that the insert loop, which is lacking in this construct, is able to directly interact with PI(4,5)P_2 or allosterically regulate the structure of PIP5K, allowing for the kinase to interact with PI(4,5)P_2 away from its active site. Again, the differences in PIP5K isoform insert loops (similarity 56-69%, identity 42-57%) leads us to hypothesize that there is some type of differential regulation or even differences in PI(4,5)P_2 binding affinities between the isoforms. Altogether, PIP5K is localized with the PM due to an interaction between PI4P and PI(4,5)P_2 and the basic C-terminal tail residues. These specific interactions set up a potential positive feedback mechanism for the rapid production or maintenance of homeostatic PI(4,5)P_2 levels upon the activation of cellular signaling, in agreement with previously published literature (*418*).

3.5 Experimental Procedures

3.5.1 Cell culture and lipofection

HeLa (ATCC CCL-2) and HEK293A (Thermo Fisher R705-07) cells were cultured in DMEM (low glucose; Life Technologies 10567022) supplemented with 10% heat-inactivated fetal bovine serum (Life Technologies 10438-034), 100 units/ml penicillin, 100µg/ml streptomycin (Life Technologies 15140122), and 1:1,000 chemically defined lipid supplement (Life Technologies 11905031) and were held at 37˚C with a humidified atmosphere and 5% CO_2. Cells were passaged twice weekly diluting the stock suspension 1 in 5 after dissociation in TrpLE (Life Technologies 12604039). HEK293A cells with endogenous PIP5K1A alleles tagged with NeonGreen2 (NG2) were generated similarly as described (*430*) using a protocol we have described (*323*). In brief, Platinum Cas9 (Thermo Fisher B25640) was precomplexed with gRNA and electroporated into HEK293A cells in combination with a single-stranded HDR Template (IDT). HDR sequence is provided in **Table 3.2**. The HDR template contains 70 bp homology-arms, the NG2 sequence, and a flexible linker in frame with PIP5K1A. After cells recovered, FACS (University of Pittsburgh Flow Cytometry Core) was used to sort NG2-positive cells. These NG2-PIP5K1A (ePIP5K1A) cells were cultured under identical conditions to the HeLa and HEK293A cells.

3.5.2 Chemicals and reagents

Rapamycin (Thermo Fisher BP2963-1) was dissolved in DMSO at 1 mM and stored as a stock at -20˚C, it was used in cells at 1 µM. EGTA (VWR EM-4100) was dissolved in water at 0.5

M and stored at room temperature, it was used in cells at 5 mM. Ionomycin (EMD Millipore 407952) was dissolved in DMSO at 10 mM and stored as a stock at -20˚C, it was used in cells at 10 μM. Dibucaine (Sigma D0638) was dissolved in DMSO at 200 mM and stored as a stock at -20˚C, it was used in cells at 5 mM.

3.5.3 Plasmids and cloning

The EGFP (Aequorea victoria GFP containing F64L and S65T mutations) (*319*), mCherry (Discoma DsRed monomeric variant) (*320*), mTagBFP2 (Entacmaea quadricolor protein eqFP578) (*321*), and iRFP713 (Rhodopseudomonas palustris [Rp] bacteriophytochrome BphP2) (*322*) fluorophores were used in the Clontech pEGFP-C1, -C2, and -N1 backbones as described previously (*323*). Mutated constructs were generated using site-directed mutagenesis using targeted pairs of DNA oligos which were custom made and supplied by Thermo Fisher. New plasmids used in this study were generated using standard restriction-ligation or by using NEBuilder HiFi DNA Assembly (New England Biolabs E552OS). Otherwise, plasmids were obtained from the sources listed in Table 1. All constructs were sequence verified using Sanger DNA sequencing. Plasmids constructed for this study will be available through Addgene.

3.5.4 Microscopy

For all live-cell imaging experiments, cells were imaged in 1.6 mL of experiment specific imaging media. Base imaging media contained FluoroBrite DMEM (Life Technologies A1896702) supplemented with 25 mM HEPES (pH 7.4) and 1:1000 chemically defined lipid supplement (SF CHIM). Media was then further supplemented with either 10% fetal bovine serum

(CHIM) or 0.1% BSA (0.1% BSA CHIM). Alternatively, Ca^{2+} free Ringer's solution (Ca^{2+} Free) was used, containing 160 mM NaCl, 2.5 mM KCl, 1 mM $MgCl_2$, 8 mM glucose and 10 mM NaHEPES, pH 7.5. For treatments, 0.4 mL of experiment specific imaging media containing fivefold final concentration of compound was applied to the dish (or 0.5 ml for a second addition).

Confocal imaging was performed on a Nikon TiE A1R platform with acquisition in resonant mode with a 100x 1.45 NA plan-apochromatic objective. The signal-to-noise ratio was improved by taking 8 or 16 frame averages. Excitation of fluorophores was accomplished using a dual fiber-coupled LUN-V laser launch with 405-nm (BFP), 488-nm (EGFP and NG2), 561-nm (mCherry), and 640-nm (iRFP) lines. Emission was collected on four separate photomultiplier tubes with blue (425-475 nm), green (500-550 nm), yellow/orange (570-620 nm), and far-red (663-737 nm) filters. Blue and yellow/orange channels were recorded concurrently, as were green and far-red. The confocal pinhole was defined as 1.2x the Airy disc size of the longest wave-length channel used in the experiment. Nikon Elements denoising software was used to further enhance the signal-to-noise ratio.

For TIRFM and single-molecule imaging (SMol), a separate Nikon TiE platform coupled with a Nikon TIRF illuminator arm and 100x 1.45 NA plan-apochromatic objective was used. Excitation of fluorophores was accomplished using an Oxxius L4C laser launch with 405-nm (BFP), 488-nm (EGFP and NG2), 561-nm (mCherry), and 638-nm (iRFP) lines. Emission was collected through dual-pass filters (Chroma) with blue (420-480 nm) and yellow/orange (570-620 nm) together, and green (505-550 nm) and far-red (650-850 nm) together. An ORCA-Fusion BT sCMOS camera (Hamamatsu) was used to capture images. For TIRF micrscopy, images were captured with 2x2 pixel binning. For SMol, the NG2 channel was excited with 20% power for 50

ms from the 488-nm laser in a 16x16 μm region of the PM. Images were registered in rolling shutter mode with 2x2 pixel binning with a 1.5x magnifier lens.

For all types of imaging, Nikon Elements software was used to acquire all images for all experiments and all data was saved with the ND2 file extension.

3.5.5 Image analysis

Analysis of all images was accomplished using Fiji software (*324*) using the LOCI BioFormats importer (*325*). Custom macros were written to generate channel-specific montages displaying all x,y positions captured in an experiment in concatenated series. In these montages, individual regions of interest (ROIs) were generated around displayed cells.

For confocal images, the ratio or fluorescence intensity between specific compartments was analyzed as described previously (*323*). In brief, a custom macro was used to generate a compartment of interest specific binary mask through à trous wavelet decomposition (*326*). This mask was applied to measure the fluorescence intensity within the given compartment while normalizing to the mean pixel intensity in the ROI.

For TIRFM images, a minimum intensity projection was used to generate ROIs within the smallest footprint of the cells. Background fluorescence was measured and subtracted from all images at all timepoints. The average pixel intensity in each frame (F_t) was normalized to the mean pixel intensity in the ROI of the time points before treatment (F_{pre}) to yield F_t/F_{pre}.

Quantitative data was imported into Prism 8 (GraphPad) for statistical analysis and the generation of graphs and plots. D'Agostino and Pearson normality tests showed data that significantly varied from normal distribution, data were then subjected to a nonparametric Kruskal-

Wallis test. If significant difference was found between sample medians, a post hoc Dunn's multiple comparison test was run.

Representative images were selected based on fluorescence measurements near the median of the sampled population, displayed typical morphology, and robust signal-to-noise ratio. If adjusting brightness or contrast, any changes were made across the entire image.

3.5.6 Single Molecule Analysis using Thunderstorm

Mean photon count was estimated using the Fiji ThunderSTORM plugin (*431*). Either HEK293A cells expressing PH-PLCδ1-mNG2x1-3 or ePIP4K2C cells were imaged using SMol settings. Raw images were run through Fiji using the ThunderSTORM plugin. Settings for molecule localization were determined using a wavelet filter with a local maximum method and integrated Gaussian point spread function. To determine fluorescence intensity per spot, histograms of photon counts, in each condition, were generated using a 5-photon bin size.

Table 3.1 Plasmids used in this study

Plasmid	Vector	Insert	Reference
EGFP	pEGFP-C1	EGFP	This study
EGFP-PIP5K1A	pEGFP-C1	EGFP:PIP5K1A	This study
EGFP-PIP5K1A^{D322K}	pEGFP-C1	EGFP:PIP5K1A(D322K)	This study
EGFP-PIP5K1B	pEGFP-C1	EGFP:PIP5K1B	This study
EGFP-PIP5K1B^{D266K}	pEGFP-C1	EGFP:PIP5K1B(D266K)	This study
EGFP-PIP5K1C	pEGFP-C2	EGFP:PIP5K1C	(*432*)
EGFP-PIP5K1C^{D316K}	pEGFP-C2	EGFP:PIP5K1C(D316K)	(*432*)
TagBFP2	pTagBFP2-C1	mTagBFP2	This study
TagBFP2-PIP4K2A	pTagBFP2-C1	mTagBFP2:PIP4K2A	(*60*) This study
TagBFP2-PIP4K2A^{D273K}	pTagBFP2-C1	mTagBFP2:PIP4K2A(D273K)	This study
EGFP-PIP5K1A_Kina	pEGFP-C1	EGFP:PIP5K1A(81-450)	This study
EGFP-PIP5K1A_KinaCTail	pEGFP-C1	EGFP:PIP5K1A(81-562)	This study
EGFP-PIP5K1A_Kina^{++}	pEGFP-C1	EGFP:PIP5K1A(81-452)	This study
Lyn$_{11}$-FRB-iRFP	piRFP-N1	LYN(1-11):MTOR(2021-2113):iRFP	(*408*)
mCherry-FKBP-PJ	pmCherry-C1	mCherry:FKBP1A(3-108):[GGSA]$_4$GG: SACM1L(2-517):INPP5E(214-644)	(*408*)
mCherry-FKBP-INPP5E	pmCherry-C1	mCherry:FKBP1A(3-108):[GGSA]$_4$GG:INPP5E(214-644)	(*408*)
mCherry-FKBPSAC1$^{\Delta TMD}$	pmCherry-C1	mCherry:FKBP1A(3-108):[GGSA]4GG:SACM1L(1-521)	(*407*)
mRFP-FKBP-PLCß3	pmRFP-C1	RFP:FKBP1A(3-108):[GGSA]$_4$GG:PLCB3(10-848Δ472-585)	This study
EGFP-PIP5K1C_Kina	pEGFP-C2	EGFP:PIP5K1C(79-444)	This study
EGFP-PIP5K1C_KinaCTail	pEGFP-C2	EGFP:PIP5K1C(79-640)	This study
EGFP-PIP5K1C_Kina^{++}	pEGFP-C2	EGFP:PIP5K1C(79-446)	This study
EGFP-PIP5K1C_Kina^{++}ΔIns	pEGFP-C2	EGFP:PIP5K1C(79-446Δ328-376)	This study
EGFP-PIP5K1C_Kina^{++}ΔAct	pEGFP-C2	EGFP:PIP5K1C(79-446Δ401-424)	This study
Tubby$_C$-mCherry	pmCherry-N1	*Mus musculus* Tub(243-505):mCherry	(*405*)
Tubby$_C^{R332H}$-mCherry	pmCherry-N1	*Mus musculus* Tub(243-505)(R332H):EGFP	(*405*)
Tubby$_C$-TagBFP2	TagBFP2-N1	*Mus musculus* Tub(243-505):mCherry	(*405*)
Tubby$_C^{R332H}$- TagBFP2	TagBFP2-N1	*Mus musculus* Tub(243-505)(R332H):EGFP	(*405*)

Table 3.2 HDR sequence for PIP5K1A

Gene	HDR sequence
PIP5K1A	gtattaaatgttttgtgatattcgacaccttaacgtctctgacttgacaccagtactcccgcagagagttctttcctgggttaggaatttcagaggactt ggcggaccgactcttgtcccgagttcagatcactcgacccagtcctagcaaagaactgaacctaagaggacctgccgagccaccgtagggact gtcggccaacccgcgcgcgcacatcttccacccgtggactcgtcagggcgtgaggacccacctcacgtgaccattagcagcctcccgattggtt ttgctccttttttctccccaatgagtgggctgatgccccgagaaggtcgggcgcatgcgcagtgctcggatttttgcttggctacccggagtgaag cggccgggttgggcgattaacaggccgtggttaggaaggacggagaaggggcgttcgctcctttgggacttttcatgcctcgtttttttttcagatg tggcttggtctgggcgcaaggtcccagcagccagcttaagcttactcttctgtgaaaggggaaagtatcccctgtggaaagcggttaaacttgtgg agggggtgcgggacgtgagttcttccccatgccaggcgaatggtgtggccttgagctggtccaggagccggctcgacgtgtctgagggaggc cccggaggggggcggggaggtggcccacagaacgcgggttctgtaaagagacgttgggaagattcgattccgagaagaggaagaaccggatt gaaagagagccaggccgctgaggggggaggggctgctaagATGGTGAGCAAGGGCGAGGAGGATAACATGG CCTCTCTCCCAGCGACACATGAGTTACACATCTTTGGCTCCATCAACGGTGTGGACTTT GACATGGTGGGTCAGGGCACCGGCAATCCAAATGATGGTTATGAGGAGTTAAACCTGA AGTCCACCAAGGGTGACCTCCAGTTCTCCCCCTGGATTCTGGTCCCTCATATCGGGTAT GGCTTCCATCAGTACCTGCCCTACCCTGACGGGATGTCGCCTTTCCAGGCCGCCATGGT AGATGGCTCCGGATACCAAGTCCATCGCACAATGCAGTTTGAAGATGGTGCCTCCCTTA CTGTTAACTACCGCTACACCTACGAGGGAAGCCACATCAAAGGAGAGGCCCAGGTGAA GGGGACTGGTTTCCCTGCTGACGGTCCTGTGATGACCAACTCGCTGACCGCTGCGGACT GGTGCAGGTCGAAGAAGACTTACCCCAACGACAAAACCATCATCAGTACCTTTAAGTG GAGTTACACCACTGGAAATGGCAAGCGCTACCGGAGCACTGCGCGGACCACCTACACC TTTGCCAAGCCAATGGCGGCTAACTATCTGAAGAACCAGCCGATGTACGTGTTCCGTAA GACGGAGCTCAAGCACTCCAAGACCGAGCTCAACTTCAAGGAGTGGCAAAAGGCCTTT ACCGATGTGATGGGCATGGACGAGCTGTACAAGGGTGGCGGCgcgtcggcctcctccgggccgtcgt cttcggtcggtttttcatcctttgatcccgcggtcccttcctgtaccttgtcctcaggtaagcccggcagggcgtgggtagggagctggtgaggaat atgcgatgggaggaagagcgagacctaagagggtacctgtagctgggaatgtcctacgtgttaccggtaagtgggcgcgagctgggctttcaa atagggatttatgagcgggcaggagtttgaggaaaggataagtttgattaagaagttgtcgaaaactttggttgtctttgaggaggacggatggag attgaaggtgggggtagggtggcccggcgcggtggctcacgcctgtaatctcagcactttgggaggccttggcgggcggatcatttgaggtca gaagttcgagacgagcctggccaacatagagaaatctcgtccctactaaaaatacaaaaattatccggacagtagtggcgtgcatctgtaatccc agctacttgggaggctgaggcaggataatcccttgagcctgggaggcagagcttgcggtgagccgagattgggccactgctctccagtctggg cgagagagtgagaccctgtctcaaaaaaaTaaaaaaagaagttgcggtaggaaacaagagaaacggaagggagtagagaaactaagaaag taaatggaggcctaagaagtagagagaactacttagtgtgagaggcaggtggaatctaagttgattgtgggctaattggatgaaaatgttgaaga gaagccatgggacttaaaagata

4.0 A novel negative feedback mechanism tempers $PI(4,5)P_2$ synthesis at the PM

The text in this chapter, at the time of this dissertation submission, is expanded from a manuscript currently under review at Review Commons.

4.1 Overview

The lipid molecule phosphatidylinositol (4,5)-bisphosphate ($PI(4,5)P_2$) controls many aspects of plasma membrane (PM) function in animal cells, from membrane selective permeability to the attachment of the cytoskeleton. Although disruption of $PI(4,5)P_2$ is associated with a wide range of diseases, it remains unclear how cells sense and maintain $PI(4,5)P_2$ levels to support various cell functions. Here, we show that the PIP4K family of enzymes that synthesize $PI(4,5)P_2$ via a minor pathway also function as sensors of tonic $PI(4,5)P_2$ levels, inactivating synthesis of the lipid via interaction with the major PIP5K-catalyzed pathway when $PI(4,5)P_2$ levels rise. Perturbation of this simple homeostatic mechanism reveals differential sensitivity of $PI(4,5)P_2$-dependent signaling to elevated $PI(4,5)P_2$ levels. These findings reveal that a subset of $PI(4,5)P_2$-driven functions may drive diseases associated with disrupted $PI(4,5)P_2$ homeostasis.

4.2 Introduction

The lipid molecule phosphatidylinositol-4,5-bisphosphate ($PI(4,5)P_2$) is a master regulator of animal cell plasma membranes (PMs). By recruiting or activating scores of membrane proteins,

it controls the transport of ions and solutes across the membrane (*8*, *409*), attaches the underlying cytoskeleton (*411*), regulates the traffic of proteinaceous cargo to and from the membrane (*410*), disseminates extracellular signals (*409*), facilitates the entry, assembly and egress of bacterial and viral pathogens (*409*, *433*), and serves as a substrate for the generation of second messengers such as (IP_3), diacylglycerol (DAG) (*36*), and ($PI(3,4,5)P_3$) (*100*, *413*). As a result, the capacity to synthesize $PI(4,5)P_2$ is essential for life in mammals (*434*, *435*). Nonetheless, genetic defects occur in humans that either increase or decrease $PI(4,5)P_2$ levels, disrupting cellular physiology in unpredictable ways. These manifest in diseases ranging from cancer (*436*) to kidney disease (*437*) to dysentery (*438*) Clearly, there is a central physiological imperative to tightly control $PI(4,5)P_2$ levels for harmonious PM function. Yet, a detailed homeostatic mechanism that can sense and maintain $PI(4,5)P_2$ levels has proven elusive to date.

In mammals, $PI(4,5)P_2$ can be synthesized by the phosphorylation of either phosphatidylinositol 4-phosphate (PI4P) or phosphatidylinositol 5-phosphate (PI5P). There are two families of lipid kinases responsible for production of $PI(4,5)P_2$ (*62*, *63*, *69*, *416*) The first family is phosphatidylinositol 5-phosphate 4-kinase (PIP4K) which phosphorylates PI5P at the 4-OH position of the inositol ring (*37–39*). As PI5P comprises a relatively minor portion of the phosphatidylinositol phosphate pool (*9*, *57*), it is thought that PIP4K is not the main route for synthesis of $PI(4,5)P_2$ (*39*). Loss of PIP4K has been implicated in increased insulin sensitivity (*439*), PI3K signaling (*440*), and TORC1 signaling (*441*). On the other hand, increased expression of PIP4K has been observed in breast cancer (*442*). Taken together, this work suggests that PIP4K may play a role in PI3K signaling.

The second family of kinases responsible for $PI(4,5)P_2$ production is the phosphatidylinositol 4-phosphate 5-kinase (PIP5K) which phosphorylates PI4P on the 5-OH

position of the inositol headgroup (*62–65*). PIP5K is associated with the PM due to electrostatic interactions (*71*), substrate binding (*72*, *73*, *292*) product interaction (*92*, *418*), and directly embeds into the membrane (*42*). Evidence has suggested that the PIP5K-PI(4,5)P_2 interaction functions as a positive feedback mechanism for PI(4,5)P_2 synthesis at the PM (*92*, *418*). On the other hand, upon PLC mediated PI(4,5)P_2 depletion and resynthesis, the level of PI(4,5)P_2 recovers before PI4P levels (*124*, *419*). Furthermore, the levels of PI(4,5)P_2 reach a plateau, while PI4P levels continue to rise, suggesting that PIP5K is also negatively regulated. However, this mechanism of negative regulation has not been identified. Here, we identify a potential mechanism by which PIP5K is inhibited by a direct interaction with PIP4K which acts as a low affinity PI(4,5)P_2 sensor.

4.3 Results

4.3.1 Reciprocal regulation of PM PI(4,5)P_2 levels by PIP5K and PIP4K

The yeast PIP5K homolog, multicopy suppressor of Stt4 mutation (Mss4) (*66*, *67*), has an interesting and well characterized negative regulatory system. Opy1, a tandem PH domain containing protein, acts as a coincidence detector for both PI(4,5)P_2 and Mss4 (*67*). Opy1 is recruited to the PM in a PI(4,5)P_2 dependent manor and is then able to negatively regulate Mss4 mediated PI(4,5)P_2 synthesis (*67*). To date, the mechanism of regulation similar to that of Mss4 has yet to be detected in mammals. To elucidate the negative feedback mechanism, we initially, independently, over-expressed all three isoforms of human PIP5K (A,B,C) (*64*, *65*, *68*, *69*). We observed any differences in PI(4,5)P_2 by using a low affinity Tubby$_C^{R332H}$ biosensor (*316*). The over-expression of PIP5K, responsible for phosphorylating PI4P, is predicted to increase PI(4,5)P_2

at the PM. Indeed, confocal imaging revealed the expected increase in $PI(4,5)P_2$ at the PM upon Mss4 or PIP5K expression (*84*, *443*, *444*), compared with an EGFP control (**Figure 4.1A**). We next sought to compare active PIP5K with the expression of a catalytically dead mutant (*74*, *292*, *422*). Expression of $Mss4^{D636K(CatDead)}$ yielded expected results that mimic the control - the mean $PI(4,5)P_2$ ratio did not increase - indicating that there was no $PI(4,5)P_2$ production. Unexpectedly, over-expressed mammalian $PIP5K^{CatDead}$ constructs ($PIP5K1A^{D322K}$, $PIP5K1B^{D266K}$, and $PIP5K1C^{D316K}$) resulted in a striking increase in $PI(4,5)P_2$ levels at the PM, which nearly mimicked that of the active enzymes. After similarly puzzling observations were made upon knocking out the PIP4K family by Wang et al (*56*), we performed over-expression experiments of PIP4K to observe changes in $PI(4,5)P_2$ levels at the PM. As PIP4K is expected to produce $PI(4,5)P_2$ from PI5P (**Figure 4.1B, left**), we still expected to see increased PM $PI(4,5)P_2$ levels. Conversely, when PIP4K enzymes were over-expressed in HeLa cells, we observed the opposite effect on $PI(4,5)P_2$. The PM/cell ratio of $Tubby_C^{R332H}$ was lower than control, and more closely matched the effect of over-expressed INPP5E, a $PI(4,5)P_2$ phosphatase (**Figure 4.1B**). $PIP4K2A^{D273K(CatDead)}$ over-expression also resulted in the same changes in $PI(4,5)P_2$ as the catalytically active versions, indicating that the effects on PI(4,5)P2 are not dependent on catalytic activity of either PIP5K or PIP4K. These observations, along with those made by (*53*, *56*) led us to further hypothesize that PIP4K interacts with and inhibits the activity of PIP5K. In our system, over-expressed $PIP5K^{CatDead}$ sequesters endogenous PIP4K leaving endogenous PIP5K to continue to produce $PI(4,5)P_2$ without negative regulation (**Figure 4.1C**).

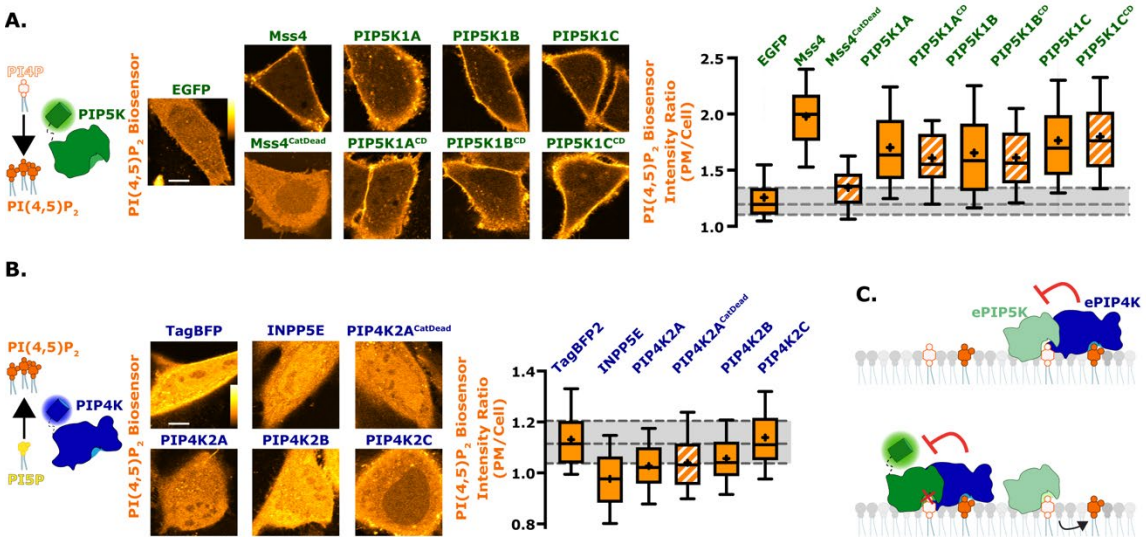

Figure 4.1 Reciprocal regulation of PM PI(4,5)P_2 levels by PIP5K and PIP4K.

(**A**) PIP5Ks increase PM PI(4,5)P_2 independently of catalytic activity. Cartoon denotes the catalytic activity of PIP5K. Images show equatorial confocal sections of HeLa cells expressing the low affinity $Tubby_C^{R332H}$ PI(4,5)P_2 sensor (orange), co-transfected with EGFP-tagged catalytically active or dead PIP5K constructs (yeast Mss4 or mammalian A, B, or C isoforms), or EGFP alone as control. Increased PI(4,5)P_2 is apparent from increased $Tubby_C^{R332H}$ fluorescence in the PM. Box and whisker plots show the mean fluorescence intensity ratio (PM/cell) of the PI(4,5)P_2 sensor from >90 cells imaged across at least three independent experiments (boxes displaying median and interquartile range, whiskers representing 10-90% of data and "+" represents mean), scale bar is 10 µm. (**B**) PIP4Ks decrease PM PI(4,5)P_2 independently of catalytic activity. Cartoon shows the catalytic activity of PIP4K. Images show PI(4,5)P_2 sensor in HeLa cells as in A, co-transfected with different PIP4K isoforms (A, B, C), catalytically dead PIP4K2A or a PI(4,5)P_2 5-phosphatase(pptase) (INPP5E). Box and whiskers from >90 cells imaged across at least three independent experiments as in A, scale bar is 10 µm. (**C**) Proposed inhibition of ePIP5K (endogenous PIP5K) by ePIP4K. With the overexpression of a fluorescently tagged version of PIP5K, regardless of catalytic activity, ePIP4K is sequestered. This relieves endogenous PIP5K from inhibition, increasing PI(4,5)P_2 levels.

4.3.2 PIP4K attenuates PIP5K kinase activity

In each of the previous experiments we over-expressed solely PIP5K or PIP4K, which would likely saturate the feedback mechanism proposed in **Figure 4.1C**. To better balance the established over-expression system, we visualized changes in $PI(4,5)P_2$ levels in cells expressing PIP5K or PIP4K or both PIPKs in combination. As we had previously observed, the PIP5K expression resulted in increased $Tubby_C^{R332H}$ localization at the PM and PIP4K expression resulted in a reduction of $Tubby_C^{R332H}$ PM association (**Figure 4.2A**). When PIP5K isoforms were expressed with any PIP4K isoform there was a reduction in $Tubby_C$ localization at the PM when compared to PIP5K overexpression alone (**Figure 4.2A**). This provides further evidence that the inhibitory effect we see on PIP5K by PIP4K is due to a protein mass effect, rather than exclusively catalytic activity.

To test real-time negative regulation of PIP5K activity by PIP4K, we triggered PM recruitment of cytosolic, FKBP-tagged PIP4K by chemically induced dimerization (CID) with a membrane targeted FRB domain, using rapamycin (*154*) (**Figure 4.2B, cartoon**). For these experiments we used $Tubby_C$ (*316*), a high affinity $PI(4,5)P_2$ sensor, to more easily visualize decreases in $PI(4,5)P_2$ levels at the PM. Within minutes of PM recruitment, all three isoforms of PIP4K induced a steady decline in PM $PI(4,5)P_2$ levels (**Figure 4.2B**). Finally, we recruited $PIP4K2A^{CatDead}$ and, as in **Figure 4.1** we observed the same decrease in PM localized $Tubby_C$ (**Figure 4.2B**). This further indicated that PIP4K was able to inhibit both the production and maintenance of PM $PI(4,5)P_2$, and this was not dependent on enzymatic activity.

To measure PIP4K2A dependent inhibition of PIP5K1A activity biochemically, we turned to our collaborator, Scott Hansen, who established a TIRF microscopy based assay to monitor the kinetics of $PI(4,5)P_2$ production in real time on supported lipid bilayers (SLBs) (*418*). Lipid

phosphorylation reactions catalyzed by PIP5K1A proceeded until completion, as indicated by the plateau in membrane binding intensity of a $PI(4,5)P_2$ biosensor, PH-PLCδ1 (**Figure 4.2C**). In the presence of PIP4K2A, we observed a nearly 2-fold increase in the time required for PIP5K1A dependent lipid phosphorylation reactions to plateau. Furthermore, the presence of PIP4K2A caused the PIP5K1A lipid phosphorylation reaction to exhibit biphasic reaction kinetics. The onset of PIP5K1A inhibition was delayed until a threshold density of approximately 2% $PI(4,5)P_2$ was generated (**Figure 4.2C**). In contrast, lipid phosphorylation reactions catalyzed by Mss4 were unaffected by PIP4K2A (**Figure 4.2C, inset**). This indicates inhibition of PIP5K1A is not simply due to PIP4K2A membrane binding and sequestration of PPIns lipids, which have been shown to modulate PIP5K1A membrane recruitment and activity (*275*, *418*). These data also indicate that PIP5K1A rapidly and efficiently converts PI4P to $PI(4,5)P_2$, but the inclusion of PIP4K2C, even in a purified system, slows this reaction. Taken together, this indicates that PIP4K over-expression seems to negatively regulate PM $PI(4,5)P_2$ levels, in both cells and SLBs.

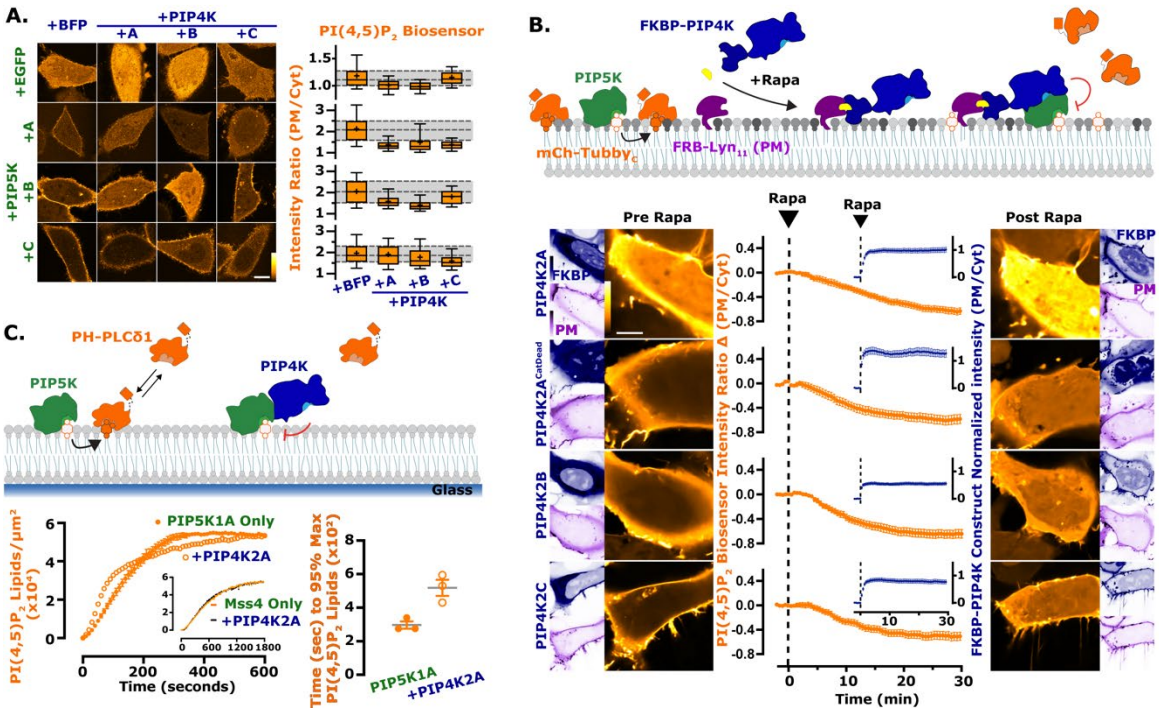

Figure 4.2 The activity of PIP5K is blunted by PIP4K.

(**A**) PIP4Ks antagonize PIP5K-mediated PI(4,5)P_2 increases. HeLa cells expressing PI(4,5)P_2 indicator Tubby$_C^{R332H}$ (orange) were co-transfected with the indicated EGFP- or TagBFP2-tagged constructs. Images show confocal equatorial sections of representative cells. Box and whiskers from 90 cells imaged across at least three independent experiments, displayed as in A, scale bar is 10 μm. (**B**) PIP4K recruitment acutely inhibits PM PI(4,5)P_2 levels. Cartoon schematics show the chemically induced dimerization (CID) system for FKBP-tagged PIP4K isoforms (A, B, C), which dimerize with the PM-anchored FRB-Lyn$_{11}$ upon the addition of rapamycin (rapa). HEK293A cells were transfected with FKBP-tagged proteins, the high affinity PI(4,5)P_2 indicator Tubby$_C$ and FRB-Lyn$_{11}$. During time-lapse confocal microscopy, cells were stimulated with 1 μM rapa as indicated. Graphs represent mean change in PI(4,5)P_2 sensor intensity ratio (PM/cell) ± s.e. for 35-60 cells imaged across three independent experiments, scale bar is 10 μm. (**C**) PIP4K2A attenuates the kinetics of PI(4,5)P_2 production driven by PIP5K1A, but not Mss4. Kinetics of PI(4,5)P_2 production measured on SLBs in the presence of 1 nM PIP5K1A, 20 nM PH-PLCδ1, +/- 50 nM PIP4K2A. Inhibition of PIP5KA activity is delayed until a threshold density of approximately 2% PI(4,5)P_2 is created to support membrane recruitment of PIP4K2A. Inset shows kinetics of reactions executed in the presence of 50 nM Mss4, 20 nM PH-PLCδ1, +/- 50 nM PIP4K2A. Initial membrane composition: 76% DOPC, 20% DOPS, 4% PI4P. Right graphs show the quantification of time required for reactions to reach 95% completion (n = 3 technical replicates).

4.3.3 Endogenous PIP4K2C is localized at the PM

The over-expression of proteins can skew experimental observations in many ways (*307*) To probe the interaction of endogenous PIP4Ks with PM $PI(4,5)P_2$, we used a split fluorescent protein approach (*407*, *445*, *446*) to add a NeonGreen2 (NG2) tag to PIP4K2C, the most abundant PIP4K in HEK293A cells (*52*) (**Figure 4.3A**). We used HEK293A cells stably over-expressing NG1-10 ($293^{NG1\text{-}10}$). We then edited these cells to add the NG11 tag to the N-terminus of the PIP4K2C protein. Successful integration of the split NG2 tag was evident at both the genomic and protein levels (**Figure 4.3A**). The ePIP4K2C cells were genotyped using a NG11-specific forward primer and a PIP4K2C specific reverse primer to produce an expected amplicon of ~200 bp in the edited, but not the parental HEK293ANG cell line (**Figure 4.3A**). Similarly, using a PIP4K2C specific antibody, we probed both HEK293A and ePIP4K2C cells and observed the expected ~3 kDa increase in molecular weight with the addition of the NG11 tag. As expected, endogenous ePIP4K2C has a mainly cytosolic distribution when viewed in confocal, with a slight enrichment at the cell periphery (**Figure 4.3B**). More specifically, we also observed a slight enrichment in fluorescence intensity of ePIP4K2C at the PM (**Figure 4.3B**). Analysis of the ventral PM by TIRFM revealed individual, diffraction-limited and uniform intensity puncta that were dynamically associated with the membrane (**Figure 4.3C**). We compared the intensity of these puncta in ePIP4K2C cells to cells expressing a $PI(4,5)P_2$ biosensor tagged with single, tandem-dimer or -trimer mNeonGreen expressed at single molecule levels (PHmNGx*N*). This revealed that the NG2-PIP4K2C puncta contained an average of 1.64 NG molecules, consistent with dimeric PIP4K2C complexes (*41*) containing either one or two NG2-tagged protein copies (**Figure 4.3C**). It is likely that a single allele or two of three alleles in HEK293A cells may have been tagged in our cell line, yielding a combination of monomeric and dimeric structures (*447*). As we

observed the presence of ePIP4K2C at the PM, we sought to determine the mechanism by which this localization occurred.

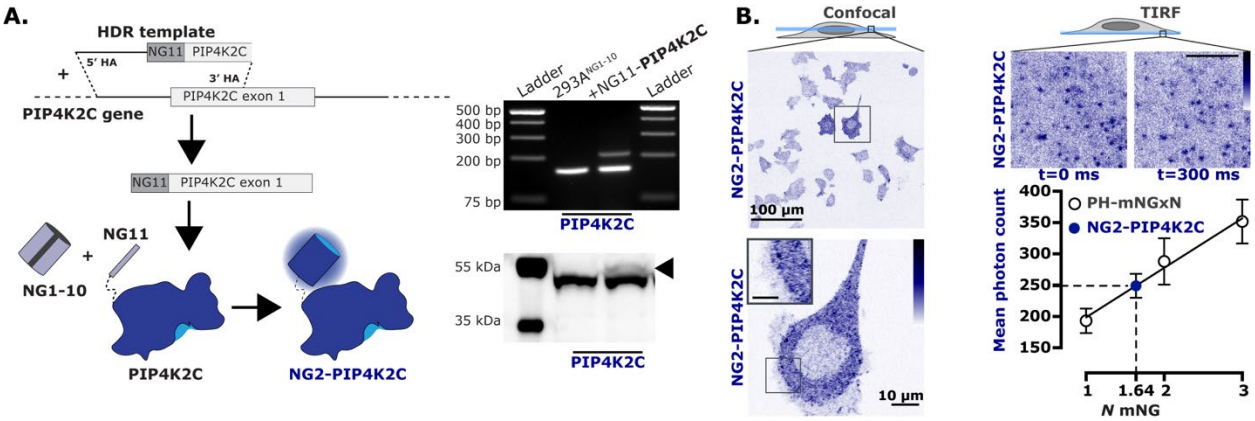

Figure 4.3 Endogenously tagged PIP4K2C is partly associated with the PM.

(**A**) Endogenous tagging of PIP4K2C. Brief cartoon schematic showing the mechanism of endogenous tagging employed for PIP4K2C with mNeonGreen2 (NG2). The resulting cell line was termed NG2-PIP4K2C. Cells were genotyped with a mNG specific forward primer and a PIP4K2C specific reverse primer yielding an edited product of ~200bp. Cells were also probed with a PIP4K2C specific antibody showing the expected ~3 kDa shift in weight (arrowhead). (**B**) Image based characterization of NG2-PIP4K2C. Confocal images display the NG2-PIP4K2C (blue) in cells localized mainly to the cytosol, but the zoomed in image shows slight association of the enzyme to the PM. When imaged live by TIRF, dynamic, diffraction limited spots are observed on the membrane (compare differential localization at 0 and +0.3 s). These have an intensity consistent with a mixed population of 1 or 2 mNG molecules when calibrated against single, dimeric or trimeric mNG molecules fused to a PI(4,5)P_2 binding domain (graph). This correlates to the mean photon count of a heterogeneously tagged cell population (single or double alleles tagged with NG11), scale bar is 2.5 µm unless otherwise annotated.

4.3.4 PI(4,5)P_2 is required for membrane association of PIP4K2A

Given the dynamic PM localization of ePIP4K2C, we set out to determine if 1) PIP4K can directly interact with PI(4,5)P_2 (the enzymatic product) on the PM, or 2) PIP4K interacts directly with PIP5K at the PM. We have previously established three criteria to use to determine whether

lipid binding proteins, specifically biosensors (*123*, *305*), interact selectively with a given lipid. In brief, is the protein binding specific for the target lipid? Is the localization dependent on that lipid? And, if it is dependent, is the lipid alone sufficient to localize the protein? To determine whether PIP4K2C was localized in a $PI(4,5)P_2$ dependent manner, we utilized the CID system to recruit INPP5E (5E) to the PM. Using TIRF microscopy, we observed a rapid loss of the $PI(4,5)P_2$ biosensor, $Tubby_C$, fluorescence upon recruitment of INPP5E (**Figure 4.4A**). We also observed a loss of ePIP4K2C puncta from the PM upon recruitment of INPP5E (**Figure 4.4A**). On the other hand, we recruited $INPP5E^{D477N}$($5E^{CatDead}$) (*448*, *449*) and observed no changes in either $Tubby_C$ fluorescence or ePIP4K2C puncta at the PM. Parallel to live-cell imaging experiments, Scott Hansen measured the dynamics of PIP4K2A membrane dissociation on SLBs. PIP4K2A and PH-PLCδ1 were allowed to equilibrate on supported membranes containing 4% $PI(4,5)P_2$. To test whether stable membrane association of PIP4K2A requires $PI(4,5)P_2$ after membrane docking, inositol polyphosphate-5-phosphatase (OCRL) was added to catalyze the dephosphorylation of $PI(4,5)P_2$. This resulted in the rapid dissociation of PIP4K2A and PH-PLCδ1 (**Figure 4.4B**). Taken together, these data suggest that PM localization of ePIP4K2C is dependent on $PI(4,5)P_2$.

We have also previously established that a critical criterion for lipid binding selectivity is whether the lipid alone is sufficient to drive localization (*123*, *305*, *318*). To test this, we generated a recruitable mutant of the previously used PIP5K1C. We generated a truncation of PIP5K1C which contained only the kinase domain, as well as the homodimeric mutant $PIP5K1C\_Kina^{D101R/R304D}$ (PIP5K1C-HD) (*70*). Again, using the CID system, we recruited PIP5K1C-HD to the PM and, with confocal, observed an increase in PM association of $Tubby_C^{R332H}$ over time (**Figure 4.4C**). Similarly, there was a concomitant increase in ePIP4K2C intensity at the PM (**Figure 4.4C**). To test if PIP4K recruitment was dependent upon PIP5K

activity, we generated a similar catalytically inactive mutant as previously described, PIP5K1C_Kina$^{D101R/R304D/D316K}$ (PIP5K1C-HD^{CatDead}) (*70*, *74*). We similarly recruited this construct to the PM and observed no changes in Tubby$_C^{R332H}$ localization (**Figure 4.4C**). Additionally, here were no measurable increases in ePIP4K2C localization (**Figure 4.4C**), indicating that ePIP4K2C localizes to the PM in a manner that was dependent on catalytic activity of the PIP5K.

Utilizing the PIP5K construct does not fully discern whether PI(4,5)P_2 alone is sufficient for PIP4K PM localization, as these two proteins may directly interact. We next used our Mss4 constructs to similarly increase PM PI(4,5)P_2 levels. With the over-expression of Mss4 we observed an increase in ePIP4K2C at the PM, but there was no change in ePIP4K2C localization with the Mss4^{CatDead} construct (**Figure 4.4D**). Finally, Scott Hansen visualized interactions between purified PIP4K2A and SLBs in the presence of varying densities of PI(4,5)P_2 lipids. We observed highly cooperative PIP4K2A membrane recruitment when Mss4 was added to SLBs to catalyze the production of PI(4,5)P_2 (**Figure 4.4E**). Here, these data suggest that increased PM PI(4,5)P_2 is sufficient to localize ePIP4K2C.

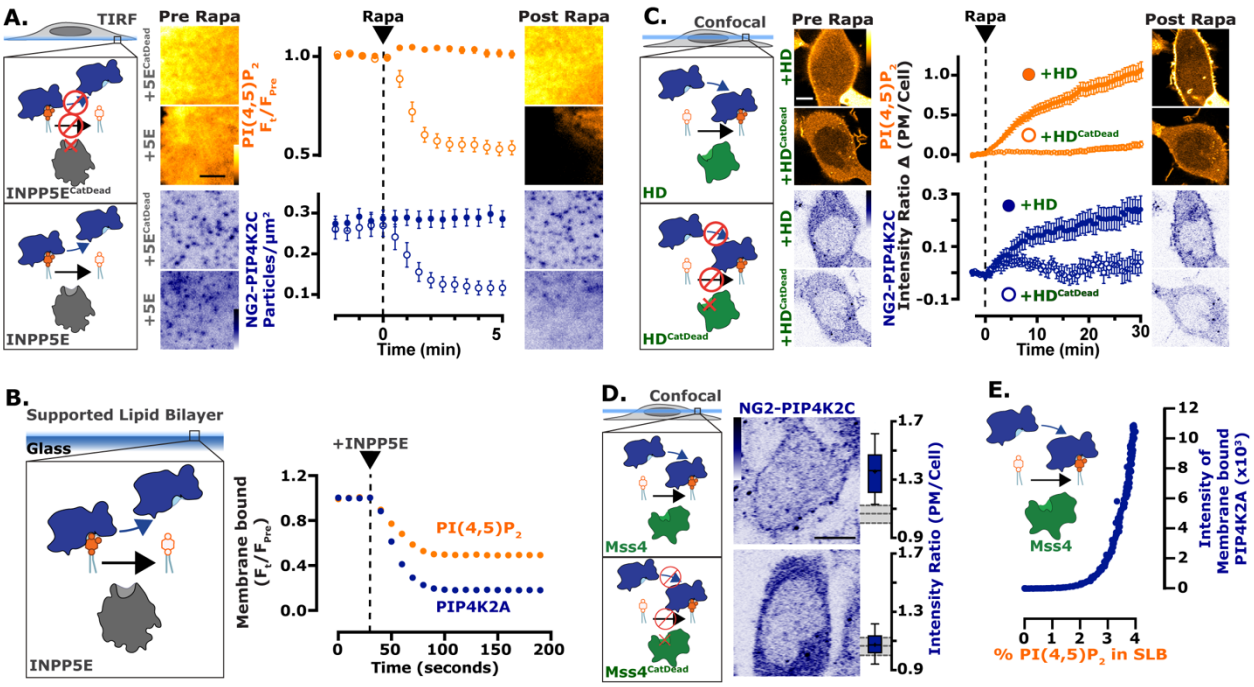

Figure 4.4 PI(4,5)P2 is necessary and sufficient for the PM localization of PIP4K.

(**A**) Depletion of PI(4,5)P_2 causes PIP4K2C (eNG and purified) to dissociate from the membrane. Cartoons show the CID system, in TIRF, for FKBP-tagged INPP5E (catalytically active or dead) dimerizing with the PM-anchored Lyn_{11}-FRB. NG2-PIP4K2C (blue) cells were transfected with FKBP-tagged proteins, the high affinity PI(4,5)P_2 indicator $Tubby_C$ (orange) and Lyn_{11}-FRB. During time-lapse TIRF microscopy, cells were stimulated with 1μM rapa, as indicated. $Tubby_C$ traces represent mean change in fluorescence intensity (F_t/F_{pre} normalized to pre-stimulation levels) ± s.e. The NG2-PIP4K2C traces represent the mean change in puncta per μm^2 ± s.e. of 36-37 cells that were imaged across three independent experiments, scale bar is 2.5 μm. (**B**) Imaging chambers containing 50 nM PIP4K2A and 20 nM PH-PLCδ1 at equilibrium with SLBs composed of 96% DOPC and 4% PI(4,5)P_2 were visualized by TIRF microscopy. At 30 seconds, 100 nM OCRL was added to catalyze the dephosphorylation of PI(4,5)P_2 and membrane dissociation of PIP4K2A and PH-PLCδ1. (**C**) Acute enrichment of PI(4,5)P_2 causes PIP4K2C to increase association with the membrane. Cartoons show the CID system, in confocal, for the interaction of catalytically active or dead FKBP-tagged homo-dimeric PIP5K1C kinase with the PM-anchored Lyn_{11}-FRB. NG2-PIP4K2C (blue) cells were transfected with FKBP-tagged proteins, the low affinity PI(4,5)P_2 indicator $Tubby_C^{R332H}$ (orange) and Lyn_{11}-FRB. During time-lapse confocal microscopy, cells were stimulated with 1μM rapa, as indicated. Traces represent mean change in fluorescence intensity (PM/cell normalized to pre-stimulation levels) ± s.e. of 48-52 cells imaged across at

least three independent experiments, scale bar is 10 μm. (**D**) Chronic enrichment of $PI(4,5)P_2$ causes NG2-PIP4K2C to associate with the membrane. Cartoons show the expression of catalytically active or dead Mss4. Images show equatorial confocal sections of representative NG2-PIP4K2C cells transfected with Mss4 and the low affinity $PI(4,5)P_2$ indicator $Tubby_C^{R332H}$. Box and whisker plots show the mean fluorescence intensity ratio (PM/cell) of the $PI(4,5)P_2$ sensor from 88-90 cells images across at least three independent experiments (boxes display median and interquartile range, whiskers represent 10-90% of data and "+" represents mean) , scale bar is 10 μm. (**E**) Enrichment of $PI(4,5)P_2$ causes dynamic membrane recruitment of purified PIP4K2A. In SLBs, membrane recruitment of 50 nM PIP4K2A monitored during Mss4 catalyzed phosphorylation of PI4P. Membranes containing 4% PI4P were converted to $PI(4,5)P_2$ using 10 nM Mss4.

4.3.5 PIP4KA binds cooperatively to $PI(4,5)P_2$ containing membranes

Using a fixed solution concentration of 50 nM PIP4K2A, Scott Hansen compared the membrane absorption and equilibration dynamics of PIP4K2A on SLBs containing varying densities of $PI(4,5)P_2$ lipids (**Figure 4.5A**). PIP4K2A exhibited a nearly 125-fold increase in membrane binding over the range of 1 to 4% $PI(4,5)P_2$ (**Figure 4.5A**). Additionally, PIP4K2A displayed a similar degree of cooperativity when we converted PI4P to $PI(4,5)P_2$ on SLBs in the presence of Mss4 (**Figure 4.5A**). Parallel biochemical experiments confirmed that PIP4K and Mss4 do not physically interact (**figure 4.6D**), indicating that the change in PIP4K2A localization was solely dependent on the production of $PI(4,5)P_2$.

To test this in live cells, we assessed the kinetics of PM binding during $PI(4,5)P_2$ re-synthesis after strong PLC activation. Cells with over-expressed muscarinic M3 receptors were stimulated with carbachol (CCh) to activate PLCβ3 and decrease $PI(4,5)P_2$ levels (*124*, *419*). Indeed, we observed a rapid decrease in both $Tubby_C$ localization and ePIP4K2C puncta at the PM (**Figure 4.5B**). Atropine was then added as an M_3 receptor antagonist, allowing for $PI(4,5)P_2$

resynthesis (*124*). We observed Tubby$_C$ re-localized at the PM after ~60 sec of atropine treatment (~300 sec total) (**Figure 4.5B**). Following this increase in PI(4,5)P_2, we observed a slower re-emergence (~180 sec post atropine or ~480 sec total) of ePIP4K2C puncta on the PM (**Figure 4.5B**). In examining purified PIP4K2A in SLBs, there was a PI(4,5)P_2 dose dependence on PIP4K membrane localization (**Figure 4.5A**). As SLB PI(4,5)P_2 levels changed from 0% to 4% there was an exponential fold increase in PIP4K2A association with the membrane (**Figure 4.5A**). These data taken together indicate that PIP4K seems to localize with the PM in a PI(4,5)P_2 dependent manner. Collectively, these data demonstrate that PIP4Ks are low-affinity PI(4,5)P_2 effectors, poised to sense both decreases and crucially, elevations in PI(4,5)P_2 levels in the PM.

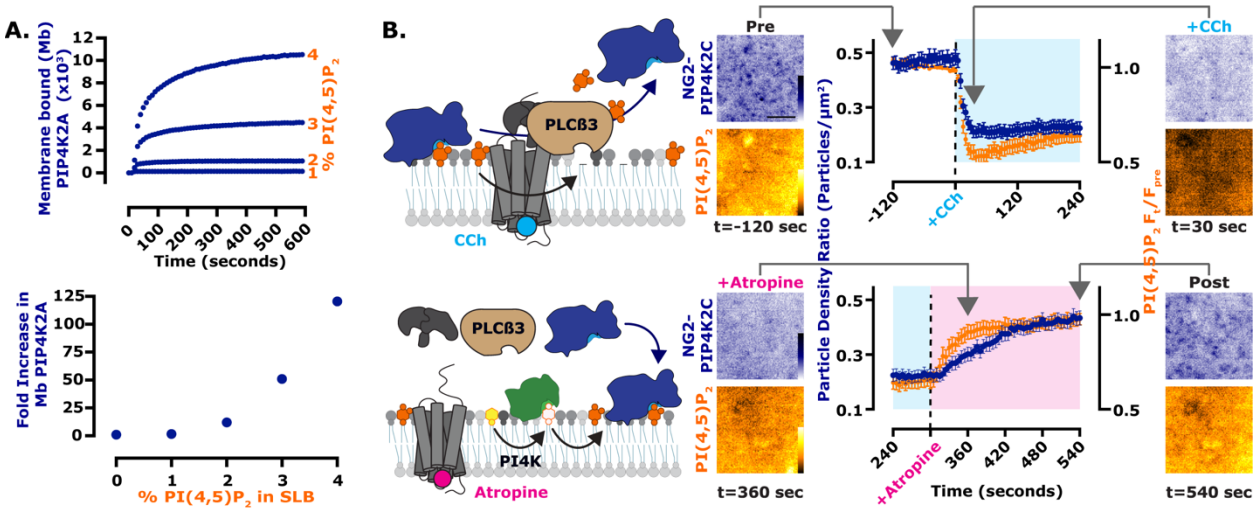

Figure 4.5 PI(4,5)P_2 is necessary and sufficient for membrane association of purified PIP4K.

(**A**) Purified PIP4K2A localizes to PI(4,5)P_2 in a concentration dependent manner. Membrane absorption and equilibration kinetics of 50 nM Alexa488-PIP4K2A measured by TIRF microscopy on SLBs containing 1–4% PI(4,5)P_2. PIP4K2A membrane binding exhibited non-linearity with respect to the PI(4,5)P_2 lipid density. Quantification of the fold increase in membrane bound PIP4K2A relative to the equilibrium fluorescence intensity of PIP4K2A on a membrane containing 0% PI(4,5)P_2. (**B**) PM localization of PIP4K2C follows resynthesis of PI(4,5)P_2. Cartoons show PLCβ3 mediated loss of PI(4,5)P_2 and eNG-PIP4K2C followed by the subsequent reappearance of PI(4,5)P_2 and eNG-PIP4K2C. eNG-PIP4K2C (blue) cells were transfected with FKBP-tagged proteins, the high affinity PI(4,5)P_2 indicator Tubby$_C$ (orange) and Lyn$_{11}$-FRB. During time-lapse TIRF microscopy, cells were

stimulated with 100 μM carbachol (CCh) and then stimulated with 5 μM atropine as indicated. $Tubby_C$ traces represent mean change in fluorescence intensity (F_t/F_{pre} normalized to pre-stimulation levels) ± s.e. The eNG-PIP4K traces represent the mean change in puncta per μm^2 ± s.e. 40 cells were imaged across at least three independent experiments, scale bar is 2.5 μm.

4.3.6 PIP4K interacts with PIP5K for inhibition

The inhibition of PIP5K activity by PIP4Ks (**Figure 4.1 and 4.2**), and the low-affinity $PI(4,5)P_2$ binding by PIP4K (**Figure 4.3 and 4.4**) suggest the following mechanism: when $PI(4,5)P_2$ levels rise due to PIP5K activity, PIP4K is recruited to the PM, where it can directly bind to $PI(4,5)P_2$ and inhibit PIP5K. The possibility of PIP4K directly interacting with PIP5K at the PM has not yet been ruled out by our previous experiments. In fact, (*420*) showed that PIP4K2A was able to co-localize with the various isoforms of PIP5K. In **figure 4.2A**, we expressed combinations of PIP4K and PIP5K isoforms to look at the effects on $Tubby_C^{R332H}$ localization. Using the same experimental data but observing the localization of each of the PIP5K or PIP4K constructs, we could determine if the co-expression of these two proteins influenced either of their subcellular localizations (**Figure 4.6A**). We observe PM localization of each of the three PIP5K isoforms, alone and in combination with any of the PIP4K isoforms (**Figure 4.6A, green**). The three PIP4K isoforms all displayed a mostly cytosolic localization with a slight increase in PM localization compared to the expression of a fluorophore alone (**Figure 4.6A, blue**). However, with the expression of any PIP5K isoform each of the PIP4K isoforms were found more strongly associated with the PM (**Figure 4.6A, blue**). These data could indicate that PIP4K localization is influenced by PIP5K PM localization. While this is consistent with a direct interaction between PIP4Ks and PIP5Ks, another possibility exists: the PIP5K dependent increase in $PI(4,5)P_2$ (**Figure 4.1**)

enhances PM recruitment of PIP4K and **Figures 4.4 and 4.5** show that that PIP4K PM localization is impacted by PI(4,5)P_2 levels. Furthermore, prior pull-downs of PIP5K and PIP4K from lysates required cross-linking the proteins when the enzymes may still have been co-localized on the PM (*56*).

We, therefore, sought to distinguish between a direct PIP5K-PIP4K binding interaction versus PI(4,5)P_2-induced co-enrichment on membranes. To this end, we devised an experiment whereby a bait protein (either PIP5K or control proteins) could be acutely localized to domains of the PM. This was achieved using CID of baits with an endoplasmic reticulum ER-localized tail of CyB5A (*407*), causing recruitment of the bait protein to ER-PM contact sites (**Figure 4.6B, cartoon**). Using TIRF, we visualized ePIP4K2C puncta localization with each of these constructs. Enrichment of endogenous ePIP4K2C at ER-PM contact sites was only observed when PIP5K1A was the bait; an unrelated peptide (myristoylated and palmitoylated peptide from Lyn kinase, Lyn_{11}) or Mss4 did not enrich ePIP4K2C (**Figure 4.6B**). The use of Mss4 ruled out an effect of enhanced PI(4,5)P_2 generation at contact sites, as this enzyme increases PI(4,5)P_2 as potently as PIP5K1A (**Figure 4.6B**), yet does not cause recruitment of PIP4K2C. Furthermore, data from Scott Hansen's lab used purified proteins in SLBs also showed a robust association of both PIP4K2A and PIP5K1A with the membrane when both proteins are present (**Figure 4.6C**). However, there was no additional membrane association of PIP4K2A when purified Mss4 was added to SLBs (**Figure 4.6D**). Altogether, our data show that PIP4K PM localization is dependent both on the presence of PI(4,5)P_2 and PIP5K for PM localization.

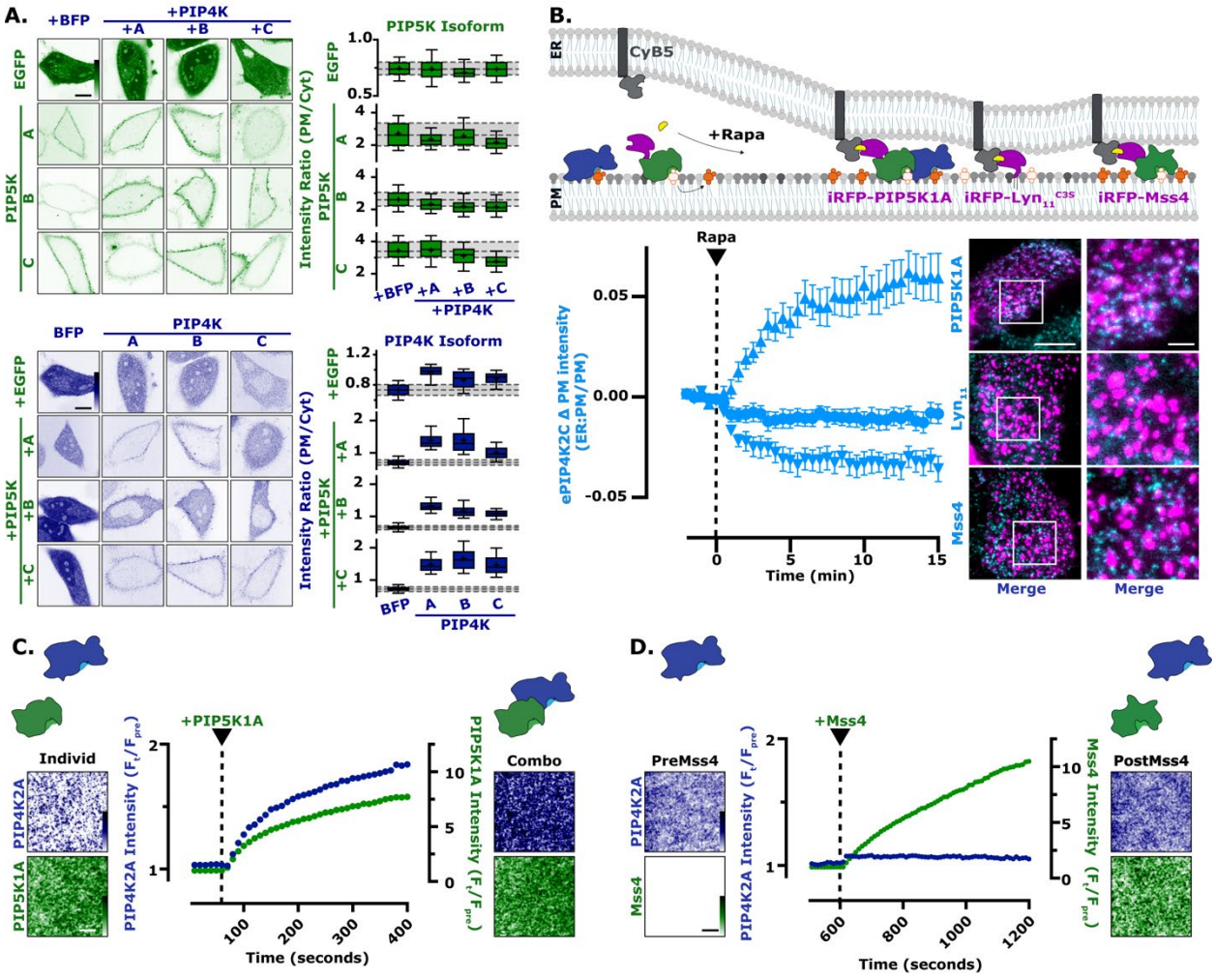

Figure 4.6 PIP4K interacts with mammalian PIP5K for inhibition.

(**A**) PIP5K expression increases PIP4K PM localization. The same experimental data set from Figure 1E is used here. HeLa cells expressing PIP5K (green) or PIP4K (blue) were co-transfected with the indicated EGFP- or TagGFP2-tagged isoform constructs. Images show equatorial sections in confocal of representative cells. For box and whisker plots, boxes display median and interquartile range and whiskers representing 10-90% of the data and "+" represents the mean of 90 cells imaged across at least three independent experiments, scale bar is 10 µm. (**B**) PIP4K2C interacts with PIP5K1A. Cartoon schematic show the CID system for the generation of ER-PM contact sites between ER-anchored FKBP-CyB5 and PM-anchored FRB-tagged constructs. eNG-PIP4K2C (cyan) cells were transfected with FKBP-CyB5, the low affinity PI(4,5)P_2 indicator $Tubby_C^{R332H}$, and the indicated FRB-tagged construct (magenta). During time-lapse TIRF microscopy, cells were stimulated with 1µM rapa. TIRF images are representative and color-coded to represent fluorescence intensity, as indicated. eNG-PIP4K2C traces represent mean fluorescence intensities

(ER:PM/PM) ± s.e. of 32-39 cells imaged across a minimum of three independent experiments, scale bar is 10 μm, inset scale bar is 2.5 μm. (**C**) Dynamic PIP5K1A dependent membrane recruitment of PIP4K2A. In the absence of PIP5K, 50 nM PIP4K2A displays a low level of membrane recruitment. The addition of 10 nM PIP5K1A, stimulates an immediate and steady increase in both PIP4K2A and PIP5K1A membrane localization. Membrane composition: 2% PI(4,5)P_2, 98% DOPC. TIRF images are representative and color-coded to represent fluorescence intensity, as indicated, scale bar is 5 μm. (**D**) Membrane binding of PIP4K2A is insensitive to yeast Mss4 membrane localization. TIRF microscopy images show the membrane localization of PIP4K2A in the absence and presence of Mss4. Following membrane equilibration of 50 nM PIP4KA, 10 nM Mss4 was added to the imaging chamber. No appreciable change in PIP4K2A localization was observed during membrane absorption of Mss4. Membrane composition: 4% PI(4,5)P_2 and 96% DOPC. TIRF images are representative and color-coded to represent fluorescence intensity, as indicated, scale bar is 5 μm.

4.3.7 The N-terminus of PIP4K mediates the interaction with PIP5K

We next sought to determine the point of physical interaction and therefore inhibition between PIP5K and PIP4K. The PIP4K protein lacks predictable structural features near the linear N-terminus of the protein (*426*, *427*, *450*). We hypothesized that this N-terminus could form a protein-protein interaction domain with PIP5K present, and this may form the interaction motif between the proteins. We generated a construct of PIP4K2A which lacked the first 32aa residues, PIP4K2A^{Kina}, and a fragment which consisted of only the first 32aa residues, NTerm (**Figure 4.7A**). Again, we utilized our CID system to recruit the full-length, the kinase fragment, or the N-terminus of PIP4K to the PM. Following recruitment of full-length PIP4K2A we observed the expected decrease in Tubby$_C$ biosensor localization with the PM. However, recruitment of PIP4K2A^{Kina} did not result in any change in PI(4,5)P_2 at the PM (**Figure 4.7B**). On the other hand, we observed no changes in PI(4,5)P_2 at the PM with the recruitment of NTerm alone (**Figure 4.7B**). This observation shows that PIP4K specifically requires the N-terminus to inhibit PIP5K

mediated PI(4,5)P_2 synthesis, however, the N-terminus is not sufficient on its own to mediate this inhibition.

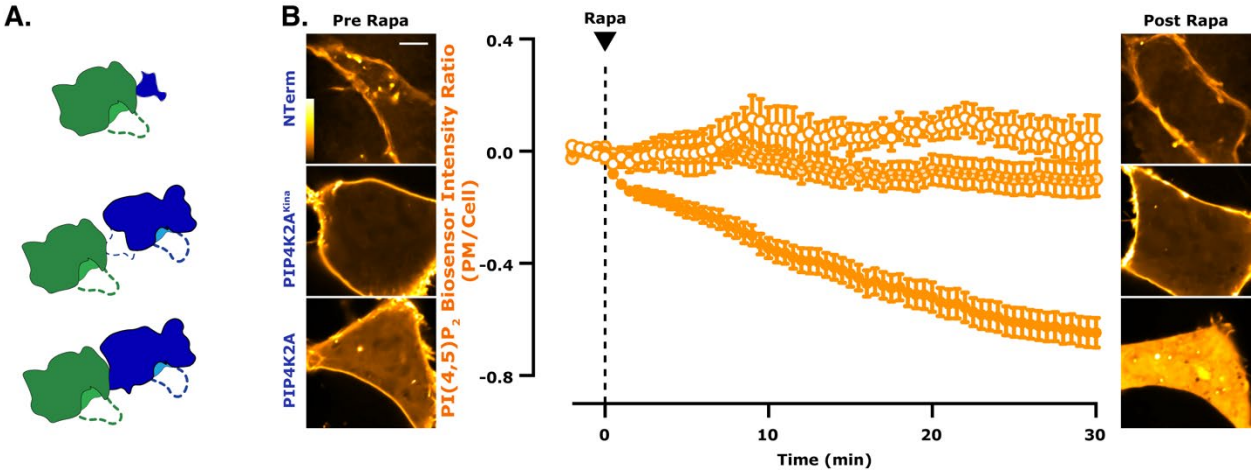

Figure 4.7 The N-terminus of PIP4K interacts with PIP5K.

(**A**) Proposed interaction between the N-terminus of PIP5K and PIP5K. Cartoons show the potential interaction mechanism between PIP4K2A and PIP5K. The lack of interaction is shown in the PIP4K2A^{Kina} fragment construct. (**B**) Recruitment of PIP4K2A^{Kina} does not result in changes in PM PI(4,5)P_2. HEK293A cells were transfected with FKBP-tagged proteins, the high affinity PI(4,5)P_2 indicator Tubby$_C$ (orange) and Lyn$_{11}$-FRB. During time-lapse confocal microscopy, cells were stimulated with 1μM rapa, as indicated. Traces represent mean change in fluorescence intensity (PM/cell normalized to pre-stimulation levels) ± s.e. of 24-74 cells imaged across at least three independent experiments (two independent experiments in the case of NTerm), scale bar is 10 μm.

4.3.8 Regulation of PIP5K by the low affinity PI(4,5)P_2 interaction of PIP4K

Synthesizing all of these observations, we propose a simple homeostatic feedback loop that maintains PI(4,5)P_2 levels in the PM (**Figure 4.8A**): when PI(4,5)P_2 levels increase, PIP4K is recruited to the PM in sufficient quantities to inhibit PIP5K, halting further PI(4,5)P_2 synthesis. If

$PI(4,5)P_2$ levels fall, PIP4K is one of the first $PI(4,5)P_2$ binding proteins to be released (due to its low affinity), causing disinhibition of PIP5K and recovery of $PI(4,5)P_2$. We next sought to test how perturbations of this homeostat would affect physiological function.

We first assessed $PI(4,5)P_2$ levels in cells with one of three different $PI(4,5)P_2$ biosensors: PH-PLCδ1, $Tubby_C$, $Tubby_C^{R332H}$ (*305*, *316*, *451*, *452*). We could produce graded changes in resting $PI(4,5)P_2$ levels by over-expression of various components of the homeostat: enhanced PIP5K1A expression, either catalytically active or inactive, increases $PI(4,5)P_2$; a myristoylated PIP4K2A retains PM localization even at low $PI(4,5)P_2$, causing sustained reductions in $PI(4,5)P_2$; and a PM-localized $PI(4,5)P_2$ 5-OH phosphatase causes near complete ablation of the lipid. These constructs all show the expected changes in PM $PI(4,5)P_2$ compared to a control, reported by three different $PI(4,5)P_2$ biosensors. Of these, $Tubby_c$ showed the most linear response across all changes in $PI(4,5)P_2$ levels (**Figure 4.8B**). We then used these graded changes in steady-state PM $PI(4,5)P_2$ to investigate the concentration requirements for the lipid.

4.3.9 PLC-mediated Ca^{2+} signals saturate at elevated $PI(4,5)P_2$ levels

$PI(4,5)P_2$ is the substrate for PLC, the enzyme that cleaves it into second messengers diacylglycerol and inositol (1,4,5)-trisphosphate (IP_3), triggering calcium release from ER stores

We set out to determine if changes in baseline $PI(4,5)P_2$ had any impact on IP_3 production and downstream Ca^{2+} flux. We observed CCh mediated PLCβ3 activation in HEK293A cells using the Ca^{2+} biosensor R-GECO1.2 (*453*) (**Figure 4.8C**). Cells expressed one of the previously used constructs and R-GECO1.2 for the detection of intracellular Ca^{2+}. Cells were visualized using confocal microscopy and R-GECO1.2 intensity was measured before and after CCh stimulation (F_t/F_{pre}). In the $PI(4,5)P_2$ control condition ($myrLyn_{11}$), we observed a rapid and transient increase

in R-GECO1.2 fluorescence which approached baseline fluorescence by the end of the 5 min of stimulation (**Figure 4.8C**). The expression of INPP5E had shown the lowest amount of $PI(4,5)P_2$ (**Figure 4.8C**) at the PM and likewise we observed very little R-GECO1.2 fluorescence increase which immediately returned to baseline (**Figure 4.8C**). Similarly, the over-expression of myrPIP4K2C produced a decreased R-GECO1.2 response which returned to baseline in less than a minute (**Figure 4.8C**). In the case of increased basal $PI(4,5)P_2$, with over-expression of $PIP5K1A^{CatDead}$ or PIP5K1A, we again observed a rapid increase in R-GECO1.2 fluorescence. However, the R-GECO1.2 fluorescence did not return to baseline 5 min after stimulation in either of these conditions (**Figure 4.8C**). Influx of extracellular calcium was increased by elevated $PI(4,5)P_2$ levels, consistent with a prior report that store-operated calcium entry is enhanced by increased PIP5K activity (*454*).

We next focused specifically on IP_3 mediated intracellular Ca^{2+} by repeating the previous experiments using a Ca^{2+}-free imaging media. The results obtained here were like those previously discussed. Over-expression of $myrLyn_{11}$ resulted in a transient increase in R-GECO1.2 fluorescence that recovered within 1 min after CCh stimulation (**Figure 4.8C**). Stimulation of the INPP5E condition resulted in a very minor increase in R-GECO1.2 fluorescence which returned to baseline after ~30 sec (**Figure 4.8C**). Over-expression of myrPIP4K2C resulted in a transient spike in fluorescence of R-GECO1.2, which returned to baseline after ~30 sec (**Figure 4.8C**). The over-expression of either $PIP5K1A^{CatDead}$ or PIP5K1A resulted in transient increases in R-GECO1.2 fluorescence, which both returned to baseline within 2 min of stimulation (**Figure 4.8C**). We then compared either the peak response or the total area under the curve (AUC) of each experimental set up (Ca or Ca-free media) with the $Tubby_C$ intensity ratio obtained in (**Figure 4.8C**). Overall, we observed a correlation between decreased starting $PI(4,5)P_2$ levels with a

decreased peak Ca^{2+} response. Following PIP5K1A^{CatDead} or PIP5K1A over-expression and increased basal PI(4,5)P_2, there seems to be a plateaued effect in the peak response when compared with myrLyn11 (**Figure 4.8C**). In the case of the AUC there were differences between the experimental Ca^{2+} conditions. In the case of Ca^{2+} containing media, there was an almost linear increase in the duration of the R-GECO1.2 fluorescence (**Figure 4.8C**). This is likely the result of extracellular Ca^{2+} flux during these experiments. In the Ca2+ free media, there again was a similar plateau effect seen in the peak response data, where decreased starting amounts of PI(4,5)P_2 resulted in decreased R-GECO1.2 fluorescence (**Figure 4.8C**). However, an increased basal PI(4,5)P_2 level did not result in any increase in AUC, compared to control (**Figure 4.8C**). It suggests that IP_3-triggered calcium release appears saturated at resting PI(4,5)P_2.

4.3.10 PI3K mediated PI(3,4,5)P_3 synthesis is linearly dependent on PI(4,5)P_2 levels

Next, we sought to determine if the changes in baseline PI(4,5)P_2 had any impact on PI(3,4,5)P_3 production. We observed EGF mediated PI3K activation in HEK293A cells using the PI(3,4,5)P_3 biose(*280*)PH-ARNO$^{2G\text{-}I303E}$x2 (aPHx2) (*318*) (**Figure 4.8D**). Cells expressing one of the above constructs and aPHx2 were stimulated with EGF after 2 mins and we observed the translocation of our probe to the PM (PM/Cyto) using confocal microscopy. With myrLyn$_{11}$ expression, and baseline levels of PI(4,5)P_2, we observed an EGF-dependent increase in aPHx2 levels at the PM (**Figure 4.8D**). These levels approached baseline by the end of the 15' experiment (**Figure 4.8D**). Over-expression of either myrPIP4K2C or INPP5E, achieving a baseline reduction in basal PI(4,5)P_2 levels, resulted in little to no PM association of aPHx2, respectively (**Figure 4.8D**). Finally, over-expression of either PIP5K1A^{CatDead} or PIP5K1A resulted in the greatest increase in aPHx2 levels at the PM (**Figure 4.8D**). Interestingly, when plotting either peak or AUC

of the aPHx2 response against $PI(4,5)P_2$ levels in each condition, we can see a linear relationship between the two (**Figure 4.8D**). The more $PI(4,5)P_2$ available at baseline translates to more $PI(3,4,5)P_3$ produced after EGF-mediated PI3K activation (**Figure 4.8D**).

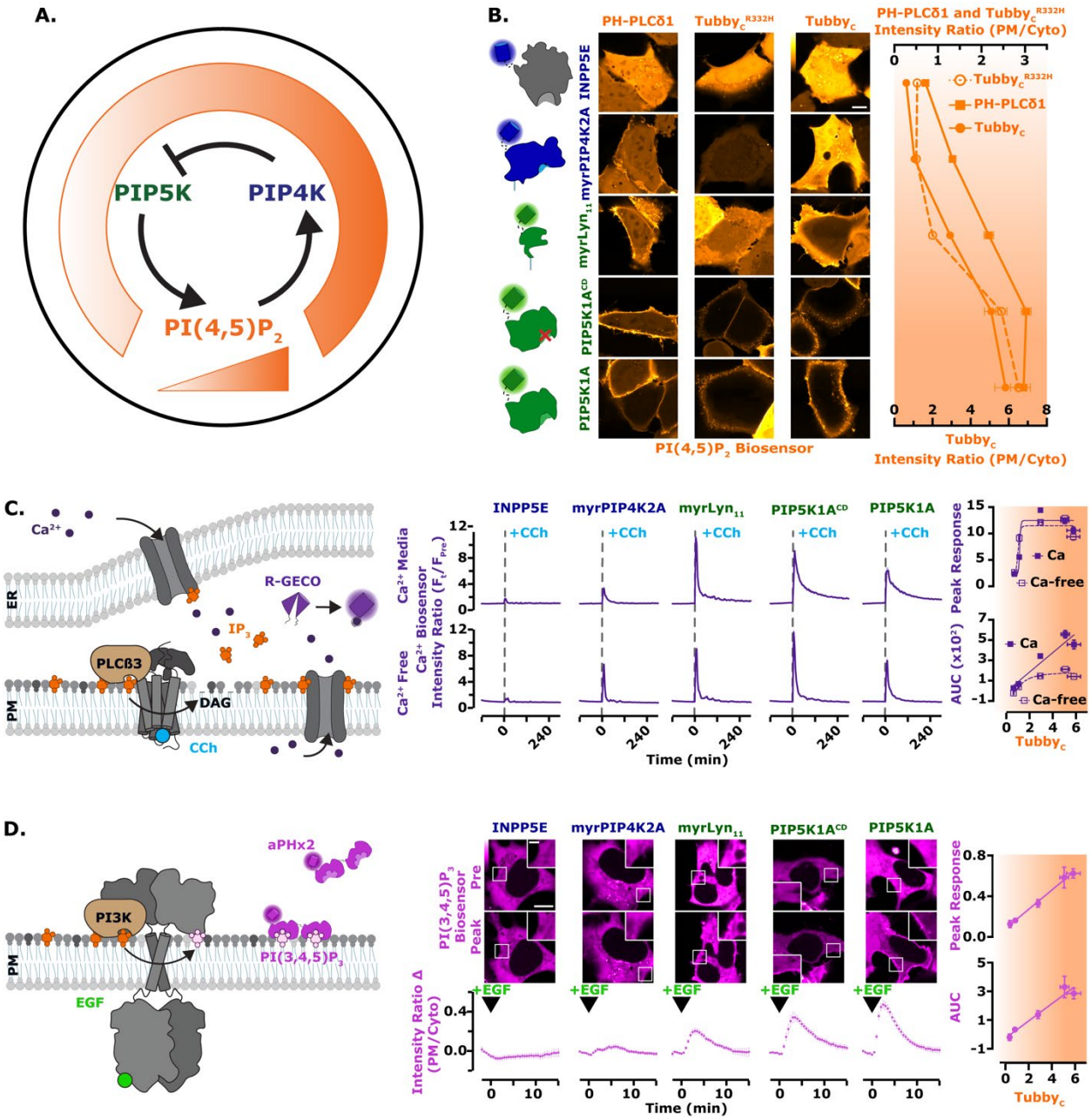

Figure 4.8 PI3K, but not calcium signaling, are modulated across all concentration ranges of PI(4,5)P$_2$.

(**A**) Proposed regulation of PIP5K by the low affinity PI(4,5)P$_2$ interaction of PIP4K. The working model for negative feedback of PIP5K via PIP4K resembles the thermostat regulation of temperature. When PI(4,5)P$_2$ levels are high, PIP4K is recruited and held at the PM, via a direct low affinity interaction with PI(4,5)P$_2$. At the PM, PIP4K interacts with and inhibits the catalytic activity of PIP5K, causing reduced PI(4,5)P$_2$ synthesis. (**B**) PI(4,5)P$_2$ biosensors detect a gradient of lipid levels. HEK293A cells were transfected with the indicated fluorescently tagged PI(4,5)P$_2$ modulating proteins (INPP5E, myrPIP4K2A, myrLyn$_{11}$, PIP5K1A catalytic dead or active) and the indicated

$PI(4,5)P_2$ biosensor (PH-PLCδ1, $Tubby_C$, or $Tubby_C^{R332H}$ displayed in orange) for 16-24 hours. Mean fluorescence intensity (PM/cyto) are shown as points with error bars representing s.e. of >120 cells imaged across three independent experiments, scale bar is 10 μm. (**C**) PLC-mediated Ca^{2+} signals saturate at elevated $PI(4,5)P_2$ levels. Cartoon schematics of PLC mediated Ca^{2+} signaling and detection. HEK293A cells were transfected with the indicated fluorescently tagged construct and the calcium sensor R-GECO (purple). During time-lapse confocal microscopy (performed with either compete imaging media [Ca^{2+}] or calcium free Ringer's media [Ca^{2+}-Free]), cells were stimulated with 100 μM CCh as indicated. Traces represent the peak response of mean change in fluorescence intensity (F_t/F_{Pre} normalized to pre-stimulation levels) ± s.e. of >100 cells imaged across a minimum of three independent experiments. The peak response and total area under the curve (AUC) were plotted against the normalized ratio of $Tubby_C$. (**D**) PI3K mediated $PI(3,4,5)P_3$ synthesis is linearly dependent on $PI(4,5)P_2$ levels. Cartoon schematics show PI3K mediated signaling and detection of $PI(3,4,5)P_3$ upon the addition of EGF. HEK293A cells were transfected with the indicated fluorescently tagged construct and the $PI(3,4,5)P_3$ biosensor, $PH\text{-}ARNO^{2G\text{-}I303Ex2}$ (aPHx2) (magenta). During time-lapse confocal microscopy, cells were stimulated with 10 ng/mL EGF, as indicated. Traces represent the peak response of mean change in fluorescence intensity (PM/cell normalized to pre-stimulation levels) ± s.e. of 35 cells imaged across a minimum of three independent experiments. The peak response and AUC were plotted against the normalized ratio of $Tubby_C$, scale bar is 10 μm, inset scale bar is 2.5 μm.

4.4 Discussion

In conclusion, our results reveal a remarkably simple homeostatic mechanism that controls PM $PI(4,5)P_2$ levels (**Figure 4.8A**). In this study we show that PIP4K, independent of catalytic activity, negatively regulates PIP5K activity. Specifically overexpressed PIP4K decreases cellular $PI(4,5)P_2$ levels at the PM. This is also recapitulated in a purified system, where PIP4K2A inhibits the activity of PIP5K1A on a membrane. This system can help explain why a loss of PIP4K leads to increased PI3K signaling pathways (*439–441*). Likely, the negative regulation of PIP5K results

in increased $PI(4,5)P_2$ and downstream signaling. Similarly, the increased PIP4K protein expression observed in breast cancer (*442*) could be viewed as a physiological attempt to dampen PI3K signaling by further inhibiting PIP5K catalytic activity.

Our results also indicate that PIP4K acts as a low affinity $PI(4,5)P_2$ binding protein which localizes to the PM in a $PI(4,5)P_2$ dependent manner. The depletion of $PI(4,5)P_2$ in cells and SLBs resulted in a loss of ePIP4K2C or PIP4K2A, respectively. Elevations in $PI(4,5)P_2$ resulted in increases in PIP4K association with either the PM or SLBs. This $PI(4,5)P_2$ dependent recruitment was further shown in cells stimulated with CCh and then atropine. Specifically, the cellular levels of $PI(4,5)P_2$ recovered more quickly than ePIP4K2C puncta. Upon increases in $PI(4,5)P_2$ synthesis, PIP4K can be recruited to the PM to inhibit further PIP5K mediated synthesis. When $PI(4,5)P_2$ levels are low or decrease, PIP4K remains cytosolically localized.

Our data indicate that the N-terminus of PIP4K mediates the interaction with PIP5K at the PM to inhibit catalytic activity. Our data supports previous evidence that PIP5K can interact with PIP4K (*420*). Here we show that ePIP4K2C is colocalized with ER-PM contact sites which contain PIP5K1A, but not Mss4. Similarly, purified PIP5K1A enhances the ability of PIP4K2A to associate with SLBs, but again there is no association between Mss4 and PIP4K2A. PIP4Ks appear to be recruited in a $PI(4,5)P_2$ dependent manner to directly interact with and inhibit the activity of PIP5K. Furthermore, truncation of the PIP4K enzyme revealed that the N-terminus of PIP4K2A is necessary for this inhibitory effect. It is yet unknown where PIP4K interacts with PIP5K, that is to be the topic of future studies.

We show that perturbation of this homeostasis reveals different sensitivities of PLC and PI3K signaling, with the latter showing enhanced activation with elevated $PI(4,5)P_2$. This likely explains why the PI3K, and not the PLC pathway, drives the phenotype of PIP4K-null fruit flies

(*53*). More broadly, such differences in the sensitivity of $PI(4,5)P_2$-dependent PM functions to lipid concentration may go a long way to explaining the phenotypic diversity of diseases associated with dysregulated $PI(4,5)P_2$ metabolism. For example, they may explain why a selective inhibitor of PI3Kα can correct aberrant kidney function associated with Lowe syndrome models (*437*). Indeed, experimental manipulation of $PI(4,5)P_2$ homeostasis will now afford the ability to determine which of the panoply of $PI(4,5)P_2$-dependent PM functions are dysregulated by pathological alterations – finally bringing potential therapeutic targets into view.

4.5 Experimental Procedures

4.5.1 Cell culture and lipofection

HeLa (ATCC CCL-2) and HEK293A (ThermoFisher R705-07) cells were cultured in DMEM (low glucose; Life Technologies 10567022) supplemented with 10% heat-inactivated fetal bovine serum (Life Technologies 10438-034), 100 units/ml penicillin, 100µg/ml streptomycin (Life Technologies 15140122), and 1:1,000 chemically defined lipid supplement (Life Technologies 11905031) at 37˚C with a humidified atmosphere with 5% CO_2. Cells were passaged twice per week diluting 1 in 5 after dissociation in TrpLE (Life Technologies 12604039). 293A cells with endogenous PIP4K2C alleles tagged with split NeonGreen2 (NG2) were generated similarly as described (*430*) using a protocol we have described (*323*). In brief, Platinum Cas9 (Thermo Fisher B25640) was precomplexed with gRNA and electroporated into $HEK293A^{NG2\text{-}1\text{-}10}$ cells in combination with a single-stranded HDR Template (IDT). Sequences are provided in **table 2**. The HDR template contains 70 bp homology-arms, the NG2-11 sequence, and a flexible

linker in frame with PIP4K2C (ATGACCGAGCTCAACTTCAAGGAGTGGCAAAAGGCCTTT-ACCGATATGATGGGTGGCGGC). After recovery, FACS (University of Pittsburgh Flow Cytometry Core) was used to sort NG2-positive cells. These NG2-PIP4K2C (ePIP4K2C) cells were cultured under identical conditions to the HeLa and HEK293A cells.

4.5.2 Chemicals and reagents

Rapamycin (Thermo Fisher BP2963-1) was dissolved in DMSO at 1 mM and stored as a stock at -20˚C, it was used in cells at 1 μM. EGTA (VWR EM-4100) was dissolved in water at 0.5 M and stored at room temperature, it was used in cells at 5 mM. EGF (Corning CB-40052) was dissolved in water at 100 μg/ml and stored as a stock at -20˚C, it was used in cells at 10 ng/ml. Carbachol (Thermo Fisher AC10824-0050) was dissolved in water at 50 mM and stored as a stock at -20˚C, it was used in cells at 100 μM. Atropine (Thermo Fisher AC226680100) was dissolved in 100% ethanol at 25 mM and stored as a stock at -20˚C, it was used in cells at 5 μM.

4.5.3 Plasmids and cloning

The EGFP (Aequorea victoria GFP containing F64L and S65T mutations) (*319*), mCherry (Discoma DsRed monomeric variant) (*320*), mTagBFP2 (Entacmaea quadricolor protein eqFP578) (*321*), iRFP713 (Rhodopseudomonas palustris [Rp] bacteriophytochrome BphP2) (*322*) and iRFP670 (RpBphP6 iRFP702 containing V112I, K174M and I247C mutations) (*455*) fluorophores were used in the Clontech pEGFP-C1, -C2, and -N1 backbones as described previously (*323*). Mutated constructs were generated using site-directed mutagenesis using

targeted pairs of DNA oligos which were custom made and supplied by Thermo Fisher. New plasmids used in this study were generated using standard restriction-ligation or by using NEBuilder HiFi DNA Assembly (New England Biolabs E552OS). HsPIP5K1A, HsPIP5K1B, Mss4_Kina, and HsPIP4K2C were obtained as human codon optimized synthetic gBlocks (IDT). Otherwise, plasmids were obtained from the sources listed in Table 1. All constructs were sequence verified using Sanger DNA sequencing. Plasmids constructed for this study are available through Addgene.

4.5.4 Purification of PIP5K1A and Mss4

Gene sequences encoding human PIP5K1A and yeast Mss4 kinase domain were cloned into a FastBac1 vector to create the following vectors: His6-MBP-TEV-(Gly)5-PIP5K1A (1-546aa) and His6-MBP-TEV-(Gly)5-Mss4 (379-779aa). BACMIDs and baculovirus were generated as previously described (*456*). ES-Sf9 cells were infected with baculovirus using an optimized multiplicity of infection (MOI), typically 2% vol/vol, that was empirically determined from small-scale test expression. Infected cells were typically grown for 48 hours at 27ºC in ESF 921 Serum-Free Insect Cell Culture medium (Expression Systems, Cat# 96-001-01) and then harvested by centrifugation. Insect cell pellets were then washed with 1x PBS [pH 7.2] and centrifuged (3500 rpm for 10 minutes). The final cell pellet was combined with an equal volume of buffer containing 1x PBS [pH 7.2], 10% glycerol, and 2x Sigma protease inhibitor cocktail tablet solution before transferring to the -80ºC freezer for storage. For purification, frozen cells were thawed in an ambient water bath and then resuspended in buffer containing 50 mM Na_2HPO_4 [pH 8.0], 10 mM imidazole, 400 mM NaCl, 5% glycerol, 1 mM PMSF, 5 mM BME, 100 µg/mL DNase, and 1x Sigma protease inhibitor cocktail tablet. Cells were lysed using a glass dounce

homogenizer. Lysate was then centrifuged at 35,000 rpm (140,000 x g) for 60 minutes in a Beckman Ti-45 rotor at 4ºC. High speed supernatant was combined with 6 mL of Ni-NTA Agarose (Qiagen, Cat# 30230) and stirred in a beaker for 1-2 hour(s) at 4ºC. Following batch binding, resin was collected in 50 mL tubes, centrifuged, and washed with buffer containing 50 mM Na_2HPO_4 [pH 8.0], 10 mM imidazole, 400 mM NaCl, and 5 mM BME. Ni-NTA resin with His6-MBP-(Asn)10-TEV-(Gly)5-PIP5KA bound was washed in a gravity flow column with 100 mL of 50 mM Na_2HPO_4 [pH 8.0], 30 mM imidazole, 400 mM NaCl, 5% glycerol, and 5 mM BME buffer. Protein elution was achieved by washing the resin with buffer containing 50 mM Na_2HPO_4 [pH 8.0], 500 mM imidazole, 400 mM NaCl, 5% glycerol, and 5 mM BME. Peak fractions were pooled, combined with 200 µg/mL His6-TEV(S291V) protease, and dialyzed against 4 liters of buffer containing 20 mM Tris [pH 8.0], 200 mM NaCl and 2.5 mM BME for 16-18 hours at 4ºC. The next day, dialysate was combined 1:1 volumes with 20 mM Tris [pH 8.0], 1 mM TCEP to reduce the NaCl to a final concentration of 100 mM. Precipitate was removed by centrifugation (3500 rpm for 10 minutes) and a 0.22 µm syringe filtration. Clarified dialysate was bound to a MonoS cation exchange column (GE Healthcare, Cat# 17-5168-01) equilibrated with buffer containing 20 mM Tris [pH 8.0], 100 mM NaCl, and 1 mM TCEP. Proteins were resolved over a 10-100% linear gradient (0.1-1 M NaCl, 45 CV, 45 mL total, 1 mL/min flow rate). $(Gly)_{x5}$-PIP5K1A and $(Gly)_{x5}$-Mss4 eluted from the MonoS in the presence of 375-450 mM NaCl. Peak fractions containing PIP5K1A were pooled, concentrated in a 30 kDa MWCO Vivaspin 6 centrifuge tube (GE Healthcare, Cat# 28-9323-17), and loaded onto a 24 mL Superdex 200 10/300 GL (GE Healthcare, Cat# 17-5174-01) size exclusion column equilibrated in 20 mM Tris [pH 8.0], 200 mM NaCl, 10% glycerol, 1 mM TCEP. Peak fractions were concentrated to 10-50 µM using a 30 kDa MWCO

Amicon centrifuge tube (Millipore Sigma) before snap freezing with liquid nitrogen. PIP5K1A and Mss4 were stored in -80ºC as single use aliquots.

4.5.5 Purification of PIP4K2A

The gene encoding human PIP4K2A was cloned into a pETM derived bacterial expression vector to create the following fusion protein: His6-SUMO3-(Gly)5-PIP4K2A (1-406aa). Recombinant PIP4KA was expressed in BL21 (DE3) Star E. coli (i.e. lack endonuclease for increased mRNA stability). Using 4 liters of Terrific Broth, bacterial cultures were grown at 37ºC until OD_{600}=0.6. Cultures were then shifted to 18ºC for 1 hour to cool down. Protein expression was induced with 50 µM IPTG and bacteria expressed protein for 20 hours at 18ºC before being harvested by centrifugation. For purification, cells were lysed into buffer containing 50 mM Na_2HPO_4 [pH 8.0], 400 mM NaCl, 0.4 mM BME, 1 mM PMSF (add twice, 15 minutes intervals), DNase, and 1 mg/mL lysozyme using a microtip sonicator. Lysate was centrifuged at 16,000 rpm (35,172 x g) for 60 minutes in a Beckman JA-17 rotor chilled to 4ºC. Lysate was circulated over 5 mL HiTrap Chelating column (GE Healthcare, Cat# 17-0409-01) that had been equilibrated with 100 mM $CoCl_2$ for 1 hour, washed with MilliQ water, and followed by buffer containing 50 mM Na_2HPO_4 [pH 8.0], 400 mM NaCl, 0.4 mM BME. Recombinant PIP4K2A was eluted with a linear gradient of imidazole (0-500 mM, 8 CV, 40 mL total, 2 mL/min flow rate). Peak fractions were pooled, combined with 50 µg/mL of His6-SenP2 (SUMO protease), and dialyzed against 4 liters of buffer containing 25 mM Na_2HPO_4 [pH 8.0], 400 mM NaCl, and 0.4 mM BME for 16-18 hours at 4ºC. Following overnight cleavage of the SUMO3 tag, dialysate containing His6-SUMO3, His6-SenP2, and GGGGG-PIP4K2A was recirculated for at least 1 hour over a 5 mL HiTrap(Co^{2+}) chelating column. Flow-through containing GGGGG-PIP4K2A was then concentrated in a 30 kDa

MWCO Vivaspin 6 before loading onto a Superdex 200 size exclusion column equilibrated in 20 mM HEPES [pH 7], 200 mM NaCl, 10% glycerol, 1 mM TCEP. In some cases, cation exchange chromatography was used to increase the purity of GGGGG-PIP4K2A before loading on the Superdex 200. In those cases, we equilibrated a MonoS column with 20 mM HEPES [pH 7], 100 mM NaCl, 1 mM TCEP buffer. PIP4K2A (pI = 6.9) bound to the MonoS was resolved over a 10-100% linear gradient (0.1-1 M NaCl, 30 CV, 30 mL total, 1.5 mL/min flow rate). Peak fractions collected from the Superdex 200 were concentrated in a 30 kDa MWCO Amicon centrifuge tube and snap frozen at a final concentration of 20-80 μM using liquid nitrogen.

4.5.6 Purification of PH-PLCδ1 domain

The coding sequence of human PH-PLCδ1 (11-140aa) was expressed in BL21 (DE3) E. coli as a His6-SUMO3-(Gly)5-PLCδ1 (11-140aa) fusion protein. Bacteria were grown at 37ºC in Terrific Broth to an OD_{600} of 0.8. Cultures were shifted to 18ºC for 1 hour, induced with 0.1 mM IPTG, and allowed to express protein for 20 hours at 18ºC before being harvested. Cells were lysed into 50 mM Na_2HPO_4 [pH 8.0], 300 mM NaCl, 0.4 mM BME, 1 mM PMSF, 100 μg/mL DNase using a microfluidizer. Lysate was then centrifuged at 16,000 rpm (35,172 x g) for 60 minutes in a Beckman JA-17 rotor chilled to 4ºC. Lysate was circulated over 5 mL HiTrap Chelating column (GE Healthcare, Cat# 17-0409-01) charged with 100 mM $CoCl_2$ for 1 hour. Bound protein was then eluted with a linear gradient of imidazole (0-500 mM, 8 CV, 40 mL total, 2 mL/min flow rate). Peak fractions were pooled, combined with SUMO protease (50 μg/mL final concentration), and dialyzed against 4 liters of buffer containing 50 mM Na_2HPO_4 [pH 8.0], 300 mM NaCl, and 0.4 mM BME for 16-18 hours at 4ºC. Dialysate containing SUMO cleaved protein was recirculated for 1 hour over a 5 mL HiTrap Chelating column. Flow-through containing $(Gly)_5$-PLCδ1 (11-

140aa) was then concentrated in a 5 kDa MWCO Vivaspin 20 before being loaded on a Superdex 75 size exclusion column equilibrated in 20 mM Tris [pH 8.0], 200 mM NaCl, 10% glycerol, 1 mM TCEP. Peak fractions containing $(Gly)_5$-PLCδ1 (11-140aa) were pooled and concentrated to a maximum of 75 µM (1.2 mg/mL) before freezing in liquid nitrogen.

4.5.7 Purification of OCRL

The coding sequence of human 5-phosphatase OCRL (234-539aa of 901aa isoform) was expressed in BL21 (DE3) E. coli as a His6-MBP-(Asn)10-TEV-(Gly)5-OCRL fusion protein. Bacteria were grown at 37ºC in Terrific Broth to an OD600 of 0.8. Cultures were shifted to 18ºC for 1 hour, induced with 0.1 mM IPTG, and allowed to express protein for 20 hours at 18ºC before being harvested. Cells were lysed into 50 mM Na H_2PO_4 [pH 8.0], 300 mM NaCl, 0.4 mM BME, 1 mM PMSF, 100 µg/mL DNase using a microfluidizer. Lysate was then centrifuged at 16,000 rpm (35,172 x g) for 60 minutes in a Beckman JA-17 rotor chilled to 4ºC. Lysate was circulated over 5 mL HiTrap Chelating column (GE Healthcare, Cat# 17-040901) charged with 100 mM CoCl2 for 1 hour. Bound protein was eluted with a linear gradient of imidazole (0-500 mM, 8 CV, 40 mL total, 2 mL/min flow rate). Peak fractions were pooled, combined with TEV protease (75 µg/mL final concentration), and dialyzed against 4 liters of buffer containing 50 mM Na H_2PO_4 [pH 8.0], 300 mM NaCl, and 0.4 mM BME for 16-18 hours at 4ºC. Dialysate containing TEV protease cleaved protein was recirculated for 1 hour over a 5 mL HiTrap Chelating column. Flow-through containing (Gly)5-protein was then concentrated in a 5 kDa MWCO Vivaspin 20 before being loaded on a Superdex 75 (10/300 GL) size exclusion column equilibrated in 20 mM Tris [pH 8.0], 200 mM NaCl, 10% glycerol, 1 mM TCEP. Peak fractions were pooled and concentrated before snap freezing in liquid nitrogen.

4.5.8 Sortase mediated peptide ligation

PIP4K2A, PIP5K1A, and PH-PLCδ1 were labeled on a N-terminal (Gly)5 motif using sortase mediated peptide ligation (*456*, *457*). Initially, a LPETGG peptide was labeled with either Alexa488, Alexa647, or Cy5 conjugated to an amine reactive N-Hydroxysuccinimide (NHS) (e.g. NHS-Alexa488). Protein labeling was achieved by combining the fluorescently labeled LPETGG peptide with the following reagents: 50 mM Tris [pH 8.0], 150 mM NaCl, 50 μM $(Gly)_5$-protein, 500 μM Alexa488-LPETGG, and 10-15 μM His_6-Sortase. This reaction mixture was incubated at 16-18ºC for 16-20 hours, before buffer exchange with a G25 Sephadex column (e.g. PD10) to remove the majority of dye and dye-peptide. The His_6-Sortase was then captured on Ni-NTA agarose resin (Qiagen) and unbound labeled protein was separated from remaining fluorescent dye and peptide using a Superdex 75 or Superdex 200 size exclusion column (24 mL bed volume).

4.5.9 Preparation of small unilamellar vesicles

The following lipids were used to generated small unilamellar vesicles (SUVs): 1,2-dioleoyl-sn-glycero-3-phosphocholine (18:1 DOPC, Avanti # 850375C), L-α-phosphatidylinositol-4-phosphate (Brain PI(4)P, Avanti Cat# 840045X), L-α-phosphatidylinositol-4,5-bisphosphate (Brain $PI(4,5)P_2$, Avanti # 840046X), and 1,2-dioleoyl-sn-glycero-3-phospho-L-serine (18:1 DOPS, Avanti # 840035C). Lipids were purchased as single use ampules containing between 0.1-5 mg of lipids dissolved in chloroform. Brain PI(4)P and $PI(4,5)P_2$ were purchased as 0.25 mg/mL stocks dissolved in chloroform:methanol:water (20:9:1). To make liposomes, 2 μmoles total lipids were combined in a 35 mL glass round bottom flask containing 2 mL of chloroform. Lipids were dried to a thin film using rotary evaporation with the

glass round-bottom flask submerged in a 42ºC water bath. After evaporating all the chloroform, the round bottom flask was flushed with nitrogen gas for at least 30 minutes. We resuspended the lipid film in 2 mL of PBS [pH 7.2], making a final concentration of 1 mM total lipids. All lipid mixtures expressed as percentages (e.g. 98% DOPC, 2% PI(4)P) are equivalent to molar fractions. For example, a 1 mM lipid mixture containing 98% DOPC and 2% PI(4)P is equivalent to 0.98 mM DOPC and 0.02 mM PI(4)P. To generate 30-50 nm SUVs, 1 mM total lipid mixtures were extruded through a 0.03 μm pore size 19 mm polycarbonate membrane (Avanti #610002) with filter supports (Avanti #610014) on both sides of the PC membrane. Hydrated lipids at a concentration of 1 mM were extruded through the PC membrane 11 times.

4.5.10 Preparation of supported lipid bilayers

Supported lipid bilayers were formed on 25x75 mm coverglass (IBIDI, #10812). Coverglass was first cleaned with 2% Hellmanex III (Fisher, Cat#14-385-864) heated to 60-70ºC in a glass coplin jar and incubated for at least 30 minutes. We washed the coverglass extensively with MilliQ water and then etched with Pirahna solution (1:3, hydrogen peroxide:sulfuric acid) for 10-15 minutes the same day SLBs were formed. Etched coverglass, in water, was rapidly dried with nitrogen gas before adhering to a 6-well sticky-side chamber (IBIDI, Cat# 80608). SLBs were formed by flowing 30 nm SUVs diluted in PBS [pH 7.2] to a total lipid concentration of 0.25 mM. After 30 minutes, IBIDI chambers were washed with 5 mL of PBS [pH 7.2] to remove non-absorbed SUVs. Membrane defects were blocked for 15 minutes with a 1 mg/mL beta casein (ThermoFisherSci, Cat# 37528) diluted in 1x PBS [pH 7.4]. Before use as a blocking protein, frozen 10 mg/mL beta casein stocks were thawed, centrifuged for 30 minutes at 21,370 x g, and

0.22 µm syringe filtered. After blocking SLBs with beta casein, membranes were washed again with 1mL of PBS, followed by 1 mL of kinase buffer before TIRFM.

4.5.11 Microscopy

For all live-cell imaging experiments, cells were imaged in 1.6 mL of experiment specific imaging media. Base imaging media contained FluoroBrite DMEM (Life Technologies A1896702) supplemented with 25 mM HEPES (pH 7.4) and 1:1000 chemically defined lipid supplement (SF CHIM). Media was then further supplemented with either 10% fetal bovine serum (CHIM) or 0.1% BSA (0.1% BSA CHIM). Alternatively, Ca^{2+} free Ringer's solution (Ca^{2+} Free) was used, containing 160 mM NaCl, 2.5 mM KCl, 1 mM $MgCl_2$, 8 mM glucose and 10 mM NaHEPES, pH 7.5. For treatments, 0.4 mL of experiment specific imaging media containing fivefold final concentration of compound was applied to the dish (or 0.5 ml for a second addition).

Confocal imaging was performed on a Nikon TiE A1R platform with acquisition in resonant mode with a 100x 1.45 NA plan-apochromatic objective. The signal-to-noise ratio was improved by taking 8 or 16 frame averages. Excitation of fluorophores was accomplished using a dual fiber-coupled LUN-V laser launch with 405-nm (BFP), 488-nm (EGFP and NG2), 561-nm (mCherry), and 640-nm (iRFP) lines. Emission was collected on four separate photomultiplier tubes with blue (425-475 nm), green (500-550 nm), yellow/orange (570-620 nm), and far-red (663-737 nm) filters. Blue and yellow/orange channels were recorded concurrently, as were green and far-red. The confocal pinhole was defined as 1.2x the Airy disc size of the longest wave-length channel used in the experiment. Nikon Elements denoising software was used to further enhance the signal-to-noise ratio.

For TIRFM and single-molecule imaging (SMol), a separate Nikon TiE platform coupled with a Nikon TIRF illuminator arm and 100x 1.45 NA plan-apochromatic objective was used. Excitation of fluorophores was accomplished using an Oxxius L4C laser launch with 405-nm (BFP), 488-nm (EGFP and NG2), 561-nm (mCherry), and 638-nm (iRFP) lines. Emission was collected through dual-pass filters (Chroma) with blue (420-480 nm) and yellow/orange (570-620 nm) together, and green (505-550 nm) and far-red (650-850 nm) together. An ORCA-Fusion BT sCMOS camera (Hamamatsu) was used to capture images. For TIRFM, images were captured with 2x2 pixel binning. For SMol, the NG2 channel was excited with 20% power for 50 ms from the 488-nm laser in a 16x16 μm region of the PM. Images were registered in rolling shutter mode with 2x2 pixel binning with a 1.5x magnifier lens.

For all types of imaging, Nikon Elements software was used to acquire all images for all experiments and all data was saved with the ND2 file extension.

Membrane binding and lipid phosphorylation reactions reconstituted on supported lipid bilayers (SLBs) were visualized using an inverted Nikon Eclipse Ti2 microscope using a 100x Nikon (1.49 NA) oil immersion TIRF objective. TIRF microscopy images of SLBs were acquired using an iXion Life 897 EMCCD camera (Andor Technology Ltd., UK). Fluorescently labeled proteins were excited with either a 488 nm, 561 nm, or 637 nm diode laser (OBIS laser diode, Coherent Inc. Santa Clara, CA) controlled with a Vortran laser drive with acousto-optic tunable filters (AOTF) control. The power output measured through the objective for single particle imaging was 1-2 mW. Excitation light was passed through the following dichroic filter cubes before illuminating the sample: (1) ZT488/647rpc and (2) ZT561rdc (ET575LP) (Semrock). Fluorescence emission was detected on the iXion Life 897 EMCCD camera position after a Nikon emission filter wheel housing the following emission filters: ET525/50M, ET600/50M,

ET700/75M (Semrock). All experiments were performed at room temperature (23ºC). Microscope hardware was controlled by Nikon NIS elements.

4.5.12 Image analysis

Analysis of all images was accomplished using Fiji software (*324*) using the LOCI BioFormats importer (*325*). Custom macros were written to generate channel-specific montages displaying all x,y positions captured in an experiment in concatenated series. In these montages, individual regions of interest (ROIs) were generated around displayed cells.

For confocal images, the ratio or fluorescence intensity between specific compartments was analyzed as described previously (*323*). In brief, a custom macro was used to generate a compartment of interest specific binary mask through à trous wavelet decomposition (*326*). This mask was applied to measure the fluorescence intensity within the given compartment while normalizing to the mean pixel intensity in the ROI.

For TIRFM images, a minimum intensity projection was used to generate ROIs within the smallest footprint of the cells. Background fluorescence was measured and subtracted from all images at all timepoints. The average pixel intensity in each frame (F_t) was normalized to the mean pixel intensity in the ROI of the time points before treatment (F_{pre}) to yield F_t/F_{pre}.

Quantitative data was imported into Prism 8 (GraphPad) for statistical analysis and the generation of graphs and plots. D'Agostino and Pearson normality tests showed data that significantly varied from normal distribution, data were then subjected to a nonparametric Kruskal-Wallis test. If significant difference was found between sample medians, a post hoc Dunn's multiple comparison test was run.

Representative images were selected based on fluorescence measurements near the median of the sampled population, displayed typical morphology, and robust signal-to-noise ratio. If adjusting brightness or contrast, any changes were made across the entire image.

4.5.13 Single Molecule Analysis using Thunderstorm

Mean photon count was estimated using the Fiji ThunderSTORM plugin (*431*). Either HEK293A cells expressing PH-PLCδ1-mNG2x1-3 or NG2-PIP4K2C cells were imaged using SMol settings. Raw images were run through Fiji using the ThunderSTORM plugin. Settings for molecule localization were determined using a wavelet filter with a local maximum method and integrated Gaussian point spread function. To determine fluorescence intensity per spot, histograms of photon counts, in each condition, were generated using a 5-photon bin size.

4.5.14 Kinetic measurements of PI(4,5)P_2 production

The kinetics of PI(4)P phosphorylation was measured on SLBs formed in IBIDI chambers and visualized using TIRF microscopy as previously described (*456*). Reaction buffer contained 20 mM HEPES [pH 7.0], 150 mM NaCl, 1 mM ATP, 5 mM $MgCl_2$, 0.5 mM EGTA, 20 mM glucose, 200 µg/mL beta casein (ThermoScientific, Cat# 37528), 20 mM BME, 320 µg/mL glucose oxidase (Serva, #22780.01 Aspergillus niger), 50 µg/mL catalase (Sigma, #C40-100MG Bovine Liver), and 2 mM Trolox (UV treated, see methods below). Perishable reagents (i.e. glucose oxidase, catalase, and Trolox) were added 5-10 minutes before image acquisition. For all experiments, we monitored the change in PI(4)P or PI(4,5)P_2 membrane density using solution concentrations of 20 nM Alexa647-DrrA(544-647) or 20 nM Alexa488-PLCδ1, respectively.

Table 4.1 Plasmids used in this study

Plasmid	Vector	Insert	Reference
EGFP	pEGFP-C1	EGFP	This study
EGFP-PIP5K1A	pEGFP-C1	EGFP:PIP5K1A	This study
EGFP-PIP5K1A^{D322K}	pEGFP-C1	EGFP:PIP5K1A(D322K)	This study
EGFP-PIP5K1B	pEGFP-C1	EGFP:PIP5K1B	This study
EGFP-PIP5K1B^{D266K}	pEGFP-C1	EGFP:PIP5K1B(D266K)	This study
EGFP-PIP5K1C	pEGFP-C2	EGFP:PIP5K1C	(*432*)
EGFP-PIP5K1C^{D316K}	pEGFP-C2	EGFP:PIP5K1C(D316K)	(*432*)
TagBFP2-Mss4-Kina	pTagBFP2-C1	mTagBFP2:*S. cerevisiae* Mss4(377-756)	This study
TagBFP2-Mss4^{D636K}-Kina	pTagBFP2-C1	mTagBFP2:*S. cerevisiae* Mss4(377-756)(D636K)	This study
TagBFP2	pTagBFP2-C1	mTagBFP2	This study
TagBFP2-PIP4K2A	pTagBFP2-C1	mTagBFP2:PIP4K2A	(*60*) This study
TagBFP2-PIP4K2A^{D273K}	pTagBFP2-C1	mTagBFP2:PIP4K2A(D273K)	This study
TagBFP2-PIP4K2B	pTagBFP2-C1	mTagBFP2:PIP4K2B	(*60*) This study
TagBFP2-PIP4K2C	pTagBFP2-C1	mTagBFP2:PIP4K2A	This study
mCherry-FKBP-PIP4K2A	pmCherry-C1	mCherry:FKBP1A(3-108):[GGSA]$_4$GG:PIP4K2A	(*60*) This study
mCherry-FKBP-PIP4K2A^{D273K}	pmCherry-C1	mCherry:FKBP1A(3-108):[GGSA]$_4$GG:PIP4K2A(D273K)	This study
mCherry-FKBP-PIP4K2B	pmCherry-C1	mCherry:FKBP1A(3-108):[GGSA]$_4$GG:PIP4K2B	(*60*) This study
mCherry-FKBP-PIP4K2C	pmCherry-C1	mCherry:FKBP1A(3-108):[GGSA]$_4$GG:PIP4K2C	This study
EGFP-INPP5E	pEGFP-C2	EGFP:*Mus musculus* INPP5E	(*458*)
Lyn$_{11}$-FRB-iRFP	piRFP-N1	LYN(1-11):MTOR(2021-2113):iRFP	(*408*)
TagBFP2-FKBP-INPP5E	pTagBFP2-C1	mCherry:FKBP1A(3-108):[GGSA]$_4$GG:INPP5E(214-644)	(*408*)
TagBFP2-FKBP-INPP5E^{D477N}	pTagBFP2-C1	mCherry:FKBP1A(3-108):[GGSA]$_4$GG:INPP5E(214-644)(D477N)	This study
mCherry-Mss4-Kina	pmCherry-C1	mCherry:*S. cerevisiae* Mss4 (377-756)	This study
mCherry-Mss4^{D636K}-Kina	pmCherry-C1	mCherry:*S. cerevisiae* Mss4 (377-756)(D636K)	This study
TagBFP2-FKBP-PIP5K1C_Kina-HD	pTagBFP2-C1	mTagBFP2:FKBP1A(3-108):[GGSA]$_4$GG:PIP5K1C(79-366)(D101R/R304D)	This study
TagBFP2-FKBP-PIP5K1C_Kina-HD^{D316K}	pTagBFP2-C1	mTagBFP2:FKBP1A(3-108):[GGSA]$_4$GG:PIP5K1C(79-366)(D101R/R304D/D316K)	This study
HAx3-AChR-M3	pcDNA3.1	HAx3:CHRM3(2-590)	J. Wess

Table 4.1 Continued

TagBFP2-HRAS-CAAX	pTagBFP2-C1	TagBFP2:HRAS(172-189)	(*459*)
iRFP713-FRB-PIP5K1A	piRFP-C1	iRFP713:MTOR(2021-2113):GGSA$_2$:PIP5K1A	This study

iRFP713-FRB-Mss4-Kina	piRFP-C1	iRFP713:MTOR(2021-2113):$GGSA_2$:*S. cerevisiae* Mss4 (377-756)	This study
TagBFP2-FKBP-CYB5Atail	pTagBFP2-C1	mTagBFP2:FKBP1A(3-108):$[GGSA]_4$GG:CYB5A(100-134)	(*323*)
mCherry-FKBP-PIP4K2A-Kina	pmCherry-C1	mCherry:FKBP1A(3-108):$[GGSA]_4$GG:PIP4K2A(33-406)	This study
mCherry-FKBP-PIP4K2A-NTerm	pmCherry-C1	mCherry:FKBP1A(3-108):$[GGSA]_4$GG:PIP4K2A(1-32)	This study
EGFP-INPP5E-CAAX	pEGFP-C1	EGFP:INPP5E(214-644):HRAS(172-189)	This study
Lyn_{11}^{C3S}-EGFP	pEGFP-N1	LYN(1-11)(C3S):EGFP	This study
EGFP-Lyn_{11}^{C32S}-PIP4K2A	pEGFP-C1	EGFP:LYN(1-11)(C3S):PIP4K2A	This study
$Tubby_C$-EGFP	pEGFP-N1	*Mus musculus* Tub(243-505):EGFP	(*316*)
$Tubby_C^{R332H}$-EGFP	pEGFP-N1	*Mus musculus* Tub(243-505)(R332H):mCherry	(*316*)
$Tubby_C$-mCherry	pmCherry-N1	*Mus musculus* Tub(243-505):mCherry	(*316*)
$Tubby_C^{R332H}$-mCherry	pmCherry-N1	*Mus musculus* Tub(243-505)(R332H):EGFP	(*316*)
PH-PLCδ1-EGFP	pEGFP-N1	PLCD1v2(1-170):EGFP	(*451*)
NES-EGFP-PH-$ARNO^{2G-I303Ex2}$	pEGFP-C1	*X. Laevis* map2k1.L(32-44):EGFP:CYTH2(252-399)(I303E):GGSGGVDM:CYTH2(252-399)(I303E)	(*459*)
R-GECO1.2	pcDNA3	R-GECO1 (M164R / I166V / V174L / F222L / N267S / S270T / I330M / L419I)	(*460*)
iRFP670-PIP5K1A	piRFP670-C1	iRFP670:PIP5K1A	This study
iRFP670-PIP4K2C	piRFP670-C1	iRFP670:PIP4K2C	This study
PH-PLCδ1-mNGx1	pmNG2-N1	PLCD1v2(1-170):mNG2	This study
PH-PLCδ1-mNGx2	pmNG2-N1	PLCD1v2(1-170): mNG2:mNG2	This study
PH-PLCδ1-mNGx3	pmNG2-N1	PLCD1v2(1-170): mNG2:mNG2:mNG2	This study
His6-OCRL	pFastBac1	His6-MBP-Asn10-TEV-Gly5-OCRL (901isoform)(234-539)	(*418*)
His6-PIP4K2A	pETM	His6-SUMO3- Gly5-PIP4K2A(1-406)	This study
His6-Mss4	pFastBac1	His6-MBP-TEV-Gly5-Mss4(379-779)	(*92*)
His6-PIP5K1A	pFastBac1	His6-MBP-TEV-Gly5-PIP5K1A(1-546)	(*92*)
His6-PH-PLCδ1	pETM	His6-SUMO3-Gly5-PLCD1(11-140)	(*418*)

Table 4.2 HDR and gRNA sequences for PIP4K2C.

Gene	**crRNA sequence**
PIP4K2C	TAATACGACTCACTATAGGGGAGACTATGGCGTCCTCCTGTTTAAGAGCTATGCTGGAA
	HDR sequence
PIP4K2C	CCGCTTCCGGGGTCGGGCGCCTGGATAGCTGCCGGCTCCGGCTTCCACTTGGTCGGTTG CGCGGGAGACTATGACCGAGCTCAACTTCAAGGAGTGGCAAAAGGCCTTTACCGATAT GATGGGTGGCGGCATGGCGTCCTCCTCGGTCCCACCAGCCACGGTATCGGCGGCGACA GCAGGCCCCGGCCCAGGTTTCGGCT

5.0 Discussion and Perspectives

5.1 Study Synopses

The plasma membrane (PM) of mammalian cells is an ever-bustling hub of activity. A myriad of activities are coordinated by phosphatidylinositol 4,5-bisphosphate ($PI(4,5)P_2$), a master regulator of PM dynamics; ranging from the generation of second messengers (*36*, *100*, *413*) to attachment of the cytoskeleton (*411*) to assembly of retroviruses (*409*, *433*). In these works, we have focused on four major aspects of $PI(4,5)P_2$ metabolism:

1) Detection and manipulation of lipids, particularly $PI(4,5)P_2$, with biosensors,

2) The mechanism of PM targeting by PIP5K,

3) The mechanism of $PI(4,5)P_2$ homeostasis at the PM, and

4) Physiological impacts of aberrant $PI(4,5)P_2$ homeostasis.

This all comes together to reveal a surprisingly simple mechanism of $PI(4,5)P_2$ homeostatic control revolving around two proteins involved in the biochemical synthesis of this critical lipid (**Figure 4.8A**).

5.1.1 $PI(4,5)P_2$ detection and manipulation

Genetically encoded lipid biosensors remain a prevalent tool used to study the function and metabolism of discrete lipid populations in living cells using microscopy. Here, we have shown that $PI(4,5)P_2$ can be visualized and quantified while simultaneously chronically or acutely modifying lipid levels using kinases or phosphatases in living cells (*305*, *316*, *451*, *452*). We

briefly discussed potential caveats when using lipid biosensors; the interpretation of biosensor localization should be used as a part of a holistic story when interpreting lipid dynamics in cells. For these reasons and more, we believe that biosensors are an incredibly useful tool for the study of lipid dynamics in living cells, in real time.

5.1.2 PI(4,5)P_2 synthesis is rapidly re-initiated after stimulated depletion

Phosphatidylinositol 4-phosphate 5-kinase (PIP5K) plays the primary role in PM PI(4,5)P_2 synthesis in cells (*62–65*). This enzyme appears to be exclusively localized to the PM; due, in part, to an interaction with its product, PI(4,5)P_2. Our data support previous work showing that PIP5K is positively regulated at the PM due to an interaction with its catalytic product (*418*). This interaction appears to be facilitated, in part, by two basic residues in the C-terminal tail immediately proximal to the kinase domain. Moreover, this interaction requires both the activation loop as well as the insert loop. Structurally, the yet uncharacterized insert loop is located near the two basic residues and immediately opposite the activation loop of PIP5K. We propose that the interaction with PI(4,5)P_2 may be mediated in part by the insert loop, either by direct binding or by conformational change to the PIP5K kinase domain.

5.1.3 PI(4,5)P_2 synthesis is negatively regulated

We identified a mechanism of PI(4,5)P_2 driven positive feedback mechanism for PIP5K. Knowing that levels of PI(4,5)P_2 do not exceed the baseline, we hypothesized that cells must also be able to negatively regulate PI(4,5)P_2 production. In our second study, we show that phosphatidylinositol 5-phosphate 4-kinase (PIP4K) negatively regulates PIP5K activity.

Furthermore, this negative regulation occurs independent of PIP4K catalytic activity. The over-expression of PIP4K decreases the level of $PI(4,5)P_2$ at the PM of cells and this effect is seen between PIP4K2A and PIP5K1A in a minimal purified system. Like PIP5K, PIP4K binds to $PI(4,5)P_2$, though with low affinity. Through this mechanism, PIP4K is recruited to the PM in a $PI(4,5)P_2$ dependent manner to interact with and inhibit the activity of PIP5K. We propose that this generates a negative feedback mechanism for $PI(4,5)P_2$ synthesis.

5.1.4 Physiological impacts of aberrant $PI(4,5)P_2$ homeostasis

The cellular mechanisms for both positive and negative regulation of $PI(4,5)P_2$ homeostasis illustrate the overall importance of this essential lipid. Perturbations in this system of feedback can lead to changes in both Ca^{2+}-specific PLC signaling and PI3K signaling. Specifically, we show that decreases in $PI(4,5)P_2$ lead to reductions in Ca^{2+} signaling, but that increases in baseline $PI(4,5)P_2$ do not seem to impact Ca^{2+} signaling, as it may already be saturated. PI3K, on the other hand, seems to be impacted linearly by changes in baseline $PI(4,5)P_2$. Using this knowledge as a foundation, PIP5K or PIP4K protein abundance can be used as biomarkers for predictive models to assess downstream physiological impacts from aberrant $PI(4,5)P_2$ homeostasis.

5.2 Perspectives

This text has been pulled from a combination of grant submissions to the American Heart Association and the National Institutes of Health, most recently a National Cancer Institute Grant Awarded to Rachel C Wills (F531CA247349).

5.2.1 Potential PIP5K interactions

We have shown that the insert loop of PIP5K has a role in PM association, and potentially, PI(4,5)P_2 binding. An interesting observation is that the spatial localization of the insert loop and the basic C-terminal tail residues are on the opposite face of the protein when compared to the activation loop and active site. The unstructured insert loop is approximately 50 amino acid residues in length. This loop contains five conserved basic residues and structurally lies in close proximity to the necessary basic residues in the C-terminal tail. These residues may assist in the formation of a basic pocket which could interact with the negatively charged PI(4,5)P_2 headgroup. Furthermore, the insert loop contains several hydrophobic residues which could integrate with the PM, similar to the interaction between the activation loop and the PM (*42*). Additionally, the insert loop may be required for the allosteric regulation of PIP5K, potentially revealing a cryptic PM / PI(4,5)P_2 binding site (*461*, *462*). Finally, there are four conserved Tyr, Ser, or Thr residues in the insert loop which could easily be targeted for phosphorylated, though there is no evidence to date that this occurs physiologically (*463–465*). This phosphorylation event could also induce a confirmational change or allow for a protein-protein interaction at the PM. Ultimately, a specific interaction between PIP5K and PI(4,5)P_2 would need to be determined both in the presence and the absence of the insert loop. Point mutants should be used to specifically map the PI(4,5)P_2 interaction site and determine which residues are necessary for PM association, PI(4,5)P_2 binding, and catalytic activity. Given the spatial location and amino acid composition of the insert loop, it is easy to see how this domain could have any number of functions in PIP5K PM association, and these specific functions have yet to be elucidated. Regardless, these lipid binding regions of PIP5K further prolong the PM association as PIP5K “searches” for substrate.

Work has been done to map the specific region of interaction between PIP5K and PIP4K (**Figure 4.7**) (*56*). This work has mainly focused on identifying the region of PIP4K that is responsible for the negative regulation. Therefore, identifying the point of PIP5K where this inhibitory interaction takes place is still important. Our data support that PIP5K and PIP4K directly interact with one another (Figure 4.8). In brief, our data suggests that the over-expression of a catalytically inactive minimal construct of PIP5K ($Kina^{++CatDead}$) also yields the same increase in $PI(4,5)P_2$ biosensor at the PM as the full-length active overexpression constructs (data not shown). We interpret this data to mean that PIP4K interacts not only with full-length PIP5K, but with this minimal fragment. We further hypothesize that the N-terminus of PIP4K mediates the interaction with the PIP5K kinase domain. Again, the PIP5K G-loop, insert loop, and activation loop all make excellent candidates for places to study the region of interaction with PIP4K. Furthermore, the crystal structure of the PIP5K kinase domain reveals specific residues which may facilitate an interaction between these two proteins that could be easily mutated (*70*). Of special interest, there are several Lys and Tyr residues which are exposed in the PIP5K kinase domain. These residues can be genetically altered to introduce an artificial caged amino acid at these residues (*466*). Following optical illumination of cells transfected with these engineered constructs the caged residue is freed (*318*, *466*). We can use this technique to acutely determine which ones mediate the interaction with PIP4K. This would allow us the ability to observe the proposed mechanism from **Figure 4.1C** in real-time.

Other potential regions of the PIP5K which could be assessed for their contribution in PM binding are the G-loop, the N-terminus, and the C-terminal tail regions. The specific functions or interaction partners of the G-loop and the N-terminus are still unknown (*48*). These regions are likely to fold and influence the structure of the PIP5K kinase domain or allosterically regulate

points of contact between other lipids or proteins. The different isoforms of PIP5K are found concentrated in different subcellular locations due to differing protein-protein interactions (*84*, *85*, *87–89*). Furthermore, the C-terminal tail of several of the various PIP5K1C splice variants have also been shown to play a role in the targeted localization (*65*, *74*, *75*, *86–89*). Of final note, these regions lack structural information, both from crystallography (*70*) or predictive modeling (*426*, *427*), lending them to be excellent candidates for further study and work.

5.2.2 Protein-lipid interactions

It has been proposed that PIP5K interacts with multiple lipids: PI4P, $PI(4,5)P_2$, and PA. The interaction with PI4P is well characterized and required for PIP5K activity (*73*, *292*). The interaction with $PI(4,5)P_2$ is less well understood. It has been proposed that the PIP5K interaction with $PI(4,5)P_2$ can be involved in either positive feedback mechanism (this work and (*92*)) or an inhibitory mechanism (*64*, *69*). Understanding the mechanism of this interaction and the impact that it plays on PIP5K catalytic activity and cellular localization is essential in the cellular context. Finally, it is possible that PIP5K localization is driven by the binding to PA, an acidic phospholipid, at the PM, and that this interaction stimulates PIP5K activity to produce $PI(4,5)P_2$ (*65*, *69*, *171*). We believe that PA is unlikely the crucial lipid, as $PI(4,5)P_2$ depletion is sufficient for PIP5K1B and PIP5K1C to dissociate from the PM. However, we could test this by generating $PI(4,5)P_2$ or PA containing SLBs and assessing both binding and activity. These experiments will still be useful in determining the roles of both $PI(4,5)P_2$ and PA in PIP5K activity.

We propose that the mechanism by which PIP4K is recruited to the PM is dependent on a low affinity interaction with $PI(4,5)P_2$ (**Figure 4.4**). It could be hypothesized that the site of $PI(4,5)P_2$ binding is the PIP4K active site, however the residues necessary for this interaction have

not been determined. This could easily be done by mutating the active site or by mutating basic regions/residues of PIP4K which may interact with $PI(4,5)P_2$ and repeating the SLB experiments from **Figure 4.6** to determine the mechanism by which PIP4K interacts with $PI(4,5)P_2$. In doing so, the affinity for $PI(4,5)P_2$ may also be calculated, which would confirm the low affinity interaction that was proposed. By mapping the residues required for the protein-lipid interactions listed, we can shed light on the mechanisms by which PIP5K may become activated or inactivated. Using these sites of interaction, small molecules could be generated to recapitulate the desired effect on PIP5K catalytic activity.

5.2.3 Health and disease

The role of $PI(4,5)P_2$ has been implicated in several diseases (*8*). As part of understanding the role of $PI(4,5)P_2$ in disease, it may first be important to understand the physiological range for $PI(4,5)P_2$ in certain cell types. However, the mol % of $PI(4,5)P_2$ in various cells types is not well characterized. For example, the pineal gland, cultured human embryonic kidney cells, and Chinese hamster ovary cells all have different basal levels of $PI(4,5)P_2$ (*11*, *467*, *468*). Furthermore, the range of $PI(4,5)P_2$ that is necessary to carry out cell specific $PI(4,5)P_2$ dependent functions has also not been defined. **Figure 4.8** showed some of the differential effects that alterations in baseline $PI(4,5)P_2$ can have on either PI3K or Ca^{2+} signaling.

One area of future study encompasses defining the physiological range of $PI(4,5)P_2$ for contractile signaling in vascular smooth muscle cells (VSMCs). In hypertension, although multiple treatment options are available, 75% of patients require combination therapy to achieve a healthy blood pressure. Moreover, it is estimated that 10% of patients do not respond to combinatorial treatments (*469*). Many medications target different steps in VSMC contraction. $PI(4,5)P_2$ plays a

central role at each of these steps. However, the mechanism by which $PI(4,5)P_2$ abundance is regulated in VSCMs to maintain stimulus-coupled contraction is poorly understood. The goal of this proposal is to determine the mechanism of $PI(4,5)P_2$ homeostasis and the physiological range of $PI(4,5)P_2$ in VSMCs for stimulus-coupled contraction. Vasodilating hormones, such as angiotensin II and vasopressin, stimulate VSMCs and trigger phospholipase C mediated $PI(4,5)P_2$ degradation. This generates IP_3, which both triggers intracellular Ca^{2+} release and depolarizes the cell to allow for extracellular Ca^{2+} flux via $PI(4,5)P_2$ dependent channels (see Section 1.4 for additional details). The acto-myosin network directly connects to the PM to allow for contraction; specifically, dense bodies are linked to actin by vinculin and alpha-actinin, which are both activated by $PI(4,5)P_2$ (*470*). $PI(4,5)P_2$ is thus absolutely essential for VSMC stimulation-contraction coupling, and even slight alterations in $PI(4,5)P_2$ abundance are expected to have a profound effect on contractile ability. However, it is unknown how $PI(4,5)P_2$ metabolism is regulated in VSMCs, or how alterations in this metabolism may contribute to diseases, such as hypertension. We have shown that there are some alterations in Ca^{2+} signaling with decreased amounts of $PI(4,5)P_2$, but there are few changes to intracellular IP_3-mediated Ca^{2+} levels with increases in basal $PI(4,5)P_2$. However, in the presence of extracellular media containing Ca^{2+}, SOCE increased in a $PI(4,5)P_2$ dependent manner. Furthermore, changes in basal $PI(4,5)P_2$ may have a profound impact on NCX and the PMCA ATPase. Further study could determine how each of these processes are independently impacted by altered $PI(4,5)P_2$ levels. Additionally, changes in either PKC mediated signaling or acto-myosin based contraction have yet to be determined. We hypothesize that increased $PI(4,5)P_2$ increases PKC signaling and acto-myosin contraction. We can test this hypothesis by altering the baseline $PI(4,5)P_2$ levels in cells, such as A10 VSMCs (*471*). Again, we can measure changes in Ca^{2+}, myosin light chain phosphorylation, and assembly

of dense body structural components (vinculin and α-actinin). This will allow us to determine how changes in $PI(4,5)P_2$ concentration lead to either hypo- or hyper-responsiveness. The proposed research is expected to be the identification of key molecular components involved in the homeostasis of $PI(4,5)P_2$ in VSMCs, and to determine how changes in metabolism affects contractility in VSMCs.

Another proposed area of study includes defining the role of altered $PI(4,5)P_2$ homeostasis in driving PI3K signaling, and its effect on breast cancer cell proliferation. PI3K, which produces a majority of $PI(3,4,5)P_3$, is overactive in over 40% of breast cancer cases (cBioPortal: March2019: PIK3CA or PIK3CB: BreastCancer) (*472*, *473*). Most commonly, the PI3Kα isoform (encoded by PIK3CA) is amplified and/or acquires activating mutations, accounting for the majority of the ~40% of breast cancer cases (*474*, *475*). With approximately 120,000 new breast cancer patients possessing overactivated PI3Kα, there has been a significant effort to develop PI3K inhibitors as targeted therapies (*472*, *473*, *476*, *477*). The PI3Kα-specific inhibitor, Alpelisib (BYL719), has recently shown a doubling of progression-free survival for patients with hormone receptor positive (HR+) advanced breast cancer (*478*). The phase III trial, SOLAR-1, was able utilize genetic testing to specifically target patients with activated PI3Kα and thus elevated $PI(3,4,5)P_3$ levels (*478*, *479*). $PI(3,4,5)P_3$ is a driver of cell proliferation and increased $PI(3,4,5)P_3$ levels are found in tumors (*473*, *480*, *481*).

PIP5K1A has been implicated as a driver in numerous cancers including breast cancer (*293*, *482*, *483*), prostate cancer (*484*, *485*), and lymphoma (*486–488*). In breast cancer, PIP5K1A is found amplified in over 18% of tumors, and this amplification is found independent of PI3Kα mutations in half of these cases (*474*, *475*). It has been demonstrated that amplified PIP5K results in increased $PI(4,5)P_2$ levels (*65*, *489*). However, it is not yet understood whether PIP5K1A

amplification and elevated $PI(4,5)P_2$ levels drive tumor growth by enhancing $PI(3,4,5)P_3$ production. We have shown that altered $PI(4,5)P_2$ homeostasis drives PI3K signaling in a linear fashion (**Figure 4.8**). However, the downstream impacts of this signaling are not yet known. Our hypothesis is that increased levels of $PI(4,5)P_2$ result in increased PI3K signaling. This hypothesis can be tested by utilizing biosensors to measure changes in $PI(3,4,5)P_3$ levels and AKT phosphorylation after manipulation of $PI(4,5)P_2$ levels. Furthermore, we can test cancer cell proliferation and migration after the same $PI(4,5)P_2$ modulations. We propose that these experiments will identify increased $PI(4,5)P_2$ as a driver of breast cancer cell proliferation via enhanced PI3K signaling.

Tamas Balla once quipped that "It may be an exaggeration, but with some efforts every human disease can be linked to altered inositol lipid metabolism." I would whole heartedly agree, though would like to push that even further and say that, with some effort, every human disease can be linked to altered $PI(4,5)P_2$ levels.

Appendix A Quantification of genetically encoded lipid biosensors

Appendix A.1 Materials

Appendix A.1.1 Tissue Culture

1. Glass-bottom culture dishes. 35 mm, #1.5 glass-bottom dishes, with 200 mm glass aperture (In vitro Scientific).
2. Extracellular matrix for coating dishes. Fibronectin solution,1 mg/mL in DDiH2O.
3. Extracellular matrix for coating dishes. Entactin–Collagen IV–Laminin (ECL) Cell Attachment Matrix.
4. Phosphate-buffered saline (PBS). Purchased directly from suppliers.
5. Cell dissociation reagent. Trypsin or TrypLE.
6. Complete cell culture media. DMEM (low glucose), 10% fetal bovine serum (FBS), 100 U/mL penicillin, 100 U/mL streptomycin, 1:1000 chemically defined lipid supplement (CDLS).
7. HeLa cells. The HeLa cervical cancer immortalized cell line can be purchased from the American Type Culture Collection (ATCC).
8. HEK293A cells. The HEK293A embryonic kidney immortalized cell line can be purchased from ThermoFisher Scientific.
9. Transfection reagent. Cationic liposomal transfection reagent, such as Lipofectamine 2000.
10. Reduced serum medium for transfection. Minimal essential medium (MEM), such as Opti-MEM.

11. Plasmids for the expression of lipid sensors are readily available at Addgene (https://www.addgene.org/). The different options are listed in **Table 1**.

Appendix A.1.2 Microscopy

1. Complete HEPES Imaging Media (CHIM). Phenol red-free DMEM (FluorBrite), 10% FBS, 2 mM GlutaMax, 25 mM HEPES, pH 7.4, 1:1000 CDLS.
2. Plasma membrane stain. 1:5000 CellMask deep red.
3. Microscope. TIRF microscope, such as Nikon TiE with TIRF illuminator arm with 100X 1.45 NA plan-apochromatic objective.
4. Microscope. Confocal microscope, such as Nikon TiE A1Rwith 100X 1.45 NA plan-apochromatic objective.

Appendix A.1.3 Imaging analysis

1. Image processing software package. ImageJ or Fiji Image Analysis software (*490*, *491*) (see Note 1).
2. Statistics software package. Excel or Prism 8—GraphPad Prism.

Appendix A.2 Methods

Appendix A.2.1 Seeding cells

For each glass-bottom culture dish, coat glass with either FN or ECL (see Note 2).

Coating Dishes with FN

1. Dilute 5µL of 1 mg/mL stock FN into 500µL of DDiH2O and add to the glass inset at the bottom of the 35-mm dish.
2. Incubate for 30–60 min in an incubator.
3. Aspirate DDiH2O and FN and add 2 mL of complete DMEM and return to the incubator to continue to warm.

Coating Dishes with ECL

1. Dilute 10µL of 1 mg/mL stock ECL into 500µL of DMEM and add to the glass inset at the bottom of the 35-mm dish.
2. Incubate for 60 min in an incubator.
3. Aspirate DMEM and ECL and add 2 mL of complete DMEM and return to the incubator to continue to warm.

Appendix A.2.2 Splitting and seeding cells

1. Using a sterile aspirating pipette, aspirate media from a confluent T75 flask (see Note 3).
2. Wash the adherent layer of cells once with 10 mL of PBS (see Note 4).
3. Add 1 mL of TrypLE and place the flask in an incubator for 1–5 min until cells have detached from the surface of the flask.
4. Add 4 mL of complete DMEM to neutralize the TrypLE and to resuspend the cells in a total volume of 5 mL.
5. Seed cells in previously coated dishes at an appropriate volume (see Note 5). For a next day transfection, seed 160 µL of cell suspension, or seed cells at 25%.

6. Allow cells to settle and adhere for >1 h before transfecting. **Appendix Table 1.1** shows an overview of the cell suspension volumes for variations in seeding before transfection.

Appendix A.2.3 Transfect cells

Per 35-mm glass-bottom dish:

1. Dilute 3.1 µL of Lipofectamine 2000 into 96.9 µL of OptiMEM in a 1.7-mL tube and mix. Generate a master mix for multiple transfections.
2. Dilute up to 1 µg total plasmid DNA (10 µL total) into a total of 100 µL Opti-MEM in a 1.7-mL tube and mix (see Note 6). Again, generate a master mix for multiple transfections. Below is an example of a single transfection mix for EGFP with biosensors for PI4P and for $PI(4,5)P_2$ (see Note 7).
    a. 0.25 µg EGFP-C1.
    b. 0.25 µg mCherry-Tubby$_C^{R332H}$.
    c. 0.25 µg TagBFP2-P4Mx1 (see Note 8).
    d. 92.5 µL Opti-MEM (see Note 9).
3. Combine the 100-µL diluted Lipofectamine 2000 and the 100-µL diluted DNA, and mix gently by flicking. Incubate for ~15 min at room temperature to allow for the formation of lipid–DNA complexes.
4. Add the total 200-µL volume of lipid–DNA complex to the pre-seeded 35-mm glass-bottom dish.
5. After ~4 h, aspirate the transfection mix off of the cells and replace with 2 mL of fresh, prewarmed, complete DMEM.
6. For transient transfections, visualize cells 16–48 h after transfection

Appendix A.3 Microscope set up and imaging

Appendix A.3.1 TIRF microscopy

1. Use appropriate excitation for each fluorescent protein. For example, we use a fiber-coupled device with 405-nm (for TagBFP2), 488-nm (for EGFP), 561-nm (for mCherry), and 640-nm (for iRFP) laser lines to excite the indicated fluorescent protein.
2. Collect fluorescence emission with appropriate bandwidth filters. For example, blue and yellow/orange channels are imaged through a dual-pass 420–480 nm and 570–620 nm Chroma filter, respectively, and green and far/infrared are imaged through a dual-pass 505–550 nm and 650–850 nm Chroma filter, respectively.
3. Optimize the incidence angle of the illuminating beam to greater than the critical angle, pixel binning, excitation intensity, and/or camera exposure time to maximize the signal-tonoise ratio in images and minimize phototoxicity (i.e., set the minimal excitation power and exposure time) (see Note 10).
4. A motorized XY positioning stage is used to register up to 30 fields during the recording period (see Note 11).
5. Configure software acquisition to take one image over the 30 marked XY positions with no lag between images (see Note 12).

Appendix A.3.2 Confocal microscopy

1. Use appropriate excitation for each fluorescent protein. For example, we use a fiber-coupled device with 405-nm (for TagBFP2), 488-nm (for EGFP), 561-nm (for mCherry), and 640-nm (for iRFP) laser lines to excite the indicated fluorescent protein.
2. Collect fluorescence emission with appropriate bandwidth filters. We use Chroma filters with 425–475 nm (for TagBFP2), 500–550 nm (for EGFP), 570–620 nm (for mCherry), and 663–737 nm (for iRFP). Differential interference contrast (DIC) is used on a transmitted light channel for confocal imaging.
3. Set confocal pinhole at diameter for maximal axial resolution based on the longest wavelength channel (e.g., 1.2x Airy disc size on our Nikon A1R).
4. Optimize confocal scan speed, line averaging, detector gain, excitation intensity, and/or camera exposure time for maximal signal-to-noise ratio in images with minimal phototoxicity (i.e., minimal excitation power and exposure time possible) (see Note 13).
5. A motorized stage is used to register up to 30 fields during the whole recording period (see Note 11).
6. Configure software acquisition to take one image over the 30 marked XY positions with no lag between images.

Appendix A.3.3 Imaging 35-mm dishes

1. Prewarm CHIM media (2.5 mL per dish) (see Note 14).
2. Prepare CellMask (500 μL per dish at 1:5000 in prewarmed CHIM, i.e., 0.1 μL per dish).

3. Aspirate media off dish and add 500 μL of prediluted CellMask in CHIM. Allow to incubate for 3 min.
4. Aspirate the CellMask mix and replace with 2 mL of fresh CHIM.
5. Apply immersion oil on the 100X plan-apochromatic, 1.45 NA objective lens.
6. Mount the dish on the microscope.
7. Find the focus plane and look for healthy cells showing fluorescent signals in the channels required (see Note 15).
8. Save up to 30 positions for acquisition during the experiment.
9. Optimize the scan path and record the data to a file location of choice.

Appendix A.4 Data analysis

The above microscopy experiment results in images at single data points, which can be used to determine changes in lipid levels due to chronic effects, such as expression changes in lipid metabolizing enzymes. These differences can be observed at the plasma membrane using TIRFM or other membranes using confocal microscopy. We note that the quantification of data from TIRF microcopy is better suited for time-lapse imaging; refer to **Appendix B** for a detailed protocol. The following analysis best applies for images acquired by confocal microscopy.

1. Import files into ImageJ (or its cell biology optimized build, Fiji) using the Laboratory for Optical and Computational Instrumentation (LOCI) Bio-Formats importer (*490*, *491*) (see Note 16).
2. Draw ROIs in the iRFP channel, around the CellMask-stained PM, of each cell to be analyzed using the Freehand selection tool (see Note 17).

3. Select the image(s) to be used to generate the mask and duplicate this image three separate times (Image -> Duplicate). Rename the starting image of I0 (Image -> Rename). Rename the other three duplicates I1, I2, and I3.
4. Each of these images will be processed using a Gaussian blur filter with a progressively larger radius determined by the point spread function (PSF) of the channel used to generate the mask (Process -> Filters -> Gaussian Blur).
5. PSF = Wavelength/ 2 x NA = 640/2 x 1:45 = 0:22 μm.
6. The radius for the filter in I1 = 0.22 μm, I2 = 0.44 μm, and I3 = 0.66 μm.
7. I0–I3 can then be used to generate wavelets 1–3.
8. Using the image calculator function, generate the three wavelets by subtracting each smoothed image from the previous image (Process -> Image Calculator).
    a. I0–I1 = W1
    b. I1–I2 = W2
    c. I2–I3 = W3
9. Determine the standard deviation (SD) of each resulting wavelet and threshold each by 0.5*SD (Analyze -> Measure).
10. Generate the product of the three wavelets to generate a filtered image (Process -> Image Calculator).
    a. W 1 * W2 * W3 10.
11. Convert this image to a binary Mask by converting to 32-bit and dividing the image by itself (Image -> Type -> 32-bit -> Process -> Image Calculator). Set the brightness and contrast on this image between 0 and 1 (Image -> Adjust -> Brightness/Contrast -> Set).
12. Save this as Mask.

13. Measure and determine the mean intensity of all ROIs in each channel (Analyze -> Measure).
14. Normalize the intensity of each ROI to the mean intensity of each channel.
15. Measure the intensity of each channel within the mask by multiplying the image by the mask (Process -> Image Calculator).
16. Calculate the ratio of intensity within the mask relative to the intensity in the ROI (organelle/cyt or PM/cyt here).
17. Copy and paste data into GraphPad Prism or other data analysis software and format as desired.
18. This process is illustrated in **Figure 1X** (see Note 18).
19. The data collected from this process are then illustrated in **Figure 1X**.

Appendix A.5 Notes

1. Fiji is a free version of ImageJ2, which includes the LOCI Bio-Formats importer. The Fiji software is also regularly updated using a built-in macro.
2. Dishes can be coated with FN for most cells; however, ECL coating should be used for poorly adherent HEK293A cells.
3. To ensure reproducibility of experiments, it is recommended that cells have been passaged no more than 30 times.
4. Prewarm complete DMEM, PBS, and TrypLE to 37˚C for >20 min before culturing cells. DMEM can be prewarmed in a vented tissue culture flask in the incubator to allow for gas exchange.

5. Consider a doubling time of 24 h for cells, recommended seeding density of 50% for a same day transfection, or a seeding density of 25% for a next day transfection. Volume of cell suspension per dish = (confluence at seeding/100) x (dish surface area/surface area of flask) x resuspension volume (**see Appendix Table 1.1**).
6. The volume of DNA can be controlled by diluting all plasmids to 100 ng/μL before storing and using them.
7. Transfecting high concentrations of lipid biosensor has the potential to sequester the target lipid and effect normal cellular interactions. As such, biosensors should be expressed at the lowest concentration possible. This may require optimization depending on cell type and promoter driving expression of biosensor protein.
8. Appropriate spectral separation is obtained by using these fluorescent proteins.
9. This plasmid mix does not contain an iRFP-labeled PM marker. Cell Mask Deep Red will be used as a PM marker in this setup. However, an iRFP-tagged PM marker (iRFP-CAAX) could easily be included and transfected alongside the other plasmids.
10. TIRF image acquisition parameters should be made to obtain the greatest sensitivity, resolution, and acquisition speed. The settings used in our lab are TIRF slider = 2150, 2x2 pixel binning on our Andor Zyla 5.5 sCMOS camera (giving ~130 nm image pixel size through the 100X objective), <5%excitation, and 100 ms exposure time. These parameters maximize sensitivity and resolution and minimize photobleaching of the fluorophores.
11. This setup is for cells taken at a single time point; refer to XX for a detailed setup for time-lapse imaging.
12. The time to acquire each image depends on the optimization of the settings in Note 10. The higher the signal-to-noise ratio and resolution, the slower the acquisition speed. The

conditions outlined above result in about a 3-s acquisition time per image, or about a 90-s total acquisition time for 30 images.

13. Again, image acquisition parameters for confocal should be made to get the greatest sensitivity, resolution, and acquisition speed. The settings used in our lab are resonant scan mode, line average of 8 or 16 frames, and gain and excitation varying between different fluorophores, but these should be set to the lowest value possible. These settings maximize sensitivity and resolution and minimize photobleaching of the fluorophores.
14. This DMEM-based formulation lacks phenol red and therefore has low background to increase the signal-to-noise ratio on fluorophores.
15. In this case, healthy cells are defined by morphology visualized in DIC. Cells should be fully adherent to the dish and fully spread. Avoid imaging cells that have rounded up or those with blebbing or protrusions around the membrane, as these are dead or dying cells.
16. LOCI developed Bio-Formats, which allows for ImageJ or Fiji to open all file formats, including proprietary formats from specific microscope vendors.
17. Draw each ROI around a maximum intensity projection of all frames in the time-lapse to capture the maximum PM footprint for the generation of the PM mask in each frame.
18. This process can be recorded into an automated macro using the ImageJ IJ1 macro language.

Appendix B Induced dimerization tools to deplete specific phosphatidylinositol phosphates

Appendix B.1 Materials

Generally speaking, this protocol uses a dimerization system to target localization of a phosphatase to deplete a specific pool of PPIns (**Appendix Figure 1**). A membrane-bound recruiter carrying an FRB domain is used to target the enzyme fused with the FKBP domain. Simultaneously, a lipid-binding domain fused to a fluorescent protein can be used to observe how lipid levels change at the specific cellular location. A prototypical protocol of depletion of $PI(4,5)P_2$ from the plasma membrane (PM) is described here. However, lipid biosensors, enzymes, and membrane recruiters are interchangeable according to the experimenter's scope (**Appendix Table 1.2**).

Appendix B.1.1 Plasmids

A wide range of phosphatases and biosensors for PPIns fused with a full spectrum of fluorescent protein are available from Addgene. For detailed directions about plasmid manipulations, refer to **Appendix A** (see Note 1). As an example, $PI(4,5)P_2$ depletion is described in this protocol by using the following plasmids:

1. piRFP-N1-Lyn11-FRB (recruiter).
2. pTagBFP2-N1-Tubby (lipid biosensor).
3. pmCherry-C1-FKBP-INPP5E (phosphatase that hydrolyzes 5-phosphate of $PI(4,5)P_2$).

Appendix B.1.2 Cell culture and transfection

Standard cell culture and transfection materials are used:

1. TrpLE (Life Technologies 12604039) for cell dissociation.
2. Low glucose DMEM (Life Technologies) supplemented with penicillin (100 U/mL), streptomycin (100 μg/mL), 10% of heat-inactivated fetal bovine serum (FBS), and 0.1% chemically defined lipid supplement (Life Technologies).
3. T75 flask (VWR International) and 35-mm glass-bottom dishes with 20-mm glass aperture (In Vitro Scientific).
4. Opti-MEM (Life Technologies).
5. Human Plasma Fibronectin (Life Technologies).
6. Phosphate-buffered saline (PBS).
7. Lipofectamine 2000.
8. Cell culture incubator at 37˚C in a humidified atmosphere with 5% CO_2.

Appendix B.1.3 Live-cell imaging

The steps provided below describe an experiment performed on a confocal microscope. However, this protocol is also applicable for the TIRF microscope, depending on the scope of the experiment.

1. FluoroBrite DMEM (Life Technologies) supplemented with 10% of heat-inactivated fetal bovine serum, 25 mM HEPES(pH 7.4), and 0.1% chemically defined lipid supplement (see Note 2).
2. 1 mM rapamycin in DMSO. Store as 20 μL aliquots at -20˚C.

3. Confocal microscope equipped with at least three laser lines. Experiments are optimized for a Nikon Eclipse TiE inverted microscope equipped with a 100X, plan apochromatic, 1.45 NA oil-immersion objective lens and a Nikon A1R confocal scan head with a laser unit (LU-NV) containing four laser lines (405, 488, 561, and 640 nm).
4. Motorized stage.
5. Image acquisition software such as Elements (Nikon).

Appendix B.1.4 Image analysis

1. Open-access image analysis package Fiji.
2. Analysis software such as GraphPad Prism.

Appendix B.2 Methods

Instructions to maintain cell culture and transfection procedures are standard. Particular indications are provided in **Appendix A**.

Appendix B.2.1 Transfection

Per 35-mm glass-bottom dish at ~50% confluence:

1. Dilute 3.1µL of lipofectamine 2000 into 96.9 µL of Opti-MEM in a sterile 1.5-mL plastic tube and mix.

2. Dilute up to 1μg of total plasmid DNA into a total of 100 μL of Opti-MEM in a 1.5-mL plastic tube and mix. As a preliminary experiment, begin with the following masses of DNA (see Note 3):
    a. 300 ng of piRFP-N1-Lyn11-FRB,
    b. 300 ng of pmCherry-C1-FKBP-INPP5E,
    c. 400 ng of pTagBFP2-N1-Tubby (see Note 4).
3. Combine tubes containing plasmids and lipofectamine dilution.
4. Incubate for 20 min at room temperature to allow lipid–DNA complex formation.
5. Gently add complex lipid–DNA to cells and mix by swirling the dish.
6. Incubate for 4 h and replace the transfection mix with 2 mL of fresh DMEM.
7. Cells are imaged 18–24 h after transfection.

Appendix B.2.2 Microscope setup

1. Use a fiber-coupled laser device equipped with 405-nm (for TagBFP2), 561-nm (for mCherry), and 640-nm (for iRFP) laser lines to excite the indicated fluorescent protein (see Note 5).
2. Collect fluorescence emission with bandwidths at 425–475 nm (for TagBFP2), 570–620 nm (for mCherry), and 663–737 nm (for iRFP). Differential interference contrast (DIC) is used on a transmitted light channel (see Note 6).
3. Our experiments are optimized with the Nikon A1R laser scanning confocal microscope. If available, use the resonant mode of A1R confocal scan head (see Note 7).
4. Set pinhole at 1.2x Airy disc size based on the longest wavelength channel (see Note 8).

5. A motorized stage is used to register up to 16 fields for each time frame during the whole recording (see Note 9).
6. Our experiments are optimized with the acquisition software “Elements” by Nikon (see Note 10).
7. Configure software acquisition to take a sequence of frames each 30 s for 17 m (see Note 11).

Appendix B.2.3 Time-lapse imaging and rapamycin addition

1. Turn on a microscope at least 20 min before starting the experiment to allow stabilization of the optical system.
2. Prepare a fresh dilution of rapamycin at 5 μM in FluorBrite DMEM (see Note 12).
3. Clean 100X objective lens with appropriate wipes and cleaning solution.
4. Apply immersion oil on the 100X plan apochromatic, 1.45 NA objective lens.
5. Before placing the dish on the microscope, remove growth medium and rinse once with 1 mL of pre-warmed FluoroBrite DMEM.
6. Add 1.6 mL of FluroBrite DMEM and mount the dish on the microscope.
7. Find the focus plane and look for cells showing fluorescent signal in the three channels (see Note 13).
8. Save the number of positions to register during the experiment (see Note 14).
9. Start acquisition allowing 2 min of baseline before inducing recruitment of mCherry-FKBP-INPP5E with rapamycin (see Note 15).
10. Add 400 μL of 5 μM rapamycin (see Note 16).
11. Continue acquisition and save experiment.

Appendix B.3 Data Analysis

Using the above plasmids and protocol, depletion of $PI(4,5)P_2$ on the PM can be performed. In addition, the strategy described above leaves the green channel to record an additional fluorescent reporter (e.g., a second GFP-tagged lipid biosensor). Using these image data, we can obtain fluorescence intensity measurements on a given cellular location for each channel. These selective measurements over a cellular compartment of interest are done by producing a binary mask. Usually, the recruiter channel is used to construct the mask.

Appendix B.3.1 Confocal microscopy

1. Import images into the open-access image analysis platform Fiji (see Note 17).
2. Single series are analyzed, first producing a binary mask using the recruiter channel (Lyn_{11}-FRB-iRFP) for each frame along the whole time-series (see Note 18).
3. Draw regions of interest (ROIs) containing the whole cell (see Note 19).
4. Measure fluorescence intensity on each mask at a specific timeframe for all channels, including the recruiter channel (see Note 20).
5. Normalize signal between experiments by using the ratio of fluorescence intensity raw data divided by the fluorescence at the first frame for the same cell.
6. Expected results must show an increase in fluorescence intensity of mCherry-FKBP-INPP5E after inducing dimerization with rapamycin. As consequence, a decrease of the signal of $Tubby_C$-TagBFP2 must occur and no changes on Lyn_{11}-FRB-iRFP are expected to happen.

Appendix B.3.2 TIRF microscopy

1. Import files into Fiji using the LOCI Bio-Formats importer.
2. Draw an ROI in the background of the image(s) to be analyzed.
3. Measure the intensity of the background ROI.
4. Subtract the background data from the images.
5. Draw ROIs around labeled cells in each frame (see Note 21).
6. Measure the intensity within the ROI in each channel at each timepoint.
7. Copy and paste data into GraphPad Prism and format as desired.

Appendix B.4 Notes

1. Keep in mind the topology of protein of interest. The FKBP-tagged protein must be cytosolic. If you are working with an enzyme that has a membrane-interacting domain, it will be necessary to remove it and test that the enzymatic function of protein remains unaltered. Verify plasmids by DNA sequencing before using them.
2. Experiments were optimized for this reagent. Fluorobrite is a DMEM-based formulation presenting low background to enhance signal-to-noise ratio on fluorophores.
3. The amount of FRB expression is limiting to recruit FKBP (Appendix Figure 1). For this reason, the first time the experiment is run, different ratios of FRB/FKBP expression should be tested. Because transfection efficiency is variable for each plasmid and several factors affect the expression of the protein of interest, this step is experimentally determined by changing plasmid concentrations during transfection (Fig. 2).

4. An appropriate spectral separation is performed by using these three fluorescent proteins. In addition, this configuration allows an extra emission window to add another fluorophore in the green channel.
5. Under this configuration, a 488-nm laser line is available to excite another fluorophore. This excitation is most commonly used to excite GFP with an emission of 500–550 nm.
6. To avoid crosstalk, images are sequentially acquired by avoiding spectral overlapping: TagBFP2 followed by mCherry, then GFP, and lastly iRFP.
7. Other microscope systems equipped with similar settings as mentioned above can be used.
8. Increasing Airy disc size increases signal but decreases both Z and X–Y resolution.
9. A total of 8 or 16 frames are averaged to improve the signal to noise ratio. This step is optional, but registering more than one field per dish makes for more efficient and robust data gathering and statistically tractable results. It also minimizes cell variability effects and obtains more reliable data when single treatment experiments are performed, as occurs with irreversible chemical dimerizers. The number of positions is determined as the maximum number of fields accommodated by the time frame.
10. Other systems and proprietary image acquisition software may be used, though the user may need to optimize.
11. High affinity and fast permeability of rapamycin induces dimerization in the order of seconds. In this way, kinetics of depletion of PPIns can be recorded in 5 min, with 2 min of baseline signal. For custom experiments, establish time-lapses by considering the time frame of changes that will be observed. This later point is determined in pilot experiments.
12. Final concentration of rapamycin in cells is 1 μM. A dilution 1:5 is used at the moment of the experiment.

13. Set confocal Z-axis position on the equatorial section of cells to reduce out-of-focus changes during acquisition. In addition, the maximal signal on the PM is recorded at this z-section.
14. Increase movement efficiency of motorized stage by using a looping pattern.
15. Pre-addition frames will be used to normalize baseline correction.
16. Add rapamycin gently after the fifth frame capture.
17. Use LOCI's Bio-Formats plugin to open images on a standard ImageJ compatible format. A series containing information of three or four channels will be open. Each series represents one field of acquisition along the time.
18. Detailed instructions about the mask constructions are provided in Appendix A.
19. Measurements of total fluorescent intensity are performed on the respective mask for each frame; ROIs delimit signal by cell in order to get an average signal of all the cells.
20. Basic protocol registers the depletion of specific PPIns on the recruiter localization, but another subcellular region can be monitored simultaneously, taking advantage of additional channels.
21. Draw each ROI around a minimum intensity projection to capture PM footprint, which is always in contact with the glass-bottom dish.

Appendix Table 1.1 Suggested cell suspension volumes to seed cells for transfections.

Volume of Suspension (µL)	Days Post Seeding for Transfection	Confluence at Seeding (%)	Ending Surface Area (cm^2)	Starting Surface Area (cm^2)	Resuspension Volume (mL)
80	2	12.5	9.6	75	5
160	1	25	9.6	75	5
320	0 (same day)	50	9.6	75	5

Appendix Table 2.2 Representative phosphoinositide phosphatases.

Categorization	Phosphatase	Lipid substrate[1]	Product[1]
3-phosphatase (pptase)	TPIP	$PI(3,4,5)P_3$	$PI(4,5)P_2$
	MTM and MTMR	$PI(3,5)P_2$ *and/or* PI3P	PI3P *and/or* PI
	PTEN	$PI(3,4,5)P_3$ *and/or* $PI(3,4)P_2$	$PI(4,5)P_2$ *and/or* PI(3)P
4-pptase	Sac1	PI4P *and/or* PI3P	PI
	INPP4A/B	$PI(3,4)P_2$	PI3P
5-pptase	ORCL	$PI(4,5)P_2$ *and/or* $PI(3,4,5)P_3$ *and/or* $PI(3,5)P_2$	PI(4)P *and/or* $PI(3,4)P_2$ *and/or* PI(3)P
	Synaptojanins	$PI(3,4,5)P_3$ *and/or* $PI(3,5)P_2$	$PI(3,4)P_2$ *and/or* PI(3)P
	INPP5B	$PI(4,5)P_2$ *and/or* $PI(3,4,5)P_3$	PI(4)P *and/or* $PI(3,4)P_2$
	SKIP	$PI(4,5)P_2$ *and/or* $PI(3,4,5)P_3$	PI4P *and/or* $PI(3,4)P_2$
	SHIP1	$PI(3,4,5)P_3$ *and/or* $PI(4,5)P_2$	$PI(3,4)P_2$ *and/or* PI4P
	SHIP2	$PI(4,5)P_2$ *and/or* $PI(3,4,5)P_3$ *and/or* $PI(3,5)P_2$	PI4P *and/or* $PI(3,4)P_2$ *and/or* PI3P
	INPP5E	$PI(3,4,5)P_3$ *and/or* $PI(4,5)P_2$	$PI(3,4)P_2$ *and/or* PI4P

1 (*9*)

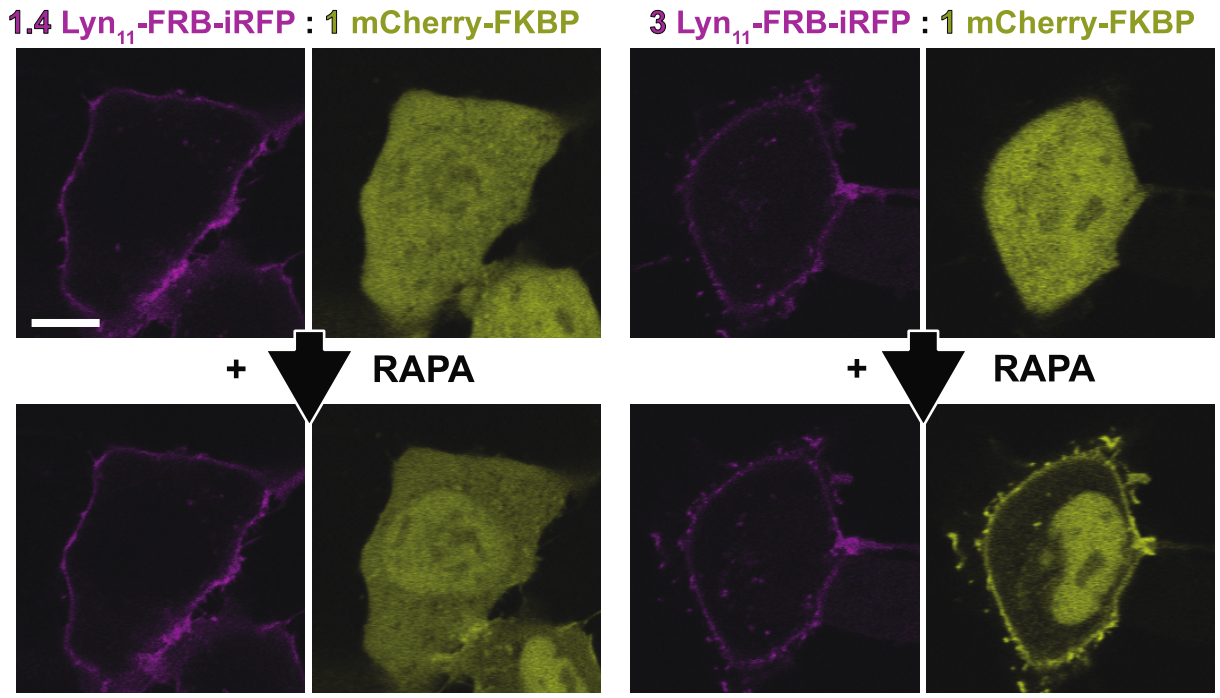

Appendix Figure 1 Rapamycin induces recruitment at different efficiencies of FRB-FKBP ratios.

Plasmid encoding Lyn_{11}-FRB-iRFP transfected at a ratio of 1.4:1 with plasmid encoding mCherry-FKBP produces little apparent localization change. When the plasmid encoding Lyn_{11}-FRB-iRFP is transfected at a ratio of 3:1 to the plasmid encoding mCherry-FKBP instead, then rapamycin induces clear localization of mCherry at the PM. Scale Bar ~10 μm.

Bibliography

1. G. van Meer, A. I. P. M. de Kroon, Lipid map of the mammalian cell. *J Cell Sci*. **124**, 5–8 (2011).

2. G. van Meer, D. R. Voelker, G. W. Feigenson, Membrane lipids: where they are and how they behave. *Nat Rev Mol Cell Bio*. **9**, 112–124 (2008).

3. T. Balla, Phosphoinositides: Tiny Lipids With Giant Impact on Cell Regulation. *Physiological reviews*. **93**, 1019–1137 (2012).

4. G. R. V. Hammond, M. J. Fischer, K. E. Anderson, J. Holdich, A. Koteci, T. Balla, R. F. Irvine, PI4P and PI(4,5)P2 Are Essential But Independent Lipid Determinants of Membrane Identity. *Science*. **337**, 727–730 (2012).

5. R. V. Stahelin, Lipid binding domains: more than simple lipid effectors. *J Lipid Res*. **50**, S299–S304 (2009).

6. V. Narwal, R. Deswal, B. Batra, V. Kalra, R. Hooda, M. Sharma, J. S. Rana, Cholesterol Biosensors: A review. *Steroids*. **143**, 6–17 (2018).

7. B. M. Quinville, N. M. Deschenes, A. E. Ryckman, J. S. Walia, A Comprehensive Review: Sphingolipid Metabolism and Implications of Disruption in Sphingolipid Homeostasis. *Int J Mol Sci*. **22**, 5793 (2021).

8. E. J. Dickson, B. Hille, Understanding phosphoinositides: rare, dynamic, and essential membrane phospholipids. *Biochemical Journal*. **476**, 1–23 (2019).

9. T. Balla, Phosphoinositides: Tiny Lipids With Giant Impact on Cell Regulation. *Physiol Rev*. **93**, 1019–1137 (2013).

10. B. W. Agranoff, Turtles All the Way: Reflections on myo-Inositol. *J Biol Chem*. **284**, 21121–21126 (2009).

11. A. Traynor-Kaplan, M. Kruse, E. J. Dickson, G. Dai, O. Vivas, H. Yu, D. Whittington, B. Hille, Fatty-acyl chain profiles of cellular phosphoinositides. *Biochimica Et Biophysica Acta Bba - Mol Cell Biology Lipids*. **1862**, 513–522 (2017).

12. L. N. Bone, R. M. Dayam, M. Lee, N. Kono, G. D. Fairn, H. Arai, R. J. Botelho, C. N. Antonescu, The acyltransferase LYCAT controls specific phosphoinositides and related membrane traffic. *Mol Biol Cell*. **28**, 161–172 (2016).

13. H. Paulus, E. P. Kennedy, The Enzymatic Synthesis of Inositol Monophosphatide. *J Biol Chem*. **235**, 1303–1311 (1960).

14. B. W. Agranoff, R. M. Bradley, R. O. Brady, The Enzymatic Synthesis of Inositol Phosphatide. *J Biol Chem*. **233**, 1077–1083 (1958).

15. T. Icho, C. P. Sparrow, C. R. Raetz, Molecular cloning and sequencing of the gene for CDP-diglyceride synthetase of Escherichia coli. *J Biol Chem*. **260**, 12078–12083 (1985).

16. W. THOMPSON, K. STRICKLAND, R. ROSSITER, Biosynthesis of phosphatidylinositol in rat brain. *Biochem J*. **87**, 136–142 (1963).

17. X. Liu, Y. Yin, J. Wu, Z. Liu, Structure and mechanism of an intramembrane liponucleotide synthetase central for phospholipid biosynthesis. *Nat Commun*. **5**, 4244 (2014).

18. S. Tanaka, J. Nikawa, H. Imai, S. Yamashita, K. Hosaka, Molecular cloning of rat phosphatidylinositol synthase cDNA by functional complementation of the yeast Saccharomyces cerevisiae pis mutation. *Febs Lett*. **393**, 89–92 (1996).

19. S. Kim, A. Kedan, M. Marom, N. Gavert, O. Keinan, M. Selitrennik, O. Laufman, S. Lev, The phosphatidylinositol-transfer protein Nir2 binds phosphatidic acid and positively regulates phosphoinositide signalling. *Embo Rep*. **14**, 891–899 (2013).

20. Y. J. Kim, M.-L. Guzman-Hernandez, E. Wisniewski, T. Balla, Phosphatidylinositol-Phosphatidic Acid Exchange by Nir2 at ER-PM Contact Sites Maintains Phosphoinositide Signaling Competence. *Dev Cell*. **33**, 549–561 (2015).

21. Y. J. Kim, M. L. Guzman-Hernandez, E. Wisniewski, N. Echeverria, T. Balla, Phosphatidylinositol and phosphatidic acid transport between the ER and plasma membrane during PLC activation requires the Nir2 protein. *Biochem Soc T*. **44**, 197–201 (2016).

22. C.-L. Chang, T.-S. Hsieh, T. T. Yang, K. G. Rothberg, B. D. Azizoglu, E. Volk, J.-C. Liao, J. Liou, Feedback Regulation of Receptor-Induced Ca2+ Signaling Mediated by E-Syt1 and Nir2 at Endoplasmic Reticulum-Plasma Membrane Junctions. *Cell Reports*. **5**, 813–825 (2013).

23. J. P. Zewe, A. M. Miller, S. Sangappa, R. C. Wills, B. D. Goulden, G. R. V. Hammond, Probing the subcellular distribution of phosphatidylinositol reveals a surprising lack at the plasma membrane. *J Cell Biol*. **219**, e201906127 (2020).

24. J. G. Pemberton, Y. J. Kim, J. Humpolickova, A. Eisenreichova, N. Sengupta, D. J. Toth, E. Boura, T. Balla, Defining the subcellular distribution and metabolic channeling of phosphatidylinositol. *J Cell Biology*. **219**, e201906130 (2020).

25. H. BROCKERHOFF, C. E. BALLOU, Phosphate incorporation in brain phosphionositides. *J Biological Chem*. **237**, 49–52 (1962).

26. S. Yoshida, Y. Ohya, M. Goebl, A. Nakano, Y. Anraku, A novel gene, STT4, encodes a phosphatidylinositol 4-kinase in the PKC1 protein kinase pathway of Saccharomyces cerevisiae. *J Biol Chem*. **269**, 1166–1172 (1994).

27. A. Balla, T. Balla, Phosphatidylinositol 4-kinases: old enzymes with emerging functions. *Trends Cell Biol*. **16**, 351–361 (2006).

28. A. L. Marat, V. Haucke, Phosphatidylinositol 3-phosphates—at the interface between cell signalling and membrane traffic. *Embo J*. **35**, 561–579 (2016).

29. S. N. Zolov, D. Bridges, Y. Zhang, W.-W. Lee, E. Riehle, R. Verma, G. M. Lenk, K. Converso-Baran, T. Weide, R. L. Albin, A. R. Saltiel, M. H. Meisler, M. W. Russell, L. S. Weisman, In vivo, Pikfyve generates PI(3,5)P2, which serves as both a signaling lipid and the major precursor for PI5P. *Proc National Acad Sci*. **109**, 17472–17477 (2012).

30. P. Berger, S. Bonneick, S. Willi, M. Wymann, U. Suter, Loss of phosphatase activity in myotubularin-related protein 2 is associated with Charcot–Marie–Tooth disease type 4B1. *Hum Mol Genet*. **11**, 1569–1579 (2002).

31. M. Velichkova, J. Juan, P. Kadandale, S. Jean, I. Ribeiro, V. Raman, C. Stefan, A. A. Kiger, Drosophila Mtm and class II PI3K coregulate a PI(3)P pool with cortical and endolysosomal functions. *J Cell Biology*. **190**, 407–425 (2010).

32. R. S. Rana, L. E. Hokin, Role of phosphoinositides in transmembrane signaling. *Physiol Rev*. **70**, 115–164 (1990).

33. S. G. Rhee, REGULATION OF PHOSPHOINOSITIDE-SPECIFIC PHOSPHOLIPASE C*. *Annu Rev Biochem*. **70**, 281–312 (2001).

34. M. J. Berridge, Inositol trisphosphate and calcium signalling mechanisms. *Biochimica Et Biophysica Acta Bba - Mol Cell Res*. **1793**, 933–940 (2009).

35. M. J. Berridge, R. F. Irvine, Inositol trisphosphate, a novel second messenger in cellular signal transduction. *Nature*. **312**, 315–321 (1984).

36. M. J. Berridge, Inositol trisphosphate and diacylglycerol as second messengers. *Biochem J*. **220**, 345–360 (1984).

37. L. E. Ling, J. T. Schulz, L. C. Cantley, Characterization and Purification of Membrane-associated Phosphatidylinositol-4-phosphate Kinase from Human Red Blood Cells. *J Biol Chem*. **264**, 5080–5088 (1989).

38. C. E. Bazenet, A. R. Ruano, J. L. Brockman, R. A. Anderson, The human erythrocyte contains two forms of phosphatidylinositol-4-phosphate 5-kinase which are differentially active toward membranes. *J Biol Chem*. **265**, 18012–18022 (1990).

39. L. E. Rameh, K. F. Tolias, B. C. Duckworth, L. C. Cantley, A new pathway for synthesis of phosphatidylinositol-4,5-bisphosphate. *Nature*. **390**, 192–196 (1997).

40. L. E. Rameh, A. Arvidsson, K. L. Carraway, A. D. Couvillon, G. Rathbun, A. Crompton, B. VanRenterghem, M. P. Czech, K. S. Ravichandran, S. J. Burakoff, D.-S. Wang, C.-S. Chen, L. C. Cantley, A Comparative Analysis of the Phosphoinositide Binding Specificity of Pleckstrin Homology Domains. *J Biol Chem*. **272**, 22059–22066 (1997).

41. V. D. Rao, S. Misra, I. V. Boronenkov, R. A. Anderson, J. H. Hurley, Structure of type IIβ phosphatidylinositol phosphate kinase: A protein kinase fold flattened for interfacial phosphorylation. *Cell*. **94**, 829–839 (1998).

42. A. Liu, D. Sui, D. Wu, J. Hu, The activation loop of PIP5K functions as a membrane sensor essential for lipid substrate processing. *Science Advances*. **2** (2016), doi:10.1126/sciadv.1600925.

43. K. A. Hinchliffe, A. Ciruela, A. J. Letcher, N. Divecha, R. F. Irvine, Regulation of type IIα phosphatidylinositol phosphate kinase localisation by the protein kinase CK2. *Curr Biol*. **9**, 983-S1 (1999).

44. J. P. Richardson, M. Wang, J. H. Clarke, K. J. Patel, R. F. Irvine, Genomic tagging of endogenous Type IIβ Phosphatidylinositol 5-phosphate 4-kinase in DT40 cells reveals a nuclear localisation. *Cell Signal*. **19**, 1309–1314 (2007).

45. J. H. Clarke, P. C. Emson, R. F. Irvine, Localization of phosphatidylinositol phosphate kinase IIγ in kidney to a membrane trafficking compartment within specialized cells of the nephron. *Am J Physiology - Ren Physiology*. **295**, F1422–F1430 (2008).

46. M. Wang, N. J. Bond, A. J. Letcher, J. P. Richardson, K. S. Lilley, R. F. Irvine, J. H. Clarke, Genomic tagging reveals a random association of endogenous PtdIns5P 4-kinases IIα and IIβ and a partial nuclear localization of the IIα isoform. *Biochem J*. **430**, 215–221 (2010).

47. Y. Bultsma, W.-J. Keune, N. Divecha, PIP4Kβ interacts with and modulates nuclear localization of the high-activity PtdIns5P-4-kinase isoform PIP4Kα. *Biochem J*. **430**, 223–235 (2010).

48. J. H. Clarke, R. F. Irvine, Evolutionarily conserved structural changes in phosphatidylinositol 5-phosphate 4-kinase (PI5P4K) isoforms are responsible for differences in enzyme activity and localization. *Biochem J*. **454**, 49–57 (2013).

49. R. Fiume, D. R. Jones, N. Divecha, PIP4K2B: Coupling GTP Sensing to PtdIns5P Levels to Regulate Tumorigenesis. *Trends Biochem Sci*. **41**, 473–475 (2016).

50. K. Sumita, Y.-H. Lo, K. Takeuchi, M. Senda, S. Kofuji, Y. Ikeda, J. Terakawa, M. Sasaki, H. Yoshino, N. Majd, Y. Zheng, E. Kahoud, T. Yokota, B. M. Emerling, J. M. Asara, T. Ishida, J. W. Locasale, T. Daikoku, D. Anastasiou, T. Senda, A. T. Sasaki, The Lipid Kinase PI5P4Kβ Is an Intracellular GTP Sensor for Metabolism and Tumorigenesis. *Molecular Cell*. **61**, 187–198 (2016).

51. T. Geiger, A. Wehner, C. Schaab, J. Cox, M. Mann, *Mol Cell Proteom Mcp*, in press, doi:10.1074/mcp.m111.014050.

52. N. H. Cho, K. C. Cheveralls, A.-D. Brunner, K. Kim, A. C. Michaelis, P. Raghavan, H. Kobayashi, L. Savy, J. Y. Li, H. Canaj, J. Y. S. Kim, E. M. Stewart, C. Gnann, F. McCarthy, J. P. Cabrera, R. M. Brunetti, B. B. Chhun, G. Dingle, M. Y. Hein, B. Huang, S. B. Mehta, J. S. Weissman, R. Gómez-Sjöberg, D. N. Itzhak, L. A. Royer, M. Mann, M. D. Leonetti, OpenCell: Endogenous tagging for the cartography of human cellular organization. *Science*. **375**, eabi6983 (2022).

53. S. Sharma, S. Mathre, V. Ramya, D. Shinde, P. Raghu, Phosphatidylinositol 5 Phosphate 4-Kinase Regulates Plasma-Membrane PIP3 Turnover and Insulin Signaling. *Cell Reports*. **27**, 1979-1990.e7 (2019).

54. A. Wilcox, K. A. Hinchliffe, Regulation of extranuclear PtdIns5P production by phosphatidylinositol phosphate 4-kinase 2α. *Febs Lett*. **582**, 1391–1394 (2008).

55. D. R. Jones, Y. Bultsma, W.-J. Keune, J. R. Halstead, D. Elouarrat, S. Mohammed, A. J. Heck, C. S. D'Santos, N. Divecha, Nuclear PtdIns5P as a Transducer of Stress Signaling: An In Vivo Role for PIP4Kbeta. *Mol Cell*. **23**, 685–695 (2006).

56. D. G. Wang, M. N. Paddock, M. R. Lundquist, J. Y. Sun, O. Mashadova, S. Amadiume, T. W. Bumpus, C. Hodakoski, B. D. Hopkins, M. Fine, A. Hill, T. J. Yang, J. M. Baskin, L. E. Dow, L. C. Cantley, PIP4Ks Suppress Insulin Signaling through a Catalytic-Independent Mechanism. *Cell Reports*. **27**, 1991-2001.e5 (2019).

57. M. R. Wenk, L. Lucast, G. D. Paolo, A. J. Romanelli, S. F. Suchy, R. L. Nussbaum, G. W. Cline, G. I. Shulman, W. McMurray, P. D. Camilli, Phosphoinositide profiling in complex lipid mixtures using electrospray ionization mass spectrometry. *Nat Biotechnol*. **21**, 813–817 (2003).

58. S. J. Bulley, J. H. Clarke, A. Droubi, M.-L. Giudici, R. F. Irvine, Exploring phosphatidylinositol 5-phosphate 4-kinase function. *Adv Biological Regul*. **57**, 193–202 (2015).

59. D. G. Wang, M. N. Paddock, M. R. Lundquist, J. Y. Sun, O. Mashadova, S. Amadiume, T. W. Bumpus, C. Hodakoski, B. D. Hopkins, M. Fine, A. Hill, T. J. Yang, J. M. Baskin, L. E. Dow, L. C. Cantley, PIP4Ks Suppress Insulin Signaling Through a Catalytic-Independent Mechanism. *Biorxiv*, 370544 (2018).

60. M. R. Lundquist, M. D. Goncalves, R. M. Loughran, E. Possik, T. Vijayaraghavan, A. Yang, C. Pauli, A. Ravi, A. Verma, Z. Yang, J. L. Johnson, J. C. Y. Wong, Y. Ma, K. S.-K. Hwang, D.

Weinkove, N. Divecha, J. M. Asara, O. Elemento, M. A. Rubin, A. C. Kimmelman, A. Pause, L. C. Cantley, B. M. Emerling, Phosphatidylinositol-5-Phosphate 4-Kinases Regulate Cellular Lipid Metabolism By Facilitating Autophagy. *Mol Cell*. **70**, 531-544.e9 (2018).

61. A. Ravi, L. Palamiuc, R. M. Loughran, J. Triscott, G. K. Arora, A. Kumar, V. Tieu, C. Pauli, M. Reist, R. J. Lew, S. L. Houlihan, C. Fellmann, C. Metallo, M. A. Rubin, B. M. Emerling, PI5P4Ks drive metabolic homeostasis through peroxisome-mitochondria interplay. *Dev Cell*. **56**, 1661-1676.e10 (2021).

62. N. Divecha, C. E. L. Brooksbank, R. F. Irvine, Purification and characterization of phosphatidylinositol 4-phosphate 5-kinases. *Biochem J*. **288**, 637–642 (1992).

63. N. Divecha, O. Truong, J. J. Hsuan, K. A. Hinchliffe, R. F. Irvine, The cloning and sequence of the C isoform of PtdIns4 P 5-kinase. *Biochem J*. **309**, 715–719 (1995).

64. H. Ishihara, Y. Shibasaki, N. Kizuki, H. Katagiri, Y. Yazaki, T. Asano, Y. Oka, Cloning of cDNAs encoding two isoforms of 68-kDa type I phosphatidylinositol-4-phosphate 5-kinase. *J Biol Chem*. **271**, 23611–23614 (1996).

65. H. Ishihara, Y. Shibasaki, N. Kizuki, T. Wada, Y. Yazaki, T. Asano, Y. Oka, Type I phosphatidylinositol-4-phosphate 5-kinases. Cloning of the third isoform and deletion/substitution analysis of members of this novel lipid kinase family. *The Journal of biological chemistry*. **273**, 8741–8 (1998).

66. K. Homma, S. Terui, M. Minemura, H. Qadota, Y. Anraku, Y. Kanaho, Y. Ohya, Phosphatidylinositol-4-phosphate 5-Kinase Localized on the Plasma Membrane Is Essential for Yeast Cell Morphogenesis. *J Biol Chem*. **273**, 15779–15786 (1998).

67. Y. Ling, C. J. Stefan, J. a MacGurn, A. Audhya, S. D. Emr, The dual PH domain protein Opy1 functions as a sensor and modulator of PtdIns(4,5)P2 synthesis. *Embo J*. **31**, 2882–2894 (2011).

68. J. C. Loijens, R. A. Anderson, Type I Phosphatidylinositol-4-phosphate 5-Kinases Are Distinct Members of This Novel Lipid Kinase Family. *J Biol Chem*. **271**, 32937–32943 (1996).

69. J. C. Loijens, I. V. Boronenkov, G. J. Parker, R. A. Anderson, The phosphatidylinositol 4-phosphate 5-kinase family. *Adv Enzyme Regul*. **36**, 115–140 (1996).

70. J. Hu, Q. Yuan, X. Kang, Y. Qin, L. Li, Y. Ha, D. Wu, Resolution of structure of PIP5K1A reveals molecular mechanism for its regulation by dimerization and dishevelled. *Nat Commun*. **6**, 8205 (2015).

71. G. D. Fairn, K. Ogata, R. J. Botelho, P. D. Stahl, R. A. Anderson, P. D. Camilli, T. Meyer, S. Wodak, S. Grinstein, An electrostatic switch displaces phosphatidylinositol phosphate kinases from the membrane during phagocytosis. *J Cell Biology*. **187**, 701–714 (2009).

72. Y. Muftuoglu, Y. Xue, X. Gao, D. Wu, Y. Ha, Mechanism of substrate specificity of phosphatidylinositol phosphate kinases. *Proceedings of the National Academy of Sciences*. **113**, 8711–8716 (2016).

73. J. Kunz, M. P. Wilson, M. Kisseleva, J. H. Hurley, P. W. Majerus, R. A. Anderson, The Activation Loop of Phosphatidylinositol Phosphate Kinases Determines Signaling Specificity. *Molecular Cell*. **5**, 1–11 (2000).

74. M.-L. GIUDICI, P. C. EMSON, R. F. IRVINE, A novel neuronal-specific splice variant of Type I phosphatidylinositol 4-phosphate 5-kinase isoform gamma. *Biochem J*. **379**, 489–496 (2004).

75. N. J. Schill, R. A. Anderson, Two novel phosphatidylinositol-4-phosphate 5-kinase type Iγ splice variants expressed in human cells display distinctive cellular targeting. *Biochem J*. **422**, 473–482 (2009).

76. Y. Xia, R. F. Irvine, M.-L. Giudici, Phosphatidylinositol 4-phosphate 5-kinase Iγ_v6, a new splice variant found in rodents and humans. *Biochem Bioph Res Co*. **411**, 416–420 (2011).

77. Y. Kanaho, A. Kobayashi-Nakano, T. Yokozeki, The Phosphoinositide Kinase PIP5K That Produces the Versatile Signaling Phospholipid PI4,5P2. *Biological Pharm Bulletin*. **30**, 1605–1609 (2007).

78. P. A. Weernink, M. Schmidt, K. H. Jakobs, Regulation and cellular roles of phosphoinositide 5-kinases. *European Journal of Pharmacology*. **500**, 87–99 (2004).

79. I. van den Bout, N. Divecha, PIP5K-driven PtdIns(4,5)P2 synthesis: regulation and cellular functions. *Journal of Cell Science*. **122**, 3837–3850 (2009).

80. S. Choi, R. A. Anderson, IQGAP1 is a phosphoinositide effector and kinase scaffold. *Adv Biological Regul*. **60**, 29–35 (2016).

81. L. E. Rameh, A. M. Mackey, IQGAP1 makes PI(3)K signalling as easy as PIP, PIP2, PIP3. *Nat Cell Biol*. **18**, 1263–1265 (2016).

82. V. S. Yerramilli, A. H. Ross, S. Scarlata, A. Gericke, IQGAP1 scaffolding links phosphoinositide kinases to cytoskeletal reorganization. *Biophys J*. **121**, 793–807 (2022).

83. S. Choi, M. Chen, V. L. Cryns, R. A. Anderson, A nuclear phosphoinositide kinase complex regulates p53. *Nature Cell Biology*. **21**, 462–475 (2019).

84. R. L. Doughman, A. J. Firestone, M. L. Wojtasiak, M. W. Bunce, R. A. Anderson, Membrane Ruffling Requires Coordination between Type Iα Phosphatidylinositol Phosphate Kinase and Rac Signaling*. *J Biol Chem*. **278**, 23036–23045 (2003).

85. C. M. Szalinski, C. J. Guerriero, W. G. Ruiz, B. E. Docter, Y. Rbaibi, N. M. Pastor-Soler, G. Apodaca, M. A. Puthenveedu, O. A. Weisz, PIP5KIβ Selectively Modulates Apical Endocytosis in Polarized Renal Epithelial Cells. *Plos One*. **8**, e53790 (2013).

86. S. F. Bairstow, K. Ling, X. Su, A. J. Firestone, C. Carbonara, R. A. Anderson, Type Iγ661 Phosphatidylinositol Phosphate Kinase Directly Interacts with AP2 and Regulates Endocytosis*. *J Biol Chem*. **281**, 20632–20642 (2006).

87. J. R. Thieman, S. K. Mishra, K. Ling, B. Doray, R. A. Anderson, L. M. Traub, Clathrin Regulates the Association of PIPKIγ661 with the AP-2 Adaptor β2 Appendage*. *J Biol Chem*. **284**, 13924–13939 (2009).

88. K. Ling, R. L. Doughman, A. J. Firestone, M. W. Bunce, R. A. Anderson, Type Iγ phosphatidylinositol phosphate kinase targets and regulates focal adhesions. *Nature*. **420**, 89–93 (2002).

89. G. D. Paolo, L. Pellegrini, K. Letinic, G. Cestra, R. Zoncu, S. Voronov, S. Chang, J. Guo, M. R. Wenk, P. D. Camilli, Recruitment and regulation of phosphatidylinositol phosphate kinase type 1γ by the FERM domain of talin. *Nature*. **420**, 85–89 (2002).

90. M.-L. Giudici, K. Lee, R. Lim, R. F. Irvine, The intracellular localisation and mobility of Type Iγ phosphatidylinositol 4P 5-kinase splice variants. *Febs Lett*. **580**, 6933–6937 (2006).

91. Y. V. Shulga, R. A. Anderson, M. K. Topham, R. M. Epand, Phosphatidylinositol-4-phosphate 5-Kinase Isoforms Exhibit Acyl Chain Selectivity for Both Substrate and Lipid Activator. *J Biol Chem*. **287**, 35953–35963 (2012).

92. S. D. Hansen, A. A. Lee, J. T. Groves, *Biorxiv*, in press, doi:10.1101/2021.09.21.461304.

93. G. H. Jenkins, P. L. Fisette, R. A. Anderson, Type I phosphatidylinositol 4-phosphate 5-kinase isoforms are specifically stimulated by phosphatidic acid. *J Biological Chem*. **269**, 11547–54 (1994).

94. A. Moritz, P. N. D. Graan, W. H. Gispen, K. W. Wirtz, Phosphatidic acid is a specific activator of phosphatidylinositol-4-phosphate kinase. *J Biological Chem*. **267**, 7207–10 (1992).

95. N. Divecha, M. Roefs, J. R. Halstead, S. D'Andrea, M. Fernandez-Borga, L. Oomen, K. M. Saqib, M. J. O. Wakelam, C. D'Santos, Interaction of the Type Iα PIPkinase with phospholipase D: a role for the local generation of phosphatidylinositol 4,5-bisphosphate in the regulation of PLD2 activity. *Embo J*. **19**, 5440–5449 (2000).

96. J. H. Lorent, K. R. Levental, L. Ganesan, G. Rivera-Longsworth, E. Sezgin, M. Doktorova, E. Lyman, I. Levental, Plasma membranes are asymmetric in lipid unsaturation, packing and protein shape. *Nat Chem Biol*. **16**, 644–652 (2020).

97. J. C. Bozelli, J. Yune, D. Takahashi, F. Sakane, R. M. Epand, Membrane morphology determines diacylglycerol kinase α substrate acyl chain specificity. *Faseb J*. **35**, e21602 (2021).

98. G. R. Masson, R. L. Williams, Structural Mechanisms of PTEN Regulation. *Csh Perspect Med*. **10**, a036152 (2020).

99. L. R. Stephens, T. R. Jackson, P. T. Hawkins, Agonist-stimulated synthesis of phosphatidylinositol(3,4,5)-trisphosphate A new intracellular signalling system? *Biochimica Et Biophysica Acta Bba - Mol Cell Res*. **1179**, 27–75 (1993).

100. P. T. Hawkins, T. R. Jackson, L. R. Stephens, Platelet-derived growth factor stimulates synthesis of Ptdlns(3,4,5)P3 by activating a Ptdlns(4,5)P2 3-OH kinase. *Nature*. **358**, 157–159 (1992).

101. M. A. Lemmon, Membrane recognition by phospholipid-binding domains. *Nature Reviews Molecular Cell Biology*. **9**, nrm2328 (2008).

102. L. E. Rameh, L. C. Cantley, The Role of Phosphoinositide 3-Kinase Lipid Products in Cell Function*. *J Biol Chem*. **274**, 8347–8350 (1999).

103. N. Vasan, L. C. Cantley, At a crossroads: how to translate the roles of PI3K in oncogenic and metabolic signalling into improvements in cancer therapy. *Nat Rev Clin Oncol*, 1–15 (2022).

104. M. Zhang, H. Jang, R. Nussinov, PI3K Driver Mutations: A Biophysical Membrane-Centric Perspective. *Cancer Res*. **81**, 237–247 (2021).

105. M. Pirruccello, P. Camilli, Inositol 5-phosphatases: insights from the Lowe syndrome protein OCRL. *Trends in Biochemical Sciences*. **37**, 134–143 (2012).

106. S. E. Conduit, J. M. Dyson, C. A. Mitchell, Inositol polyphosphate 5-phosphatases; new players in the regulation of cilia and ciliopathies. *Febs Lett*. **586**, 2846–2857 (2012).

107. L. Staiano, M. A. D. Matteis, Phosphoinositides in the kidney. *J Lipid Res*. **60**, 287–298 (2019).

108. F. Nakatsu, R. M. Perera, L. Lucast, R. Zoncu, J. Domin, F. B. Gertler, D. Toomre, P. D. Camilli, The inositol 5-phosphatase SHIP2 regulates endocytic clathrin-coated pit dynamics. *J Cell Biology*. **190**, 307–315 (2010).

109. G. R. V. Hammond, G. Schiavo, R. F. Irvine, Immunocytochemical techniques reveal multiple, distinct cellular pools of PtdIns4P and PtdIns(4,5)P2. *Biochem J*. **422**, 23–35 (2009).

110. D. Sarkes, L. E. Rameh, A novel HPLC-based approach makes possible the spatial characterization of cellular PtdIns5P and other phosphoinositides. *Biochem J*. **428**, 375–384 (2010).

111. P. T. Hawkins, L. R. Stephens, PI3K signalling in inflammation. *Biochimica Et Biophysica Acta Bba - Mol Cell Biology Lipids*. **1851**, 882–897 (2015).

112. S. Kolay, U. Basu, P. Raghu, Control of diverse subcellular processes by a single multi-functional lipid phosphatidylinositol 4,5-bisphosphate [PI(4,5) P 2]. *Biochem J*. **473**, 1681–1692 (2016).

113. H. Choudhry, M. Aggarwal, P.-Y. Pan, Mini-review: Synaptojanin 1 and its implications in membrane trafficking. *Neurosci Lett*. **765**, 136288–136288 (2021).

114. B. K. Kay, M. P. Williamson, M. Sudol, The importance of being proline: the interaction of proline-rich motifs in signaling proteins with their cognate domains. *Faseb J*. **14**, 231–241 (2000).

115. R. Dong, T. Zhu, L. Benedetti, S. Gowrishankar, H. Deng, Y. Cai, X. Wang, K. Shen, P. D. Camilli, The inositol 5-phosphatase INPP5K participates in the fine control of ER organization. *J Cell Biology*. **217**, 3577–3592 (2018).

116. R. Gurung, A. Tan, L. M. Ooms, M. J. McGrath, R. D. Huysmans, A. D. Munday, M. Prescott, J. C. Whisstock, C. A. Mitchell, Identification of a Novel Domain in Two Mammalian Inositol-polyphosphate 5-Phosphatases That Mediates Membrane Ruffle Localization THE INOSITOL 5-PHOSPHATASE SKIP LOCALIZES TO THE ENDOPLASMIC RETICULUM AND TRANSLOCATES TO MEMBRANE RUFFLES FOLLOWING EPIDERMAL GROWTH FACTOR STIMULATION*. *J Biol Chem*. **278**, 11376–11385 (2003).

117. J. Xie, I. Vandenbroere, I. Pirson, SHIP2 associates with intersectin and recruits it to the plasma membrane in response to EGF. *Febs Lett*. **582**, 3011–3017 (2008).

118. T. Pawson, G. D. Gish, P. Nash, SH2 domains, interaction modules and cellular wiring. *Trends Cell Biol*. **11**, 504–511 (2001).

119. M.-J. Park, R. Sheng, A. Silkov, D.-J. Jung, Z.-G. Wang, Y. Xin, H. Kim, P. Thiagarajan-Rosenkranz, S. Song, Y. Yoon, W. Nam, I. Kim, E. Kim, D.-G. Lee, Y. Chen, I. Singaram, L. Wang, M. H. Jang, C.-S. Hwang, B. Honig, S. Ryu, J. Lorieau, Y.-M. Kim, W. Cho, SH2 Domains Serve as Lipid-Binding Modules for pTyr-Signaling Proteins. *Molecular Cell*. **62** (2016), doi:10.1016/j.molcel.2016.01.027.

120. S. Sipeki, K. Koprivanacz, T. Takács, A. Kurilla, L. László, V. Vas, L. Buday, Novel Roles of SH2 and SH3 Domains in Lipid Binding. *Cells*. **10**, 1191 (2021).

121. T. Balla, Z. Szentpetery, Y. J. Kim, Phosphoinositide Signaling: New Tools and Insights. *Physiology*. **24**, 231–244 (2009).

122. M. Maekawa, G. D. Fairn, Molecular probes to visualize the location, organization and dynamics of lipids. *J Cell Sci*. **127**, 4801–4812 (2014).

123. G. R. V. Hammond, T. Balla, Polyphosphoinositide binding domains: Key to inositol lipid biology. *Biochimica Et Biophysica Acta Bba - Mol Cell Biology Lipids*. **1851**, 746–758 (2015).

124. J. T. Tóth, G. Gulyás, D. J. Tóth, A. Balla, G. R. V. Hammond, L. Hunyady, T. Balla, P. Várnai, BRET-monitoring of the dynamic changes of inositol lipid pools in living cells reveals a PKC-dependent PtdIns4P increase upon EGF and M3 receptor activation. *Biochimica Et Biophysica Acta Bba - Mol Cell Biology Lipids*. **1861**, 177–187 (2016).

125. P. Várnai, G. Gulyás, D. J. Tóth, M. Sohn, N. Sengupta, T. Balla, Quantifying lipid changes in various membrane compartments using lipid binding protein domains. *Cell Calcium*. **64**, 72–82 (2017).

126. G. van Meer, A. I. P. M. de Kroon, Lipid map of the mammalian cell. *J Cell Sci*. **124**, 5–8 (2011).

127. F. Zambrano, S. Fleischer, B. Fleischer, Lipid composition of the golgi apparatus of rat kidney and liver in comparison with other subcellular organelles. *Biochimica Et Biophysica Acta Bba - Lipids Lipid Metabolism*. **380**, 357–369 (1975).

128. J. E. Ferrell, W. H. Huestis, Phosphoinositide metabolism and the morphology of human erythrocytes. *J Cell Biology*. **98**, 1992–1998 (1984).

129. G. Griffiths, S. D. Fuller, R. Back, M. Hollinshead, S. Pfeiffer, K. Simons, The dynamic nature of the Golgi complex. *J Cell Biology*. **108**, 277–297 (1989).

130. G. Griffiths, R. Back, M. Marsh, A quantitative analysis of the endocytic pathway in baby hamster kidney cells. *J Cell Biology*. **109**, 2703–2720 (1989).

131. G. van Meer, D. R. Voelker, G. W. Feigenson, Membrane lipids: where they are and how they behave. *Nat Rev Mol Cell Bio*. **9**, 112–124 (2008).

132. G. D. Paolo, P. D. Camilli, Phosphoinositides in cell regulation and membrane dynamics. *Nature*. **443** (2006), doi:10.1038/nature05185.

133. C. Xu, J. Watras, L. M. Loew, Kinetic analysis of receptor-activated phosphoinositide turnover. *The Journal of Cell Biology*. **161**, 779–791 (2003).

134. D. W. Hilgemann, Local PIP2 signals: when, where, and how? *Pflügers Archiv - European J Physiology*. **455**, 55–67 (2007).

135. D. J. James, C. Khodthong, J. A. Kowalchyk, T. F. J. Martin, Phosphatidylinositol 4,5-bisphosphate regulates SNARE-dependent membrane fusion. *J Cell Biology*. **182**, 355–366 (2008).

136. C.-L. Chang, J. Liou, Homeostatic regulation of the PI(4,5)P2–Ca2+ signaling system at ER–PM junctions. *Biochimica Et Biophysica Acta Bba - Mol Cell Biology Lipids*. **1861**, 862–873 (2016).

137. R. H. Michell, C. J. Kirk, L. M. Jones, C. P. Downes, J. A. Creba, The stimulation of inositol lipid metabolism that accompanies calcium mobilization in stimulated cells: defined characteristics and unanswered questions. *Philosophical Transactions Royal Soc Lond B Biological Sci*. **296**, 123–138 (1981).

138. Y. Zhou, X. Cai, R. M. Nwokonko, N. A. Loktionova, Y. Wang, D. L. Gill, The STIM-Orai coupling interface and gating of the Orai1 channel. *Cell Calcium*. **63**, 8–13 (2017).

139. P. G. Hogan, A. Rao, Store-operated calcium entry: Mechanisms and modulation. *Biochem Bioph Res Co*. **460**, 40–49 (2015).

140. M. K. Korzeniowski, M. A. Popovic, Z. Szentpetery, P. Varnai, S. S. Stojilkovic, T. Balla, Dependence of STIM1/Orai1-mediated Calcium Entry on Plasma Membrane Phosphoinositides*. *J Biol Chem*. **284**, 21027–21035 (2009).

141. J. Maléth, S. Choi, S. Muallem, M. Ahuja, Translocation between PI(4,5)P2-poor and PI(4,5)P2-rich microdomains during store depletion determines STIM1 conformation and Orai1 gating. *Nature Communications*. **5**, 5843 (2014).

142. M. Periasamy, A. Kalyanasundaram, SERCA pump isoforms: Their role in calcium transport and disease. *Muscle Nerve*. **35**, 430–442 (2007).

143. K. Rahate, L. K. Bhatt, K. S. Prabhavalkar, SERCA stimulation: A potential approach in therapeutics. *Chem Biol Drug Des*. **95**, 5–15 (2020).

144. C.-L. Chang, Y.-J. Chen, J. Liou, ER-plasma membrane junctions: Why and how do we study them? *Biochimica Et Biophysica Acta Bba - Mol Cell Res*. **1864**, 1494–1506 (2017).

145. N. Déliot, B. Constantin, Plasma membrane calcium channels in cancer: Alterations and consequences for cell proliferation and migration. *Biochimica Et Biophysica Acta Bba - Biomembr*. **1848**, 2512–2522 (2015).

146. A. L. Duncan, W. Song, M. S. P. Sansom, Lipid-Dependent Regulation of Ion Channels and G Protein–Coupled Receptors: Insights from Structures and Simulations. *Annu Rev Pharmacol*. **60**, 1–20 (2019).

147. A. A. Rodríguez-Menchaca, S. K. Adney, L. Zhou, D. E. Logothetis, Dual Regulation of Voltage-Sensitive Ion Channels by PIP2. *Frontiers in Pharmacology*. **3**, 170 (2012).

148. T. Rohacs, B. Nilius, Regulation of transient receptor potential (TRP) channels by phosphoinositides. *Pflügers Archiv - European J Physiology*. **455**, 157–168 (2007).

149. B. Nilius, F. Mahieu, Y. Karashima, T. Voets, Regulation of TRP channels: a voltage–lipid connection. *Biochem Soc T*. **35**, 105–108 (2007).

150. L. Wu, C. S. Bauer, X. Zhen, C. Xie, J. Yang, Dual regulation of voltage-gated calcium channels by PtdIns(4,5)P2. *Nature*. **419**, 947–952 (2002).

151. N. Gamper, V. Reznikov, Y. Yamada, J. Yang, M. S. Shapiro, Phosphotidylinositol 4,5-Bisphosphate Signals Underlie Receptor-Specific Gq/11-Mediated Modulation of N-Type Ca2+ Channels. *J Neurosci*. **24**, 10980–10992 (2004).

152. M. Rousset, T. Cens, A. Gouin-Charnet, F. Scamps, P. Charnet, Ca2+ and Phosphatidylinositol 4,5-Bisphosphate Stabilize a Gβγ-sensitive State of CaV2 Ca2+ Channels*. *J Biol Chem*. **279**, 14619–14630 (2004).

153. B. Hille, E. J. Dickson, M. Kruse, O. Vivas, B.-C. Suh, Phosphoinositides regulate ion channels. *Biochimica Et Biophysica Acta Bba - Mol Cell Biology Lipids*. **1851**, 844–856 (2015).

154. P. Varnai, B. Thyagarajan, T. Rohacs, T. Balla, Rapidly inducible changes in phosphatidylinositol 4,5-bisphosphate levels influence multiple regulatory functions of the lipid in intact living cells. *J Cell Biology*. **175**, 377–382 (2006).

155. S. Bandara, S. Malmersjö, T. Meyer, Regulators of Calcium Homeostasis Identified by Inference of Kinetic Model Parameters from Live Single Cells Perturbed by siRNA. *Sci Signal*. **6**, ra56–ra56 (2013).

156. D. W. Hilgemann, R. Ball, Regulation of Cardiac Na+,Ca2+ Exchange and KATP Potassium Channels by PIP2. *Science*. **273**, 956–959 (1996).

157. M. Brini, E. Carafoli, The Plasma Membrane Ca2+ ATPase and the Plasma Membrane Sodium Calcium Exchanger Cooperate in the Regulation of Cell Calcium. *Cold Spring Harbor Perspectives in Biology*. **3**, a004168 (2011).

158. D. W. Hilgemann, S. Feng, C. Nasuhoglu, The Complex and Intriguing Lives of PIP2 with Ion Channels and Transporters. *Sci. STKE*. **2001**, re19–re19 (2001).

159. M. J. Berridge, Inositol Trisphosphate and Diacylglycerol: Two Interacting Second Messengers. *Annu Rev Biochem*. **56**, 159–193 (1987).

160. F. Colón-González, M. G. Kazanietz, C1 domains exposed: From diacylglycerol binding to protein–protein interactions. *Biochimica Et Biophysica Acta Bba - Mol Cell Biology Lipids*. **1761**, 827–837 (2006).

161. J. Chen, F. Deng, J. Li, Q. J. Wang, Selective binding of phorbol esters and diacylglycerol by individual C1 domains of the PKD family. *Biochem J*. **411**, 333–342 (2008).

162. M.-C. Domart, T. M. C. Hobday, C. J. Peddie, G. H. C. Chung, A. Wang, K. Yeh, N. Jethwa, Q. Zhang, M. J. O. Wakelam, R. Woscholski, R. D. Byrne, L. M. Collinson, D. L. Poccia, B. Larijani, Acute Manipulation of Diacylglycerol Reveals Roles in Nuclear Envelope Assembly & Endoplasmic Reticulum Morphology. *Plos One*. **7**, e51150 (2012).

163. R. V. Stahelin, M. A. Digman, M. Medkova, B. Ananthanarayanan, H. R. Melowic, J. D. Rafter, W. Cho, Diacylglycerol-induced Membrane Targeting and Activation of Protein Kinase Cϵ MECHANISTIC DIFFERENCES BETWEEN PROTEIN KINASES Cδ AND Cϵ. *J Biol Chem*. **280**, 19784–19793 (2005).

164. J. H. Hurley, T. Meyer, Subcellular targeting by membrane lipids. *Current Opinion in Cell Biology*. **13**, 146–152 (2001).

165. C. Lehel, Z. Olah, G. Jakab, W. B. Anderson, Protein kinase C epsilon is localized to the Golgi via its zinc-finger domain and modulates Golgi function. *Proc National Acad Sci*. **92**, 1406–1410 (1995).

166. D. J. Erle, D. Sheppard, The cell biology of asthma. *J Cell Biology*. **205**, 621–631 (2014).

167. T. J. Eddinger, Smooth Muscle-Protein Translocation and Tissue Function. *The Anatomical Record*. **297**, 1734–1746 (2014).

168. T. Chatila, L. Silverman, R. Miller, R. Geha, Mechanisms of T cell activation by the calcium ionophore ionomycin. *J Immunol Baltim Md 1950*. **143**, 1283–9 (1989).

169. D. S. Regier, K. A. Waite, R. Wallin, L. C. McPhail, A Phosphatidic Acid-activated Protein Kinase and Conventional Protein Kinase C Isoforms Phosphorylate p22 phox , an NADPH Oxidase Component*. *J Biol Chem*. **274**, 36601–36608 (1999).

170. M. A. Rizzo, K. Shome, S. C. Watkins, G. Romero, The recruitment of Raf-1 to membranes is mediated by direct interaction with phosphatidic acid and is independent of association with Ras. *J Biol Chem*. **275**, 23911–23918 (2000).

171. C. A. Kraft, J. L. Garrido, E. Fluharty, L. Leiva-Vega, G. Romero, Role of Phosphatidic Acid in the Coupling of the ERK Cascade*. *J Biol Chem*. **283**, 36636–36645 (2008).

172. M. Whitman, C. P. Downes, M. Keeler, T. Keller, L. Cantley, Type I phosphatidylinositol kinase makes a novel inositol phospholipid, phosphatidylinositol-3-phosphate. *Nature*. **332**, 644–646 (1988).

173. A. E. Traynor-Kaplan, A. L. Harris, B. L. Thompson, P. Taylor, L. A. Sklar, An inositol tetrakisphosphate-containing phospholipid in activated neutrophils. *Nature*. **334**, 353–356 (1988).

174. K. R. Auger, L. A. Serunian, S. P. Soltoff, P. Libby, L. C. Cantley, PDGF-dependent tyrosine phosphorylation stimulates production of novel polyphosphoinositides in intact cells. *Cell*. **57**, 167–175 (1989).

175. K. Mariniello, Y. Min, K. Ghebremeskel, Phosphorylation of protein kinase B, the key enzyme in insulin-signaling cascade, is enhanced in linoleic and arachidonic acid-treated HT29 and HepG2 cells. *Nutrition (Burbank, Los Angeles County, Calif.)*. **57**, 52–58 (2018).

176. Y. Miao, S. Bhattacharya, T. Banerjee, B. Abubaker-Sharif, Y. Long, T. Inoue, P. A. Iglesias, P. N. Devreotes, Wave patterns organize cellular protrusions and control cortical dynamics. *Molecular Systems Biology*. **15**, e8585 (2019).

177. H. Zhan, S. Bhattacharya, H. Cai, P. A. Iglesias, C.-H. Huang, P. N. Devreotes, An Excitable Ras/PI3K/ERK Signaling Network Controls Migration and Oncogenic Transformation in Epithelial Cells. *Dev Cell*. **54**, 608-623.e5 (2020).

178. B. P. Ziemba, J. J. Falke, A PKC-MARCKS-PI3K regulatory module links Ca2+ and PIP3 signals at the leading edge of polarized macrophages. *Plos One*. **13**, e0196678 (2018).

179. K.-K. Wong, J. A. Engelman, L. C. Cantley, Targeting the PI3K signaling pathway in cancer. *Curr Opin Genet Dev*. **20**, 87–90 (2010).

180. D. A. Fruman, H. Chiu, B. D. Hopkins, S. Bagrodia, L. C. Cantley, R. T. Abraham, The PI3K Pathway in Human Disease. *Cell*. **170**, 605–635 (2017).

181. M. N. Paddock, S. J. Field, L. C. Cantley, Treating cancer with phosphatidylinositol-3-kinase inhibitors: increasing efficacy and overcoming resistance. *Journal of lipid research* (2019), doi:10.1194/jlr.S092130.

182. K. L. Pierce, R. T. Premont, R. J. Lefkowitz, Seven-transmembrane receptors. *Nat Rev Mol Cell Bio*. **3**, 639–650 (2002).

183. D. M. Rosenbaum, S. G. F. Rasmussen, B. K. Kobilka, The structure and function of G-protein-coupled receptors. *Nature*. **459**, 356–363 (2009).

184. P. G. de Oliveira, M. L. S. Ramos, A. J. Amaro, R. A. Dias, S. I. Vieira, Gi/o-Protein Coupled Receptors in the Aging Brain. *Front Aging Neurosci*. **11**, 89 (2019).

185. K. Palczewski, T. Kumasaka, T. Hori, C. A. Behnke, H. Motoshima, B. A. Fox, I. L. Trong, D. C. Teller, T. Okada, R. E. Stenkamp, M. Yamamoto, M. Miyano, Crystal Structure of Rhodopsin: A G Protein-Coupled Receptor. *Science*. **289**, 739–745 (2000).

186. Q. Zhou, D. Yang, M. Wu, Y. Guo, W. Guo, L. Zhong, X. Cai, A. Dai, W. Jang, E. I. Shakhnovich, Z.-J. Liu, R. C. Stevens, N. A. Lambert, M. M. Babu, M.-W. Wang, S. Zhao, Common activation mechanism of class A GPCRs. *Elife*. **8**, e50279 (2019).

187. H.-Y. Yen, K. K. Hoi, I. Liko, G. Hedger, M. R. Horrell, W. Song, D. Wu, P. Heine, T. Warne, Y. Lee, B. Carpenter, A. Plückthun, C. G. Tate, M. S. P. Sansom, C. V. Robinson, PtdIns(4,5)P2 stabilizes active states of GPCRs and enhances selectivity of G-protein coupling. *Nature*. **559**, 423–427 (2018).

188. W. Song, A. L. Duncan, M. S. P. Sansom, Modulation of adenosine A2a receptor oligomerization by receptor activation and PIP2 interactions. *Struct Lond Engl 1993*. **29**, 1312-1325.e3 (2021).

189. K. L. Pierce, R. J. Lefkowitz, Classical and new roles of β-arrestins in the regulation of G-PROTEIN-COUPLED receptors. *Nat Rev Neurosci*. **2**, 727–733 (2001).

190. W. Huang, M. Masureel, Q. Qianhui, J. Janetzko, A. Inoue, H. E. Kato, M. J. Robertson, K. C. Nguyen, J. S. Glenn, G. Skiniotis, B. K. Kobilka, Structure of the Neurotensin Receptor 1 in complex with β-arrestin 1. *Nature*. **579**, 303–308 (2020).

191. J. Janetzko, R. Kise, B. Barsi-Rhyne, D. H. Siepe, F. M. Heydenreich, M. Masureel, K. Kawakami, K. C. Garcia, M. von Zastrow, A. Inoue, B. K. Kobilka, *Biorxiv*, in press, doi:10.1101/2021.10.09.463790.

192. S.-R. Jung, Y. Jiang, J. B. Seo, D. T. Chiu, B. Hille, D.-S. Koh, β-arrestin–dependent PI(4,5)P2 synthesis boosts GPCR endocytosis. *Proc National Acad Sci*. **118**, e2011023118 (2021).

193. B.-C. C. Suh, B. Hille, PIP2 is a necessary cofactor for ion channel function: how and why? *Annual review of biophysics*. **37**, 175–95 (2008).

194. M. Kruse, G. R. V. Hammond, B. Hille, Regulation of voltage-gated potassium channels by PI(4,5)P2. *J Gen Physiology*. **140**, 189–205 (2012).

195. D. Liu, E. R. Liman, Intracellular Ca2+ and the phospholipid PIP2 regulate the taste transduction ion channel TRPM5. *Proc National Acad Sci*. **100**, 15160–15165 (2003).

196. Z. Zhang, H. Okawa, Y. Wang, E. R. Liman, Phosphatidylinositol 4,5-Bisphosphate Rescues TRPM4 Channels from Desensitization*. *J Biol Chem*. **280**, 39185–39192 (2005).

197. L. W. Runnels, L. Yue, D. E. Clapham, The TRPM7 channel is inactivated by PIP2 hydrolysis. *Nat Cell Biol*. **4**, 329–336 (2002).

198. B. Nilius, F. Mahieu, J. Prenen, A. Janssens, G. Owsianik, R. Vennekens, T. Voets, The Ca2+-activated cation channel TRPM4 is regulated by phosphatidylinositol 4,5-biphosphate. *Embo J*. **25**, 467–478 (2006).

199. T. Rohács, C. M. B. Lopes, I. Michailidis, D. E. Logothetis, PI(4,5)P2 regulates the activation and desensitization of TRPM8 channels through the TRP domain. *Nat Neurosci*. **8**, 626–634 (2005).

200. H. Chuang, E. D. Prescott, H. Kong, S. Shields, S.-E. Jordt, A. I. Basbaum, M. V. Chao, D. Julius, Bradykinin and nerve growth factor release the capsaicin receptor from PtdIns(4,5)P2-mediated inhibition. *Nature*. **411**, 957–962 (2001).

201. G. Dai, C. Peng, C. Liu, M. D. Varnum, Two structural components in CNGA3 support regulation of cone CNG channels by phosphoinositides. *J Gen Physiology*. **141**, 413–430 (2013).

202. Q. Zhao, M. Yang, A. T. Ting, D. E. Logothetis, PIP 2 Regulates the Ionic Current of P2X Receptors and P2X 7 Receptor-Mediated Cell Death. *Channels*. **1**, 47–56 (2007).

203. L.-P. Bernier, A. R. Ase, S. Chevallier, D. Blais, Q. Zhao, E. Boue-Grabot, D. Logothetis, P. Seguela, Phosphoinositides Regulate P2X4 ATP-Gated Channels through Direct Interactions. *J Neurosci*. **28**, 12938–12945 (2008).

204. S. Noreng, A. Bharadwaj, R. Posert, C. Yoshioka, I. Baconguis, Structure of the human epithelial sodium channel by cryo-electron microscopy. *Elife*. **7**, e39340 (2018).

205. O. Pochynyuk, Q. Tong, A. Staruschenko, J. D. Stockand, Binding and direct activation of the epithelial Na+ channel (ENaC) by phosphatidylinositides. *J Physiology*. **580**, 365–372 (2007).

206. C. R. Archer, B. T. Enslow, C. M. Carver, J. D. Stockand, Phosphatidylinositol 4,5-bisphosphate directly interacts with the β and γ subunits of the sodium channel ENaC. *J Biol Chem*. **295**, 7958–7969 (2020).

207. T. M. A. El-Aziz, A. Kaur, M. S. Shapiro, J. D. Stockand, C. R. Archer, Optogenetic Control of PIP2 Interactions Shaping ENaC Activity. *Int J Mol Sci*. **23**, 3884 (2022).

208. F. S. Choveau, V. D. la Rosa, S. M. Bierbower, C. C. Hernandez, M. S. Shapiro, Phosphatidylinositol 4,5-bisphosphate (PIP2) regulates KCNQ3 K+ channels by interacting with four cytoplasmic channel domains. *J Biol Chem*. **293**, 19411–19428 (2018).

209. C. C. Hernandez, B. Falkenburger, M. S. Shapiro, Affinity for phosphatidylinositol 4,5-bisphosphate determines muscarinic agonist sensitivity of Kv7 K+ channels. *J Gen Physiology*. **134**, 437–448 (2009).

210. Y. Jiang, A. Lee, J. Chen, V. Ruta, M. Cadene, B. T. Chait, R. MacKinnon, X-ray structure of a voltage-dependent K+ channel. *Nature*. **423**, 33–41 (2003).

211. S. B. Long, X. Tao, E. B. Campbell, R. MacKinnon, Atomic structure of a voltage-dependent K+ channel in a lipid membrane-like environment. *Nature*. **450**, 376–382 (2007).

212. A. A. Rodriguez-Menchaca, S. K. Adney, Q.-Y. Tang, X.-Y. Meng, A. Rosenhouse-Dantsker, M. Cui, D. E. Logothetis, PIP2 controls voltage-sensor movement and pore opening of Kv channels through the S4–S5 linker. *Proceedings of the National Academy of Sciences*. **109**, E2399–E2408 (2012).

213. N. A. Hager, C. K. McAtee, M. A. Lesko, A. F. O'Donnell, Inwardly Rectifying Potassium Channel Kir2.1 and its "Kir-ious" Regulation by Protein Trafficking and Roles in Development and Disease. *Frontiers Cell Dev Biology*. **9**, 796136 (2022).

214. C.-L. Huang, S. Feng, D. W. Hilgemann, Direct activation of inward rectifier potassium channels by PIP2 and its stabilization by Gβγ. *Nature*. **391**, 803–806 (1998).

215. T. Rohács, J. Chen, G. D. Prestwich, D. E. Logothetis, Distinct Specificities of Inwardly Rectifying K+Channels for Phosphoinositides*. *J Biol Chem*. **274**, 36065–36072 (1999).

216. T. Rohács, C. M. B. Lopes, T. Jin, P. P. Ramdya, Z. Molnár, D. E. Logothetis, Specificity of activation by phosphoinositides determines lipid regulation of Kir channels. *Proc National Acad Sci*. **100**, 745–750 (2003).

217. M. R. Whorton, R. MacKinnon, Crystal Structure of the Mammalian GIRK2 K+ Channel and Gating Regulation by G Proteins, PIP2, and Sodium. *Cell*. **147**, 199–208 (2011).

218. S. B. Hansen, X. Tao, R. MacKinnon, Structural basis of PIP2 activation of the classical inward rectifier K+ channel Kir2.2. *Nature*. **477**, 495–498 (2011).

219. M. R. Whorton, R. MacKinnon, X-ray structure of the mammalian GIRK2 – βγ G protein complex. *Nature*. **498**, 190–197 (2013).

220. O. Fürst, B. Mondou, N. D'Avanzo, Phosphoinositide regulation of inward rectifier potassium (Kir) channels. *Front Physiol*. **4**, 404 (2014).

221. N. Li, J.-X. Wu, D. Ding, J. Cheng, N. Gao, L. Chen, Structure of a Pancreatic ATP-Sensitive Potassium Channel. *Cell*. **168**, 101-110.e10 (2017).

222. Q.-Y. Tang, T. Larry, K. Hendra, E. Yamamoto, J. Bell, M. Cui, D. E. Logothetis, L. M. Boland, Mutations in Nature Conferred a High Affinity Phosphatidylinositol 4,5-Bisphosphate-binding Site in Vertebrate Inwardly Rectifying Potassium Channels*. *J Biol Chem*. **290**, 16517–16529 (2015).

223. O. Aharonovitz, H. C. Zaun, T. Balla, J. D. York, J. Orlowski, S. Grinstein, Intracellular Ph Regulation by Na+/H+ Exchange Requires Phosphatidylinositol 4,5-Bisphosphate. *J Cell Biology*. **150**, 213–224 (2000).

224. B. G. A. Jawdeh, S. Khan, I. Deschênes, M. Hoshi, M. Goel, J. T. Lock, K. Shinlapawittayatorn, G. Babcock, S. Lakhe-Reddy, G. DeCaro, S. P. Yadav, M. L. Mohan, S. V. N. Prasad, W. P. Schilling, E. Ficker, J. R. Schelling, Phosphoinositide Binding Differentially Regulates NHE1 Na+/H+ Exchanger-dependent Proximal Tubule Cell Survival*. *J Biol Chem*. **286**, 42435–42445 (2011).

225. H. Rasgado-Flores, H. Gonzalez-Serratos, Plasmalemmal transport of magnesium in excitable cells. *Front Biosci*. **5**, d866 (2000).

226. S. Li, C. Ghosh, Y. Xing, Y. Sun, Phosphatidylinositol 4,5-bisphosphate in the Control of Membrane Trafficking. *Int J Biol Sci*. **16**, 2761–2774 (2020).

227. K. O. Schink, K.-W. Tan, H. Stenmark, Phosphoinositides in Control of Membrane Dynamics. *Annu Rev Cell Dev Bi*. **32**, 1–29 (2015).

228. M. R. Wenk, P. D. Camilli, Protein-lipid interactions and phosphoinositide metabolism in membrane traffic: Insights from vesicle recycling in nerve terminals. *Proc National Acad Sci*. **101**, 8262–8269 (2004).

229. T. Martin, PI(4,5)P2-binding effector proteins for vesicle exocytosis. *Biochimica et Biophysica Acta (BBA) - Molecular and Cell Biology of Lipids*. **1851**, 785–793 (2015).

230. M. R. Heider, M. Munson, Exorcising the Exocyst Complex. *Traffic*. **13**, 898–907 (2012).

231. K. Mei, W. Guo, The exocyst complex. *Curr Biol*. **28**, R922–R925 (2018).

232. H. Maib, D. H. Murray, A mechanism for exocyst-mediated tethering via Arf6 and PIP5K1C-driven phosphoinositide conversion. *Curr Biol* (2022), doi:10.1016/j.cub.2022.04.089.

233. G. Kabachinski, M. Yamaga, D. M. Kielar-Grevstad, S. Bruinsma, T. F. J. Martin, CAPS and Munc13 utilize distinct PIP2-linked mechanisms to promote vesicle exocytosis. *Mol Biol Cell*. **25**, 508–521 (2014).

234. C. Capuano, R. Paolini, R. Molfetta, L. Frati, A. Santoni, R. Galandrini, PIP2-dependent regulation of Munc13-4 endocytic recycling: impact on the cytolytic secretory pathway. *Blood*. **119**, 2252–2262 (2012).

235. L. van Keimpema, R. Kooistra, R. F. Toonen, M. Verhage, CAPS-1 requires its C2, PH, MHD1 and DCV domains for dense core vesicle exocytosis in mammalian CNS neurons. *Sci Rep-uk*. **7**, 10817 (2017).

236. T. Tsuboi, E. Kanno, M. Fukuda, The polybasic sequence in the C2B domain of rabphilin is required for the vesicle docking step in PC12 cells. *J Neurochem*. **100**, 770–779 (2007).

237. S. Gonzalo, M. E. Linder, SNAP-25 Palmitoylation and Plasma Membrane Targeting Require a Functional Secretory Pathway. *Mol Biol Cell*. **9**, 585–597 (1998).

238. P. Weber, H. Batoulis, K. M. Rink, S. Dahlhoff, K. Pinkwart, T. H. Söllner, T. Lang, Electrostatic anchoring precedes stable membrane attachment of SNAP25/SNAP23 to the plasma membrane. *Elife*. **6**, e19394 (2017).

239. G. D. Paolo, H. S. Moskowitz, K. Gipson, M. R. Wenk, S. Voronov, M. Obayashi, R. Flavell, R. M. Fitzsimonds, T. A. Ryan, P. D. Camilli, Impaired PtdIns(4,5)P2 synthesis in nerve terminals produces defects in synaptic vesicle trafficking. *Nature*. **431**, 415–422 (2004).

240. R. Zoncu, R. M. Perera, R. Sebastian, F. Nakatsu, H. Chen, T. Balla, G. Ayala, D. Toomre, P. V. D. Camilli, Loss of endocytic clathrin-coated pits upon acute depletion of phosphatidylinositol 4,5-bisphosphate. *Proc National Acad Sci*. **104**, 3793–3798 (2007).

241. N. Abe, T. Inoue, T. Galvez, L. Klein, T. Meyer, Dissecting the role of PtdIns(4,5)P2 in endocytosis and recycling of the transferrin receptor. *Journal of Cell Science*. **121**, 1488–1494 (2008).

242. L. M. Traub, Common principles in clathrin-mediated sorting at the Golgi and the plasma membrane. *Biochimica Et Biophysica Acta Bba - Mol Cell Res*. **1744**, 415–437 (2005).

243. L. M. Traub, Clathrin Couture: Fashioning Distinctive Membrane Coats at the Cell Surface. *Plos Biol*. **7**, e1000192 (2009).

244. I. Gaidarov, J. H. Keen, Phosphoinositide–Ap-2 Interactions Required for Targeting to Plasma Membrane Clathrin-Coated Pits. *J Cell Biology*. **146**, 755–764 (1999).

245. N. R. Zaccai, Z. Kadlecova, V. K. Dickson, K. Korobchevskaya, J. Kamenicky, O. Kovtun, P. K. Umasankar, A. G. Wrobel, J. G. G. Kaufman, S. R. Gray, K. Qu, P. R. Evans, M. Fritzsche, F. Sroubek, S. Höning, J. A. G. Briggs, B. T. Kelly, D. J. Owen, L. M. Traub, FCHO controls AP2's initiating role in endocytosis through a PtdIns(4,5)P2-dependent switch. *Sci Adv*. **8**, eabn2018 (2022).

246. M. G. J. Ford, B. M. F. Pearse, M. K. Higgins, Y. Vallis, D. J. Owen, A. Gibson, C. R. Hopkins, P. R. Evans, H. T. McMahon, Simultaneous Binding of PtdIns(4,5)P_2 and Clathrin by AP180 in the Nucleation of Clathrin Lattices on Membranes. *Science*. **291**, 1051–1055 (2001).

247. T. Itoh, S. Koshiba, T. Kigawa, A. Kikuchi, S. Yokoyama, T. Takenawa, Role of the ENTH Domain in Phosphatidylinositol-4,5-Bisphosphate Binding and Endocytosis. *Science*. **291**, 1047–1051 (2001).

248. W. M. Henne, E. Boucrot, M. Meinecke, E. Evergren, Y. Vallis, R. Mittal, H. T. McMahon, FCHo Proteins Are Nucleators of Clathrin-Mediated Endocytosis. *Science*. **328**, 1281–1284 (2010).

249. W. Henne, H. M. Kent, M. Ford, B. G. Hegde, O. Daumke, J. P. Butler, R. Mittal, R. Langen, P. R. Evans, H. T. McMahon, Structure and Analysis of FCHo2 F-BAR Domain: A Dimerizing and Membrane Recruitment Module that Effects Membrane Curvature. *Structure*. **15**, 839–852 (2007).

250. M. Achiriloaie, B. Barylko, J. P. Albanesi, Essential Role of the Dynamin Pleckstrin Homology Domain in Receptor-Mediated Endocytosis. *Mol Cell Biol*. **19**, 1410–1415 (1999).

251. J. E. Bear, M. Krause, F. B. Gertler, Regulating cellular actin assembly. *Curr Opin Cell Biol*. **13**, 158–166 (2001).

252. J. Saarikangas, H. Zhao, P. Lappalainen, Regulation of the Actin Cytoskeleton-Plasma Membrane Interplay by Phosphoinositides. *Physiol Rev*. **90**, 259–289 (2010).

253. S. G. Heiss, J. A. Cooper, Regulation of CapZ, an actin capping protein of chicken muscle, by anionic phospholipids. *Biochemistry-us*. **30**, 8753–8758 (1991).

254. C. Solís, B. Russell, CapZ integrates several signaling pathways in response to mechanical stiffness. *J Gen Physiology*. **151**, 660–669 (2019).

255. T. J. Hartman, J. L. Martin, R. J. Solaro, A. M. Samarel, B. Russell, CapZ dynamics are altered by endothelin-1 and phenylephrine via PIP2- and PKC-dependent mechanisms. *Am J Physiol-cell Ph*. **296**, C1034–C1039 (2009).

256. V. Papayannopoulos, C. Co, K. E. Prehoda, S. Snapper, J. Taunton, W. A. Lim, A Polybasic Motif Allows N-WASP to Act as a Sensor of PIP2 Density. *Mol Cell*. **17**, 181–191 (2005).

257. H. N. Higgs, T. D. Pollard, Activation by Cdc42 and Pip2 of Wiskott-Aldrich Syndrome Protein (Wasp) Stimulates Actin Nucleation by Arp2/3 Complex. *J Cell Biology*. **150**, 1311–1320 (2000).

258. H. Higgs, T. Pollard, Regulation of actin filament network formation through ARP2/3 complex: activation by a diverse array of proteins. *Annual review of biochemistry*. **70**, 649–76 (2001).

259. L. A. Helgeson, B. J. Nolen, Mechanism of synergistic activation of Arp2/3 complex by cortactin and N-WASP. *Elife*. **2**, e00884 (2013).

260. B. A. Smith, S. B. Padrick, L. K. Doolittle, K. Daugherty-Clarke, I. R. Corrêa, M.-Q. Xu, B. L. Goode, M. K. Rosen, J. Gelles, Three-color single molecule imaging shows WASP detachment from Arp2/3 complex triggers actin filament branch formation. *Elife*. **2**, e01008 (2013).

261. P. J. Goldschmidt-Clermont, L. M. Machesky, J. J. Baldassare, T. D. Pollard, The Actin-Binding Protein Profilin Binds to PIP2 and Inhibits Its Hydrolysis by Phospholipase C. *Science*. **247**, 1575–1578 (1990).

262. R. H. Sohn, J. Chen, K. S. Koblan, P. F. Bray, P. J. Goldschmidt-Clermont, Localization of a Binding Site for Phosphatidylinositol 4,5-Bisphosphate on Human Profilin (∗). *J Biol Chem*. **270**, 21114–21120 (1995).

263. A. V. Kwiatkowski, F. B. Gertler, J. J. Loureiro, Function and regulation of Ena/VASP proteins. *Trends Cell Biol*. **13**, 386–392 (2003).

264. T. Y. E. Sayegh, P. D. Arora, K. Ling, C. Laschinger, P. A. Janmey, R. A. Anderson, C. A. McCulloch, Phosphatidylinositol-4,5 Bisphosphate Produced by PIP5KIγ Regulates Gelsolin,

Actin Assembly, and Adhesion Strength of N-Cadherin Junctions. *Mol Biol Cell*. **18**, 3026–3038 (2007).

265. D. Szatmári, B. Xue, B. Kannan, L. D. Burtnick, B. Bugyi, M. Nyitrai, R. C. Robinson, ATP competes with PIP2 for binding to gelsolin. *PLOS ONE*. **13**, e0201826 (2018).

266. K.-M. Lin, E. Wenegieme, P.-J. Lu, C.-S. Chen, H. L. Yin, Gelsolin Binding to Phosphatidylinositol 4,5-Bisphosphate Is Modulated by Calcium and pH*. *J Biol Chem*. **272**, 20443–20450 (1997).

267. H. Zhao, M. Hakala, P. Lappalainen, ADF/Cofilin Binds Phosphoinositides in a Multivalent Manner to Act as a PIP2-Density Sensor. *Biophys J*. **98**, 2327–2336 (2010).

268. V. Y. Gorbatyuk, N. J. Nosworthy, S. A. Robson, N. P. S. Bains, M. W. Maciejewski, C. G. dos Remedios, G. F. King, Mapping the Phosphoinositide-Binding Site on Chick Cofilin Explains How PIP2 Regulates the Cofilin-Actin Interaction. *Mol Cell*. **24**, 511–522 (2006).

269. J. van Rheenen, X. Song, W. van Roosmalen, M. Cammer, X. Chen, V. DesMarais, S.-C. Yip, J. M. Backer, R. J. Eddy, J. S. Condeelis, EGF-induced PIP2 hydrolysis releases and activates cofilin locally in carcinoma cells. *J Cell Biology*. **179**, 1247–1259 (2007).

270. N. F. Valadares, H. d' M. Pereira, A. P. U. Araujo, R. C. Garratt, Septin structure and filament assembly. *Biophysical Rev*. **9**, 481–500 (2017).

271. A. Bertin, M. A. McMurray, L. Thai, G. Garcia, V. Votin, P. Grob, T. Allyn, J. Thorner, E. Nogales, Phosphatidylinositol-4,5- bisphosphate Promotes Budding Yeast Septin Filament Assembly and Organization. *J Mol Biol*. **404**, 711–731 (2010).

272. B. Machnicka, A. Czogalla, A. Hryniewicz-Jankowska, D. M. Bogusławska, R. Grochowalska, E. Heger, A. F. Sikorski, Spectrins: A structural platform for stabilization and activation of membrane channels, receptors and transporters. *Biochimica Et Biophysica Acta Bba - Biomembr*. **1838**, 620–634 (2014).

273. P. Zhang, S. Talluri, H. Deng, D. Branton, G. Wagner, Solution structure of the pleckstrin homology domain of Drosophila β-spectrin. *Structure*. **3**, 1185–1195 (1995).

274. R. K. H. Liem, Cytoskeletal Integrators: The Spectrin Superfamily. *Csh Perspect Biol*. **8**, a018259 (2016).

275. J. Pacheco, A. C. Cassidy, J. P. Zewe, R. C. Wills, G. R. V. Hammond, *Biorxiv*, in press, doi:10.1101/2022.01.07.475414.

276. D. T. Moore, P. Nygren, H. Jo, K. Boesze-Battaglia, J. S. Bennett, W. F. DeGrado, Affinity of talin-1 for the β3-integrin cytosolic domain is modulated by its phospholipid bilayer environment. *Proc National Acad Sci*. **109**, 793–798 (2012).

277. X. Song, J. Yang, J. Hirbawi, S. Ye, H. D. Perera, E. Goksoy, P. Dwivedi, E. F. Plow, R. Zhang, J. Qin, A novel membrane-dependent on/off switch mechanism of talin FERM domain at sites of cell adhesion. *Cell Res*. **22**, 1533–1545 (2012).

278. J.-J. Hao, Y. Liu, M. Kruhlak, K. E. Debell, B. L. Rellahan, S. Shaw, Phospholipase C–mediated hydrolysis of PIP2 releases ERM proteins from lymphocyte membrane. *J Cell Biology*. **184**, 451–462 (2009).

279. K. Hamada, T. Shimizu, T. Matsui, S. Tsukita, S. Tsukita, T. Hakoshima, Structural basis of the membrane-targeting and unmasking mechanisms of the radixin FERM domain. *Embo J*. **19**, 4449–4462 (2000).

280. P. Kanchanawong, G. Shtengel, A. M. Pasapera, E. B. Ramko, M. W. Davidson, H. F. Hess, C. M. Waterman, Nanoscale architecture of integrin-based cell adhesions. *Nature*. **468**, 580–584 (2010).

281. G. M. Goñi, C. Epifano, J. Boskovic, M. Camacho-Artacho, J. Zhou, A. Bronowska, M. T. Martín, M. J. Eck, L. Kremer, F. Gräter, F. L. Gervasio, M. Perez-Moreno, D. Lietha, Phosphatidylinositol 4,5-bisphosphate triggers activation of focal adhesion kinase by inducing clustering and conformational changes. *Proc National Acad Sci*. **111**, E3177–E3186 (2014).

282. X. Cai, D. Lietha, D. F. Ceccarelli, A. V. Karginov, Z. Rajfur, K. Jacobson, K. M. Hahn, M. J. Eck, M. D. Schaller, Spatial and Temporal Regulation of Focal Adhesion Kinase Activity in Living Cells ▿ . *Mol Cell Biol*. **28**, 201–214 (2008).

283. A. P. Gilmore, K. Burridge, Regulation of vinculin binding to talin and actin by phosphatidyl-inositol-4-5-bisphosphate. *Nature*. **381**, 531–535 (1996).

284. A. Orłowski, S. Kukkurainen, A. Pöyry, S. Rissanen, I. Vattulainen, V. P. Hytönen, T. Róg, PIP2 and Talin Join Forces to Activate Integrin. *J Phys Chem B*. **119**, 12381–12389 (2015).

285. K. Chinthalapudi, E. S. Rangarajan, T. Izard, The interaction of talin with the cell membrane is essential for integrin activation and focal adhesion formation. *Proc National Acad Sci*. **115**, 10339–10344 (2018).

286. K. Fukami, T. Endo, M. Imamura, T. Takenawa, alpha-Actinin and vinculin are PIP2-binding proteins involved in signaling by tyrosine kinase. *J Biological Chem*. **269**, 1518–22 (1994).

287. P. M. Thompson, S. Ramachandran, L. B. Case, C. E. Tolbert, A. Tandon, M. Pershad, N. V. Dokholyan, C. M. Waterman, S. L. Campbell, A Structural Model for Vinculin Insertion into PIP2-Containing Membranes and the Effect of Insertion on Vinculin Activation and Localization. *Structure*. **25**, 264–275 (2017).

288. T. Izard, D. T. Brown, Mechanisms and Functions of Vinculin Interactions with Phospholipids at Cell Adhesion Sites. *Journal of Biological Chemistry*. **291**, 2548–2555 (2016).

289. K. Chinthalapudi, E. S. Rangarajan, D. N. Patil, E. M. George, D. T. Brown, T. Izard, Lipid binding promotes oligomerization and focal adhesion activity of vinculin. *The Journal of Cell Biology*. **207** (2014), doi:10.1083/jcb.201404128.

290. A. V. Kwiatkowski, D. A. Rubinson, E. W. Dent, J. E. van Veen, J. D. Leslie, J. Zhang, L. M. Mebane, U. Philippar, E. M. Pinheiro, A. A. Burds, R. T. Bronson, S. Mori, R. Fässler, F. B. Gertler, Ena/VASP Is Required for Neuritogenesis in the Developing Cortex. *Neuron*. **56**, 441–455 (2007).

291. C. D. Merkel, Y. Li, Q. Raza, D. B. Stolz, A. V. Kwiatkowski, Vinculin anchors contractile actin to the cardiomyocyte adherens junction. *Mol Biol Cell*. **30**, 2639–2650 (2019).

292. J. Kunz, A. Fuelling, L. Kolbe, R. A. Anderson, Stereo-specific substrate recognition by phosphatidylinositol phosphate kinases is swapped by changing a single amino acid residue. *Journal of Biological Chemistry*. **277** (2002), doi:10.1074/jbc.M110775200.

293. H. Yamaguchi, S. Yoshida, E. Muroi, M. Kawamura, Z. Kouchi, Y. Nakamura, R. Sakai, K. Fukami, Phosphatidylinositol 4,5-bisphosphate and PIP5-kinase Iα are required for invadopodia formation in human breast cancer cells. *Cancer Sci*. **101**, 1632–1638 (2010).

294. P. T. Ivanova, B. A. Cerda, D. M. Horn, J. S. Cohen, F. W. McLafferty, H. A. Brown, Electrospray ionization mass spectrometry analysis of changes in phospholipids in RBL-2H3 mastocytoma cells during degranulation. *Proc National Acad Sci*. **98**, 7152–7157 (2001).

295. S. B. Milne, P. T. Ivanova, D. DeCamp, R. C. Hsueh, H. A. Brown, A targeted mass spectrometric analysis of phosphatidylinositol phosphate species. *J Lipid Res*. **46**, 1796–1802 (2005).

296. C. A. Alter, B. A. Wolf, Identification of Phosphatidylinositol 3,4,5-Trisphosphate in Pancreatic Islets and Insulin-Secreting β-Cells. *Biochem Bioph Res Co*. **208**, 190–197 (1995).

297. M. Hokin-Neaverson, K. Sadeghian, Separation of [3H]inositol monophosphates and [3H]inositol on silica gel glass-fiber sheets. *J Chromatogr A*. **120**, 502–505 (1976).

298. V. Natarajan, H. H. O. Schmid, Inositol Phospholipid Hydrolysis by Rat Sciatic Nerve Phospholipase C. *J Neurochem*. **49**, 1878–1887 (1987).

299. H. Hegewald, One-Dimensional Thin-Layer Chromatography of All Known D-3 and D-4 Isomers of Phosphoinositides. *Anal Biochem*. **242**, 152–155 (1996).

300. P. Várnai, X. Lin, S. B. Lee, G. Tuymetova, T. Bondeva, A. Spät, S. G. Rhee, G. Hajnóczky, T. Balla, Inositol Lipid Binding and Membrane Localization of Isolated Pleckstrin Homology (PH) Domains STUDIES ON THE PH DOMAINS OF PHOSPHOLIPASE C δ1AND p130*. *J Biol Chem*. **277**, 27412–27422 (2002).

301. T. Balla, P. Várnai, Visualizing Cellular Phosphoinositide Pools with GFP-Fused Protein-Modules. *Sci Stke*. **2002**, pl3 (2002).

302. M. A. Lemmon, K. M. Ferguson, C. S. Abrams, Pleckstrin homology domains and the cytoskeleton. *Febs Lett*. **513**, 71–76 (2002).

303. M. A. Lemmon, Phosphoinositide Recognition Domains. *Traffic*. **4**, 201–213 (2003).

304. G. R. V. Hammond, M. P. Machner, T. Balla, A novel probe for phosphatidylinositol 4-phosphate reveals multiple pools beyond the Golgi. *J Cell Biology*. **205**, 113–126 (2014).

305. R. C. Wills, B. D. Goulden, G. R. V. Hammond, Genetically encoded lipid biosensors. *Mol Biol Cell*. **29**, 1526–1532 (2018).

306. A. Fegan, B. White, J. C. T. Carlson, C. R. Wagner, Chemically Controlled Protein Assembly: Techniques and Applications. *Chem Rev*. **110**, 3315–3336 (2010).

307. R. DeRose, T. Miyamoto, T. Inoue, Manipulating signaling at will: chemically-inducible dimerization (CID) techniques resolve problems in cell biology. *Pflügers Archiv - European J Physiology*. **465**, 409–417 (2013).

308. D. M. Spencer, T. J. Wandless, S. L. Schreiber, G. R. Crabtree, Controlling Signal Transduction with Synthetic Ligands. *Science*. **262**, 1019–1024 (1993).

309. J. Chen, X. F. Zheng, E. J. Brown, S. L. Schreiber, Identification of an 11-kDa FKBP12-rapamycin-binding domain within the 289-kDa FKBP12-rapamycin-associated protein and characterization of a critical serine residue. *Proc National Acad Sci*. **92**, 4947–4951 (1995).

310. L. A. Banaszynski, C. W. Liu, T. J. Wandless, Characterization of the FKBP·Rapamycin·FRB Ternary Complex. *J Am Chem Soc*. **127**, 4715–4721 (2005).

311. J. H. Bayle, J. S. Grimley, K. Stankunas, J. E. Gestwicki, T. J. Wandless, G. R. Crabtree, Rapamycin Analogs with Differential Binding Specificity Permit Orthogonal Control of Protein Activity. *Chem Biol*. **13**, 99–107 (2006).

312. D. W. Lamming, Inhibition of the Mechanistic Target of Rapamycin (mTOR)–Rapamycin and Beyond. *Csh Perspect Med*. **6**, a025924 (2016).

313. S. Santagata, T. J. Boggon, C. L. Baird, C. A. Gomez, J. Zhao, W. S. Shan, D. G. Myszka, L. Shapiro, G-Protein Signaling Through Tubby Proteins. *Science*. **292**, 2041–2050 (2001).

314. S. J. Field, N. Madson, M. L. Kerr, K. A. A. Galbraith, C. E. Kennedy, M. Tahiliani, A. Wilkins, L. C. Cantley, PtdIns(4,5)P2 Functions at the Cleavage Furrow during Cytokinesis. *Curr Biol*. **15**, 1407–1412 (2005).

315. Z. Szentpetery, A. Balla, Y. J. Kim, M. A. Lemmon, T. Balla, Live cell imaging with protein domains capable of recognizing phosphatidylinositol 4,5-bisphosphate; a comparative study. *Bmc Cell Biol*. **10**, 67–67 (2009).

316. K. V. Quinn, P. Behe, A. Tinker, Monitoring changes in membrane phosphatidylinositol 4,5-bisphosphate in living cells using a domain from the transcription factor tubby. *J Physiology*. **586**, 2855–2871 (2008).

317. C. R. Halaszovich, D. N. Schreiber, D. Oliver, Ci-VSP Is a Depolarization-activated Phosphatidylinositol-4,5-bisphosphate and Phosphatidylinositol-3,4,5-trisphosphate 5′-Phosphatase. *J Biol Chem*. **284**, 2106–2113 (2009).

318. B. D. Goulden, J. Pacheco, A. Dull, J. P. Zewe, A. Deiters, G. R. V. Hammond, A high-avidity biosensor reveals plasma membrane PI(3,4)P2 is predominantly a class I PI3K signaling product. *J Cell Biology*. **218**, 1066–1079 (2019).

319. B. P. Cormack, R. H. Valdivia, S. Falkow, FACS-optimized mutants of the green fluorescent protein (GFP). *Gene*. **173**, 33–38 (1996).

320. N. C. Shaner, R. E. Campbell, P. A. Steinbach, B. N. G. Giepmans, A. E. Palmer, R. Y. Tsien, Improved monomeric red, orange and yellow fluorescent proteins derived from Discosoma sp. red fluorescent protein. *Nat Biotechnol*. **22**, 1567–1572 (2004).

321. O. M. Subach, P. J. Cranfill, M. W. Davidson, V. V. Verkhusha, An Enhanced Monomeric Blue Fluorescent Protein with the High Chemical Stability of the Chromophore. *Plos One*. **6**, e28674 (2011).

322. G. S. Filonov, K. D. Piatkevich, L.-M. Ting, J. Zhang, K. Kim, V. V. Verkhusha, Bright and stable near infra-red fluorescent protein for in vivo imaging. *Nat Biotechnol*. **29**, 757–761 (2011).

323. J. P. Zewe, R. C. Wills, S. Sangappa, B. D. Goulden, G. R. Hammond, SAC1 degrades its lipid substrate PtdIns4P in the endoplasmic reticulum to maintain a steep chemical gradient with donor membranes. *Elife*. **7**, e35588 (2018).

324. J. Schindelin, I. Arganda-Carreras, E. Frise, V. Kaynig, M. Longair, T. Pietzsch, S. Preibisch, C. Rueden, S. Saalfeld, B. Schmid, J.-Y. Tinevez, D. J. White, V. Hartenstein, K. Eliceiri, P. Tomancak, A. Cardona, Fiji: an open-source platform for biological-image analysis. *Nat Methods*. **9**, 676–682 (2012).

325. M. Linkert, C. T. Rueden, C. Allan, J.-M. Burel, W. Moore, A. Patterson, B. Loranger, J. Moore, C. Neves, D. MacDonald, A. Tarkowska, C. Sticco, E. Hill, M. Rossner, K. W. Eliceiri, J. R. Swedlow, Metadata matters: access to image data in the real world. *J Cell Biology*. **189**, 777–782 (2010).

326. J.-C. Olivo-Marin, Extraction of spots in biological images using multiscale products. *Pattern Recogn*. **35**, 1989–1996 (2002).

327. Y. Shimada, M. Maruya, S. Iwashita, Y. Ohno-Iwashita, The C-terminal domain of perfringolysin O is an essential cholesterol-binding unit targeting to cholesterol-rich microdomains. *Eur J Biochem*. **269**, 6195–6203 (2002).

328. M. Maekawa, G. D. Fairn, Complementary probes reveal that phosphatidylserine is required for the proper transbilayer distribution of cholesterol. *J Cell Sci*. **128**, 1422–1433 (2015).

329. S.-L. Liu, R. Sheng, J. H. Jung, L. Wang, E. Stec, M. J. O'Connor, S. Song, R. K. Bikkavilli, R. A. Winn, D. Lee, K. Baek, K. Ueda, I. Levitan, K.-P. Kim, W. Cho, Orthogonal lipid sensors identify transbilayer asymmetry of plasma membrane cholesterol. *Nat Chem Biol*. **13**, 268–274 (2016).

330. A. Yamaji, Y. Sekizawa, K. Emoto, H. Sakuraba, K. Inoue, H. Kobayashi, M. Umeda, Lysenin, a Novel Sphingomyelin-specific Binding Protein. **273** (1998).

331. E. Kiyokawa, T. Baba, N. Otsuka, A. Makino, S. Ohno, T. Kobayashi, Spatial and Functional Heterogeneity of Sphingolipid-rich Membrane Domains*. *J Biol Chem*. **280**, 24072–24084 (2005).

332. M. Abe, A. Makino, F. Hullin-Matsuda, K. Kamijo, Y. Ohno-Iwashita, K. Hanada, H. Mizuno, A. Miyawaki, T. Kobayashi, A Role for Sphingomyelin-Rich Lipid Domains in the Accumulation of Phosphatidylinositol-4,5-Bisphosphate to the Cleavage Furrow during Cytokinesis. *Mol Cell Biol*. **32**, 1396–1407 (2012).

333. F. Zhang, Z. Wang, M. Lu, Y. Yonekubo, X. Liang, Y. Zhang, P. Wu, Y. Zhou, S. Grinstein, J. F. Hancock, G. Du, Temporal Production of the Signaling Lipid Phosphatidic Acid by Phospholipase D2 Determines the Output of Extracellular Signal-Regulated Kinase Signaling in Cancer Cells. *Mol Cell Biol*. **34**, 84–95 (2014).

334. M. Bohdanowicz, D. Schlam, M. Hermansson, D. Rizzuti, G. D. Fairn, T. Ueyama, P. Somerharju, G. Du, S. Grinstein, Phosphatidic acid is required for the constitutive ruffling and macropinocytosis of phagocytes. *Mol Biol Cell*. **24**, 1700–1712 (2013).

335. H. Yamada, S. Mizuno, S. Honda, D. Takahashi, F. Sakane, Characterization of α-synuclein N-terminal domain as a novel cellular phosphatidic acid sensor. *Febs J*. **287**, 2212–2234 (2020).

336. T. Yeung, G. E. Gilbert, J. Shi, J. Silvius, A. Kapus, S. Grinstein, Membrane Phosphatidylserine Regulates Surface Charge and Protein Localization. *Science*. **319**, 210–213 (2008).

337. K. Maeda, K. Anand, A. Chiapparino, A. Kumar, M. Poletto, M. Kaksonen, A.-C. Gavin, Interactome map uncovers phosphatidylserine transport by oxysterol-binding proteins. *Nature*. **501**, 257–261 (2013).

338. K. D. Vecchio, R. V. Stahelin, Investigation of the phosphatidylserine binding properties of the lipid biosensor, Lactadherin C2 (LactC2), in different membrane environments. *J Bioenerg Biomembr*. **50**, 1–10 (2018).

339. J. Chen, F. Deng, J. Li, Q. J. Wang, Selective binding of phorbol esters and diacylglycerol by individual C1 domains of the PKD family. *Biochem J*. **411**, 333–342 (2008).

340. Y. J. Kim, M. L. Guzman-Hernandez, T. Balla, A Highly Dynamic ER-Derived Phosphatidylinositol-Synthesizing Organelle Supplies Phosphoinositides to Cellular Membranes. *Dev Cell*. **21**, 813–824 (2011).

341. R. V. Stahelin, M. A. Digman, M. Medkova, B. Ananthanarayanan, H. R. Melowic, J. D. Rafter, W. Cho, Diacylglycerol-induced Membrane Targeting and Activation of Protein Kinase Cϵ MECHANISTIC DIFFERENCES BETWEEN PROTEIN KINASES Cδ AND Cϵ*. *J Biol Chem*. **280**, 19784–19793 (2005).

342. M.-C. Domart, T. M. C. Hobday, C. J. Peddie, G. H. C. Chung, A. Wang, K. Yeh, N. Jethwa, Q. Zhang, M. J. O. Wakelam, R. Woscholski, R. D. Byrne, L. M. Collinson, D. L. Poccia, B. Larijani, Acute Manipulation of Diacylglycerol Reveals Roles in Nuclear Envelope Assembly & Endoplasmic Reticulum Morphology. *Plos One*. **7**, e51150 (2012).

343. J. G. Pemberton, Y. J. Kim, J. Humpolickova, A. Eisenreichova, N. Sengupta, D. J. Toth, E. Boura, T. Balla, Defining the subcellular distribution and metabolic channeling of phosphatidylinositol. *J Cell Biology*. **219**, e201906130 (2020).

344. C. G. Burd, S. D. Emr, Phosphatidylinositol(3)-Phosphate Signaling Mediated by Specific Binding to RING FYVE Domains. *Mol Cell*. **2**, 157–162 (1998).

345. J.-M. Gaullier, A. Simonsen, A. D'Arrigo, B. Bremnes, H. Stenmark, R. Aasland, FYVE fingers bind PtdIns(3)P. *Nature*. **394**, 432–433 (1998).

346. D. J. Gillooly, I. C. Morrow, M. Lindsay, R. Gould, N. J. Bryant, J. Gaullier, R. G. Parton, H. Stenmark, Localization of phosphatidylinositol 3-phosphate in yeast and mammalian cells. *Embo J*. **19**, 4577–4588 (2000).

347. V. G. Sankaran, D. E. Klein, M. M. Sachdeva, M. A. Lemmon, High-Affinity Binding of a FYVE Domain to Phosphatidylinositol 3-Phosphate Requires Intact Phospholipid but Not FYVE Domain Oligomerization †. *Biochemistry-us*. **40**, 8581–8587 (2001).

348. J.-M. Gaullier, E. Rønning, D. J. Gillooly, H. Stenmark, Interaction of the EEA1 FYVE Finger with Phosphatidylinositol 3-phosphate and early endosomes. Role of conserved residues. *J Biol Chem*. **275**, 24595–24600 (2000).

349. J. Bravo, D. Karathanassis, C. M. Pacold, M. E. Pacold, C. D. Ellson, K. E. Anderson, P. J. G. Butler, I. Lavenir, O. Perisic, P. T. Hawkins, L. Stephens, R. L. Williams, The Crystal

Structure of the PX Domain from p40phox Bound to Phosphatidylinositol 3-Phosphate. *Mol Cell*. **8**, 829–839 (2001).

350. C. D. Ellson, S. Gobert-Gosse, K. E. Anderson, K. Davidson, H. Erdjument-Bromage, P. Tempst, J. W. Thuring, M. A. Cooper, Z.-Y. Lim, A. B. Holmes, P. R. J. Gaffney, J. Coadwell, E. R. Chilvers, P. T. Hawkins, L. R. Stephens, PtdIns(3)P regulates the neutrophil oxidase complex by binding to the PX domain of p40phox. *Nat Cell Biol*. **3**, 679–682 (2001).

351. F. Kanai, H. Liu, S. J. Field, H. Akbary, T. Matsuo, G. E. Brown, L. C. Cantley, M. B. Yaffe, The PX domains of p47phox and p40phox bind to lipid products of PI(3)K. *Nat Cell Biol*. **3**, 675–678 (2001).

352. E. Brombacher, S. Urwyler, C. Ragaz, S. S. Weber, K. Kami, M. Overduin, H. Hilbi, Rab1 Guanine Nucleotide Exchange Factor SidM Is a Major Phosphatidylinositol 4-Phosphate-binding Effector Protein of Legionella pneumophila*S. *J Biological Chem*. **284**, 4846–4856 (2009).

353. S. Schoebel, W. Blankenfeldt, R. S. Goody, A. Itzen, High-affinity binding of phosphatidylinositol 4-phosphate by Legionella pneumophila DrrA. *Embo Rep*. **11**, 598–604 (2010).

354. G. R. V. Hammond, M. P. Machner, T. Balla, A novel probe for phosphatidylinositol 4-phosphate reveals multiple pools beyond the Golgi. *J Cell Biology*. **205**, 113–126 (2014).

355. R. Levin, G. R. V. Hammond, T. Balla, P. D. Camilli, G. D. Fairn, S. Grinstein, Multiphasic dynamics of phosphatidylinositol 4-phosphate during phagocytosis. *Mol Biol Cell*. **28**, 128–140 (2017).

356. S. Dolinsky, I. Haneburger, A. Cichy, M. Hannemann, A. Itzen, H. Hilbi, The Legionella longbeachae Icm/Dot Substrate SidC Selectively Binds Phosphatidylinositol 4-Phosphate with Nanomolar Affinity and Promotes Pathogen Vacuole-Endoplasmic Reticulum Interactions. *Infect Immun*. **82**, 4021–4033 (2014).

357. S. Weber, M. Wagner, H. Hilbi, Live-Cell Imaging of Phosphoinositide Dynamics and Membrane Architecture during Legionella Infection. *Mbio*. **5**, e00839-13 (2014).

358. J. P. Zewe, R. C. Wills, S. Sangappa, B. D. Goulden, G. R. Hammond, SAC1 degrades its lipid substrate PtdIns4P in the endoplasmic reticulum to maintain a steep chemical gradient with donor membranes. *Elife*. **7**, e35588 (2018).

359. J. Chung, F. Torta, K. Masai, L. Lucast, H. Czapla, L. B. Tanner, P. Narayanaswamy, M. R. Wenk, F. Nakatsu, P. D. Camilli, PI4P/phosphatidylserine countertransport at ORP5- and ORP8-mediated ER–plasma membrane contacts. *Science*. **349**, 428–432 (2015).

360. R. Ghai, X. Du, H. Wang, J. Dong, C. Ferguson, A. J. Brown, R. G. Parton, J.-W. Wu, H. Yang, ORP5 and ORP8 bind phosphatidylinositol-4, 5-biphosphate (PtdIns(4,5)P2) and regulate its level at the plasma membrane. *Nat Commun*. **8**, 757 (2017).

361. M. Sohn, M. Korzeniowski, J. P. Zewe, R. C. Wills, G. R. V. Hammond, J. Humpolickova, L. Vrzal, D. Chalupska, V. Veverka, G. D. Fairn, E. Boura, T. Balla, PI(4,5)P2 controls plasma membrane PI4P and PS levels via ORP5/8 recruitment to ER–PM contact sites. *J Cell Biol*. **217**, 1797–1813 (2018).

362. T. P. Levine, S. Munro, Targeting of Golgi-Specific Pleckstrin Homology Domains Involves Both PtdIns 4-Kinase-Dependent and -Independent Components. *Curr Biol*. **12**, 695–704 (2002).

363. Z. Szentpetery, P. Várnai, T. Balla, Acute manipulation of Golgi phosphoinositides to assess their importance in cellular trafficking and signaling. *Proc National Acad Sci*. **107**, 8225–8230 (2010).

364. M. Lenoir, M. Grzybek, M. Majkowski, S. Rajesh, J. Kaur, S. B.-M. Whittaker, Ü. Coskun, M. Overduin, Structural Basis of Dynamic Membrane Recognition by trans-Golgi Network Specific FAPP Proteins. *J Mol Biol*. **427**, 966–981 (2015).

365. O. Gozani, P. Karuman, D. R. Jones, D. Ivanov, J. Cha, A. A. Lugovskoy, C. L. Baird, H. Zhu, S. J. Field, S. L. Lessnick, J. Villasenor, B. Mehrotra, J. Chen, V. R. Rao, J. S. Brugge, C. G. Ferguson, B. Payrastre, D. G. Myszka, L. C. Cantley, G. Wagner, N. Divecha, G. D. Prestwich, J. Yuan, The PHD Finger of the Chromatin-Associated Protein ING2 Functions as a Nuclear Phosphoinositide Receptor. *Cell*. **114**, 99–111 (2003).

366. C. Pendaries, H. Tronchère, L. Arbibe, J. Mounier, O. Gozani, L. Cantley, M. J. Fry, F. Gaits-Iacovoni, P. J. Sansonetti, B. Payrastre, PtdIns(5)P activates the host cell PI3-kinase/Akt pathway during Shigella flexneri infection. *Embo J*. **25**, 1024–1034 (2006).

367. S. Dowler, R. A. Currie, D. G. Campbell, M. Deak, G. Kular, C. P. Downes, D. R. Alessi, Identification of pleckstrin-homology-domain-containing proteins with novel phosphoinositide-binding specificities. *Biochem J*. **351**, 19–31 (2000).

368. C. C. Thomas, S. Dowler, M. Deak, D. R. Alessi, D. M. van Aalten, Crystal structure of the phosphatidylinositol 3,4-bisphosphate-binding pleckstrin homology (PH) domain of tandem PH-domain-containing protein 1 (TAPP1): molecular basis of lipid specificity. *Biochem J*. **358**, 287–294 (2001).

369. W. A. Kimber, S. Watt, R. T. Javier, A. Gray, C. P. Downes, J. M. Lucocq, D. R. Alessi, Evidence that the tandem-pleckstrin-homology-domain-containing protein TAPP1 interacts with Ptd(3,4)P2 and the multi-PDZ-domain-containing protein MUPP1 in vivo. *Biochem J*. **361**, 525–536 (2002).

370. A. J. Marshall, A. K. Krahn, K. Ma, V. Duronio, S. Hou, TAPP1 and TAPP2 Are Targets of Phosphatidylinositol 3-Kinase Signaling in B Cells: Sustained Plasma Membrane Recruitment Triggered by the B-Cell Antigen Receptor. *Mol Cell Biol*. **22**, 5479–5491 (2002).

371. D. Manna, A. Albanese, W. S. Park, W. Cho, Mechanistic Basis of Differential Cellular Responses of Phosphatidylinositol 3,4-Bisphosphate- and Phosphatidylinositol 3,4,5-Trisphosphate-binding Pleckstrin Homology Domains*. *J Biol Chem*. **282**, 32093–32105 (2007).

372. S.-L. Liu, Z.-G. Wang, Y. Hu, Y. Xin, I. Singaram, S. Gorai, X. Zhou, Y. Shim, J.-H. Min, L.-W. Gong, N. Hay, J. Zhang, W. Cho, Quantitative Lipid Imaging Reveals a New Signaling Function of Phosphatidylinositol-3,4-Bisphophate: Isoform- and Site-Specific Activation of Akt. *Mol Cell*. **71**, 1092-1104.e5 (2018).

373. B. D. Goulden, J. Pacheco, A. Dull, J. P. Zewe, A. Deiters, G. R. V. Hammond, A high-avidity biosensor reveals plasma membrane PI(3,4)P2 is predominantly a class I PI3K signaling product. *J Cell Biology*. **218**, 1066–1079 (2019).

374. X. Li, X. Wang, X. Zhang, M. Zhao, W. L. Tsang, Y. Zhang, R. G. W. Yau, L. S. Weisman, H. Xu, Genetically encoded fluorescent probe to visualize intracellular phosphatidylinositol 3,5-bisphosphate localization and dynamics. *Proc National Acad Sci*. **110**, 21165–21170 (2013).

375. G. R. V. Hammond, S. Takasuga, T. Sasaki, T. Balla, The ML1Nx2 Phosphatidylinositol 3,5-Bisphosphate Probe Shows Poor Selectivity in Cells. *Plos One*. **10**, e0139957 (2015).

376. P. Garcia, R. Gupta, S. Shah, A. J. Morris, S. A. Rudge, S. Scarlata, V. Petrova, S. McLaughlin, M. J. Rebecchi, The pleckstrin homology domain of phospholipase C-.delta.1 binds with high affinity to phosphatidylinositol 4,5-bisphosphate in bilayer membranes. *Biochemistry-us*. **34**, 16228–16234 (1995).

377. M. A. Lemmon, K. M. Ferguson, R. O'Brien, P. B. Sigler, J. Schlessinger, Specific and high-affinity binding of inositol phosphates to an isolated pleckstrin homology domain. *Proc National Acad Sci*. **92**, 10472–10476 (1995).

378. T. P. Stauffer, S. Ahn, T. Meyer, Receptor-induced transient reduction in plasma membrane PtdIns(4,5)P2 concentration monitored in living cells. *Curr Biol*. **8**, 343–346 (1998).

379. P. Várnai, T. Balla, Visualization of Phosphoinositides That Bind Pleckstrin Homology Domains: Calcium- and Agonist-induced Dynamic Changes and Relationship to Myo-[3H]inositol-labeled Phosphoinositide Pools. *J Cell Biology*. **143**, 501–510 (1998).

380. K. Hirose, S. Kadowaki, M. Tanabe, H. Takeshima, M. Iino, Spatiotemporal Dynamics of Inositol 1,4,5-Trisphosphate That Underlies Complex Ca2+ Mobilization Patterns. *Science*. **284**, 1527–1530 (1999).

381. B.-C. Suh, T. Inoue, T. Meyer, B. Hille, Rapid Chemically Induced Changes of PtdIns(4,5)P2 Gate KCNQ Ion Channels. *Science*. **314**, 1454–1457 (2006).

382. S. B. Lee, P. Várnai, A. Balla, K. Jalink, S.-G. Rhee, T. Balla, The Pleckstrin Homology Domain of Phosphoinositide-specific Phospholipase Cδ4 Is Not a Critical Determinant of the Membrane Localization of the Enzyme. *J Biol Chem*. **279**, 24362–24371 (2004).

383. G. R. V. Hammond, T. Balla, Polyphosphoinositide binding domains: Key to inositol lipid biology. *Biochimica Et Biophysica Acta Bba - Mol Cell Biology Lipids*. **1851**, 746–758 (2015).

384. K. V. Quinn, P. Behe, A. Tinker, Monitoring changes in membrane phosphatidylinositol 4,5-bisphosphate in living cells using a domain from the transcription factor tubby. *J Physiology*. **586**, 2855–2871 (2008).

385. C. R. Halaszovich, D. N. Schreiber, D. Oliver, Ci-VSP Is a Depolarization-activated Phosphatidylinositol-4,5-bisphosphate and Phosphatidylinositol-3,4,5-trisphosphate 5′-Phosphatase. *J Biol Chem*. **284**, 2106–2113 (2009).

386. Z. Szentpetery, A. Balla, Y. J. Kim, M. A. Lemmon, T. Balla, Live cell imaging with protein domains capable of recognizing phosphatidylinositol 4,5-bisphosphate; a comparative study. *Bmc Cell Biol*. **10**, 67–67 (2009).

387. M. G. J. Ford, B. M. F. Pearse, M. K. Higgins, Y. Vallis, D. J. Owen, A. Gibson, C. R. Hopkins, P. R. Evans, H. T. McMahon, Simultaneous Binding of PtdIns(4,5)P_2 and Clathrin by AP180 in the Nucleation of Clathrin Lattices on Membranes. *Science*. **291**, 1051–1055 (2001).

388. T. Itoh, S. Koshiba, T. Kigawa, A. Kikuchi, S. Yokoyama, T. Takenawa, Role of the ENTH Domain in Phosphatidylinositol-4,5-Bisphosphate Binding and Endocytosis. *Science*. **291**, 1047–1051 (2001).

389. Y. Yoon, P. J. Lee, S. Kurilova, W. Cho, In situ quantitative imaging of cellular lipids using molecular sensors. *Nat Chem*. **3**, 868–874 (2011).

390. Q. Lu, J. Yu, J. Yan, Z. Wei, M. Zhang, Structural basis of the myosin X PH1N-PH2-PH1C tandem as a specific and acute cellular PI(3,4,5)P3 sensor. *Mol Biol Cell*. **22**, 4268–4278 (2011).

391. L. Plantard, A. Arjonen, J. G. Lock, G. Nurani, J. Ivaska, S. Strömblad, PtdIns(3,4,5)P3 is a regulator of myosin-X localization and filopodia formation. *J Cell Sci*. **123**, 3525–3534 (2010).

392. Hokanson, D. E., Laakso, J. M., Lin, T., Sept, D., & Ostap, E. M., Myo1c Binds Phosphoinositides through a Putative Pleckstrin Homology Domain□. *MBoC*. **17**, 4856–4865 (2006).

393. M. Frech, M. Andjelkovic, E. Ingley, K. K. Reddy, J. R. Falck, B. A. Hemmings, High Affinity Binding of Inositol Phosphates and Phosphoinositides to the Pleckstrin Homology Domain of RAC/Protein Kinase B and Their Influence on Kinase Activity*. *J Biol Chem*. **272**, 8474–8481 (1997).

394. S. J. Watton, J. Downward, Akt/PKB localisation and 3′ phosphoinositide generation at sites of epithelial cell–matrix and cell–cell interaction. *Curr Biol*. **9**, 433–436 (1999).

395. M. Fukuda, T. Kojima, H. Kabayama, K. Mikoshiba, Mutation of the Pleckstrin Homology Domain of Bruton's Tyrosine Kinase in Immunodeficiency Impaired Inositol 1,3,4,5-Tetrakisphosphate Binding Capacity. *J Biol Chem*. **271**, 30303–30306 (1996).

396. K. Salim, M. J. Bottomley, E. Querfurth, M. J. Zvelebil, I. Gout, R. Scaife, R. L. Margolis, R. Gigg, C. I. Smith, P. C. Driscoll, M. D. Waterfield, G. Panayotou, Distinct specificity in the recognition of phosphoinositides by the pleckstrin homology domains of dynamin and Bruton's tyrosine kinase. *Embo J*. **15**, 6241–6250 (1996).

397. L. E. Rameh, A. Arvidsson, K. L. Carraway, A. D. Couvillon, G. Rathbun, A. Crompton, B. VanRenterghem, M. P. Czech, K. S. Ravichandran, S. J. Burakoff, D.-S. Wang, C.-S. Chen, L. C. Cantley, A Comparative Analysis of the Phosphoinositide Binding Specificity of Pleckstrin Homology Domains*. *J Biol Chem*. **272**, 22059–22066 (1997).

398. C. D. Kontos, T. P. Stauffer, W.-P. Yang, J. D. York, L. Huang, M. A. Blanar, T. Meyer, K. G. Peters, Tyrosine 1101 of Tie2 Is the Major Site of Association of p85 and Is Required for Activation of Phosphatidylinositol 3-Kinase and Akt. *Mol Cell Biol*. **18**, 4131–4140 (1998).

399. K. Venkateswarlu, P. B. Oatey, J. M. Tavaré, P. J. Cullen, Insulin-dependent translocation of ARNO to the plasma membrane of adipocytes requires phosphatidylinositol 3-kinase. *Curr Biol*. **8**, 463–466 (1998).

400. A. Gray, J. Vanderkaay, C. P. Downes, The pleckstrin homology domains of protein kinase B and GRP1 (general receptor for phosphoinositides-1) are sensitive and selective probes for the cellular detection of phosphatidylinositol 3,4-bisphosphate and/or phosphatidylinositol 3,4,5-trisphosphate in vivo. *Biochem J*. **344**, 929–936 (1999).

401. L. A. Cohen, A. Honda, P. Varnai, F. D. Brown, T. Balla, J. G. Donaldson, Active Arf6 Recruits ARNO/Cytohesin GEFs to the PM by Binding Their PH Domains. *Mol Biol Cell*. **18**, 2244–2253 (2007).

402. C.-C. Li, T.-C. Chiang, T.-S. Wu, G. Pacheco-Rodriguez, J. Moss, F.-J. s. Lee, ARL4D Recruits Cytohesin-2/ARNO to Modulate Actin Remodeling□. *MBoC*. **18**, 4420–4437 (2007).

403. I. Hofmann, A. Thompson, C. M. Sanderson, S. Munro, The Arl4 Family of Small G Proteins Can Recruit the Cytohesin Arf6 Exchange Factors to the Plasma Membrane. *Curr Biol*. **17**, 711–716 (2007).

404. J. K. Klarlund, A. Guilherme, J. J. Holik, J. V. Virbasius, A. Chawla, M. P. Czech, Signaling by Phosphoinositide-3,4,5- Trisphosphate Through Proteins Containing Pleckstrin and Sec7 Homology Domains. *Science*. **275**, 1927–30 (1997).

405. K. V. Quinn, P. Behe, A. Tinker, Monitoring changes in membrane phosphatidylinositol 4,5-bisphosphate in living cells using a domain from the transcription factor tubby. *J Physiology*. **586**, 2855–2871 (2008).

406. P. Várnai, T. Balla, Visualization of Phosphoinositides That Bind Pleckstrin Homology Domains: Calcium- and Agonist-induced Dynamic Changes and Relationship to Myo-[3H]inositol-labeled Phosphoinositide Pools. *J Cell Biology*. **143**, 501–510 (1998).

407. J. P. Zewe, R. C. Wills, S. Sangappa, B. D. Goulden, G. R. Hammond, SAC1 degrades its lipid substrate PtdIns4P in the endoplasmic reticulum to maintain a steep chemical gradient with donor membranes. *Elife*. **7**, e35588 (2018).

408. G. R. V. Hammond, M. P. Machner, T. Balla, A novel probe for phosphatidylinositol 4-phosphate reveals multiple pools beyond the GolgiLocalization of PtdIns4P in living cells. *J Cell Biology*. **205**, 113–126 (2014).

409. G. R. V. Hammond, J. E. Burke, Novel roles of phosphoinositides in signaling, lipid transport, and disease. *Curr Opin Cell Biol*. **63**, 57–67 (2020).

410. K. O. Schink, K.-W. Tan, H. Stenmark, Phosphoinositides in Control of Membrane Dynamics. *Annu Rev Cell Dev Bi*. **32**, 1–29 (2015).

411. J. Saarikangas, H. Zhao, P. Lappalainen, Regulation of the Actin Cytoskeleton-Plasma Membrane Interplay by Phosphoinositides. *Physiol Rev*. **90**, 259–289 (2010).

412. Y. Senju, P. Lappalainen, Regulation of actin dynamics by PI(4,5)P2 in cell migration and endocytosis. *Curr Opin Cell Biol*. **56**, 7–13 (2019).

413. L. R. Stephens, K. T. Hughes, R. F. Irvine, Pathway of phosphatidylinositol(3,4,5)-trisphosphate synthesis in activated neutrophils. *Nature*. **351**, 33–39 (1991).

414. R. Nández, D. M. Balkin, M. Messa, L. Liang, S. Paradise, H. Czapla, M. Y. Hein, J. S. Duncan, M. Mann, P. D. Camilli, A role of OCRL in clathrin-coated pit dynamics and uncoating revealed by studies of Lowe syndrome cells. *Elife*. **3**, e02975 (2014).

415. C. N. Antonescu, F. Aguet, G. Danuser, S. L. Schmid, Phosphatidylinositol-(4,5)-bisphosphate regulates clathrin-coated pit initiation, stabilization, and size. *Mol Biol Cell*. **22**, 2588–2600 (2011).

416. C. E. Bazenet, A. R. Ruano, J. L. Brockman, R. A. Anderson, The human erythrocyte contains two forms of phosphatidylinositol-4-phosphate 5-kinase which are differentially active toward membranes. *J Biological Chem*. **265**, 18012–22 (1990).

417. C. E. King, L. R. Stephens, P. T. Hawkins, G. R. Guy, R. H. Michell, Multiple metabolic pools of phosphoinositides and phosphatidate in human erythrocytes incubated in a medium that permits rapid transmembrane exchange of phosphate. *Biochem J*. **244**, 209–217 (1987).

418. S. D. Hansen, W. Y. C. Huang, Y. K. Lee, P. Bieling, S. M. Christensen, J. T. Groves, Stochastic geometry sensing and polarization in a lipid kinase–phosphatase competitive reaction. *Proc National Acad Sci*. **116**, 15013–15022 (2019).

419. G. B. Willars, S. R. Nahorski, R. A. J. Challiss, Differential Regulation of Muscarinic Acetylcholine Receptor-sensitive Polyphosphoinositide Pools and Consequences for Signaling in Human Neuroblastoma Cells. *J Biol Chem*. **273**, 5037–5046 (1998).

420. K. A. HINCHLIFFE, M. L. GIUDICI, A. J. LETCHER, R. F. IRVINE, Type IIα phosphatidylinositol phosphate kinase associates with the plasma membrane via interaction with type I isoforms. *Biochem J*. **363**, 563–570 (2002).

421. T.-S. Hsieh, V. A. Lopez, M. H. Black, A. Osinski, K. Pawłowski, D. R. Tomchick, J. Liou, V. S. Tagliabracci, Dynamic remodeling of host membranes by self-organizing bacterial effectors. *Science*. **372**, 935–941 (2021).

422. Z. Wu, X. Li, M. Sunkara, H. Spearman, A. J. Morris, C. Huang, PIPKIγ Regulates Focal Adhesion Dynamics and Colon Cancer Cell Invasion. *Plos One*. **6**, e24775 (2011).

423. M. Arioka, S. Nakashima, Y. Shibasaki, K. Kitamoto, Dibasic amino acid residues at the carboxy-terminal end of kinase homology domain participate in the plasma membrane localization and function of phosphatidylinositol 5-kinase γ. *Biochemical and Biophysical Research Communications*. **319**, 456–463 (2003).

424. T. Geiger, A. Wehner, C. Schaab, J. Cox, M. Mann, *Mol Cell Proteomics*, in press, doi:10.1074/mcp.m111.014050.

425. T. Yeung, M. Terebiznik, L. Yu, J. Silvius, W. M. Abidi, M. Philips, T. Levine, A. Kapus, S. Grinstein, Receptor Activation Alters Inner Surface Potential During Phagocytosis. *Science*. **313**, 347–351 (2006).

426. M. Varadi, S. Anyango, M. Deshpande, S. Nair, C. Natassia, G. Yordanova, D. Yuan, O. Stroe, G. Wood, A. Laydon, A. Žídek, T. Green, K. Tunyasuvunakool, S. Petersen, J. Jumper, E. Clancy, R. Green, A. Vora, M. Lutfi, M. Figurnov, A. Cowie, N. Hobbs, P. Kohli, G. Kleywegt, E. Birney, D. Hassabis, S. Velankar, AlphaFold Protein Structure Database: massively expanding the structural coverage of protein-sequence space with high-accuracy models. *Nucleic Acids Res*. **50**, D439–D444 (2021).

427. J. Jumper, R. Evans, A. Pritzel, T. Green, M. Figurnov, O. Ronneberger, K. Tunyasuvunakool, R. Bates, A. Žídek, A. Potapenko, A. Bridgland, C. Meyer, S. A. A. Kohl, A. J. Ballard, A. Cowie, B. Romera-Paredes, S. Nikolov, R. Jain, J. Adler, T. Back, S. Petersen, D. Reiman, E. Clancy, M. Zielinski, M. Steinegger, M. Pacholska, T. Berghammer, S. Bodenstein, D. Silver, O. Vinyals, A. W. Senior, K. Kavukcuoglu, P. Kohli, D. Hassabis, Highly accurate protein structure prediction with AlphaFold. *Nature*, 1–11 (2021).

428. M. A. Barbieri, C. M. Heath, E. M. Peters, A. Wells, J. N. Davis, P. D. Stahl, Phosphatidylinositol-4-phosphate 5-Kinase-1β Is Essential for Epidermal Growth Factor Receptor-mediated Endocytosis*. *J Biol Chem*. **276**, 47212–47216 (2001).

429. M. Jarquin-Pardo, A. Fitzpatrick, F. J. Galiano, E. A. First, N. J. Davis, Phosphatidic acid regulates the affinity of the murine phosphatidylinositol 4-phosphate 5-kinase-Iβ for phosphatidylinositol-4-phosphate. *Journal of Cellular Biochemistry*. **100**, 112–128 (2007).

430. M. D. Leonetti, S. Sekine, D. Kamiyama, J. S. Weissman, B. Huang, A scalable strategy for high-throughput GFP tagging of endogenous human proteins. *Proceedings of the National Academy of Sciences*. **113**, E3501–E3508 (2016).

431. M. Ovesný, P. Křížek, J. Borkovec, Z. Švindrych, G. M. Hagen, ThunderSTORM: a comprehensive ImageJ plug-in for PALM and STORM data analysis and super-resolution imaging. *Bioinformatics*. **30**, 2389–2390 (2014).

432. G. D. Paolo, L. Pellegrini, K. Letinic, G. Cestra, R. Zoncu, S. Voronov, S. Chang, J. Guo, M. R. Wenk, P. D. Camilli, Recruitment and regulation of phosphatidylinositol phosphate kinase type 1γ by the FERM domain of talin. *Nature*. **420**, 85–89 (2002).

433. T. K. Phan, G. K. Bindra, S. A. Williams, I. K. H. Poon, M. D. Hulett, Combating Human Pathogens and Cancer by Targeting Phosphoinositides and Their Metabolism. *Trends Pharmacol Sci*. **40**, 866–882 (2019).

434. G. Narkis, R. Ofir, D. Landau, E. Manor, M. Volokita, R. Hershkowitz, K. Elbedour, O. S. Birk, Lethal Contractural Syndrome Type 3 (LCCS3) Is Caused by a Mutation in PIP5K1C, Which Encodes PIPKIγ of the Phophatidylinsitol Pathway. *Am J Hum Genetics*. **81**, 530–539 (2007).

435. L. A. Volpicelli-Daley, L. Lucast, L.-W. Gong, L. Liu, J. Sasaki, T. Sasaki, C. S. Abrams, Y. Kanaho, P. D. Camilli, Phosphatidylinositol-4-Phosphate 5-Kinases and Phosphatidylinositol 4,5-Bisphosphate Synthesis in the Brain*. *J Biological Chem*. **285**, 28708–28714 (2010).

436. J. Semenas, A. Hedblom, R. R. Miftakhova, M. Sarwar, R. Larsson, L. Shcherbina, M. E. Johansson, P. Härkönen, O. Sterner, J. L. Persson, The role of PI3K/AKT-related PIP5K1α and the discovery of its selective inhibitor for treatment of advanced prostate cancer. *Proc National Acad Sci*. **111**, E3689–E3698 (2014).

437. M. Berquez, J. R. Gadsby, B. P. Festa, R. Butler, S. P. Jackson, V. Berno, A. Luciani, O. Devuyst, J. L. Gallop, The phosphoinositide 3-kinase inhibitor alpelisib restores actin organization and improves proximal tubule dysfunction in vitro and in a mouse model of Lowe syndrome and Dent disease. *Kidney Int*. **98**, 883–896 (2020).

438. D. Mason, G. V. Mallo, M. R. Terebiznik, B. Payrastre, B. B. Finlay, J. H. Brumell, L. Rameh, S. Grinstein, Alteration of Epithelial Structure and Function Associated with PtdIns(4,5)P2 Degradation by a Bacterial Phosphatase. *J Gen Physiology*. **129**, 267–283 (2007).

439. K. A. Lamia, O. D. Peroni, Y.-B. Kim, L. E. Rameh, B. B. Kahn, L. C. Cantley, Increased Insulin Sensitivity and Reduced Adiposity in Phosphatidylinositol 5-Phosphate 4-Kinase β−/− Mice. *Molecular and Cellular Biology*. **24**, 5080–5087 (2004).

440. C. Pendaries, H. Tronchère, L. Arbibe, J. Mounier, O. Gozani, L. Cantley, M. J. Fry, F. Gaits-Iacovoni, P. J. Sansonetti, B. Payrastre, PtdIns(5)P activates the host cell PI3-kinase/Akt pathway during Shigella flexneri infection. *Embo J*. **25**, 1024–1034 (2006).

441. H. Shim, C. Wu, S. Ramsamooj, K. N. Bosch, Z. Chen, B. M. Emerling, J. Yun, H. Liu, R. Choo-Wing, Z. Yang, G. M. Wulf, V. Kuchroo, L. C. Cantley, Deletion of the gene Pip4k2c, a novel phosphatidylinositol kinase, results in hyperactivation of the immune system. *Proceedings of the National Academy of Sciences*. **113**, 7596–7601 (2016).

442. B. M. Emerling, J. B. Hurov, G. Poulogiannis, K. S. Tsukazawa, R. Choo-Wing, G. M. Wulf, E. L. Bell, H.-S. Shim, K. A. Lamia, L. E. Rameh, G. Bellinger, A. T. Sasaki, J. M. Asara, X. Yuan, A. Bullock, G. M. DeNicola, J. Song, V. Brown, S. Signoretti, L. C. Cantley, Depletion of a Putatively Druggable Class of Phosphatidylinositol Kinases Inhibits Growth of p53-Null Tumors. *Cell*. **155**, 844–857 (2013).

443. M. R. Wenk, L. Pellegrini, V. A. Klenchin, G. D. Paolo, S. Chang, L. Daniell, M. Arioka, T. F. Martin, P. D. Camilli, PIP Kinase Iγ Is the Major PI(4,5)P2 Synthesizing Enzyme at the Synapse. *Neuron*. **32**, 79–88 (2001).

444. D. Padrón, Y. J. Wang, M. Yamamoto, H. Yin, M. G. Roth, Phosphatidylinositol phosphate 5-kinase Iβ recruits AP-2 to the plasma membrane and regulates rates of constitutive endocytosis. *J Cell Biology*. **162**, 693–701 (2003).

445. M. D. Leonetti, S. Sekine, D. Kamiyama, J. S. Weissman, B. Huang, A scalable strategy for high-throughput GFP tagging of endogenous human proteins. *Proceedings of the National Academy of Sciences*. **113**, E3501–E3508 (2016).

446. S. Feng, S. Sekine, V. Pessino, H. Li, M. D. Leonetti, B. Huang, Improved split fluorescent proteins for endogenous protein labeling. *Nat Commun*. **8**, 370 (2017).

447. Y.-C. Lin, M. Boone, L. Meuris, I. Lemmens, N. V. Roy, A. Soete, J. Reumers, M. Moisse, S. Plaisance, R. Drmanac, J. Chen, F. Speleman, D. Lambrechts, Y. V. de Peer, J. Tavernier, N. Callewaert, Genome dynamics of the human embryonic kidney 293 lineage in response to cell biology manipulations. *Nat Commun*. **5**, 4767 (2014).

448. A. M. Kong, K. A. Horan, A. Sriratana, C. G. Bailey, L. J. Collyer, H. H. Nandurkar, A. Shisheva, M. J. Layton, J. E. J. Rasko, T. Rowe, C. A. Mitchell, Phosphatidylinositol 3-Phosphate [PtdIns(3)P] Is Generated at the Plasma Membrane by an Inositol Polyphosphate 5-Phosphatase: Endogenous PtdIns(3)P Can Promote GLUT4 Translocation to the Plasma Membrane. *Mol Cell Biol*. **26**, 6065–6081 (2006).

449. Y. Tsujishita, S. Guo, L. E. Stolz, J. D. York, J. H. Hurley, Specificity Determinants in Phosphoinositide Dephosphorylation Crystal Structure of an Archetypal Inositol Polyphosphate 5-Phosphatase. *Cell*. **105**, 379–389 (2001).

450. M. Baek, F. DiMaio, I. Anishchenko, J. Dauparas, S. Ovchinnikov, G. R. Lee, J. Wang, Q. Cong, L. N. Kinch, R. D. Schaeffer, C. Millán, H. Park, C. Adams, C. R. Glassman, A. DeGiovanni, J. H. Pereira, A. V. Rodrigues, A. A. van Dijk, A. C. Ebrecht, D. J. Opperman, T. Sagmeister, C. Buhlheller, T. Pavkov-Keller, M. K. Rathinaswamy, U. Dalwadi, C. K. Yip, J. E. Burke, K. C. Garcia, N. V. Grishin, P. D. Adams, R. J. Read, D. Baker, Accurate prediction of protein structures and interactions using a three-track neural network. *Science*, eabj8754 (2021).

451. P. Várnai, T. Balla, Visualization of Phosphoinositides That Bind Pleckstrin Homology Domains: Calcium- and Agonist-induced Dynamic Changes and Relationship to Myo-[3H]inositol-labeled Phosphoinositide Pools. *J Cell Biology*. **143**, 501–510 (1998).

452. G. R. V. Hammond, M. M. C. Ricci, C. C. Weckerly, R. C. Wills, An update on genetically encoded lipid biosensors. *Mol Biol Cell*. **33**, tp2 (2022).

453. J. Wu, L. Liu, T. Matsuda, Y. Zhao, A. Rebane, M. Drobizhev, Y.-F. Chang, S. Araki, Y. Arai, K. March, T. E. Hughes, K. Sagou, T. Miyata, T. Nagai, W. Li, R. E. Campbell, Improved Orange and Red Ca2+ Indicators and Photophysical Considerations for Optogenetic Applications. *Acs Chem Neurosci*. **4**, 963–972 (2013).

454. Y.-J. Chen, C.-L. Chang, W.-R. Lee, J. Liou, *J Cell Biol*, in press, doi:10.1083/jcb.201606047.

455. D. M. Shcherbakova, V. V. Verkhusha, Near-infrared fluorescent proteins for multicolor in vivo imaging. *Nat Methods*. **10**, 751–754 (2013).

456. S. D. Hansen, W. Y. C. Huang, Y. K. Lee, P. Bieling, S. M. Christensen, J. T. Groves, Stochastic geometry sensing and polarization in a lipid kinase–phosphatase competitive reaction. *Proc National Acad Sci*. **116**, 15013–15022 (2019).

457. C. P. Guimaraes, M. D. Witte, C. S. Theile, G. Bozkurt, L. Kundrat, A. E. M. Blom, H. L. Ploegh, Site-specific C-terminal and internal loop labeling of proteins using sortase-mediated reactions. *Nat Protoc*. **8**, 1787–1799 (2013).

458. H. F. Roberts, J. H. Clarke, A. J. Letcher, R. F. Irvine, K. A. Hinchliffe, Effects of lipid kinase expression and cellular stimuli on phosphatidylinositol 5-phosphate levels in mammalian cell lines. *Febs Lett*. **579**, 2868–2872 (2005).

459. B. D. Goulden, J. Pacheco, A. Dull, J. P. Zewe, A. Deiters, G. R. V. Hammond, A high-avidity biosensor reveals plasma membrane PI(3,4)P2 is predominantly a class I PI3K signaling product. *J Cell Biology*. **218**, 1066–1079 (2019).

460. J. Wu, L. Liu, T. Matsuda, Y. Zhao, A. Rebane, M. Drobizhev, Y.-F. Chang, S. Araki, Y. Arai, K. March, T. E. Hughes, K. Sagou, T. Miyata, T. Nagai, W. Li, R. E. Campbell, Improved Orange and Red Ca2+ Indicators and Photophysical Considerations for Optogenetic Applications. *Acs Chem Neurosci*. **4**, 963–972 (2013).

461. R. B. Berlow, H. J. Dyson, P. E. Wright, Expanding the Paradigm: Intrinsically Disordered Proteins and Allosteric Regulation. *J Mol Biol*. **430**, 2309–2320 (2018).

462. R. P. Johnson, V. Niggli, P. Durrer, S. W. Craig, A Conserved Motif in the Tail Domain of Vinculin Mediates Association with and Insertion into Acidic Phospholipid Bilayers †. *Biochemistry-us*. **37**, 10211–10222 (1998).

463. C. Cochet, O. Filhol, B. Payrastre, T. Hunter, G. N. Gill, Interaction between the epidermal growth factor receptor and phosphoinositide kinases. *J Biol Chem*. **266**, 637–644 (1991).

464. T. Itoh, H. Ishihara, Y. Shibasaki, Y. Oka, T. Takenawa, Autophosphorylation of Type I Phosphatidylinositol Phosphate Kinase Regulates Its Lipid Kinase Activity. *J Biol Chem*. **275**, 19389–19394 (2000).

465. S. J. Park, T. Itoh, T. Takenawa, Phosphatidylinositol 4-Phosphate 5-Kinase Type I Is Regulated through Phosphorylation Response by Extracellular Stimuli. *J Biol Chem*. **276**, 4781–4787 (2001).

466. T. Courtney, A. Deiters, Recent advances in the optical control of protein function through genetic code expansion. *Curr Opin Chem Biol*. **46**, 99–107 (2018).

467. A. M. Hicks, C. J. DeLong, M. J. Thomas, M. Samuel, Z. Cui, Unique molecular signatures of glycerophospholipid species in different rat tissues analyzed by tandem mass spectrometry. *Biochimica Et Biophysica Acta Bba - Mol Cell Biology Lipids*. **1761**, 1022–1029 (2006).

468. I. Pradas, K. Huynh, R. Cabré, V. Ayala, P. J. Meikle, M. Jové, R. Pamplona, Lipidomics Reveals a Tissue-Specific Fingerprint. *Front Physiol*. **9**, 1165 (2018).

469. M. P. Blaustein, Sodium ions, calcium ions, blood pressure regulation, and hypertension: a reassessment and a hypothesis. *Am J Physiol-cell Ph*. **232**, C165–C173 (1977).

470. R. P. Lifton, A. G. Gharavi, D. S. Geller, Molecular Mechanisms of Human Hypertension. *Cell*. **104**, 545–556 (2001).

471. R. S. Rao, J. M. Miano, E. N. Olson, C. L. Seidel, The A10 cell line: a model for neonatal, neointimal, or differentiated vascular smooth muscle cells? *Cardiovasc Res*. **36**, 118–126 (1997).

472. J. A. Engelman, Targeting PI3K signalling in cancer: opportunities, challenges and limitations. *Nature reviews. Cancer*. **9**, 550–62 (2009).

473. F. Janku, T. A. Yap, F. Meric-Bernstam, Targeting the PI3K pathway in cancer: are we making headway? *Nature Reviews Clinical Oncology*. **15**, 273 (2018).

474. E. Cerami, J. Gao, U. Dogrusoz, B. E. Gross, S. Sumer, B. Aksoy, A. Jacobsen, C. J. Byrne, M. L. Heuer, E. Larsson, Y. Antipin, B. Reva, A. P. Goldberg, C. Sander, N. Schultz, The cBio

Cancer Genomics Portal: An Open Platform for Exploring Multidimensional Cancer Genomics Data. *Cancer Discovery*. **2**, 401–404 (2012).

475. J. Gao, B. Aksoy, U. Dogrusoz, G. Dresdner, B. Gross, O. S. Sumer, Y. Sun, A. Jacobsen, R. Sinha, E. Larsson, E. Cerami, C. Sander, N. Schultz, Integrative Analysis of Complex Cancer Genomics and Clinical Profiles Using the cBioPortal. *Sci. Signal.* **6**, pl1–pl1 (2013).

476. P. LoRusso, Inhibition of the PI3K/AKT/mTOR Pathway in Solid Tumors. *Journal of Clinical Oncology*. **34**, 3803–3815 (2016).

477. E. Pons-Tostivint, B. Thibault, J. Guillermet-Guibert, Targeting PI3K Signaling in Combination Cancer Therapy. *Trends in Cancer*. **3**, 454–469 (2017).

478. D. Juric, F. Janku, J. Rodón, H. A. Burris, I. A. Mayer, M. Schuler, R. Seggewiss-Bernhardt, M. Gil-Martin, M. R. Middleton, J. Baselga, D. Bootle, D. Demanse, L. Blumenstein, K. Schumacher, A. Huang, C. Quadt, H. S. Rugo, Alpelisib Plus Fulvestrant in PIK3CA-Altered and PIK3CA-Wild-Type Estrogen Receptor–Positive Advanced Breast Cancer. *JAMA Oncology*. **5**, e184475 (2019).

479. F. André, E. M. Ciruelos, G. Rubovszky, M. Campone, S. Loibl, H. S. Rugo, H. Iwata, P. Conte, I. A. Mayer, B. Kaufman, T. Yamashita, Y.-S. Lu, K. Inoue, M. Takahashi, Z. Pápai, A.-S. Longin, D. Mills, C. Wilke, S. Hirawat, D. Juric, LBA3_PRAlpelisib (ALP) + fulvestrant (FUL) for advanced breast cancer (ABC): Results of the phase III SOLAR-1 trial. *Ann Oncol*. **29** (2018), doi:10.1093/annonc/mdy424.010.

480. Y. Zhang, P. K.-S. Ng, M. Kucherlapati, F. Chen, Y. Liu, Y. H. Tsang, G. de Velasco, K. J. Jeong, R. Akbani, A. Hadjipanayis, A. Pantazi, C. A. Bristow, E. Lee, H. S. Mahadeshwar, J. Tang, J. Zhang, L. Yang, S. Seth, S. Lee, X. Ren, X. Song, H. Sun, J. Seidman, L. J. Luquette, R. Xi, L. Chin, A. Protopopov, T. F. Westbrook, C. S. Shelley, T. K. Choueiri, M. Ittmann, C. V. Waes, J. N. Weinstein, H. Liang, E. P. Henske, A. K. Godwin, P. J. Park, R. Kucherlapati, K. L. Scott, G. B. Mills, D. J. Kwiatkowski, C. J. Creighton, A Pan-Cancer Proteogenomic Atlas of PI3K/AKT/mTOR Pathway Alterations. *Cancer Cell*. **31**, 820-832.e3 (2017).

481. M. D. Goncalves, B. D. Hopkins, L. C. Cantley, Phosphatidylinositol 3-Kinase, Growth Disorders, and Cancer. *New England Journal of Medicine*. **379**, 2052–2062 (2018).

482. M. Tran, E. Seo, S. Min, Q. T. Nguyen, J. Choi, U. Lee, S. Hong, H. Kang, A. Mansukhani, I. Jou, S. Lee, NEDD4-induced degradative ubiquitination of phosphatidylinositol 4-phosphate 5-kinase α and its implication in breast cancer cell proliferation. *Journal of Cellular and Molecular Medicine*. **22**, 4117–4129 (2018).

483. M. Sarwar, A. S. S. Khaja, M. Aleskandarany, R. Karlsson, M. Althobiti, N. Ødum, N. P. Mongan, N. Dizeyi, H. Johnson, A. R. Green, I. O. Ellis, E. A. Rakha, J. L. Persson, The role of PIP5K1α/pAKT and targeted inhibition of growth of subtypes of breast cancer using PIP5K1α inhibitor. *Oncogene*, 1–15 (2018).

484. M. Sarwar, J. Semenas, R. Miftakhova, A. Simoulis, B. Robinson, A. G. Wingren, N. P. Mongan, D. M. Heery, H. Johnsson, P.-A. A. Abrahamsson, N. Dizeyi, J. Luo, J. L. Persson, Targeted suppression of AR-V7 using PIP5K1α inhibitor overcomes enzalutamide resistance in prostate cancer cells. *Oncotarget*. **7**, 63065–63081 (2016).

485. J. Semenas, A. Hedblom, R. R. Miftakhova, M. Sarwar, R. Larsson, L. Shcherbina, M. E. Johansson, P. Härkönen, O. Sterner, J. L. Persson, The role of PI3K/AKT-related PIP5K1α and the discovery of its selective inhibitor for treatment of advanced prostate cancer. *Proceedings of the National Academy of Sciences*. **111**, E3689–E3698 (2014).

486. N. Porciello, M. Kunkl, A. Viola, L. Tuosto, Phosphatidylinositol 4-Phosphate 5-Kinases in the Regulation of T Cell Activation. *Front Immunol*. **7**, 186 (2016).

487. M. Kunkl, N. Porciello, M. Mastrogiovanni, C. Capuano, F. Lucantoni, C. Moretti, J. L. Persson, R. Galandrini, R. Buzzetti, L. Tuosto, ISA-2011B, a Phosphatidylinositol 4-Phosphate 5-Kinase α Inhibitor, Impairs CD28-Dependent Costimulatory and Pro-inflammatory Signals in Human T Lymphocytes. *Front Immunol*. **8**, 502 (2017).

488. C. M. Gawden-Bone, G. L. Frazer, A. C. Richard, C. Y. Ma, K. Strege, G. M. Griffiths, PIP5 Kinases Regulate Membrane Phosphoinositide and Actin Composition for Targeted Granule Secretion by Cytotoxic Lymphocytes. *Immunity* (2018), doi:10.1016/j.immuni.2018.08.017.

489. O. Le, O. Cho, M. Tran, J. Kim, S. Chang, I. Jou, S. Lee, Phosphorylation of phosphatidylinositol 4-phosphate 5-kinase γ by Akt regulates its interaction with talin and focal adhesion dynamics. *Biochimica et Biophysica Acta (BBA) - Molecular Cell Research*. **1853**, 2432–2443 (2015).

490. J. Schindelin, I. Arganda-Carreras, E. Frise, V. Kaynig, M. Longair, T. Pietzsch, S. Preibisch, C. Rueden, S. Saalfeld, B. Schmid, J.-Y. Tinevez, D. J. White, V. Hartenstein, K. Eliceiri, P. Tomancak, A. Cardona, Fiji: an open-source platform for biological-image analysis. *Nat Methods*. **9**, 676–682 (2012).

491. M. Linkert, C. T. Rueden, C. Allan, J.-M. Burel, W. Moore, A. Patterson, B. Loranger, J. Moore, C. Neves, D. MacDonald, A. Tarkowska, C. Sticco, E. Hill, M. Rossner, K. W. Eliceiri, J. R. Swedlow, Metadata matters: access to image data in the real world. *J Cell Biology*. **189**, 777–782 (2010).